Western Graduate&PostdoctoralStudies

Western University
Scholarship@Western

Electronic Thesis and Dissertation Repository

9-20-2019 10:30 AM

An integrated framework to assess compound flood risks for interdependent critical infrastructure in a coastal environment

Ying Zhang
The University of Western Ontario

Supervisor
Najafi, Mohammad Reza
The University of Western Ontario

Graduate Program in Civil and Environmental Engineering
A thesis submitted in partial fulfillment of the requirements for the degree in Master of Engineering Science
© Ying Zhang 2019

Follow this and additional works at: https://ir.lib.uwo.ca/etd

Part of the Environmental Engineering Commons

Recommended Citation

Zhang, Ying, "An integrated framework to assess compound flood risks for interdependent critical infrastructure in a coastal environment" (2019). *Electronic Thesis and Dissertation Repository*. 6560.
https://ir.lib.uwo.ca/etd/6560

This Dissertation/Thesis is brought to you for free and open access by Scholarship@Western. It has been accepted for inclusion in Electronic Thesis and Dissertation Repository by an authorized administrator of Scholarship@Western. For more information, please contact wlswadmin@uwo.ca.

Abstract

Compound flooding refers to flood events caused by multiple factors, including marine processes (e.g. storm tides and waves), hydrometeorological signals (e.g. rainfall and river flows) among others. Saint Lucia is a tropical island in eastern Caribbean Sea, which is frequently affected by weather-related extreme events such as tropical storms and the associated risks are exacerbated due to its mountainous topography and high concentrations of infrastructure and human communities close to the coast. At the southern coast of Saint Lucia, significant infrastructures such as Hewanorra International Airport and Vieux Fort Seaport, and human settlements such as towns of Vieux Fort and La Tourney are located at low-lying areas and are at risk of compound flooding. A hydrologic model (i.e. HYdrological MODel) and a two-dimensional hydrodynamic model (i.e. LISFLOOD-FP) are set up and calibrated to investigate the combined effects of storm tides, wave run-up, rainfall, and river flows on flood risks in Saint Lucia. Results indicate the necessity to consider multiple contributing factors as well as to characterize the effects of uncertain boundary conditions. In flood-prone areas, there are infrastructures supporting major services in the study area, and by extension, the economy of the Island. A network-based model, which considers direct and indirect connections between infrastructures, is set up to explore risks of assets in conditions of non-flooding and flooding. Modelling results reveal the fundamental importance of various components including electricity distribution, flood control, information and communication services, transportation, housing and human settlements, tourism, and particularly the normal operations of Hewanorra International Airport. Prioritization of risks is critical for developing effective mitigation methods for infrastructure networks.

Keywords

Compound Flooding, Hydrologic Model, Hydrodynamic Model, HYMOD, LISFLOOD-FP, Uncertainty Analysis, Interdependent Infrastructure, Risk Analysis, Network-based Model

Lay Summary

Compound flooding has multiple contributing factors, including marine processes (e.g. storm tides and waves) and hydrometeorological signals (e.g. rainfall and river flows). They can interact with each other and generate more severe flooding, which has not been recognized until recent years. The study area is located at the southern coast of Saint Lucia, which is highly exposed to hurricanes and tropical storms, such as Hurricane Dean in 2007, Hurricane Tomas in 2010, and Hurricane Matthew in 2016. The compound flooding risks are exacerbated due to the mountainous topography and high concentrations of infrastructures and human communities. The most important infrastructure is Hewanorra International Airport, whose failures in several extreme events severely impacted local and international transportation as well as the local economy. Other assets that support major services in the study area and the economy of the island include Vieux Fort Seaport as well as the towns of Vieux Fort and La Tourney. They are interdependent and the failure of one asset in flooding can propagate through the network, leading to failures of other assets and more severe consequences. To understand compound flooding and its associated risks in the study area, a hydrological model (i.e. HYdrological MODel) and a two-dimensional hydrodynamic model (i.e. LISFLOOD-FP) are set up and calibrated to investigate the combined effects of storm tides, wave run-up, rainfall, and river flows on flood risks in the study area. A network-based risk analysis model is set up to explore risks of interdependent assets. Results indicate that it is important to consider multiple factors in flood analysis. Hewanorra International Airport has the fundamental significance in the study area, along with other high-risk assets in flooding such as electricity distribution, flood control, information and communication services, transportation, housing and human settlements, and tourism. This study provides insights of compound flooding and helps prioritize risks of infrastructures in local flood management.

Acknowledgments

First of all, I would like to express my sincere gratitude to my thesis supervisor Dr. Mohammad Reza Najafi, who believed in my potential and offered me the valuable opportunity to work with him two years ago. I am always encouraged to gain new skills and knowledge under his guidance. It was a wonderful journey, and I am thankful for all his support in my research.

I am grateful for my parents, who always believed in me and supported my decisions. I would not have come to Canada and pursued my research interest without your love and encouragement. Thank you for being with me and providing advices when I face challenges.

I would like to thank Deep Logic Solutions Inc., particularly Nick Martyn, Alec Hay, Charles Chamberlain, Jeff Farnworth, and Rory Kilburn, for providing topography data, holding a 3-day workshop on RiskLogik platform at Western University, providing initial RiskLogik setup for the study region, as well as answering my questions regarding the platform and data. This project was funded by an NSERC CRD grant. Also, thanks to Hahn Chul Jung from NASA for his suggestions on processing the Sentinel-1 imagery. My thesis project would not have been completed without the help and support from those people.

I would also like to thank my examination committee members, Dr. Slobodan Simonovic, Dr. Hassan Peerhossaini, and Dr. Katsu Goda, for taking time to review this dissertation and giving valuable suggestions.

Last but not least, I am grateful for my friends, who have made my life full of laughter, and for my research team members, who gave helpful comments on my research.

Table of Contents

Abstract ii

Lay Summary iii

Acknowledgments iv

Table of Contents v

List of Tables viii

List of Figures xi

Chapter 1 1

1 Thesis Overview 1

1.1 Background 1

1.2 Research Objectives 2

1.3 Research Questions 2

1.4 Summary of Chapters 3

1.5 References 4

Chapter 2 5

2 Background Literature 5

2.1 Compound Flooding 5

2.2 Two-dimensional Hydrodynamic Modelling 7

2.3 Flood Risk Assessment of Critical Infrastructure 10

2.4 References 14

Chapter 3 22

3. Analysis of Compound Flooding in Saint Lucia 22

3.1. Introduction 22

3.2. Study Area 27

3.3. Data and Methods 30
3.3.1. Input Data for the Hydrodynamic Model 31
3.3.2. Hydrologic Modelling 41
3.3.3. Observational Data 52
3.3.4. Hydrodynamic Modelling 58
3.4. Results and Discussions 72
3.4.1. Model Performance and Validation 72
3.4.2. Sensitivity Analysis 76
3.4.3. Scenario Analysis 87
3.4.4. Probabilistic Flood Hazard Analysis 96
3.5. Conclusions 100
3.6. References 102
Chapter 4 112
4 Flood Risk Analysis in Saint Lucia 112
4.1 Introduction 112
4.2 Methodology 115
4.2.1 Terminology 115
4.2.2 Scoring Systems 117
4.2.3 Analytical Tools 120
4.3 Model Setup 123
4.4 Results and Discussions 165
4.4.1 Risk Assessment under Normal Condition 165
4.4.2 Risk Assessment under Flood Scenarios 169
4.5 Conclusions 181
4.6 References 183

Chapter 5 185

5 Concluding Remarks and Future Work 185

References 188

Curriculum Vitae 189

List of Tables

Table 1. Manning's roughness coefficients for different land cover types. 32

Table 2. Characteristics of rainfall data derived from different sources during the event of Tropical Storm Matthew..... 34

Table 3. The mean sea level and observed peak water levels in the event of Tropical Storm Matthew for each tide gauge, extreme sea levels in Monioudi et al. (2018), and the rescaling factors calculated for each tide gauge. 39

Table 4. Surges and wave run-up heights in different return periods for Vieux Fort, Saint Lucia. 41

Table 5. Descriptions and the feasible ranges of HYMOD parameters. 42

Table 6. Monthly mean rainfall calculated from observed records at the rainfall gauge operated by WRMA in Saint Lucia, monthly mean rainfall calculated from the raw TMPA-3B42 V7 rainfall data, and the derived monthly bias factors..... 44

Table 7. Performance of the bias correction conducted to TMPA-3B42 V7 product. 45

Table 8. Runoff estimations obtained from the calibrated HYMOD model and the associated uncertainty bounds. 50

Table 9. Runoff estimations of the calibrated HYMOD model when using rainfall inputs derived from different sources. 51

Table 10. Information of the Pléiades-1 imageries..... 53

Table 11. Information of all utilized Sentinel-1A images in the study. 54

Table 12. Characteristics of input data for the LISFLOOD-FP model in model validation and sensitivity analysis. 64

Table 13. Characteristics of input data for the LISFLOOD-FP model in the scenario analysis of including wave run-up. 68

Table 14. Descriptions of boundary conditions used for the LISFLOOD-FP model in the probabilistic flood hazard analysis..... 72

Table 15. Characteristics of rainfall derived from different sources and corresponding flood inundation estimations. 83

Table 16. Flood area estimations when considering the uncertainties in coastal water levels. 84

Table 17. Flood area estimations when considering the uncertainties in river flow estimations associated with the selection of model parameters. 85

Table 18. Flood area estimations when considering the uncertainties in upstream river inflows associated with the sources of rainfall data used in the HYMOD model. 86

Table 19. Flood area estimations in scenarios of excluding wave run-up and including wave run-up in the coastal boundary conditions. 88

Table 20. Flood area estimations in scenarios of excluding wave run-up and including wave run-up in the coastal boundary conditions. 91

Table 21. Flood area estimations in scenarios of excluding wave run-up and including wave run-up in the coastal boundary conditions..... 94

Table 22. Defined terminology in Strongest Path Method. 116

Table 23. Operational status of an entity. 118

Table 24. Criteria used for assigning the Likelihood of Failure of an entity. 119

Table 25. Criteria used for assigning the Degree of Impact of an entity. 119

Table 26. Criteria used for assigning the Degree of Dependence to a direct connection between two entities. 120

Table 27. The hierarchical system of considered entities. 124

Table 28. Pre-defined parameters values in the model setup..... 134

Table 29. Scenario number and failed entities in each scenario. 181

List of Figures

Figure 1. The topography map and the geographic location of Saint Lucia (Sources: Esri, DigitalGlobe, GeoEye, i-cubed, USDA FSA, USGS, AEX, Getmapping, Aerogrid, IGN, IGP, swisstopo, and the GIS User Community; National Geographic, Esri, DeLorme, HERE, UNEP-WCMC, USGS, NASA, ESA, METI, NRCAN, GEBCO, NOAA, iPC; Esri, GEBCO, NOAA, National Geographic, DeLorme, HERE, Geonames.org, and other contributors; Saint Lucia Digital Elevation Model that is downloaded from http://www.charim-geonode.net/layers/geonode:dem). 25

Figure 2. The drainage basin and study area (Sources: Saint Lucia Digital Elevation Model downloaded from http://www.charim-geonode.net/layers/geonode:dem; Saint Lucia river networks downloaded from http://www.charim-geonode.net/layers/geonode:rivers; Map data © OpenStreetMap contributors, Map layer by Esri). 29

Figure 3. Map showing the topographic characteristics of the study area (Sources: Map data © OpenStreetMap contributors, Map layer by Esri; Saint Lucia Topographic Map downloaded from http://www.charim-geonode.net/maps/217; Digital Surface Model provided by Deep Logic Solutions Inc.). 29

Figure 4. Land cover map of the study area (Sources: Saint Lucia 2014 Land Cover Map downloaded from http://www.charim-geonode.net/layers/geonode:landcover_2014_improved1). 30

Figure 5. Time series of hourly or half-hourly rainfall intensities derived from different sources during the simulated period (from 00:00 am AST on September 28, 2016 to 00:00 am AST on September 30, 2016)). 35

Figure 6. Locations of utilized tide gauges in surrounding islands (Sources: Esri, DigitalGlobe, GeoEye, i-cubed, USDA FSA, USGS, AEX, Getmapping, Aerogrid, IGN, IGP, swisstopo, and the GIS User Community). 36

Figure 7. Observed and derived time series of coastal water levels. Solid colored lines (a) are the observed time series of tide gauges, and the dotted grey lines (a) are the scaled water levels based on the rescaling factors. Observed and rescaled time series are all used to calculate the mean and the standard deviation (σ) of water levels for each hour. Derived time series based on the mean and σ, represented as colored lines in (b), are used as boundary conditions for LISFLOOD-FP. 38

Figure 8. Time series of coastal water levels used in the scenario analysis when excluding and including the heights of wave run-up..... 41

Figure 9. Simulated streamflow and observed streamflow at the watershed outlet (a) from 1998 to 2018, and (b) from 2010 to 2016. Red dots correspond to the observed streamflow records, and the black line indicates the daily runoff estimates from the HYMOD model (i.e. the mean out of all simulations that utilize the 1000 derived parameter sets). The light grey shaded area denotes the 95% hydrograph prediction uncertainty associated with selection of parameter sets derived using the SCE-UA algorithm. Green dots are estimated runoff for the event. 49

Figure 10. The Pléiades-1 pre-event (left) and post-event (right) imageries (Copyright PLEIADES © CNES 2016, Distribution Airbus DS)..... 52

Figure 11. Workflow used to derive flood extent from the SAR imagery. 55

Figure 12. The flood map that is generated based on the combination of flood area derived from the Pléiades-1 and Sentinel-1 imagery..... 57

Figure 13. Example channel shapes. 59

Figure 14. Map showing the maximum flood depth for each pixel over the course of the simulation R0 in the event of Tropical Storm Matthew. 73

Figure 15. Map showing the maximum flood depth for each pixel over the course of th simulation R0 in the event of Tropical Storm Matthew within boundaries of Hewanorra International Airport. 74

Figure 16. Comparison of the maximum flood extent from the model and flood extents derived from the satellite imageries. 76

Figure 17. Map showing the maximum flood depth for each pixel over the course of the simulation R1 in the event of Tropical Storm Matthew. 77

Figure 18. Map showing the maximum flood depth for each pixel over the course of the simulation R2 (left) and simulation R3 (right) in the event of Tropical Storm Matthew. 78

Figure 19. Map showing the maximum flood depth for each pixel over the course of the simulation R4 (left) and simulation R5 (right) in the event of Tropical Storm Matthew. 79

Figure 20. Maps showing the maximum flood depth for each pixel over the course of simulations when the rainfall input is derived from (a) rainfall gauge (WRMA), (b) rainfall gauge (DS3505), (c) ERA5, (d) MERRA-2, (e) TMPA-3B42 V7, and (f) IMERGHH V05. 81

Figure 21. Graphs showing the flood inundation area over the course of simulations when the rainfall input is from (a) rainfall gauge (WRMA), (b) rainfall gauge (DS3505), (c) ERA5, (d) MERRA-2, (e) TMPA-3B42 V7, and (f) IMERGHH V05. 82

Figure 22. Map showing the maximum flood depth for each pixel over the course of simulations in scenarios of including wave run-up in the coastal boundary conditions. 89

Figure 23. Maps showing the maximum flood depth for each pixel within the Hewanorra International Airport boundary over the course of simulations when the heights of wave run-up are (a) 2.5m, (b) 3.5m, (c) 4.5m, (d) 5.5m, and (e) 6m..... 90

Figure 24. Maps showing the maximum flood depth for each pixel within the Hewanorra International Airport boundary over the course of simulations when the heights of wave run-up are (a) 0m, (b) 0.5m, (c) 1.5m, (d) 2.5m, (e) 3.5m, (f) 4.5m, (g) 5.5m, and (h) 6m. 93

Figure 25. Maps showing the maximum flood depth for each pixel over the course of simulations when the heights of wave run-up are (a) 0m, (b) 0.5m, (c) 1.5m, (d) 2.5m, (e) 3.5m, (f) 4.5m, (g) 5.5m, and (h) 6m. 96

Figure 26. Maximum flood inundation area over the course of simulations in the probabilistic flood hazard analysis. 97

Figure 27. Map showing the ranges of maximum flood depth estimations for each pixel. 98

Figure 28. Map showing the probability of flooding calculated from all simulations for each pixel in the study area. 99

Figure 29. Map showing the probability of flooding calculated from all simulations for each pixel within the Hewanorra International Airport. 99

Figure 30. The directed graph set up in the RiskLogik software. 133

Figure 31. Risk indices of each entity in the non-flood condition: (a) global vulnerability and global impact; (b) risk index. 166

Figure 32. Risk indices of entities that are at high/very high/extreme risk in the non-flood condition: (a) global vulnerability and global impact; (b) risk index. 167

Figure 33. Results of the Monte Carlo analysis in the non-flood condition. 169

Figure 34. Map showing the flood conditions when flood extents reach the maximum value over the course of the simulation R0 in the event of Tropical Storm Matthew within the boundary of Hewanorra International Airport. 170

Figure 35. Risk indices of each entity in flood conditions when not considering the effects of wave run-up: (a) global vulnerability and global impact; (b) risk index. 171

Figure 36. Risk indices of entities that are at high/very high/extreme risk in flood conditions when not considering effects of wave run-up: (a) global vulnerability and global impact; (b) risk index. 172

Figure 37. Results of the Monte Carlo analysis in flood conditions when not considering the effects of wave run-up. 173

Figure 38. Maps showing the maximum flood depth of each pixel within the airport boundary when wave run-up heights are: (a) 1.5m, (b) 2.5m, (c) 3.5m, (d) 4.5m, (e) 5.5m, and (f) 6m. .. 175

Figure 39. Risk indices of each entity in the first scenario of flooding when considering the effects of wave run-up: (a) global vulnerability and global impact; (b) risk index. 176

Figure 40. Risk indices of entities that are at high/very high/extreme risk in the first scenario of flooding when considering the effects of wave run-up: (a) global vulnerability and global impact; (b) risk index. 177

Figure 41. Results of the Monte Carlo analysis in the first scenario of flooding when considering the effects of wave run-up..... 178

Figure 42. Results of the Monte Carlo analysis in the second scenario of flooding when considering the effects of wave run-up..... 178

Figure 43. Risk indices of each entity in the second scenario of flooding when considering the effects of wave run-up: (a) global vulnerability and global impact; (b) risk index. 179

Figure 44. Risk indices of entities that are at high/very high/extreme risk in the second scenario of flooding when considering the effects of wave run-up: (a) global vulnerability and global impact; (b) risk index. 180

Figure 45. Risk index of entities that are at extreme/very high/high risk in each scenario. 182

Chapter 1

1 Thesis Overview

1.1 Background

Saint Lucia, a volcanic island in eastern Caribbean Sea, is located in the tropical cyclone belts and therefore highly exposed to multiple natural disasters such as storm surges, rogue waves, as well as heavy rainfall associated with tropical storms (ICF GHK, 2012). Compound flooding is expected in those weather-related extreme events when there are simultaneous occurrences of high river flows, high sea levels, and extreme rainfall. Resultant damage can be disastrous due to the mountainous topography cut by fast-flowing water drainage networks, as well as the high concentration of human settlements and significant infrastructure at the confined coastal lowlands in Saint Lucia (Global Facility for Disaster Reduction and Recovery, 2019; ICF GHK, 2012; United Nations Conference on Trade and Development, 2017).

Historical events have revealed the high vulnerability of critical infrastructure in Saint Lucia to flooding and landslides. For example, damages in the infrastructure sector account for 43% of the total impact caused by Hurricane Tomas in 2010 and 78.75% of the total impact resulted from a tropical trough system in 2013. Infrastructure along with other vulnerable sectors, such as agriculture and tourism, are key economic sectors in Saint Lucia. Major assets in those sectors do not function individually but are interdependent to ensure their normal activities and operations. For example, when Hewanorra International Airport was closed in several extreme events, arrivals and departures of visitors were greatly disrupted, accordingly affecting the tourism industry.

Although the failures of assets and the propagation of failures through the infrastructure networks have caused huge economic losses in Saint Lucia, there are no existing high-resolution hydrodynamic models set up to simulate compound flooding, and no network analysis models set up to conduct flood risk assessment for critical infrastructure.

1.2 Research Objectives

The overall objective of this study is to combine a hydrodynamic model with a risk assessment platform to evaluate compound flood risks to critical infrastructure. The first objective is to set up and calibrate a hydrologic and a hydrodynamic model using available (sparse) ground-based data, reanalysis products, and satellite imagery. The second objective is to characterize the individual and combined contributions of storm tides, wave run-up, heavy rainfall, and river overflows to flooding. The third objective is to identify direct connections between major assets in key economic sectors and to set up a network analysis model for evaluating the effects of indirect connections as well as prioritizing risks of assets in the system. The study area, bounded by the coastline, is at the southern coast of Saint Lucia. Major assets pertaining to key economic sectors, including Hewanorra International Airport (HIA), Vieux Fort Seaport, the town of Vieux Fort and La Tourney, coastal agricultural lands, as well as the main north-south highway, are located at low-lying areas and vulnerable to compound floods caused by heavy rainfall, high sea levels, and river overflows in the La Tourney river. We study flood risks to HIA as a critical infrastructure.

1.3 Research Questions

Following are the research questions addressed in the study.

(1) How to address problems associated with data availability for the hydrologic and hydraulic model setup?

(2) How important is it to consider the combined effects of multiple flood factors?

(3) How to characterize compound flood events and the contribution of individual flood factors?

(4) How to account for uncertainties in hydrologic and hydraulic modelling?

(5) How to combine a hydrodynamic model with a risk assessment platform to analyze flood risks to critical infrastructure?

(6) What are compound flood risks over Saint Lucia particularly Hewanorra International Airport?

(7) How to determine the relative importance of interdependent assets in different sectors and prioritize risks under the conditions of non-flooding and flooding?

1.4 Summary of Chapters

This thesis consists of three main chapters. Chapter 2 is the background literature that provides an overview of previous works in the analysis of compound flooding and in the flood risk assessment for interdependent infrastructures. In the perspective of compound flooding, this chapter covers its definition, interactions between its different contributing factors, as well as current frameworks, progress, and limitations in its analysis. In the perspective of risk analysis, this chapters provides the definition of risk, the definition of interdependent infrastructure and the impacts of its interdependency by giving a real-world example, as well as current frameworks for the flood risk analysis of critical infrastructure.

Chapter 3 introduces the study area and explains the reasons why it is at high risk of compound flooding particularly in the changing climate. Historical extreme events have revealed the high vulnerability of major assets in the study area to flooding and landslides. Detailed information is subsequently given on the analysis of compound flooding in this study, including data collection, preparations of boundary conditions, the hydrologic and hydrodynamic model setup, model validation, sensitivity analysis to explore the effects of uncertain boundary conditions, scenario analysis to account for the effects of wave run-up, as well as the probabilistic flood hazard analysis to derive a probabilistic flood hazard map. Simulation results of flood extents and flood depths are analyzed in this chapter and used in Chapter 4 for risk assessment.

Chapter 4 provides a review of several historical extreme events and their significant impacts on critical infrastructure. Interdependency of infrastructure will be defined. The framework used for the risk assessment in this study is clarified. Based on the Strong Path Method theory, the RiskLogik software was utilized to set up a network analysis model in order to explore the effects of direct and indirect connections among interdependent entities. The relative importance of entities was determined for scenarios of non-flooding and flooding, providing valuable insights on prioritization of risk and on the design of flood risk mitigation strategies.

1.5 References

Global Facility for Disaster Reduction and Recovery. (2019). Saint Lucia. Retrieved from https://www.gfdrr.org/en/saint-lucia

ICF GHK. (2012). *Climate Change Adaptation Planning in Latin American and Caribbean Cities Complete Report: Castries, Saint Lucia* Retrieved from http://www.worldbank.org/content/dam/Worldbank/document/LAC/Climate%20Change%20Adaptation%20Planning%20for%20Castries_FINAL.pdf

United Nations Conference on Trade and Development. (2017). *Climate change impacts on coastal transportation infrastructure in the Caribbean: enhancing the adaptive capacity of Small Island Developing States (SIDS), SAINT LUCIA: a case study UNDA Project 1415O.*

Chapter 2

2 Background Literature

2.1 Compound Flooding

Coastal regions are at risk of flooding caused by a combination of multiple factors including heavy precipitation, high river discharge rates and river overflows, as well as storm surges and waves generated by strong winds (Doocy et al. 2013; Kew et al. 2013; Wahl et al. 2015). This risk, which is significant particularly in low-lying densely-populated coastal environments, is projected to increase due to climate change, urbanization, population growth and expanded development (Brown et al. 2013; Condon and Sheng 2012; Creel 2003; Frazier et al. 2010; Intergovernmental Panel on Climate Change 2014; Kundzewicz et al. 2014).

Compound flooding can be defined as flooding caused by "the combined effects of marine and hydrologic processes" (Gallien et al. 2018). This definition indicates that the analysis of compound floods should consider both oceanic effects, such as waves and storm tides (the combination of astronomical tide and storm surge), and hydrologic signals, such as river flows and precipitation. Co-occurrence of these phenomena is more likely to be found in small and steep coastal catchments, such as mountainous regions near the coast, because they have a quick response to heavy rainfall that can lead to high direct runoff and/or increased riverine flows in conjunction with high sea levels caused by storm tides and waves driven by the same weather system (Klerk et al. 2015; Maskell et al. 2014; van den Hurk et al. 2015; Zheng, Westra, and Sisson 2013; Zheng et al. 2014). In this condition, peak coastal water levels and peak river discharges are highly likely to occur simultaneously and the interactions between them in the river channel can result in higher flood depths and/or larger flood extents along the river and at the coastline compared to their isolate occurrence (Svensson and Jones 2004). At the same time, heavy rainfall can lead to inland flooding and direct runoff in areas that may be saturated by high sea levels (Gallien et al. 2018). Concurrent flood hazards and the interactions among multiple contributing factors can lead to severe impacts.

Understanding of individual flood hazards and associated risks has progressed significantly, however quantitative assessments of the joint occurrences of compound flood hazards are limited.

The resultant risk is often significantly underestimated with severe consequences (Bevacqua et al. 2017; Chen et al. 2010; Kumbier et al. 2018). Until present, only a few studies have characterized compound flood hazards using process-based approaches (Tang et al. 2013; Joyce et al. 2018; Kumbier et al. 2018), statistical methods (Bevacqua et al. 2017; Klerk et al. 2015; Paprotny et al. 2018; van den Hurk et al. 2015; Wahl et al. 2015; Ward et al. 2018), and frameworks that combine them together (Lian, Xu, and Ma 2013; Thompson and Frazier 2014). Thompson & Frazier (2014) studied joint impacts of storm surges, inland precipitation and sea-level rise (SLR) over Sarasota County, Florida. Flood events of historical extreme events were depicted based on deterministic flood extents and high-risk regions for current and future hazards were determined based on probabilistic inundation extents, but this study did not consider the interactions between river flows and storm surges along waterways. Kumbier et al. (2018) developed a hydrodynamic numerical module in an estuarine environment and investigated compound flooding caused by storm tides and high river runoff, by quantifying the horizontal (flood extent) and vertical (water depth) differences in flood hazard estimates when including and excluding upstream riverine discharges during simulations. Joyce et al. (2018) utilized a coupled hydrodynamic circulation and wave-driven model to generate time series of total water levels (i.e. storm surges, astronomical tides and waves) from meteorological forcings with various hurricane characteristics, sea level rise, and rainfall. The time series are inputs of a hydrodynamic stormwater and hydrologic model to simulate flooding caused by sea levels while considering hydrological factors and interactions between them such as rainfall runoff and groundwater table fluctuations. Nevertheless, these analyses did not account for the direct impacts of extreme rainfall on flooding patterns.

Hydrodynamic models used in the flood analysis can be categorized into one-dimensional (1D), two-dimensional (2D), and three-dimensional (3D) models. It is the simplest approach to treat floodplain flows as part of the one-dimensional channel flows running parallel to the river channel, but its major drawbacks include the representation of floodplain topography as a series of cross-sections rather than as a surface, one cross-section averaged velocity to represent large variations in velocity across the floodplain, and the subjectivity of locations of cross sections (Teng et al. 2017; N.M. Hunter et al. 2007). Those problems are solved in two-dimensional models, where floodplain flows are represented as two-dimensional by assuming water depth is shallow and is insignificant compared to the other two dimensions (Teng et al. 2017). The applications of two-dimensional models to rural and urban floodplains have shown their abilities in providing

sufficient levels of physical and topographic representations (N. Hunter et al. 2008; N.M. Hunter et al. 2007). Unless when the modelling of vertical features is important, such as in cases of dam breaks and levee breaches, complex three-dimensional representations are unnecessary and the two-dimensional shallow water approximation is adequate for many scales of floodplain flows (N.M. Hunter et al. 2007; Teng et al. 2017). Coupled 1D/2D schemes were also developed, where river channels modelled as one-dimensional are coupled to floodplain flows in the 2D domain, in order to make use of the efficiency of 1D models and the accurately simulated flow dynamics in 2D models (Werner, Blazkova, and Petr 2005; Patro et al. 2009).

2.2 Two-dimensional Hydrodynamic Modelling

Two-dimensional hydrodynamic modelling is widely used in flood analysis (Fernández et al. 2016; Gallien et al. 2018; Joyce et al. 2018; Kumbier et al. 2018; Olbert et al. 2017; Saleh et al. 2017; Tang et al. 2013). Models that solve full 2D shallow water equations have proven to be able to accurately simulate flood inundation characteristics such as timing and duration (Teng et al. 2017). However, those models are computationally expensive, which is particularly unaffordable in urban flood estimations when the required model resolution is 50m or less and/or for probabilistic analyses which require a large number of simulations (Bates et al. 2005; Teng et al. 2017). Furthermore, computationally-expensive models are less likely to take advantage of the recent development in the remote sensing of topography such as high-resolution Light Detection and Ranging (LiDAR) digital elevation models due to the large computation time. In fact, improvements of other factors such as increasing the model resolution may help generate more accurate results than that of increasing physical complexity of the model itself (Lewis et al. 2013). Therefore, simplified two-dimensional hydraulic models that are computationally efficient while still capable of capturing dominant processes in flood events were developed, such as LISFLOOD-FP, Cama-Flood and JFLOW (Teng et al. 2017; N.M. Hunter et al. 2007; Horritt and Bates 2002).

Bates, Horritt, and Fewtrell (2010) developed a simplified two-dimensional model LISFLOOD-FP, which discretizes the domain into grid cells and solves two-dimensional shallow water equations without the advection term using an explicit finite difference scheme on a staggered grid. This inertial model provides water depths and discharge rates at each time step by preserving mass

balance in each cell (continuity equation, Eq. (2-1)) and handling the momentum between cells (momentum equation, Eq. (2-2)). These equations are briefly outlined here but are documented in detail in Bates, Horritt, and Fewtrell (2010) and de Almeida et al. (2012). To maintain model stability, an adaptive time-stepping method (Eq. (2-3)) is used to automatically select suitable time steps based on the Courant-Friedrichs-Lewy (CFL) condition.

$$h_{i,j}^{t+\Delta t} = h_{i,j}^{t} + \Delta t \frac{Q_{x\ i-1/2,j}^{t+\Delta t} - Q_{x\ i+1/2,j}^{t+\Delta t} + Q_{y\ i,j-1/2}^{t+\Delta t} - Q_{y\ i,j+1/2}^{t+\Delta t}}{A_{i,j}} \quad (2\text{-}1)$$

$$Q_{i+1/2}^{t+\Delta t} = \frac{Q_{i+1/2}^{t} - gA_{flow}^{t}\Delta t S_{i+1/2}^{t}}{1 + g\Delta t n^2 \left|Q_{i+1/2}^{t}\right| / \left[\left(R_{flow}^{t}\right)^{4/3} A_{flow}^{t}\right]} \quad (2\text{-}2)$$

$$\Delta t = \alpha \frac{\Delta x}{\sqrt{\max(h^t) g}} \quad (2\text{-}3)$$

where h is the water depth at the centre of each cell, Q is the flow between cells, A is the area of flows between cells, subscripts i and j are cell spatial indices in x and y directions, Δt is the time step, superscripts t and $t+\Delta t$ indicate the time t and $t+\Delta t$, R is the hydraulic radius, S is the water surface slope between cells, n is the Manning's roughness coefficient, g is the gravitational acceleration, α is the CFL coefficient ranging from 0.2 to 0.7 used to generate stable simulations for most flow situations, Δx is the cell width, and $max(h^t)$ is the maximum water depth.

Besides the extensive tests in benchmarking studies (N. Hunter et al. 2008; J. Neal et al. 2012), developments were also made for the purpose of extending the use of this inertial model. Although instabilities in low friction scenarios were reported in Bates, Horritt, and Fewtrell (2010), solutions were subsequently proposed in de Almeida et al. (2012). J. Neal, Schumann, and Bates (2012) presented a scheme to include a sub-grid channel routine in the original inertial model, which was further extended by J.C. Neal et al. (2015) through introducing a shape parameter to represent various cross-sectional shapes. The sub-grid version of LISFLOOD-FP was proven to be stable and allows for an accurate representation of river channels with any cross-sectional geometry and with any width that is below model resolution. Its successful applications in Lewis et al. (2013), Fernández et al. (2016), and García-Pintado et al. (2015) showed that the connectivity provided by sub-grid channels was essential to reproduce flow dynamics particularly in large scale simulations. The inclusion of river networks and the calibration of shape parameter led to a significant increase

in the predicting capability and accuracy in terms of water levels, wave propagation speeds, and inundation extents. Besides the introduction of sub-grid channels, considering the increasing need to directly use hydrodynamic models to simulate pluvial events particularly in complex urban areas, a constant velocity rainfall routing scheme was introduced by Sampson et al. (2013). This new scheme enables the model to route rainfall-derived water from elevated structures such as buildings without causing instabilities while reducing computation time.

The resulting inertial formulation, relatively simple yet robust, has found to be computationally efficient while yielding similar performance (in representing flood characteristics such as extents, depths and velocities) to diffusive models and full two-dimensional shallow water models especially in simulating subcritical flows that gradually vary in time and space (Bates, Horritt, and Fewtrell 2010; Fewtrell et al. 2011; Lewis et al. 2013; de Almeida and Bates 2013). Additionally, this scheme has the ability to deal with rapid wetting and drying conditions during the flood events (Bates, Horritt, and Fewtrell 2010). It provides an appropriate compromise between computational cost and physical realism, and was successfully applied in floods caused by single factor, such as river flows (Bermúdez et al. 2017; Fewtrell et al. 2011; García-Pintado et al. 2015; Wood et al. 2016), rainfall (Sampson et al. 2013), and coastal water levels (Lewis et al. 2011; Quinn et al. 2014; Seenath, Wilson, and Miller 2016), as well as compound floods caused by storm tides and river flows (Lewis et al. 2013; Maskell et al. 2014; Skinner et al. 2015). In compound flooding, it is critical to accurately simulate the interaction between river flows and coastal water levels. Maskell et al. (2014) investigated the combined influence of storm surges and river flows in an idealized estuary by using the FVCOM (a full shallow-water formulation) and LISFLOOD-FP models. Comparison of the results shows that LISFLOOD-FP has similar predicting performance (i.e. maximum flood extents) as that of FVCOM but with much-reduced computation resources. This indicates the great potential and advantage of using simplified models that capture dominant physics when the surge-river interaction caused by momentum exchange is insignificant to flood extents. In the study of Lewis et al. (2013), 3 arc-second resolution (approximately 90m) Shuttle Radar Topography Mission (SRTM) dataset was pre-processed and used as the terrain input for the LISFLOOD-FP model to simulate flooding caused by storm tides. Sub-grid channels were included to allow propagations of sea water in river channels along with backwater effects of river flows. The inundations model showed accuracy on the reproduction of flood conditions, and the overall performance (i.e. peak flood extents and

maximum water levels) was satisfactory, indicating the suitability of publicly available data as well as the ability of the sub-grid version of LISFLOOD-FP in simulating combined flooding.

Despite the successful applications of sub-grid LISFLOOD-FP in various flood analysis, its ability to simulate compound flood caused by multiple concurrent contributing factors (i.e. coastal water levels, river flows, and rainfall) has not been investigated thoroughly. In addition, the accuracy of such simplified two-dimensional hydrodynamic model strongly depends on the data quality, indicating the needs of high-resolution topographic data and correct forcing data for more accurate simulation results (J. Neal et al. 2012; Lewis et al. 2013). In data-poor regions where high-quality data is not available, it is necessary to process and improve the quality of coarse-resolution topographic data, while the uncertainties in boundary conditions and their propagations through the model to simulation results should be characterized.

2.3 Flood Risk Assessment of Critical Infrastructure

Flooding is one of the most frequent and disastrous natural hazards, which has caused significant destructions to human societies (Teng et al. 2017; Salman and Li 2018). Based on the driven factor, common flooding types include pluvial flooding that occurs when rainfall exceeds the capacity of urban drainage systems, fluvial flooding that results from river overflows, and coastal flooding caused by oceanic effects such as storm tides and waves (Hammond et al. 2015; Blanc et al. 2012). Economic losses from floods, including direct damages (e.g. property and infrastructure damages) and indirect impacts (e.g. disruptions of pubic essential services), have greatly risen over the previous decades, mainly because of the increasing exposure of human settlements and economic assets (Kundzewicz et al. 2014; Handmer et al. 2012; J. Yin, Yu, and Wilby 2016). Current flood risks are projected to be exacerbated in many regions around the world due to climate change because i) sea-level rise would amplify the impacts of coastal flooding, ii) changing local rainfall patterns could lead to more frequent riverine and inland floods, and iii) changes in the frequency and intensity of storm events would affect the characteristics and patterns of storm surges and waves (Jha et al. 2012). Small island states, where human settlements and significant infrastructure are predominate in coastal floodplains, are at particularly high risk of coastal- and weather-related flood disasters (Handmer et al. 2012). Therefore, flood risk management and cost-effective disaster

risk reduction strategies are of fundamental importance to avoid or reduce potential damages and losses while achieving basic development objectives (Mercer 2010; Handmer et al. 2012).

Effective flood risk management relies on a prior flood risk assessment, which provides sufficient insights into flood events, their consequences and possible mitigation measures that support the decision-making procedures (de Moel et al. 2015). Risk can be defined as "the combination of the probability of an event and its negative consequences" (UNISDR 2009). In the academic literature for flood risk assessment, flood risk generally refers to the product of hazard, exposure, and vulnerability (Kron 2005). To better understand and compute flood risk, the US Army Corps of Engineers (USACE) conceptually defines flood risk as a function of the flood hazard, performance, exposure, vulnerability, and consequence (USACE 2017). Flood hazard is represented by the flood characteristics such as flood extents, flow velocities, and water depths; performance depicts how the system reacts to the flood hazard; exposure describes the assets and population that are exposed to flood hazards, while vulnerability refers to their susceptibility to floods; and consequence is defined as the harm, such as economic damages and loss of life, resulting from flood hazards (USACE 2017). Extensive frameworks of flood risk assessments were set up for pluvial flooding (Szewrański et al. 2018; Z. Yin et al. 2016), coastal flooding (Christie et al. 2018; Neumann et al. 2015), and fluvial flooding (Bates et al. 2005; Feyen et al. 2012) at different scales. Urban flooding can include pluvial, coastal, and fluvial flooding. Due to the complexity and significance of urban environments, frameworks were proposed for performing flood risk analysis of urban floods (Jha et al. 2012; J. Yin et al. 2015). If different types of floods are correlated with each other in the study area and are likely to occur simultaneously (e.g. hurricanes not only induce storm surges that cause coastal floods but also heavy rainfalls that cause flash floods), flood risk assessment should consider the joint probability of different flood factors and the combined consequences of concurrent flooding (Lamb et al. 2010; Emanuelsson et al. 2014; Dawson 2015).

Infrastructures can be defined as "the basic facilities, services, and installations needed for the functioning of a community or society", and critical infrastructures are "systems and assets, whether physical or virtual, so vital to the United States that the incapacity or destruction of such systems and assets would have a debilitating effect on security, national economic security, national public health or safety, or any combination of those matters" (Bennett 2018). Critical infrastructures are the backbone of modern societies and economies, providing essential services

and covering sectors that include agriculture and food, banking and finance, drinking water and water treatment systems, energy, telecommunications, information technology, public health and healthcare, commercial facilities, emergency services, as well as transportation systems (Bennett 2018; Rinaldi, Peerenboom, and Kelly 2001). Their reliable and secure operations are of fundamental importance to national security and economic development. Infrastructures do not function in isolation from each other, but are interdependent and the state of one infrastructure may depend on the state of several other infrastructures. Rinaldi, Peerenboom, and Kelly (2001) identified four types of interdependencies, namely physical, cyber, geographic, and logical. Infrastructures can either directly or indirectly connect through one or more intervening infrastructures. These connections are described as *n*th-order interdependencies, where *n* is the number of direct and indirect linkages between the two infrastructures. The coupling of infrastructures can significantly increase the risk by triggering cascading effects. Disruptions or failures of one infrastructure can propagate through the network and subsequently cause disruptions or failures of other infrastructures thus creating first, second, and higher-order disruptions or failures and making the whole system more vulnerable in exceptional circumstances such as floods (Rinaldi, Peerenboom, and Kelly 2001). Propagation mechanisms of disruptions or failures among infrastructures are expected to aggravate the impacts of flooding, leading to more severe direct and indirect damages. For example, Hurricane Sandy hit New York City in 2012, and the associated extremely high sea levels caused extensive flooding at the coast. The flooding led to failures of several electric power systems, which subsequently led to destructions of other infrastructures, including the evacuation of the New York University Langone Medical Center and the transfer of 200 patients, destroyed and damaged houses in fire incidents due to the lack of electricity, shortage of fuel supply, business interruptions, and the breakdowns of heating networks, security systems, telecommunication services, as well as emergency power generators (Serre and Heinzlef 2018). Therefore, although risk analysis of infrastructures is challenging because of network complexity, data availability, and high degrees of interdependencies among different infrastructures, it is indispensable in order to understand how disruptions or failures propagate through the network and prevent catastrophic infrastructure breakdowns (Rinaldi, Peerenboom, and Kelly 2001).

Recent studies have highlighted that relationships between infrastructures are essential for accurate representations of infrastructure characteristics, operations, and maintenance (Alcaraz and

Zeadally 2015; Laugé, Hernantes, and Sarriegi 2015). There are several frameworks to simulate interdependencies of infrastructures, including network-based approaches, agent-based modelling, input-output models, and statistical techniques (Wang, Hong, and Chen 2012). Each framework has its advantages and limitations, and therefore, selections of the appropriate method should be based on the objectives and evaluated scopes of the study (Johansson and Hassel 2010). The major task of flood risk analysis on infrastructures is to investigate how flood damages propagate through the network of interdependent infrastructures (Hammond et al. 2015; Pant et al. 2018). Several studies successfully integrate interdependencies of infrastructures into the flood risk assessment framework by using network-based methods. The network theory is a classical and widely applied method, where a set of nodes with connecting links build up systems as networks (Ottino 2003). Emanuelsson et al. (2014) proposed a screening approach on the basis of network theory for flood risk assessment of water utility infrastructure. This framework is the combination of probability assessment, which considers the exceedance probability of a flood event and the vulnerability of each asset at the event, and consequence assessment, which accounts for not only the direct consequences of flooding of each asset but also consequences arising from interdependencies among assets. Risk scores assigned to each asset by multiplying the probability and the consequence can be utilized to rank assets, identify the potential critical assets, prioritize assets in terms of investments to reduce flood risks, and also provide information for more detailed and informative risk analysis. O'Neill (2014) proposed Strongest Path Method (SPM) for performing risk analysis on interdependent infrastructure components, which consists of standalone risk assessment for each node, identification of direct connections between each pair of nodes, and simulation of effects of indirect connections among nodes. Strongest paths, which refer to the paths between two infrastructures that constitute the most significant influence with the least intervening nodes, can be identified. Besides, multiple analytical tools can be used to analyze the relative importance of infrastructures in the system, which helps the prioritization of risks and development of effective mitigation strategies. Tsavdaroglou et al. (2018) have developed a network-based methodology to conduct the risk analysis of interdependent infrastructures under the conditions of weather-induced hazards, including coastal, fluvial, and pluvial flooding, for the current and future climate conditions. The risk estimations on infrastructure level are based on a semi-quantitative approach, using the Likert scale to estimate impacts of the event on each infrastructure and percentages to represent probabilities of event occurrences. Dependencies between infrastructures

are quantified as the product of impact on the Likert scale and likelihood as a percentage showing the degree of impact that a failure of one infrastructure can propagate to the other infrastructure. Total cascading impacts on each infrastructure are assumed to be equivalent to the highest impact among all its dependencies. This study showed that the severity of cascading effects is not only related to the relationships among assets but also strongly dependent on the recovery time of different infrastructures in different scenarios.

2.4 References

Alcaraz, Cristina, and Sherali Zeadally. 2015. "Critical infrastructure protection: Requirements and challenges for the 21st century." *International Journal of Critical Infrastructure Protection* 8: 53-66. https://doi.org/10.1016/j.ijcip.2014.12.002.

Bates, Paul D, Richard J Dawson, Jim W Hall, Matthew S Horritt, Robert J Nicholls, Jon Wicks, and Mohamed Ahmed Ali Mohamed Hassan. 2005. "Simplified two-dimensional numerical modelling of coastal flooding and example applications." *Coastal Engineering* 52 (9): 793-810.

Bates, Paul D, Matthew S Horritt, and Timothy J Fewtrell. 2010. "A simple inertial formulation of the shallow water equations for efficient two-dimensional flood inundation modelling." *Journal of Hydrology* 387 (1-2): 33-45.

Bennett, Brian T. 2018. Understanding, assessing, and responding to terrorism: Protecting critical infrastructure and personnel. John Wiley & Sons.

Bermúdez, María, Jeffrey C Neal, Paul D Bates, Gemma Coxon, Jim E Freer, Luis Cea, and Jeronimo Puertas. 2017. "Quantifying local rainfall dynamics and uncertain boundary conditions into a nested regional‐local flood modeling system." *Water Resources Research* 53 (4): 2770-2785.

Bevacqua, Emanuele, Douglas Maraun, Ingrid Hobæk Haff, Martin Widmann, and Mathieu Vrac. 2017. "Multivariate statistical modelling of compound events via pair-copula constructions: analysis of floods in Ravenna (Italy)." *Hydrology and Earth System Sciences* 21 (6): 2701-2723.

Blanc, Janice, JW Hall, Nicolas Roche, RJ Dawson, Y Cesses, A Burton, and CG Kilsby. 2012. "Enhanced efficiency of pluvial flood risk estimation in urban areas using spatial–temporal rainfall simulations." *Journal of Flood Risk Management* 5 (2): 143-152.

Brown, Sally, Robert J Nicholls, Colin D Woodroffe, Susan Hanson, Jochen Hinkel, Abiy S Kebede, Barbara Neumann, and Athanasios T Vafeidis. 2013. "Sea-level rise impacts and responses: a global perspective." In *Coastal hazards*, 117-149. Springer.

Chen, Albert S, S Djordjević, Jorge Leandro, and DA Savić. 2010. "An analysis of the combined consequences of pluvial and fluvial flooding." *Water Science and Technology* 62 (7): 1491-1498.

Christie, E. K., T. Spencer, D. Owen, A. L. McIvor, I. Möller, and C. Viavattene. 2018. "Regional coastal flood risk assessment for a tidally dominant, natural coastal setting: North Norfolk, southern North Sea." *Coastal Engineering* 134: 177-190. https://doi.org/10.1016/j.coastaleng.2017.05.003.

Condon, Andrew J, and Y Peter Sheng. 2012. "Evaluation of coastal inundation hazard for present and future climates." *Natural hazards* 62 (2): 345-373.

Creel, Liz. 2003. *Ripple effects: population and coastal regions*. Population Reference Bureau Washington, DC.

Dawson, Richard J. 2015. "Handling interdependencies in climate change risk assessment." *Climate* 3 (4): 1079-1096. https://doi.org/10.3390/cli3041079.

de Almeida, Gustavo AM, and Paul Bates. 2013. "Applicability of the local inertial approximation of the shallow water equations to flood modeling." *Water Resources Research* 49 (8): 4833-4844.

de Almeida, Gustavo AM, Paul Bates, Jim E Freer, and Maxime Souvignet. 2012. "Improving the stability of a simple formulation of the shallow water equations for 2 - D flood modeling." *Water Resources Research* 48 (5).

de Moel, H., B. Jongman, H. Kreibich, B. Merz, E. Penning-Rowsell, and P. J. Ward. 2015. "Flood risk assessments at different spatial scales." *Mitigation and Adaptation Strategies for Global Change* 20 (6): 865-890. https://doi.org/10.1007/s11027-015-9654-z.

Doocy, Shannon, Amy Daniels, Sarah Murray, and Thomas D Kirsch. 2013. "The human impact of floods: a historical review of events 1980-2009 and systematic literature review." *PLoS currents* 5.

Emanuelsson, MAE, N Mcintyre, CF Hunt, R Mawle, J Kitson, and N Voulvoulis. 2014. "Flood risk assessment for infrastructure networks." *Journal of Flood Risk Management* 7 (1): 31-41.

Fernández, Alfonso, Mohammad Reza Najafi, Michael Durand, Bryan G Mark, Mark Moritz, Hahn Chul Jung, Jeffrey Neal, Apoorva Shastry, Sarah Laborde, and Sui Chian Phang. 2016. "Testing the skill of numerical hydraulic modeling to simulate spatiotemporal flooding patterns in the Logone floodplain, Cameroon." *Journal of Hydrology* 539: 265-280.

Fewtrell, TJ, A Duncan, CC Sampson, JC Neal, and PD Bates. 2011. "Benchmarking urban flood models of varying complexity and scale using high resolution terrestrial LiDAR data." *Physics and Chemistry of the Earth* 36 (7-8): 281-291. https://doi.org/10.1016/j.pce.2010.12.011.

Feyen, Luc, Rutger Dankers, Katalin Bódis, Peter Salamon, and José I. Barredo. 2012. "Fluvial flood risk in Europe in present and future climates." *Climatic Change* 112 (1): 47-62. https://doi.org/10.1007/s10584-011-0339-7.

Frazier, Tim G., Nathan Wood, Brent Yarnal, and Denise H. Bauer. 2010. "Influence of potential sea level rise on societal vulnerability to hurricane storm-surge hazards, Sarasota County, Florida." *Applied Geography* 30 (4): 490-505. https://doi.org/https://doi.org/10.1016/j.apgeog.2010.05.005.

Gallien, Timu W., Nikos Kalligeris, Marie-Pierre C. Delisle, Bo-Xiang Tang, Joseph T. D. Lucey, and Maria A. Winters. 2018. "Coastal flood modeling challenges in defended urban backshores." *Geosciences (Switzerland)* 8 (12): 450. https://doi.org/10.3390/geosciences8120450.

García-Pintado, Javier, David C. Mason, Sarah L. Dance, Hannah L. Cloke, Jeff C. Neal, Jim Freer, and Paul D. Bates. 2015. "Satellite-supported flood forecasting in river networks: A real case study." *Journal of Hydrology* 523: 706-724. https://doi.org/10.1016/j.jhydrol.2015.01.084.

Hammond, M. J., A. S. Chen, S. Djordjević, D. Butler, and O. Mark. 2015. "Urban flood impact assessment: A state-of-the-art review." *Urban Water Journal* 12 (1): 14-29. https://doi.org/10.1080/1573062X.2013.857421.

Handmer, John, Yasushi Honda, Zbigniew W. Kundzewicz, Gerardo Benito, Ismail Fadl Mohamed, Shaohong Wu, Kiyoshi Takahashi, and Zheng Yan. 2012. *Changes in impacts of climate extremes: human systems and ecosystems. In: Managing the Risks of Extreme Events and Disasters to Advance Climate Change Adaptation*. edited by C.B. Field, V ., T.F. Stocker Barros, D. Qin, D.J. Dokken, K.L. Ebi, M.D. Mastrandrea, K.J. Mach, G.-K. Plattner, S.K., M. Tignor Allen, and P.M. and Midgley. A Special Report of Working Groups I and II of the Intergovernmental Panel on Climate Change (IPCC). Cambridge University Press, Cambridge, UK, and New York, NY, USA. A Special Report of Working Groups I and II of the Intergovernmental Panel on Climate Change (IPCC).

Horritt, MS, and PD Bates. 2002. "Evaluation of 1D and 2D numerical models for predicting river flood inundation." *Journal of hydrology* 268 (1-4): 87-99.

Hunter, Neil M, Paul D Bates, Matthew S Horritt, and Matthew D Wilson. 2007. "Simple spatially-distributed models for predicting flood inundation: a review." *Geomorphology* 90 (3-4): 208-225.

Hunter, NM, PD Bates, S Neelz, G Pender, I Villanueva, NG Wright, D Liang, Roger Alexander Falconer, B Lin, and S Waller. 2008. "Benchmarking 2D hydraulic models for urban flood simulations." Proceedings of the institution of civil engineers: water management.

Intergovernmental Panel on Climate Change. 2014. *ClimateChange 2014: Impacts, Adaptation, and Vulnerability. Part B: Regional Aspects.Contribution of Working Group II to the Fifth Assessment Report of the Intergovernmental Panel on Climate Change*. edited by

D.J. Dokken C. B. F. Barros V.R., M.D. Mastrandrea, K.J. Mach, T.E., M. Bilir, K. L. E. Chatterjee, Y.O. Estrada, R.C. Genova, B. Girma, E.S. and A.N. Kissel, & S. M. Levy, P.R. Mastrandrea, & L.L. White. Cambridge University Press, Cambridge, United Kingdom and New York, NY, USA.

Jha, Abhas, Jessica Lamond, David Proverbs, Namrata Bhattacharya-Mis, Ana Lopez, Nikolaos Papachristodoulou, A. Bird, Robin Bloch, J. Davies, and R. Barker. 2012. *Cities and Flooding: A guide to integrated urban flood risk management for the 21st Century*.

Johansson, Jonas, and Henrik Hassel. 2010. "An approach for modelling interdependent infrastructures in the context of vulnerability analysis." Reliability Engineering & System Safety 95 (12): 1335-1344.

Joyce, Justin, Ni-Bin Chang, Rahim Harji, Thomas Ruppert, and Peter Singhofen. 2018. "Cascade impact of hurricane movement, storm tidal surge, sea level rise and precipitation variability on flood assessment in a coastal urban watershed." *Climate Dynamics* 51 (1): 383-409. https://doi.org/10.1007/s00382-017-3930-4.

Kew, S. F., F. M. Selten, G. Lenderink, and W. Hazeleger. 2013. "The simultaneous occurrence of surge and discharge extremes for the Rhine delta." *Natural Hazards and Earth System Sciences* 13 (8): 2017-2029. https://doi.org/10.5194/nhess-13-2017-2013.

Klerk, W. J., H. C. Winsemius, W. J. Van Verseveld, A. M. R. Bakker, and F. L. M. Diermanse. 2015. "The co-incidence of storm surges and extreme discharges within the Rhine-Meuse Delta." *Environmental Research Letters* 10 (3): 35005. https://doi.org/10.1088/1748-9326/10/3/035005.

Kron, Wolfgang. 2005. "Flood Risk = Hazard Values Vulnerability." *Water International* 30 (1): 58-68. https://doi.org/10.1080/02508060508691837.

Kumbier, Kristian, Rafael C. Carvalho, Athanasios T. Vafeidis, and Colin D. Woodroffe. 2018. "Investigating compound flooding in an estuary using hydrodynamic modelling: A case study from the Shoalhaven River, Australia." *Natural Hazards and Earth System Sciences* 18 (2): 463-477. https://doi.org/10.5194/nhess-18-463-2018.

Kundzewicz, Zbigniew W., Shinjiro Kanae, Sonia I. Seneviratne, John Handmer, Neville Nicholls, Pascal Peduzzi, Reinhard Mechler, Laurens M. Bouwer, Nigel Arnell, Katharine Mach, Robert Muir-Wood, G. Robert Brakenridge, Wolfgang Kron, Gerardo Benito, Yasushi Honda, Kiyoshi Takahashi, and Boris Sherstyukov. 2014. "Flood risk and climate change: global and regional perspectives." *Hydrological Sciences Journal* 59 (1): 1-28. https://doi.org/10.1080/02626667.2013.857411.

Kunz, M., B. Mühr, T. Kunz-Plapp, J. E. Daniell, B. Khazai, F. Wenzel, M. Vannieuwenhuyse, T. Comes, F. Elmer, K. Schröter, J. Fohringer, T. Münzberg, C. Lucas, and J. Zschau. 2013. "Investigation of superstorm Sandy 2012 in a multi-disciplinary approach." *Natural Hazards and Earth System Sciences* 13 (10): 2579-2598. https://doi.org/10.5194/nhess-13-2579-2013.

Lamb, R., C. Keef, J. Tawn, S. Laeger, I. Meadowcroft, S. Surendran, P. Dunning, and C. Batstone. 2010. "A new method to assess the risk of local and widespread flooding on rivers and coasts." *Journal of Flood Risk Management* 3 (4): 323-336. https://doi.org/10.1111/j.1753-318X.2010.01081.x.

Laugé, Ana, Josune Hernantes, and Jose M. Sarriegi. 2015. "Critical infrastructure dependencies: A holistic, dynamic and quantitative approach." *International Journal of Critical Infrastructure Protection* 8: 16-23. https://doi.org/10.1016/j.ijcip.2014.12.004.

Lewis, Matt, Paul Bates, Kevin Horsburgh, Jeff Neal, and Guy Schumann. 2013. "A storm surge inundation model of the northern Bay of Bengal using publicly available data." *Quarterly Journal of the Royal Meteorological Society* 139 (671): 358-369. https://doi.org/10.1002/qj.2040.

Lewis, Matt, Kevin Horsburgh, Paul Bates, and Ros Smith. 2011. "Quantifying the Uncertainty in Future Coastal Flood Risk Estimates for the U.K." *Journal of Coastal Research* 27 (5): 870-881. https://doi.org/10.2112/JCOASTRES-D-10-00147.1.

Lian, J. J., K. Xu, and C. Ma. 2013. "Joint impact of rainfall and tidal level on flood risk in a coastal city with a complex river network: A case study of Fuzhou City, China." *Hydrology and Earth System Sciences* 17 (2): 679-689. https://doi.org/10.5194/hess-17-679-2013.

Maskell, John, Kevin Horsburgh, Matthew Lewis, and Paul Bates. 2014. "Investigating River-Surge Interaction in Idealised Estuaries." *Journal of Coastal Research* 30 (2): 248-259. https://doi.org/10.2112/JCOASTRES-D-12-00221.1.

Mercer, Jessica. 2010. "Disaster risk reduction or climate change adaptation: Are we reinventing the wheel?" *Journal of International Development* 22 (2): 247-264. https://doi.org/10.1002/jid.1677.

Neal, Jeffrey, Guy Schumann, and Paul Bates. 2012. "A subgrid channel model for simulating river hydraulics and floodplain inundation over large and data sparse areas." Water Resources Research 48 (11). https://doi.org/10.1029/2012WR012514.

Neal, Jeffrey, Ignacio Villanueva, Nigel Wright, Thomas Willis, Timothy Fewtrell, and Paul Bates. 2012. "How much physical complexity is needed to model flood inundation?" Hydrological Processes 26 (15): 2264-2282. https://doi.org/10.1002/hyp.8339.

Neal, Jeffrey C., Nicholas A. Odoni, Mark A. Trigg, Jim E. Freer, Javier Garcia-Pintado, David C. Mason, Melissa Wood, and Paul D. Bates. 2015. "Efficient incorporation of channel cross-section geometry uncertainty into regional and global scale flood inundation models." Journal of Hydrology 529 (1): 169-183. https://doi.org/10.1016/j.jhydrol.2015.07.026.

Neumann, Barbara, Athanasios T. Vafeidis, Juliane Zimmermann, and Robert J. Nicholls. 2015. "Future coastal population growth and exposure to sea-level rise and coastal flooding - A

global assessment." *PLoS ONE* 10 (3): e0118571. https://doi.org/10.1371/journal.pone.0118571.

Olbert, Agnieszka I., Joanne Comer, Stephen Nash, and Michael Hartnett. 2017. "High-resolution multi-scale modelling of coastal flooding due to tides, storm surges and rivers inflows. A Cork City example." *Coastal Engineering* 121: 278-296. https://doi.org/10.1016/j.coastaleng.2016.12.006.

Ottino, Julio M. 2003. "Complex systems." AIChE Journal 49 (2): 292-299.

Pant, Raghav, Scott Thacker, Jim W Hall, David Alderson, and Stuart Barr. 2018. "Critical infrastructure impact assessment due to flood exposure." *Journal of Flood Risk Management* 11 (1): 22-33.

Paprotny, Dominik, Michalis I. Vousdoukas, Oswaldo Morales-Nápoles, Sebastiaan N. Jonkman, and Luc Feyen. 2018. "Compound flood potential in Europe." *Hydrology and Earth System Sciences Discussions*: 1-34. https://doi.org/10.5194/hess-2018-132.

Patro, S, C Chatterjee, S Mohanty, R Singh, and NS Raghuwanshi. 2009. "Flood inundation modeling using MIKE FLOOD and remote sensing data." *Journal of the Indian Society of Remote Sensing* 37 (1): 107-118.

Quinn, N., M. Lewis, M. P. Wadey, and I. D. Haigh. 2014. "Assessing the temporal variability in extreme storm ‐ tide time series for coastal flood risk assessment." *Journal of Geophysical Research: Oceans* 119 (8): 4983-4998. https://doi.org/10.1002/2014JC010197.

Rinaldi, S. M., J. P. Peerenboom, and T. K. Kelly. 2001. Identifying, understanding, and analyzing critical infrastructure interdependencies. 21 (6): 11-25. https://doi.org/10.1109/37.969131.

Saleh, F., V. Ramaswamy, Y. Wang, N. Georgas, A. Blumberg, and J. Pullen. 2017. "A multi-scale ensemble-based framework for forecasting compound coastal-riverine flooding: The Hackensack-Passaic watershed and Newark Bay." *Advances in Water Resources* 110: 371-386. https://doi.org/10.1016/j.advwatres.2017.10.026.

Salman, Abdullahi M., and Yue Li. 2018. "Flood Risk Assessment, Future Trend Modeling, and Risk Communication: A Review of Ongoing Research." *Natural Hazards Review* 19 (3): 4018011. https://doi.org/10.1061/(ASCE)NH.1527-6996.0000294.

Sampson, Christopher C., Paul D. Bates, Jeffrey C. Neal, and Matthew S. Horritt. 2013. "An automated routing methodology to enable direct rainfall in high resolution shallow water models." *Hydrological Processes* 27 (3): 467-476. https://doi.org/10.1002/hyp.9515.

Seenath, Avidesh, Matthew Wilson, and Keith Miller. 2016. "Hydrodynamic versus GIS modelling for coastal flood vulnerability assessment: Which is better for guiding coastal management?" *Ocean and Coastal Management* 120: 99-109. https://doi.org/10.1016/j.ocecoaman.2015.11.019.

Serre, Damien, and Charlotte Heinzlef. 2018. "Assessing and mapping urban resilience to floods with respect to cascading effects through critical infrastructure networks." *International Journal of Disaster Risk Reduction* 30: 235-243. https://doi.org/10.1016/j.ijdrr.2018.02.018.

Skinner, Christopher J., Thomas J. Coulthard, Daniel R. Parsons, Jorge A. Ramirez, Liam Mullen, and Susan Manson. 2015. "Simulating tidal and storm surge hydraulics with a simple 2D inertia based model, in the Humber Estuary, U.K." *Estuarine, Coastal and Shelf Science* 155: 126-136. https://doi.org/10.1016/j.ecss.2015.01.019.

Svensson, Cecilia, and David A. Jones. 2004. "Dependence between sea surge, river flow and precipitation in south and west Britain." *Hydrology and Earth System Sciences* 8 (5): 973-992. https://doi.org/10.5194/hess-8-973-2004.

Szewrański, Szymon, Jakub Chrusciński, Jan Kazak, Malgorzata Swiader, Katarzyna Tokarczyk-Dorociak, and Romuald Zmuda. 2018. "Pluvial Flood Risk Assessment Tool (PFRA) for rainwater management and adaptation to climate change in newly urbanised areas." *Water (Switzerland)* 10 (4): 386. https://doi.org/10.3390/w10040386.

Tang, H. S., S. Kraatz, X. G. Wu, W. L. Cheng, K. Qu, and J. Polly. 2013. "Coupling of shallow water and circulation models for prediction of multiphysics coastal flows: Method, implementation, and experiment." *Ocean Engineering* 62: 56-67. https://doi.org/10.1016/j.oceaneng.2012.12.050.

Teng, J., A. J. Jakeman, J. Vaze, B. F. W. Croke, D. Dutta, and S. Kim. 2017. "Flood inundation modelling: A review of methods, recent advances and uncertainty analysis." *Environmental Modelling and Software* 90: 201-216. https://doi.org/10.1016/j.envsoft.2017.01.006.

Thompson, Courtney M., and Tim G. Frazier. 2014. "Deterministic and probabilistic flood modeling for contemporary and future coastal and inland precipitation inundation." *Applied Geography* 50: 1-14. https://doi.org/10.1016/j.apgeog.2014.01.013.

Tsavdaroglou, Margarita, Saad H. S. Al-Jibouri, Thomas Bles, and Johannes I. M. Halman. 2018. "Proposed methodology for risk analysis of interdependent critical infrastructures to extreme weather events." *International Journal of Critical Infrastructure Protection* 21: 57-71. https://doi.org/10.1016/j.ijcip.2018.04.002.

UNISDR. 2009. UNISDR terminology on disaster risk reduction. Geneva, Switzerland: United Nations International Strategy for Disaster Reduction (UNISDR).

USACE. 2017. Risk assessment for flood risk management studies. edited by Department of the Army. Washington, DC: U.S. Army Corps of Engineers (USACE).

van den Hurk, B. J. J. M., E. van Meijgaard, P. H. M. van der Valk, K. J. van Heeringen, and J. de Gooijer. 2015. "Analysis of a compounding surge and precipitation event in the Netherlands." *Environmental Research Letters* 10 (3): 35001. https://doi.org/10.1088/1748-9326/10/3/035001.

Wahl, Thomas, Shaleen Jain, Jens Bender, Steven D. Meyers, and Mark E. Luther. 2015. "Increasing risk of compound flooding from storm surge and rainfall for major US cities." *Nature Climate Change* 5 (12): 1093-1097. https://doi.org/10.1038/nclimate2736.

Wang, Shuliang, Liu Hong, and Xueguang Chen. 2012. "Vulnerability analysis of interdependent infrastructure systems: A methodological framework." Physica A: Statistical Mechanics and its applications 391 (11): 3323-3335.

Ward, Philip J., Anaïs Couasnon, Dirk Eilander, Ivan D. Haigh, Alistair Hendry, Sanne Muis, Ted I. E. Veldkamp, Hessel C. Winsemius, and Thomas Wahl. 2018. "Dependence between high sea-level and high river discharge increases flood hazard in global deltas and estuaries." *Environmental Research Letters* 13 (8): 84012. https://doi.org/10.1088/1748-9326/aad400.

Werner, Micha, Sarka Blazkova, and Jiri Petr. 2005. "Spatially distributed observations in constraining inundation modelling uncertainties." *Hydrological Processes: An International Journal* 19 (16): 3081-3096.

Wood, Melissa, repo dai nl info:eu, renaud hostache, J. C. Neal, thorsten wagener, laura giustarini, marco chini, giovani corato, patrick matgen, and P. D. Bates. 2016. "Calibration of channel depth and friction parameters in the LISFLOOD-FP hydraulic model using medium resolution SAR data and identifiability techniques." *Hydrology and Earth System Sciences* 20 (12): 4983-4997. https://doi.org/10.5194/hess-20-4983-2016.

Yin, Jie, Mingwu Ye, Zhane Yin, and Shiyuan Xu. 2015. "A review of advances in urban flood risk analysis over China." *Stochastic Environmental Research and Risk Assessment* 29 (3): 1063-1070. https://doi.org/10.1007/s00477-014-0939-7.

Yin, Jie, Dapeng Yu, and Rob Wilby. 2016. "Modelling the impact of land subsidence on urban pluvial flooding: A case study of downtown Shanghai, China." *Science of the Total Environment* 544: 744-753.

Yin, Zhane, Jie Yin, Dapeng Yu, Min Liu, and Qing He. 2016. "Evaluating the impact and risk of pluvial flash flood on intra-urban road network: A case study in the city center of Shanghai, China." *Journal of Hydrology* 537: 138-145. https://doi.org/10.1016/j.jhydrol.2016.03.037.

Zheng, Feifei, Seth Westra, Michael Leonard, and Scott A. Sisson. 2014. "Modeling dependence between extreme rainfall and storm surge to estimate coastal flooding risk." *Water Resources Research* 50 (3): 2050-2071. https://doi.org/10.1002/2013WR014616.

Zheng, Feifei, Seth Westra, and Scott A. Sisson. 2013. "Quantifying the dependence between extreme rainfall and storm surge in the coastal zone." *Journal of Hydrology* 505: 172-187. https://doi.org/10.1016/j.jhydrol.2013.09.054.

Chapter 3

3. Analysis of Compound Flooding in Saint Lucia

The passage of tropical storms, as the main driver of storm surges and high waves in many regions, can also generate heavy rainfalls. The resulting combination of riverine, pluvial, and coastal flooding can cause significant losses, particularly in densely-populated coastal environments. Hewanorra International Airport (HIA), located at the southern coast of Saint Lucia, is the only international airport in this island, which is susceptible to flooding caused by heavy rainfalls, high levels of water in rivers, as well as storm tides and waves. It was shut down in several extreme events (such as Hurricane Tomas in 2010) due to the flooded runway and terminal. The disruptions of HIA, as well as the flooding in surrounding human communities and significant infrastructure, have led to huge economic losses. In this study, a two-dimensional sub-grid hydrodynamic model (LISFLOOD-FP) was set up to simulate the combined effects of river flows, coastal water levels, and rainfall in the event of Tropical Storm Matthew. The model is forced with rainfall inputs that are derived from station observations and different rainfall products, as well as coastal water levels that consist of estimated storm tides and waves. A lumped rainfall-runoff model (HYMOD) was also set up and calibrated to generate upstream inflow boundary conditions for the hydrodynamic model. Validation of the LISFLOOD-FP model is based on the flood inundation map derived from available satellite imageries including the Pléiades-1 imageries and Sentinel-1 imageries. Sensitivity analysis is introduced to explore model uncertainties associated with uncertain boundary conditions. Scenario analysis is conducted to investigate the potential impacts of wave run-up. Probabilistic flood hazard analysis is completed to visualize the impacts of uncertain boundary conditions as well as to identify areas with high risks of flooding.

3.1. Introduction

In the Caribbean region, Small Island Development States (SIDS) have high exposure but limited adaptive capacities to hurricanes and tropical storm events, which were found to significantly increase since the mid-1990s, resulting in extensive damages and economic losses (Pulwarty,

Nurse, and Trotz 2010). For example, in the case of Hurricane Tomas on the island of Saint Lucia in 2010, the consequences were disastrous, which include numerous rainfall-induced landslides, the loss of electricity, destructions of houses and infrastructure, confirmed deaths of eight people, and an estimated total loss of 336.15 million U.S. dollars (Pasch and Kimberlain 2011). During the high active 2017 Atlantic hurricane season, seventeen named tropical cyclones have developed with notable collective intensity; among those extreme events, Hurricane Irma and Hurricane Maria showed the most remarkable impacts by affecting a total of 14 SIDS and 16 SIDS, respectively (Shultz et al. 2019). Besides the high sensitivity to current atmospheric conditions, Caribbean SIDS are projected to be more vulnerable in the changing climate (Pulwarty, Nurse, and Trotz 2010). They are facing critical challenges from climate-related hazards that are driven by sea level rise (SLR), increasing air and surface temperatures, as well as potential changes in the frequency and intensity of tropical storms and other extreme events (Nurse et al. 2014; Pulwarty, Nurse, and Trotz 2010; Rhiney 2015). Annual economic losses in the Caribbean in terms of hurricane damage, loss of tourism revenue, and infrastructure damage are estimated as $22 billion by 2050 and $46 billion by 2100 (Bueno et al. 2008). These estimations are believed to increase if the temperature change of 1.5˚C beyond pre-industrial levels is considered (Mycoo 2018).

As the main driver of storm tides and high waves, the passage of tropical storms in the Caribbean region can also generate heavy precipitation. Caribbean SIDS are at high risk of compound flooding not only due to their high exposure to storm events but also the inherent geophysical characteristics of small islands. Many of them can be characterized as volcanic islands with small and steep river catchments, indicating the rapid response to rainfall and generally limited storage capacity (Mycoo 2018). In addition, the majority of human communities, critical infrastructure, and development are located in low-lying areas along the coastal fringe of Caribbean SIDS, and as a result, the combined effects of storm tides, waves, heavy rainfall, and river overflows could be disastrous in those islands (Nurse et al. 2014). Coastal water levels, as well as the interactions between sea levels and river flows, can cause extensive inundation hazards along the coastline and in river floodplains, not only threatening human settlements and coastal resorts but also affecting the operations of seaports and/or airports in low-lying areas (Monioudi et al. 2018). Intense rainfall events can cause widespread disruptions of services and induce inland floods, mudslides, as well as landslides that can greatly impact transportation assets and their connecting road networks such as the major highway in the islands (Fay et al. 2017). Current challenging conditions are expected

to be worse due to climate change. SLR, one of the most widely acknowledged climate-related threats to lowlands, is believed to increase surge severity and shift higher hazards farther inland (Biondi and Guannel 2018; Lin et al. 2012). Changes in rainfall patterns are not well recognized yet, but there is a potential increase in the destructiveness of tropical cyclones and associated storm surges. Bender et al. (2010) found that the frequency of Atlantic tropical cyclones with extreme intensities (i.e. category 4 and 5 storms) is projected to double by the end of the 21st century.

As in Figure 1, the Caribbean SIDS of Saint Lucia, located in the Caribbean Sea with a land area of approximately 616 km^2, has a mountainous landscape that is characterized by steep slopes cut by fast-flowing water drainage networks, confined low-lying coastal areas, and pocket beaches (United Nations Conference on Trade and Development 2017). Coastal lowlands in Saint Lucia have a high concentration of human settlements, hotels, seaports, airports, and transportation assets that connect major communities and coasts on the island (Mycoo 2011). These highly-developed low-lying areas, however, are prone to floods and vulnerable to tropical storms and other extreme events. For example, on 24 December 2013, an unseasonal low-level trough system passed over the island. Major communities, such as Castries in the north and Vieux Fort in the south of the island, experienced substantial floods caused by heavy precipitation as well as overwhelming water in nearby river channels (Global Facility for Disaster Reduction and Recovery 2014). Both international and local transportation were impacted since the Hewanorra International Airport was shut down for nearly 48 hours due to the temporarily flooded runway and terminal building, and several sections of the main highway were collapsed due to the insufficient drainage systems (Global Facility for Disaster Reduction and Recovery 2014). The total estimated damages and losses of this event was US$99.88 million, equivalent to 8.3 per cent of the country's GDP; the transport sector was the major damage (72.3 per cent) followed by the agriculture sector (12.92 per cent) and the housing sector (3.81 per cent) (Global Facility for Disaster Reduction and Recovery 2014). Under a changing climate, flooding risks in Saint Lucia are believed to increase as the result of sea level rise, continuous damages to natural barriers such as coral reef ecosystems, reduced capacities of the drainage infrastructure, as well as potentially more frequent extreme events such as intense tropical cyclones associated with waves and storm surges (Government of Saint Lucia 2018b). Despite the high exposure and vulnerability to natural hazards, increasing development and population growth are still expected at the coastal lowlands in Saint Lucia because of the three main characteristics of the country: (i) small geographical area and limited

on-island relocation opportunities, (ii) high dependence on tourism, which accounts for 65% of GDP and serves as the main source of foreign exchange earnings for the island, and the irreplaceable role of beaches as the major tourism product, and (iii) the needs of livelihood sources such as lowland agriculture and coastal fisheries (Government of Saint Lucia 2018b; World Travel and Tourism Council 2019; Central Intelligence Agency 2019). Given the high risks of low-lying coastal areas to flooding but limited financial and human resources in Saint Lucia, flood risk assessment and efficient flood mitigation strategies are necessary for the country to protect human settlements, ecosystems, and the economy.

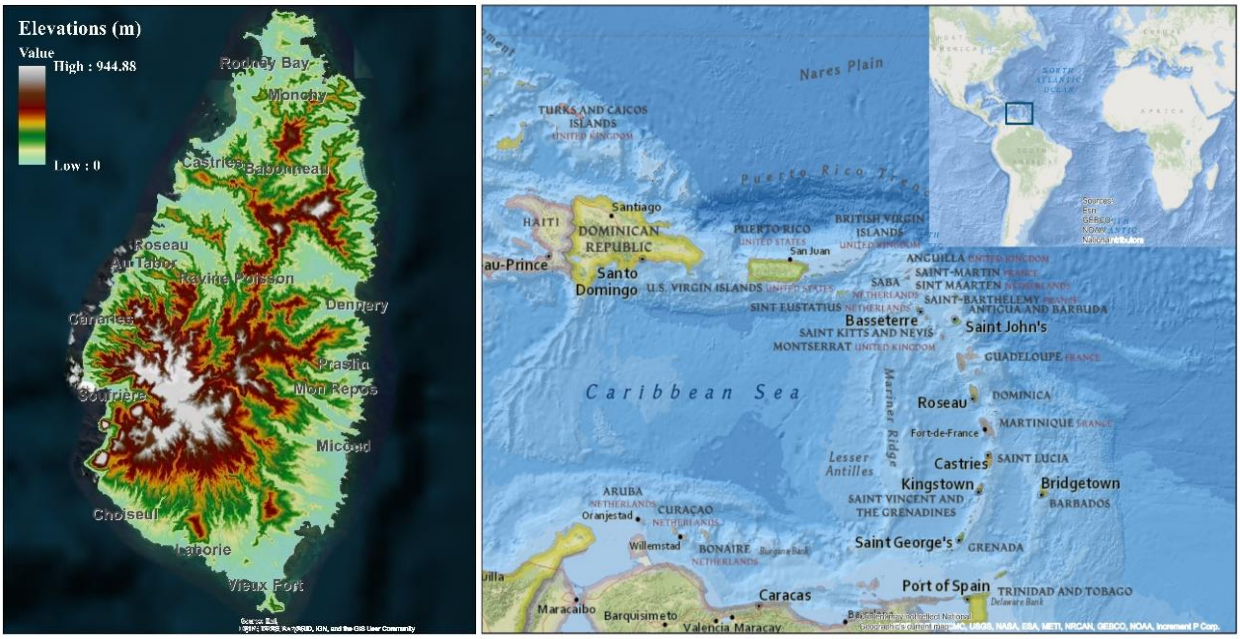

Figure 1. The topography map and the geographic location of Saint Lucia (Sources: Esri, DigitalGlobe, GeoEye, i-cubed, USDA FSA, USGS, AEX, Getmapping, Aerogrid, IGN, IGP, swisstopo, and the GIS User Community; National Geographic, Esri, DeLorme, HERE, UNEP-WCMC, USGS, NASA, ESA, METI, NRCAN, GEBCO, NOAA, iPC; Esri, GEBCO, NOAA, National Geographic, DeLorme, HERE, Geonames.org, and other contributors; Saint Lucia Digital Elevation Model that is downloaded from http://www.charim-geonode.net/layers/geonode:dem).

Two-dimensional modelling is an essential measure to understand the effects of multiple flood factors and accordingly to develop efficient flood mitigation measures. Using the integrated watershed model LImburg Soil Erosion Model (i.e. LISEM erosion/runoff model combined with the FullSWOF2D open source 2D flood module), a national flood hazard map was developed in

Saint Lucia to identify flood inundation extents in rainfall events with different return periods (Jetten 2016). In this model, the 1D kinematic wave scheme is used to route channel flows, and the 2D full Saint-Venant equations are used when channel flows spread into surrounding floodplains. However, considering the lack of model calibration and inherent uncertainties in the simulation results, estimated flood extents can only be used as a preliminary evaluation of flood hazards. The resolution of 20m is also not adequate to simulate flows around structures such as houses and buildings in communities. Furthermore, the effects of coastal water levels and river discharges are not considered in this model. Therefore, it is necessary to set up a high-resolution hydraulic model in order to comprehensively evaluate compound floods in Saint Lucia.

In this study, the latest version of the simplified two-dimensional hydrodynamic model LISFLOOD-FP (J. Neal et al. 2018) was set up to simulate flood conditions at the southern coast of Saint Lucia in the event of Tropical Storm Matthew in September 2016. This event is selected due to its severe consequences and data availability. This version of LISFLOOD-FP not only has the ability to solve inertial formulations proposed in Bates, Horritt, and Fewtrell (2010) and de Almeida et al. (2012) with much higher computation efficiency, but also includes subroutines for simulations of sub-grid river channels (J. Neal et al. 2012) and for the stable routing of rainfall-induced flows over elevated surfaces (Sampson et al. 2013). High-resolution topographic data is available for the model setup. Since observational data is limited in this data-scarce region, river discharges were simulated using a calibrated hydrologic model, coastal water levels are estimated along with corresponding uncertainty bounds, while the time series of rainfall intensities are derived from both station observations and rainfall products. Simulated river discharges, estimated coastal water levels, and derived rainfall inputs are used to force model boundaries. A flood inundation map was derived from available satellite imageries and used for the model validation. Since the accuracy of simulation results strongly depend on the forcing data, sensitivity analysis is performed to evaluate the effects of uncertain boundary conditions, and individual contributions of the three flood factors (i.e. coastal water levels, river flows, and rainfall) in flood patterns. Probabilistic flood hazard analysis is conducted based on a large number of simulations in order to explore the probability of flooding for each pixel when considering the uncertainties in river flows, sea levels, rainfall volume, as well as temporal patterns of rainfall intensities. Lastly, scenario analysis is utilized to explore the potential effects of wave run-up. Objectives of the study in this chapter are as follow.

(1) Set up and validate a simplified two-dimensional hydrodynamic model LISFLOOD-FP for the study area to comprehensively evaluate the combined effects of storm tides, waves, river discharges, as well as heavy rainfall.

(2) Conduct the sensitivity analysis to determine the impacts of uncertain boundary conditions as well as the contributions of different flood factors to the flood patterns in the event of Tropical Storm Matthew.

(3) Take uncertainties in boundary conditions into account and derive probabilistic flood hazard maps in order to examine model uncertainties associated with the input data as well as to identify high-risk flood-prone areas, which can help develop flood risk assessment and determine effective flood mitigation methods.

(4) Investigate the potential impacts of wave run-up in the scenario analysis by assuming different heights of wave run-up constantly affect the island during the simulated event.

3.2. Study Area

The study area, with a total area of 9.55 km^2, is located at the southern coast of Saint Lucia and bounded by the coastline (Figure 2). Surrounded by elevated hills and mountains, significant infrastructure and human communities are built on flat low-lying lands (Figure 3). As in Figure 4, the major land cover types are pasture (40%), shrubland and forest (31%), and buildings (9.8%). The wet season is from June to December, while tropical storms associated with heavy precipitation and storm tides typically attack the island from September to November. Flooding risks are expected to be high especially in the changing climate. Effective flood management and applicable mitigation strategies are greatly needed in this region due to the existence of significant infrastructure, lowland agriculture, transportation assets, and major communities.

Significant infrastructures, the La Tourney River, road networks, and human settlements in the study area are shown in Figure 3. The two assessed critical international transportation assets are Hewanorra International Airport (HIA) and Vieux Fort Seaport (VFSP). HIA handles 78% of all air traffic (715,955 passengers in 2017) (Government of Saint Lucia 2018a), serving as the

gateway to the international long-haul airlines. The eastern end of the HIA's runway is about 150m from the shoreline that forms on the Sandy Beach fronted by coral reefs; this seaward edge of runway is projected to be vulnerable to flooding due to SLR and possible degradation of coastal ecosystem including the beach (Government of Saint Lucia 2018b; Monioudi et al. 2018). Water from hills and mountains drains into La Tourney River, which was redirected from its original path under the runway to the west running parallel to the runway and then to the south draining to the ocean. The realignments of La Tourney River was the major cause of overbank flooding in several extreme events since the river flows with high velocities were unable to make the sharp turn near HIA and eventually followed the original course, broke the riverbanks, and flew across the runway. Surrounded by low-lying land and approached by a narrow road, VFSP is about 5km from HIA and facilitates a significant fraction of the total container traffic. The seaport is 1.5m above the local mean sea level and has the resilience to storm surges since there was no reported incidents or damages (United Nations Conference on Trade and Development 2017). As is shown in Figure 4, there are areas for woody agriculture (e.g. cacao, coconut, and banana) at the east coast. Two towns are located near the airport, namely, the town of La Tourney to the north of HIA and the town of Vieux Fort to the south of HIA. Vieux Fort has reportedly experienced flooding that was exacerbated by insufficient drainage infrastructure (United Nations Conference on Trade and Development 2017). The major north-south highway, which connects Vieux Fort to other major communities and beaches, separates the western and eastern ends of the runway from the Atlantic Ocean. Local residents and visitors rely heavily on this highway. Many people living in Vieux Fort have to travel to Castries for work, education, and health care; more than 90% of the tourists arrive at HIA and then go to their hotels that are mainly located in the north of the island such as Castries, and at west coast such as Soufriere (United Nations Conference on Trade and Development 2017).

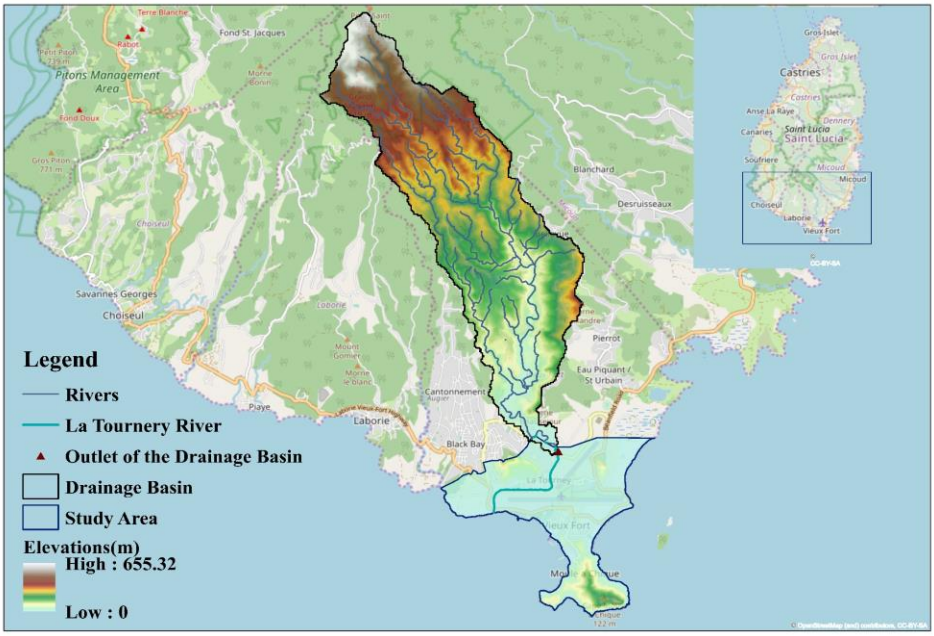

Figure 2. The drainage basin and study area (Sources: Saint Lucia Digital Elevation Model downloaded from http://www.charim-geonode.net/layers/geonode:dem; Saint Lucia river networks downloaded from http://www.charim-geonode.net/layers/geonode:rivers; Map data © OpenStreetMap contributors, Map layer by Esri).

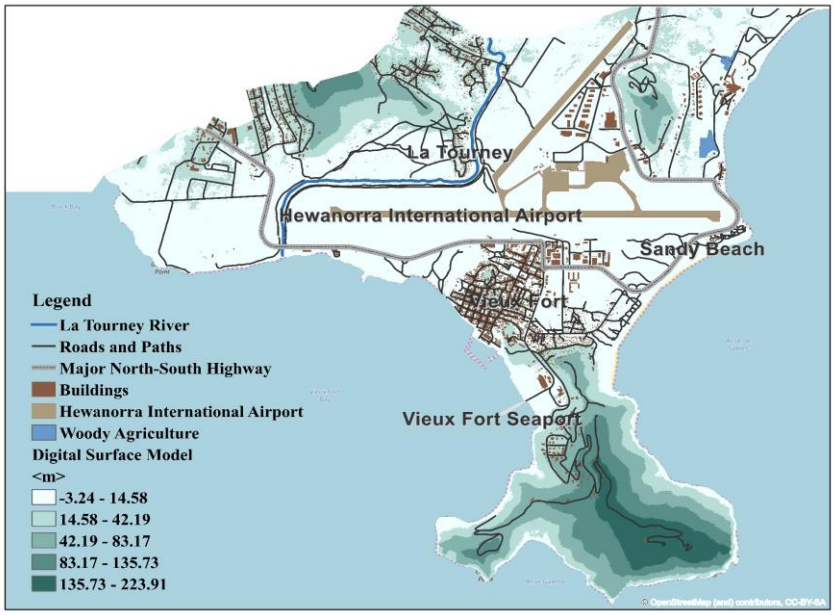

Figure 3. Map showing the topographic characteristics of the study area (Sources: Map data © OpenStreetMap contributors, Map layer by Esri; Saint Lucia Topographic Map downloaded from http://www.charim-geonode.net/maps/217; Digital Surface Model provided by Deep Logic Solutions Inc.).

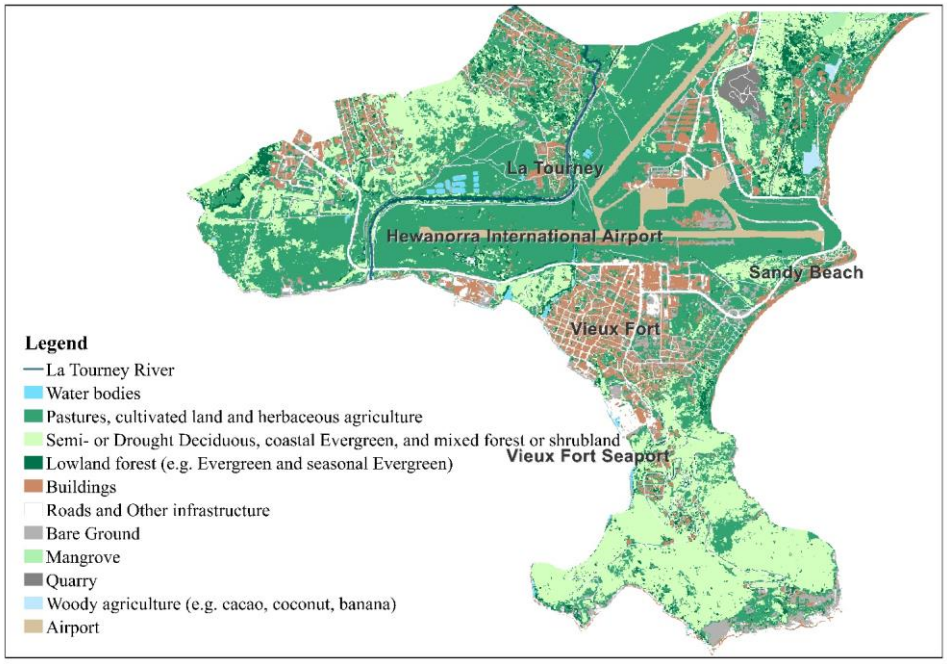

Figure 4. Land cover map of the study area (Sources: Saint Lucia 2014 Land Cover Map downloaded from http://www.charim-geonode.net/layers/geonode:landcover_2014_improved1).

3.3. Data and Methods

The 2016 Atlantic hurricane season was an above-average season since 2012 with 15 named storms and 3 intense hurricanes; among them, Hurricane Matthew, impacting across the Caribbean Region and in the United States, was the strongest and most destructive cyclone of the season (Beven 2017). Heavy rainfall, rough seas, and strong winds associated with the storm affected the island of Saint Lucia from 11:00 am Atlantic Standard Time (AST) on September 28, 2016 to 8:00 am AST on September 29, 2016 (International Federation of Red Cross and Red Crescent Societies 2017). Roofing damages and loss of services such as electricity, telephone, and internet were reported across the island; several communities including the town of Vieux Fort were flooded; landslides and fallen trees hindered accesses to some drains; blocked roads and bridges impeded the local transportation; Hewanorra International Airport was closed during the storm and restarted operations on September 29, which led to disruptions of international and regional transportation; the agriculture sector was the most adversely affected with 85 per cent of farms experiencing

damages (International Federation of Red Cross and Red Crescent Societies 2017; The Caribbean Catastrophe Risk Insurance Facility 2016).

A sub-grid version of the simplified two-dimensional hydrodynamic model LISFLOOD-FP was set up to simulate the combined effects of storm tides, waves, river flows, and heavy rainfall in the event of Tropical Storm Matthew. The model setup is challenging since the study area is a data-scarce region with limited observational data. Solutions and assumptions made during the preparations of boundary conditions are introduced in the following sections. Model results in terms of flood inundation area are validated using the flood inundation map derived from available satellite imageries. The resultant validated model is subsequently utilized to conduct sensitivity analysis, scenario analysis, as well as the probabilistic flood hazard analysis.

3.3.1. Input Data for the Hydrodynamic Model

Topographic Data

Topographic data used in this study is a Digital Surface Model (DSM) that represents the elevations of grounds as well as natural and built features such as trees and buildings (Figure 3). Provided by Deep Logic Solutions Inc., the DSM is produced from the correlated point clouds obtained from a high-resolution orthoimagery taken in April 2018. It has a spatial resolution of 0.05m with an accuracy of 3 cm (68% confidence) in both horizontal and vertical directions. The DSM was levelled to the local mean sea level, indicating that the DSM elevations are always expressed relative to local MSL = 0. The fine terrain resolution, typically 1-5m or even finer than 1m, is required to capture complex flood paths in micro-topography (T. Fewtrell et al. 2011; T.J. Fewtrell et al. 2008; Hunter et al. 2008), but the finer the resolution is the greater the computational cost would be. In this study, initial experiments have shown that the resolution of 5m can provide an appropriate compromise between computational resources and simulation accuracy. The 0.05m DSM, as a result, was resampled to 5m and used as the terrain input to provide topographic information of the study area for the hydrodynamic model. Elevations of trees and other types of vegetation are not supposed to be included in the simulations; nevertheless, the resampled DSM is used in this study considering the data availability, infeasibility of vegetation removal, and the limited impacts of vegetation elevations on simulations results in the major areas of interest.

Land Cover Map

Based on the available Pleiades imageries (acquired between 2013-2014) and RapidEye imageries (acquired between 2010-2014), a 2014 validated land cover map of Saint Lucia (Figure 4) was generated by the British Geological Survey and is available for download in the Caribbean Handbook on Risk Information Management (CHARIM) website (http://charim-geonode.net/layers/geonode:landcover_2014_improved1). Since there are minimal changes in the land cover within the study area since 2014 and there is no other available land cover map, this 2014 land cover map is resampled to 5m and used to generate spatially-varied Manning's n for each pixel. Based on the study of Jetten (2016), the land cover map is reclassified to eleven land cover types and the corresponding Manning's roughness coefficients are listed in Table1. No calibration is conducted regarding Manning's n since no relevant resources are available.

Table 1. Manning's roughness coefficients for different land cover types.

Land Cover Type	Manning's Roughness Coefficient
Mangrove	0.10
Semi-Deciduous, coastal Evergreen and mixed forest or shrubland	0.10
Lowland forest (e.g. Evergreen and seasonal Evergreen)	0.10
Woody agriculture (e.g. cacao, coconut, banana)	0.07
Pastures, cultivated land and herbaceous agriculture	0.03
Buildings	0.02
Concrete pavement	0.02
Roads and other built-up surfaces (e.g. concrete, asphalt)	0.02
Bare ground (e.g. sand, rock)	0.02
Quarry	0.02
Water	0.03

Rainfall Input

Saint Lucia has an extensive network of rain gauges, and there is one gauge located in the Hewanorra International Airport. Daily rainfall data from 1998 to 2018 and the 6-hourly accumulated rainfall records from September 28, 2016 to September 29, 2016 were provided by the Water Resource Management Agency (WRMA) in Saint Lucia. Daily rainfall data would be used to set up the hydrologic model discussed in Section 3.3.2, while the 6-hourly rainfall data would be utilized as the rainfall input for LISFLOOD-FP.

Rainfall observations provided by the WRMA is considered to be reliable in this study, but considering that the hourly rainfall pattern of the event is not known and significant inconsistency is observed in rainfall data from different sources, several precipitation datasets were used additionally to investigate the effects of uncertainties in rainfall volume and temporal precipitation distributions. Besides WRMA, the other source of 6-hourly rainfall data recorded at the Hewanorra International Airport is from the Surface Data Hourly Global (DS3505) dataset, which provides sub-daily historical observations from station networks around the world. Due to the lack of knowledge regarding the hourly rainfall patterns, hourly rainfall intensities are assumed to remain constant in each time interval of six hours, and time series of rainfall inputs could accordingly be derived from the 6-hourly rainfall records. Other than gauge records, four gridded sub-daily precipitation products were also used to obtain the time series of precipitation.

1) European Centre for Medium-range Weather Forecasts ReAnalysis 5 (ERA5) dataset (Copernicus Climate Change Service 2017) is based on the ECMWF atmospheric reanalysis that combines model data with observations (satellite and in-situ) from across the world to provide hourly atmospheric data on pressure levels or 2D parameters such as hourly precipitation on the surface/single level.

2) The second Modern-Era Retrospective analysis for Research and Applications (MERRA-2) is based on the NASA atmospheric reanalysis. The hourly time-averaged collection tavg1_2d_flx_Nx, which provides hourly bias-corrected total precipitation data, is utilized (Global Modeling and Assimilation Office 2015).

3) Tropical Rainfall Measuring Mission Multi-Satellite Precipitation Analysis 3B42 Research Version Three Hourly 0.25˚ x 0.25˚ Version 7 (TMPA-3B42 V7) dataset (Tropical Rainfall

Measuring Mission 2011) provides 3-hourly combined microwave-IR estimates with gauge adjustments in regions of latitudes 50˚N-S. Hourly rainfall intensities are assumed to remain constant in each time interval of three hours, and the time series of precipitation is accordingly derived.

4) The Integrated Multi-satellitE Retrievals for GPM Final Run Half Hourly 0.1˚ x 0.1˚ Version 5 (IMERGHH V05) dataset (Huffman 2017) combines multi-satellite and gauge data, providing global half-hourly rainfall estimates.

DS3505 dataset is accessible from the NOAA National Data Center Climatic Data Online server (https://www7.ncdc.noaa.gov/CDO/cdo). ERA5 hourly estimates of variables on single levels dataset are available for download in the Climate Data Store website (https://cds.climate.copernicus.eu/#!/home). The products of MERRA-2, TMPA-3B42 V7, and IMERGHH V05 are all accessible in the Goddard Earth Sciences (GES) Data and Information Services Center (DISC) server (https://disc.gsfc.nasa.gov/).

Table 2 summarizes the characteristics of rainfall data derived from different datasets and products. The largest total rainfall volume is observed in IMERGHH V05, while the lowest rainfall volume is found in MERRA-2. Time series of hourly or half-hourly rainfall intensities during the event, as in Figure 5, are derived from each precipitation source and are used as boundary conditions for the hydrodynamic model.

Table 2. Characteristics of rainfall data derived from different sources during the event of Tropical Storm Matthew.

Source of Rainfall Data	Temporal Resolution	Rainfall on 2016-09-28 (mm)	Rainfall on 2016-09-29 (mm)	Total Rainfall (mm)	Differences in Total Rainfall (%)
Rainfall Gauge (WRMA)	6-hour	320.60	0.10	320.7	/
Rainfall Gauge (DS3505)	6-hour	275.93	56.18	332.11	3.56
ERA5	1-hour	78.56	13.52	92.08	-71.29
MERRA-2	1-hour	58.92	11.14	70.06	-78.15

TMPA-3B42 V7	3-hour	229.73	53.32	283.05	-11.74
IMERGHH V05	30 minutes	381.48	114.18	495.66	54.56

Note: The formula for calculating the differences in the total rainfall is (total rainfall derived from sources other than WRMA – total rainfall derived from the gauge data provided by WRMA)/ total rainfall derived from the gauge data provided by WRMA.

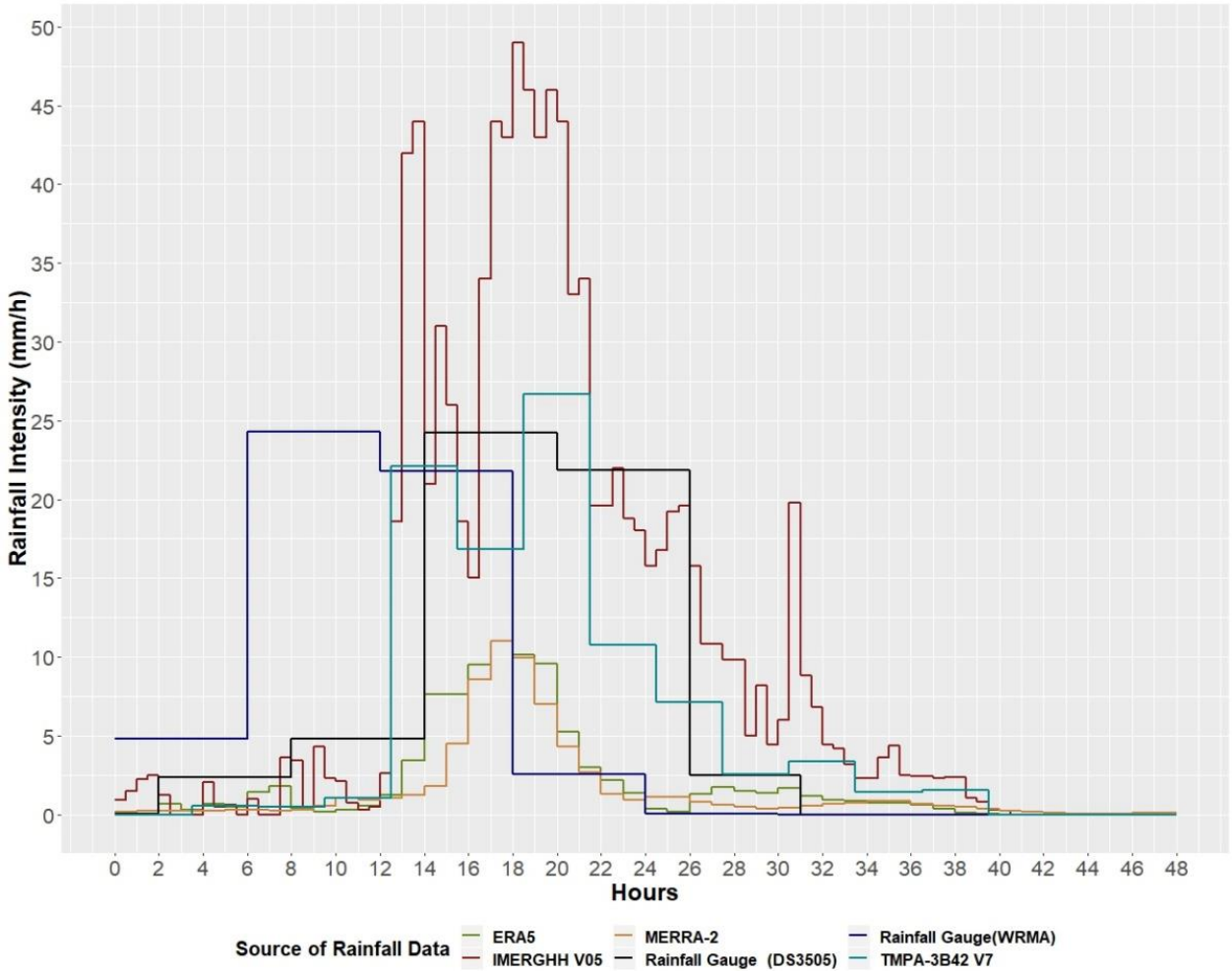

Figure 5. Time series of hourly or half-hourly rainfall intensities derived from different sources during the simulated period (from 00:00 am AST on September 28, 2016 to 00:00 am AST on September 30, 2016)).

Coastal Boundary Conditions

Figure 6. Locations of utilized tide gauges in surrounding islands (Sources: Esri, DigitalGlobe, GeoEye, i-cubed, USDA FSA, USGS, AEX, Getmapping, Aerogrid, IGN, IGP, swisstopo, and the GIS User Community).

During the events of tropical storms and hurricanes, tidal observations at gauges not only include astronomic tides, but also sea level variations caused by atmospheric pressure fluctuations, storm surge, and wave setup (i.e. rise in water levels due to breaking waves) to the degree that occurs at the location of the gauge (Federal Emergency Management Agency 2016). Tidal gauge measurements, which consists of storm tides (the combination of astronomical tide and storm surge) and limited wave setup, are extensively utilized to simulate coastal flooding (Kumbier et al. 2018; Saleh et al. 2017). There is no tidal gauge located within the study area, and therefore, tidal gauges located in surrounding islands (i.e. Fort-de-France in the Island of Martinique, Roseau in the Island of Dominica, and Prickly Bay in the Island of Grenada) are utilized to derive possible storm tides patterns in the study area. Their geographic locations are presented in Figure 6. Those gauges are operated by the University of Hawaii Sea Level Center (UHSLC) network, and their UHSLC IDs are 271, 786, and 789, respectively. The UHSLC network (Caldwell, Merrifield, and

Thompson 2015) assembles and distributes Fast Delivery (FD) and Research Quality (RQ) datasets of hourly- and daily-averaged tide gauge water-level observations around the world. The FD dataset is released within 4-6 weeks of the collection after a level 1 quality assessment (e.g. unit and timing evaluation and outlier detection), while the RQ dataset undergoes a level 2 quality assessment (e.g. tide gauge datum evaluation and comparison with nearby stations) and is available on an annual cycle. The FD data is replaced by RQ data when available. Both FD and RQ data are available for download on the UHSLC website (http://uhslc.soest.hawaii.edu/data/). Datasets used in this study is the RQ dataset for the gauge 271 and the FD datasets retrieved on March 21, 2019 for gauges 786 and 789. Mean Sea Level (MSL) for each tide gauge can be obtained in the UHSLC website (https://uhslc.soest.hawaii.edu/stations/?stn=786#datums) and/or calculated using years of tidal gauge data. Water level measurements from 00:00 am AST on September 28, 2016 to 00:00 am on September 30, 2016 at tide gauges are obtained and levelled to their corresponding MSL. The resultant time series of observed water levels (Figure 7) have similar characteristics and are considered as possible temporal distributions of storm tides at the coastline during the event.

In the study of Monioudi et al. (2018), extreme sea levels (ESLs; defined as the sum of mean sea level, the maximum astronomical tide, and the episodic water level rise due to storm surges and wave setup; wave run-up heights are not included) under different return periods from the year of 2000 to 2100 were determined for Saint Lucia. ESLs in the year of 2020 under the condition of RCP 8.5, which were levelled to the mean sea levels of tide gauges, are used to rescale the temporal distributions of observed water levels obtained from tide gauges in surrounding islands, thus generating the possible patterns of coastal water levels during the event. The rescaling procedure is based on the values of ESLs in Saint Lucia and the observed peak water levels at the gauges (i.e. Eq. (3-1) and Eq. (3-2)). Table 3 presents the rescaling factors calculated for each tide gauge for different return periods, and the resultant rescaled time series are presented in Figure 7. Based on the observed and rescaled time series (i.e. 24 time series in total), values of *mean* and *standard deviation (σ)* can be calculated for each hour during the simulated event. The composite two-day time series of coastal water levels based on the *mean* values is considered as the *true* sea levels during the event, while the time series based on *mean+σ*, *mean+2σ*, *mean-σ*, and *mean-2σ* values represent uncertainty bounds in the estimation of coastal sea levels, and are used as coastal boundary conditions in the sensitivity analysis to explore the effects of uncertainties in sea levels. The five composite time series are presented in Figure 7.

$$WL_{r,h} = WL_{o,h} \times F_r \tag{3-1}$$

$$F_r = \frac{ESLs_{MSL}}{PWL_o} \tag{3-2}$$

where $WL_{r,h}$ is the rescaled water levels for each hour, $WL_{o,h}$ is the observed water levels for each hour, F_r is the rescaling factor, $ESLs_{MSL}$ are the extreme sea levels that were levelled to mean sea levels of the corresponding tide gauge, and PWL_o is the observed peak water levels recorded at the corresponding tide gauge.

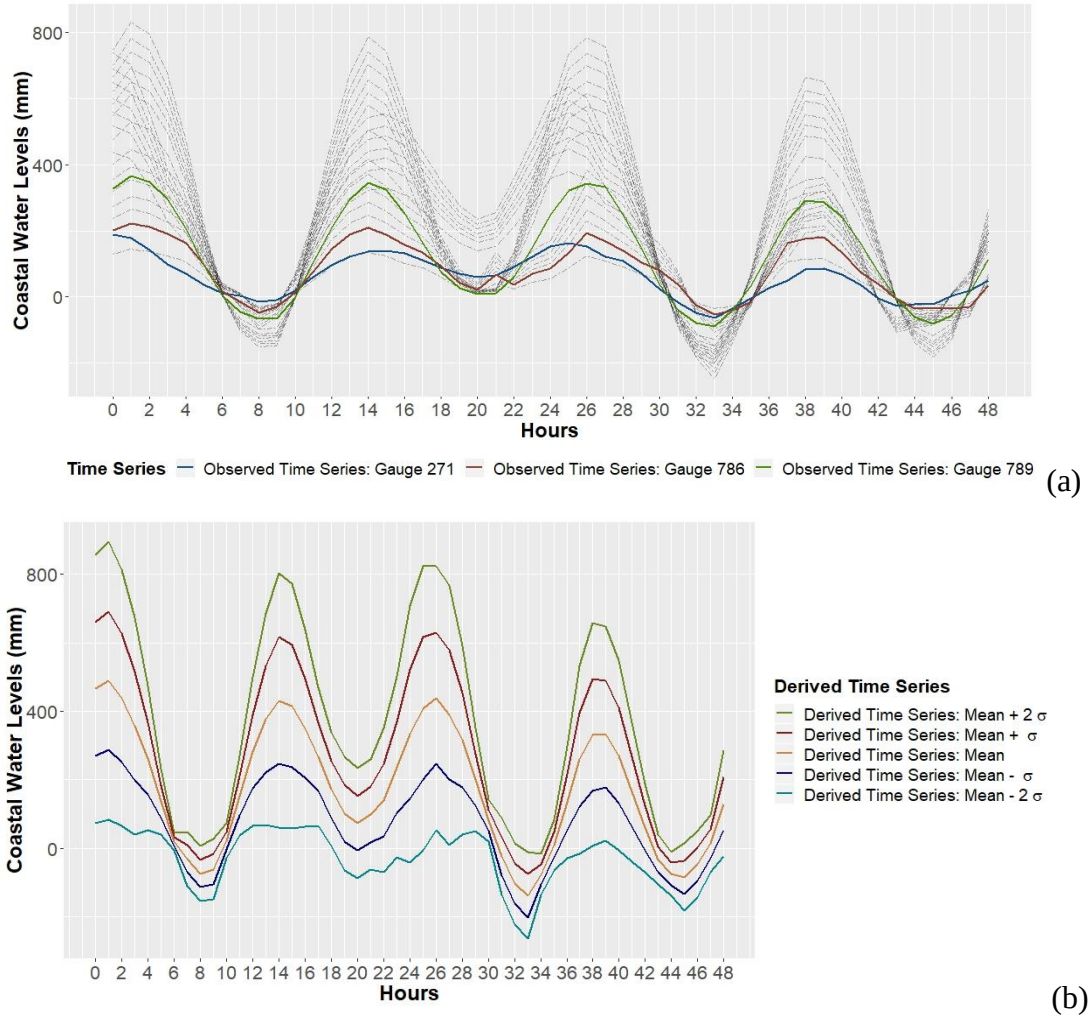

Figure 7. Observed and derived time series of coastal water levels. Solid colored lines (a) are the observed time series of tide gauges, and the dotted grey lines (a) are the scaled water levels based on the rescaling factors. Observed and rescaled time series are all used to calculate the mean and the standard deviation (σ) of water levels for each hour. Derived time series based on the mean and σ, represented as colored lines in (b), are used as boundary conditions for LISFLOOD-FP.

Table 3. The mean sea level and observed peak water levels in the event of Tropical Storm Matthew for each tide gauge, extreme sea levels in Monioudi et al. (2018), and the rescaling factors calculated for each tide gauge.

Tide Gauge ID	Mean Sea Level (mm)	Observed Peak Water Level (PWL_o; mm; referenced to tide gauge MSL)	Return Period	$ESLs_{MSL}$[3]	Rescaling Factors
271	700.34[1]	188.06	1	439.06	2.33
			5	519.06	2.76
			10	559.06	2.97
			20	599.06	3.19
			50	649.06	3.45
			100	689.06	3.66
			200	739.06	3.93
786	995.00[2]	223.00	1	145.00	0.65
			5	225.00	1.01
			10	265.00	1.19
			20	305.00	1.37
			50	355.00	1.59
			100	395.00	1.77
			200	445.00	2.00
789	608.00[2]	365.00	1	532.00	1.46
			5	612.00	1.68
			10	652.00	1.79
			20	692.00	1.90
			50	742.00	2.03
			100	782.00	2.14
			200	832.00	2.28

Note: Data are calculated from the tide gauge records (2013-2016) (Caldwell, Merrifield, and Thompson 2015)[1], obtained from the UHSLC website (https://uhslc.soest.hawaii.edu/stations/?stn=786#datums)[2], and retrieved from Monioudi et al. (2018)[3].

Wave run-up is defined as the difference between the maximum water level elevation measured on the foreshore and the still water elevation (i.e. the water level in the absence of waves and their effects), consisting of two dynamically different processes: i) maximum setup, the time-averaged water level elevation at the shoreline, representing the increase in the mean water level caused by wave shoaling and breaking; and ii) swash, representing the time-varying, vertical oscillations from the temporal mean (Stockdon et al. 2006; U.S. Army Corps of Engineers 2002). The contribution of wave run-up to coastal water levels strongly depends on the topography, bathymetry, and coastal bottom types (Marcos et al. 2019). Neglecting wave run-up and its compound effects with the presence of storm surges, particularly in areas where wave run-up can be the major driver of coastal floods, might lead to underestimated values of coastal water levels and thus significantly different flood estimates in extreme events (Armaroli et al. 2009; Perini et al. 2016; Stockdon et al. 2006).

Atlas of Probable Storm Effects in the Caribbean Sea, sponsored by the Caribbean Disaster Mitigation Project (CDMP), has used the Arbiter of Storms (TAOS) hazard model to estimate the surge and wave heights throughout the Caribbean basin for 10-, 25-, 50- and 100-year return periods. The data for Vieux Fort, Saint Lucia is available for download on the website (http://www.oas.org/cdmp/document/reglstrm/) and summarized in Table 4. Since the heights of wave run-up are significantly higher than that of surges, the effects of wave run-up can be dominant in the study area and induce severe flooding in extreme events.

Since extreme sea levels presented in Monioudi et al. (2018) do not include wave run-up heights, simulated flooding risks could be greatly underestimated, indicating the need to conduct scenario analysis and investigate the impacts of wave run-up. Due to the lack of knowledge regarding the interactions between storm tides and wave run-up during the event, the worst scenarios are considered by simply adding 0.5m, 1.5m, 2.5m, 3.5m, 4.5m, 5.5m, and 6m to the *mean* time series from 11:00 am AST on September 28, 2016 to 8:00 am AST on September 29, 2016. The resultant time series of coastal water levels used in the scenario analysis is presented in Figure 8.

Table 4. Surges and wave run-up heights in different return periods for Vieux Fort, Saint Lucia.

Return Period	Surges Heights (m; including astronomical tide and setups from pressure, wind and wave, but not wave run-up)	Wave Run-up Heights (m)
10	0.1	3.4
25	0.2	4.5
50	0.3	5.2
100	0.5	5.9

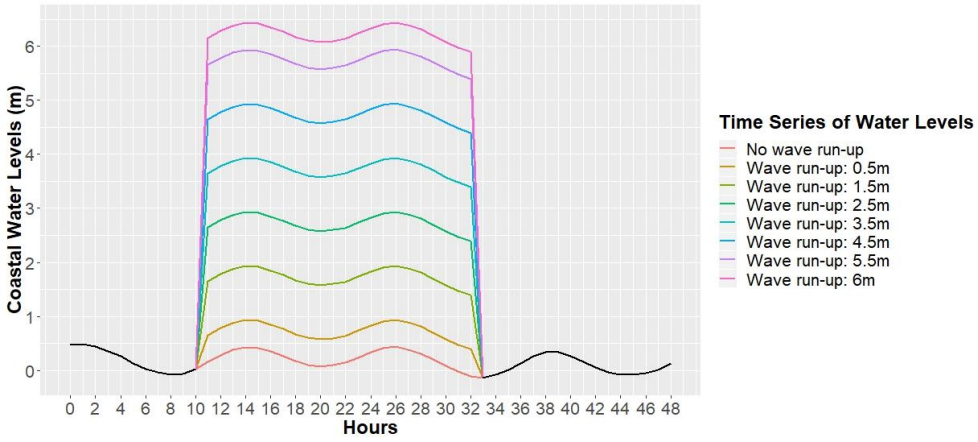

Figure 8. Time series of coastal water levels used in the scenario analysis when excluding and including the heights of wave run-up.

3.3.2. Hydrologic Modelling

There are limited discharge records available for the La Tourney River, and there are no observed records during the simulated event. A simple conceptual rainfall-runoff model, HYdrological MODel (HYMOD), was set up and calibrated for the drainage basin as in Figure 2. The total drainage area is 23.57 km^2 and the watershed outlet is at the location near La Resource (13.74˚N, 60.95˚W; Figure 2). Streamflow at the outlet, simulated by the HYMOD model, is utilized as upstream inflow boundary conditions for the hydrodynamic model LISFLOOD-FP.

Model Introduction

Based on the probability-distributed principle proposed by Moore (1985), HYMOD was originally developed by Boyle (2001) and subsequently applied in the analysis of parameter estimations and model uncertainties (Dechant and Moradkhani 2012; Moradkhani et al. 2005; Schaefli and Gupta 2007; Wagener et al. 2001). HYMOD consists of a rainfall excess model, which connects to a sequence of three quick-flow reservoirs to route surface flows, in parallel to a single slow-flow reservoir to describe subsurface flows. Details of the model structure can be found in Boyle (2001) and Wagener et al. (2001). This model includes five parameters: C_{max} is the maximum soil moisture capacity in the watershed; *Alpha* is the partitioning factor distributing surface flows and subsurface flows; *Beta* is the variability of soil moisture capacity in the domain; and R_q and R_s are the residence time of linear quick-flow and slow-flow reservoirs, respectively. Their descriptions and feasible ranges are presented in Table 5.

Table 5. Descriptions and the feasible ranges of HYMOD parameters.

Parameter	Description	Range
C_{max} (mm)	Maximum soil moisture capacity in the watershed	100-1000
Alpha	Partitioning factor distributing the surface flows and subsurface flows	0.6-0.99
Beta	Variability of soil moisture capacity	0-2
R_q (day)	The residence time of the quick-flow reservoirs	0-0.99
R_s (day)	The residence time of the slow-flow reservoir	0.001-0.5

Model Calibration and Validation

It is necessary for hydrological models to conduct model calibration in order to estimate optimal values of parameters that can ensure reliable runoff estimations. In this study, the model calibration of HYMOD is based on the comparison of simulated and observed discharges using a goodness-of-fit measure, also called an objective function. The derived parameter sets are used in model validation to examine the prediction abilities of the calibrated HYMOD model.

- **Input Data**

In the model calibration, HYMOD requires observed daily streamflow, observed daily rainfall, and daily potential evapotranspiration (PET) as inputs. In the model validation, required inputs are observed daily rainfall and daily potential evapotranspiration (PET).

Both streamflow and rainfall data are provided by WRMA in Saint Lucia. A total of 35 observed daily streamflow records extending from 2013 to 2018 are available at the outlet of the simulated drainage watershed. Daily precipitation data recorded from 1998 to 2018 are available at the rainfall gauge of Hewanorra International Airport, but a total of 15 per cent of data is found missing in the record. To fill in the missing values, daily rainfall estimates obtained from the TMPA-3B42 V7 product is utilized. Rainfall values from the product is bias corrected on a daily basis from 1998 to 2018 using the linear scaling method (i.e. Eq. (3-3) and Eq. (3-4)), aiming to match the monthly mean of the corrected values with that of the observed values (Lenderink, Buishand, and Van Deursen 2007). Monthly bias factors are presented in Table 6.

$$P_{cor,m,d}^{TMPA} = P_{m,d}^{OBS} \times F_m \tag{3-3}$$

$$F_m = \frac{\mu(P_m^{OBS})}{\mu(P_{raw,m}^{TMPA})} \tag{3-4}$$

where $P_{cor,m,d}^{TMPA}$ is bias-corrected TMPA-3B42 V7 rainfall data on the *d*th day of the *m*th month, $P_{m,d}^{OBS}$ is the observed rainfall data on the *d*th day of the *m*th month, F_m is the monthly bias factor of the *m*th month, $\mu(P_m^{OBS})$ is the monthly mean of observed rainfall of the *m*th month, and $\mu(P_{raw,m}^{TMPA})$ is the monthly mean of raw TMPA-3B42 V7 rainfall data of the *m*th month.

Performance of the bias correction is presented using statistical metrics (Table 7), including bias and relative bias (Rbias) that measure systematic differences (Eq. (3-5) and Eq. (3-6)), the root mean square error (RMSE) that measures the average error (Eq. (3-7)), and the correlation coefficient (CC) that assesses the agreement between the rainfall gauge observations and data from the rainfall product (Eq. (3-8)). Bias, Rbias, and RMSE have a perfect score of 0.00 to show a complete match between the observed daily rainfall and bias-corrected daily rainfall. CC ranges from -1 to 1 with a perfect score of 1. Results show that the bias correction conducted for the TMPA-3B42 V7 rainfall data has led to significant decreases in bias and Rbias.

$$Bias = \frac{\sum(P_{TMPA,m,d} - P_{OBS,m,d})}{N} \quad (3\text{-}5)$$

$$Rbias = \frac{\sum(P_{TMPA,m,d} - P_{OBS,m,d})}{\sum P_{OBS,m,d}} \times 100\% \quad (3\text{-}6)$$

$$RMSE = \sqrt{\frac{\sum(P_{TMPA,m,d} - P_{OBS,m,d})^2}{N}} \quad (3\text{-}7)$$

$$CC = \frac{\sum[(P_{TMPA,m,d} - \overline{P_{TMPA,m,d}})(P_{OBS,m,d} - \overline{P_{OBS,m,d}})]}{\sqrt{\sum(P_{TMPA,m,d} - \overline{P_{TMPA,m,d}})^2}\sqrt{\sum(P_{OBS,m,d} - \overline{P_{OBS,m,d}})^2}} \quad (3\text{-}8)$$

where $P_{TMPA,m,d}$ is the raw/bias-corrected TMPA-3B42 V7 rainfall data on the *d*th day of the *m*th month, $P_{OBS,m,d}$ is the observed rainfall on the *d*th day of the *m*th month, $\overline{P_{TMPA,m,d}}$ is the mean of the raw/bias-corrected TMPA-3B42 V7 rainfall of all days, $\overline{P_{OBS,m,d}}$ is the mean of observed rainfall of all days, and *N* is the number of total days.

Table 6. Monthly mean rainfall calculated from observed records at the rainfall gauge operated by WRMA in Saint Lucia, monthly mean rainfall calculated from the raw TMPA-3B42 V7 rainfall data, and the derived monthly bias factors.

Month	Monthly Mean of Raw TMPA-3B42 V7 Rainfall Data (mm)	Monthly Mean of Observed Records at the Rainfall Gauge Operated by WRMA (mm)	Monthly Bias Factors
1	1.03	3.24	3.14
2	0.55	2.52	4.60
3	0.72	2.25	3.11
4	1.14	3.96	3.47
5	1.50	3.17	2.11
6	3.05	5.67	1.86
7	4.05	5.89	1.45
8	3.97	6.31	1.59
9	4.01	6.06	1.51

10	5.63	8.40	1.49
11	3.79	7.13	1.88
12	1.57	4.09	2.60

Table 7. Performance of the bias correction conducted to TMPA-3B42 V7 product.

Metrics	Raw Rainfall Estimates from TMPA-3B42 V7	Bias-corrected Rainfall Estimates from TMPA-3B42 V7
Bias	-2.058	-0.505
Rbias	-41.2%	10.1%
RMSE	13.31	16.77
CC	0.380	0.377

Monthly PET is calculated using Thornthwaite Equation (Eq. (3-9) and Eq. (3-10)) (Thornthwaite 1948), and the daily PET required for the model is obtained by assuming daily PET to be constant throughout each month (i.e. Eq. (3-11)). Records of daily temperature at the Hewanorra International Airport station are available for download in the Global Summary of the Day (GSOD) dataset, which provides daily historical weather data and is accessible in the NOAA National Data Center Climatic Data Online server (https://www7.ncdc.noaa.gov/CDO/cdo). Records of day hours at Vieux Fort, Saint Lucia are available at a weather website (https://www.timeanddate.com/sun/saint-lucia/vieux-fort). Daily temperature and day length (hours) of each month are used to calculate average daily temperature and average day length (hours) of each month, respectively.

$$PET_m = 16\left(\frac{L_m}{12}\right)\left(\frac{N_m}{30}\right)\left(\frac{10T_{avg,m}}{I}\right)^{\alpha} \quad (3\text{-}9)$$

$$I = \sum_{i=1}^{12}\left(\frac{T_{avg,m_i}}{5}\right)^{1.514} \quad (3\text{-}10)$$

$$PET_{m,d} = \frac{PET_m}{N_m} \quad (3\text{-}11)$$

where PET_m and $PET_{m,d}$ is the estimated monthly and daily potential evapotranspiration of the *m*th month, L_m is the average day length (hours) of the *m*th month, N_m is the number of days of the *m*th month, $T_{avg,m}$ is the average daily temperature of the *m*th month, and I is the heat index calculated based on the Equation (3-10).

- **Calibration Method**

Model calibration of HYMOD includes the optimization of five parameters, which are C_{max}, *Alpha*, *Bate*, R_q, and R_s. The Shuffled Complex Evolution - University of Arizona (SCE-UA) algorithm (Q. Duan, Sorooshian, and Gupta 1992; Q.Y. Duan, Gupta, and Sorooshian 1993) was used for the parameter optimization. The SCE-UA method combines the strength of multiple search strategies, including (i) controlled random search, (ii) the simplex method, (iii) competitive evolution, and (iv) complex shuffling (Q. Duan, Sorooshian, and Gupta 1992). This optimization algorithm has proven to be an effective search algorithm and was extensively applied in the calibration of various rainfall-runoff models (Ajami et al. 2004; Jiang et al. 2015; Q. Duan, Sorooshian, and Gupta 1994; Lee, Jayawardena, and Muttil 2006; Madsen 2000; Vrugt et al. 2003; Najafi, Moradkhani, and Jung 2011).

General descriptions of the steps taken in the SCE-UA algorithm are given below. The detailed explanations can be found in Q. Duan, Sorooshian (1992) and Gupta and Q.Y. Duan, Gupta, and Sorooshian (1993).

(1) Generate sample points randomly in the feasible parameter space and compute the objective function value at each point;

(2) Rank the points in the order of increasing objective function value;

(3) Partition the sorted points accordingly into *p* complexes, each containing *m* points;

(4) The competitive complex evolution (CCE) algorithm is applied to each complex independently to evolve each complex towards the global optimum;

(5) Points in the evolved complexes are combined into a single sample population and sorted in the order of increasing function value. The sample population is then shuffled (i.e. re-partitioned) into *p* complexes.

(6) Above five steps are iterated until the pre-defined convergence criteria are satisfied, ensuring the entire population converges to the global optimum or near global optimum.

To initialize the SCE-UA algorithm, several parameters should be pre-determined, including (i) the number of complexes (*p*), (ii) the number of minimum complexes (p_{min}), (iii) the number of points in each complex (*m*), (iv) the number of points in each subcomplex constructed at the CCE algorithm (*q*), (v) the number of consecutive offspring generated by each subcomplex (α), and (vi) the number of evolution steps taken by each complex before complexes are shuffled (β). Suggested values of the algorithmic parameters were provided in Duan et al. (1994): (i) $p_{min} = p$; (ii) $m = 2n+1$, where *n* is the number of parameters to be optimized on; (iii) $q = n+1$; (iv) $\alpha = 1$; and (v) $\beta = 2n+1$. Duan et al. (1994) also found that the dimensionality was the primary factor determining the proper choice of parameter *p*; in the two- and four-parameter cases (i.e. $n = 2$ and $n = 4$), $p \geq 1$ was sufficient to ensure all optimization are successful, while for six-parameter cases (i.e. n = 6), a *p* value equals to two or larger is sufficient. In this study, sensitivity analysis was conducted to select the proper value of *p*. Results indicate that $p = 2$ is sufficient to ensure successful optimization trials and obtain better function values.

The objective function used in the optimization process is Kling-Gupta efficiency (KGE) (Gupta et al. 2009). Different from the traditional measures such as the mean squared error (MSE) and the Nash-Sutcliffe efficiency (NSE), the KGE provides a multi-objective perspective to the model calibration as well as diagnostic insights into the model performance because of the decomposition into three components representing the correlation, variability term, and bias term. The KGE is calculated as:

$$KGE = 1 - \sqrt{(r-1)^2 + (\beta-1)^2 + (\gamma-1)^2} \tag{3-12}$$

$$\beta = \frac{\mu_s}{\mu_o} \tag{3-13}$$

$$\gamma = \frac{\sigma_s}{\sigma_o} \tag{3-14}$$

where r is the linear correlation coefficient between observed and simulated discharges, β is the bias ratio, γ is the variability ratio, μ is the mean value of flows, σ is the standard deviation of flows, and the subscripts s and o represent the simulated and observed flows, respectively. KGE, r, β, and γ have their optimum at unity.

Based on Q.Y. Duan, Gupta, and Sorooshian (1993), convergence criteria used in this study to stop the shuffling loops are as follows. In each case, the trial is deemed a success when the best function value becomes less than 10^{-3} and/or the per cent of changes in the function value of the current shuffling loop and that of several shuffling loops before is less than 0.01%. The trial is regarded as fail and is automatically stopped if the convergence criteria have not been satisfied when reaching 25,000 function evaluations or 5 shuffling loops.

Due to the limited observed streamflow records, leave-n-out cross-validation method was used, enabling the maximum use of observation data for the model calibration and validation. Preliminary results have shown that n = 3 can lead to the maximum function value. In this study, three out of thirty-five sample points are randomly selected for the model validation while the remaining are used as the data sets for model calibration. With the simulated period from the year 1998 to 2018, the calibration procedure on the basis of the SCE-UA algorithm is repeated for 1000 times by using different randomly selected calibration data sets generated from the cross-validation process. This process can not only maximize the use of observed records but also help explore model uncertainties associated with the selection of model parameters.

- **Calibration Results and Analysis**

A total of 1000 parameter sets are derived after the calibration procedure, and each of them can be regarded as a set of optimal parameters and be applied to the HYMOD model for simulations, thus resulting in 1000 streamflow estimations for each day in the simulated period. Mean value is calculated on a daily basis from the 1000 simulation results and regarded as the daily runoff estimate from the HYMOD model, while the standard deviation is also calculated to explore model uncertainties of the HYMOD model associated with the selection of parameters.

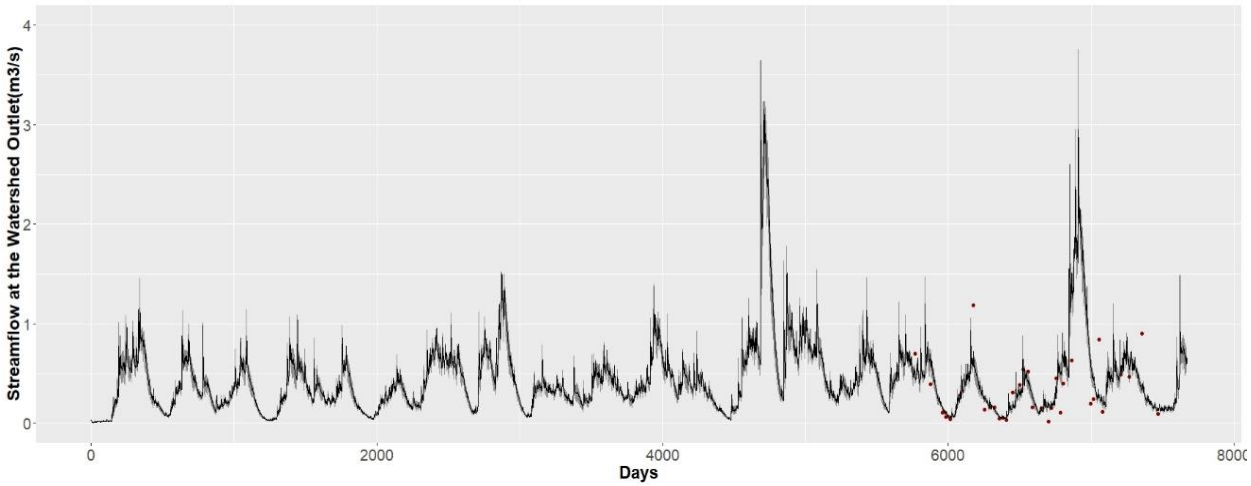

(a)

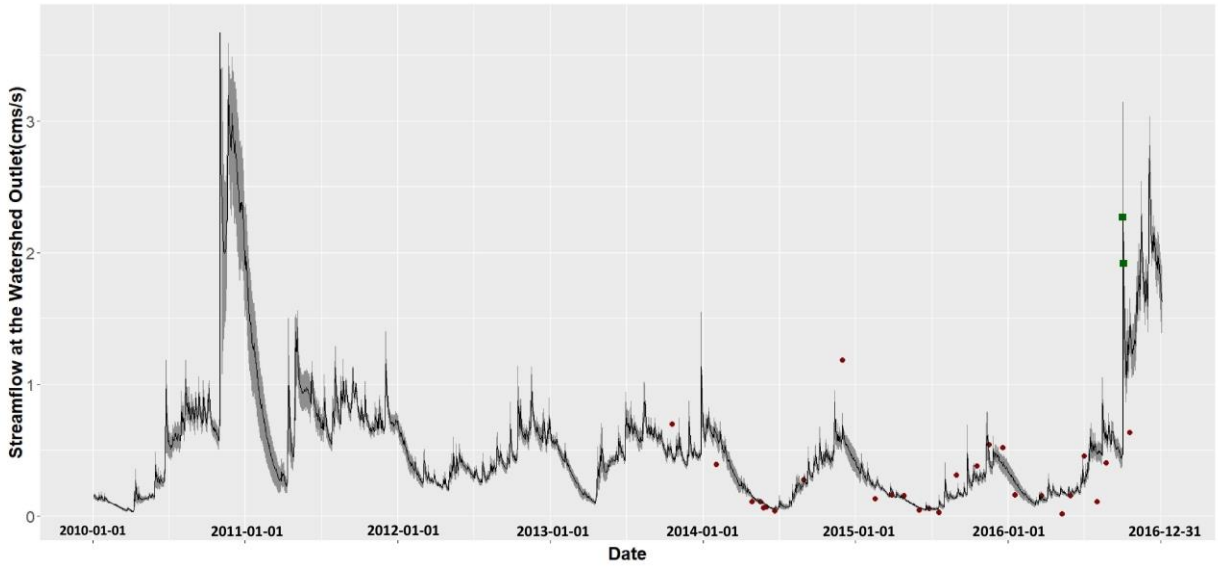

(b)

Figure 9. Simulated streamflow and observed streamflow at the watershed outlet (a) from 1998 to 2018, and (b) from 2010 to 2016. Red dots correspond to the observed streamflow records, and the black line indicates the daily runoff estimates from the HYMOD model (i.e. the mean out of all simulations that utilize the 1000 derived parameter sets). The light grey shaded area denotes the 95% hydrograph prediction uncertainty associated with selection of parameter sets derived using the SCE-UA algorithm. Green dots are estimated runoff for the event.

Figure 9 presents the observed streamflow, daily runoff estimates (i.e. the mean value out of all estimations), and the 95% hydrograph prediction uncertainty associated with the selection of parameter sets derived using the SCE-UA algorithm. The uncertainty bound is narrow, indicating

that model uncertainties associated with the selection of parameters are low. Furthermore, the KGE metric was calculated to explore the agreement between observed runoff and daily runoff estimations. Considering the limited number of observed records, the resultant KGE value of 0.544 indicates that the performance of the HYMOD model is acceptable and the parameter sets derived from the leave-three-out cross-validation method can be used for reliable runoff simulations.

- **Runoff Estimations and Associated Uncertainties**

Based on the 1000 parameter sets derived from the calibration procedure, daily runoff estimates (i.e. the values of *mean* calculated out of all simulation results) and the associated uncertainty bounds (i.e. the values of *mean+σ, mean+2σ, mean-σ,* and *mean-2σ* calculated out of all simulation results) are obtained for each day from the year of 1998 to 2018. During the event of Tropical Storm Matthew (i.e. from September 28, 2016 to September 29, 2016), as in Table 8, daily runoff estimates (i.e. the *mean*) of these two days are utilized as riverine inputs for the hydrodynamic model to simulate the effects of river flows, while the uncertainty bounds (i.e. the *mean+σ, mean+2σ, mean-σ,* and *mean-2σ*) in runoff estimations are used in the sensitivity analysis to investigate how the uncertainties in riverine inputs affect the simulated flood patterns.

Table 8. Runoff estimations obtained from the calibrated HYMOD model and the associated uncertainty bounds.

	Estimated Runoff (m^3/s) on September 28, 2016 (AST)	Estimated Runoff (m^3/s) on September 29, 2016 (AST)
mean	2.27	1.92
mean+σ	2.71	2.23
mean+2σ	3.15	2.54
mean-σ	1.83	1.60
mean-2σ	1.39	1.29

The HYMOD model is set up and calibrated based on the rainfall gauge records provided by WRMA in Saint Lucia; however, as in Table 2, rainfall data derived from different sources have different characteristics in rainfall patterns such as daily rainfall volume during the event, and as a result, the selection of rainfall sources can affect the resultant runoff estimations and accordingly affect the simulations of flood patterns. To comprehensively examine the effects of rainfall inputs to HYMOD, daily rainfall volumes derived from DS3505 dataset, ERA5, MERRA-2, TMPA-3B42 V7, and IMERGHH V05 product are also used as rainfall inputs to the calibrated HYMOD model, and the corresponding runoff estimates (Table 9) are used as the upstream inflow boundary conditions for the hydrodynamic model in the sensitivity analysis.

Table 9. Runoff estimations of the calibrated HYMOD model when using rainfall inputs derived from different sources.

Source of Rainfall Data	Estimated Runoff (m^3/s) on September 28, 2016 (AST)	Estimated Runoff (m^3/s) on September 29, 2016 (AST)
Rainfall Gauge (WRMA)	2.27	1.92
Rainfall Gauge (DS3505)	1.94	2.10
ERA5	0.78	0.76
MERRA-2	0.69	0.67
TMPA-3B42 V7	1.64	1.79
IMERGHH V05	2.71	3.08

Note: Estimated runoff is the mean value out of 1000 simulations using the derived parameter sets.

In conclusion, the *mean* value calculated for each day from all 1000 simulation results is regarded as the daily runoff estimate from the calibrated HYMOD model. However, the calibrated HYMOD model has two major sources of uncertainties: (i) the selection of parameter sets, and (ii) the selection of rainfall inputs to the model. Their impacts on the flood estimates would be investigated in the sensitivity analysis.

3.3.3. Observational Data

There are no ground observations such as recorded flood depths in the event of Tropical Storm Matthew. Available remote-sensing data is therefore utilized to provide valuable information on flood extents for the validation of the hydrodynamic model.

Pléiades-1 Satellite Imagery

Two high-resolution Airbus Defence and Space Pléiades-1 satellite images, purchased from Harris Geospatial Solutions Inc., have captured the surface features of the study area before and after the event, respectively. The images are presented in Figure 10, and the image information is presented in Table 10. No image was taken during the event. Through visual comparisons of the pre-event and post-event images, it is found that there is no presence of flood water after the event but flood-related eroded areas are observed. Those eroded regions are identified and assumed to be severely flooded, thus deriving a map to reflect flood conditions in the event of Tropical Storm Matthew. The resultant flood area derived from the Pléiades-1 satellite images is presented in Figure 12. However, the flood condition during the event is supposed to be more severe than the one indicated in the derived map not only because most of the flood water has receded and only the areas that went through severe flooding had the potential to be eroded but also because there are unidentifiable areas in the images due to the presence of clouds and high-density buildings in the human communities.

Figure 10. The Pléiades-1 pre-event (left) and post-event (right) imageries (Copyright PLEIADES © CNES 2016, Distribution Airbus DS).

Table 10. Information of the Pléiades-1 imageries

Imagery	Acquisition Date	Resolution
Pre-event Pléiades-1 Imagery	2016-09-19 10:30am AST	0.5m
Post-event Pléiades-1 Imagery	2016-09-30 10:45am AST	0.5m

Sentinel-1 Satellite Imagery

Increasing efforts on the integration of remotely sensed flood extent derived from the Synthetic Aperture Radar (SAR) imageries with hydraulic models have revealed the great potential of SAR data in flood detection and supporting timely flood management, as the all-weather, day-night operation of SAR sensors can also penetrate clouds that is often associated with flood events and are reflected by the open water surface (G. Schumann et al. 2009; G.J.P. Schumann and Moller 2015; Woodhouse and Press 2017; Yan et al. 2015). In order to derive flood inundation area, various SAR imagery-processing techniques were proposed, including visual interpretation, image histogram thresholding, automatic classification algorithms, image texture algorithms, and multi-temporal change detection methods. Each method has its advantages and disadvantages, and therefore, researchers should choose the appropriate method based on characteristics of the study area, features of the simulated flood event, and availabilities of SAR imagery. No SAR imagery is available during the event of Tropical Storm Matthew, but there is a C-band Sentinel-1A image taken after the event at 6:10 pm (AST) on September 30, 2016. Since this image has the potential to capture anomalies in areas where erosions are not noticeable in Pléiades-1 images, it was used to complement the flood map derived from the Pléiades-1 imagery. Among multiple imagery-processing techniques developed for Sentinel-1 images, the Change Detection and Thresholding (CDAT) method proposed in Long, Fatoyinbo, and Policelli (2014) is adopted due to its simplicity, applicability, and reliability. CDAT method compares the brightness information of flood imagery with the reference brightness information derived from the reference images (pre-event). Areas with significant differences in backscattering behaviour are identified as flood-affected regions.

To minimize the backscatter variability that is unrelated to flooding and establish a reliable reference profile, the reference images and the flood image should have the same orbit track, the

same polarization configuration, and preferably the same sensing period of the year especially in regions with pronounced seasonal flooding (e.g. rainy seasons in tropical areas) or significant land cover changes among seasons (Ban et al. 2012; Cian, Marconcini, and Ceccato 2018; Hostache, Matgen, and Wagner 2012; Li et al. 2018). Reference images in this study are therefore carefully chosen and the information of all selected SAR images is listed in Table 11. All images were taken in the relative orbit track of 91 by the Sentinel-1A C-band SAR instrument with the acquisition mode of Interferometric Wide swath (IW) and were delivered in Ground Range Detected High Resolution (GRDH) product with a pixel spacing of 10m (Torres et al. 2012). The reference images extend from 2014 to 2016, corresponding to the flooding season same with the flood image (i.e. September to November). No extreme event occurred when the reference images were taken. All images are pre-processed within the Google Earth Engine (GEE) (Gorelick et al. 2017) platform with steps of thermal noise removal, radiometric calibration, and terrain correction. Since initial experiments indicate the same conclusion as many other studies that VV polarization has slight advantages to identify floods (Clement, Kilsby, and Moore 2018; Twele et al. 2016), all selected images for deriving the flood extent were of the VV polarization.

Table 11. Information of all utilized Sentinel-1A images in the study.

Sensor (Band)	Sensing Date (AST)	Track	Relative Orbit	Pixel Spacing (m)	Status
Sentinel-1A (C)	2016-09-30 18:10	Ascending	91	10	Flood
Sentinel-1A (C)	2014-11-16 18:10	Ascending	91	10	Reference
Sentinel-1A (C)	2015-09-12 18:10	Ascending	91	10	Reference
Sentinel-1A (C)	2015-10-06 18:10	Ascending	91	10	Reference
Sentinel-1A (C)	2015-11-23 18:10	Ascending	91	10	Reference
Sentinel-1A (C)	2016-09-06 18:10	Ascending	91	10	Reference

Note: All images are obtained from the image collection (ID: COPERNICUS/S1_GRD) within the GEE platform (Google Earth Engine 2015).

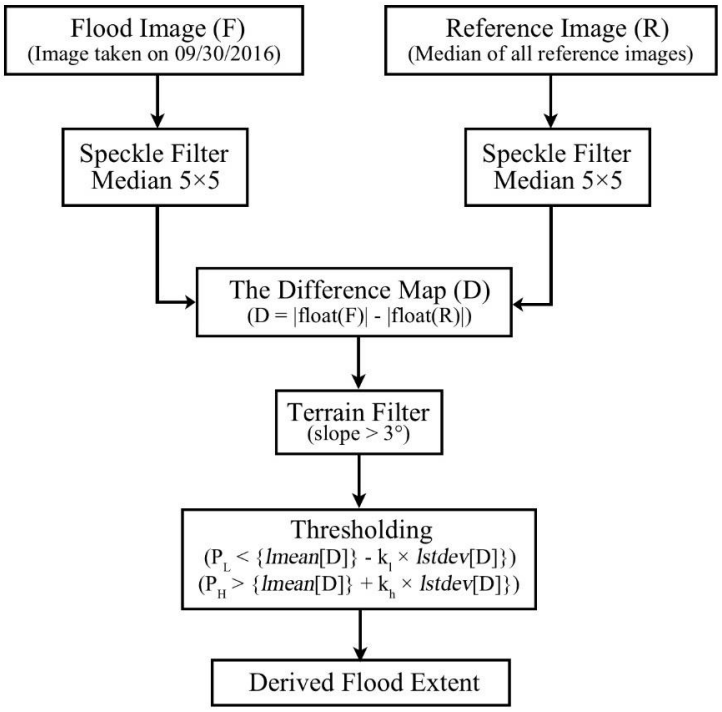

Figure 11. Workflow used to derive flood extent from the SAR imagery.

Figure 11 provides an overview of the processing steps to derive flood inundation areas. Utilized platforms include GEE and SNAP (Sentinel Application Platform) Toolbox (SNAP 2018). As listed in Table 11, the flood image is taken on September 30, 2016, while the reference profile is established based on the collection of five reference images by calculating the median backscattering values for each pixel. The reference profile represents the non-flood backscattering behaviour of the study area and is used as the final reference image (Clement, Kilsby, and Moore 2018). The median is used instead of the mean because it is less influenced by extreme values and outliers that may be caused by the instrument error (Hostache, Matgen, and Wagner 2012). SAR imagery faces the challenge of speckle noise, which is caused by the random interference with multiple backscatters on the earth surface and is generally reduced before image interpretation due to its undesirable impacts on the image quality (Argenti et al. 2013; Singh and Shree 2016; Tavus et al. 2018). Multiple filters (e.g. Boxcar, Median, Lee, Lee Sigma, Refined Lee, and Gamma Map) are available in the SNAP Toolbox. Based on the initial tests, both the flood image and the final reference image have a median 5 × 5 pixel filter applied to remove speckle and smooth the images (Bioresita et al. 2018; Tian et al. 2017; Wang et al. 2019).

A difference map (*D*) is derived by applying the difference expression (Eq. (3-15)) to obtain the difference between the absolute backscattering values of the flood image (*F*) and that of the final reference image (*R*). The difference map is subsequently filtered based on the terrain characteristics. Areas with steeper slopes (i.e. a slope larger than 3°) are masked, aiming to remove pixels that are unlikely to be flooded but show changes in backscattering behavior due to the changes in angles of signal return from steep river banks, hydraulic structures, and hill slopes (Long, Fatoyinbo, and Policelli 2014). The Shuttle Radar Topography Mission (SRTM) (Farr et al. 2007) global digital elevation model at the resolution of 1 arc-second (approximately 30m) is available at GEE platform and is used to calculate slopes for the masking process.

$$D = |float(F)| - |float(R)| \tag{3-15}$$

Surviving pixels after the terrain filter are evaluated and classified based on the threshold criteria, which is set using the brightness variance and multiplicative coefficients (Long, Fatoyinbo, and Policelli 2014). It is expected that flooding in open surface will cause a negative difference due to the specular reflection of the radar signal by the water, while flooding in vegetated or urban areas will cause a positive difference due to multiple-bounce effects of buildings and partially submerged vegetation (Brunner et al. 2008; Clement, Kilsby, and Moore 2018; Long, Fatoyinbo, and Policelli 2014; Martinis and Rieke 2015). Within non-flood areas, no significant changes are expected in the backscattering values. Therefore, the following criteria are used to determine if the pixel (P_L) is inundated in open surface or if the pixel (P_H) is inundated in vegetated or urban areas.

$$P_L < \{lmean[D]\} - k_l \times \{lstdev[D]\} \tag{3-16}$$

$$P_H > \{lmean[D]\} + k_h \times \{lstdev[D]\} \tag{3-17}$$

where *lmean[D]* and *lstdev[D]* are the mean and standard deviation of the backscattering values of surviving pixels in the difference map, and k_l and k_h are the coefficients used to determine the thresholds. Values of k_l and k_h are not fixed and need to be calibrated for the study area based on several criteria, including the amount of remaining speckle and its coverage, visual interpretation of other available observational data, and identification of characteristic flooding patterns (Long, Fatoyinbo, and Policelli 2014). The optimal values for k_l and k_h are 1.5 and 2.5 in Long, Fatoyinbo, and Policelli (2014), but in our study, in order to minimize the effects of speckle noise in the flood

image, values for k_l and k_h are both set as 2.5, which basically leads to more conservative estimations of flood inundation areas. The derived flood area from the SAR imagery is presented in Figure 12.

Derived Flood Inundation Map

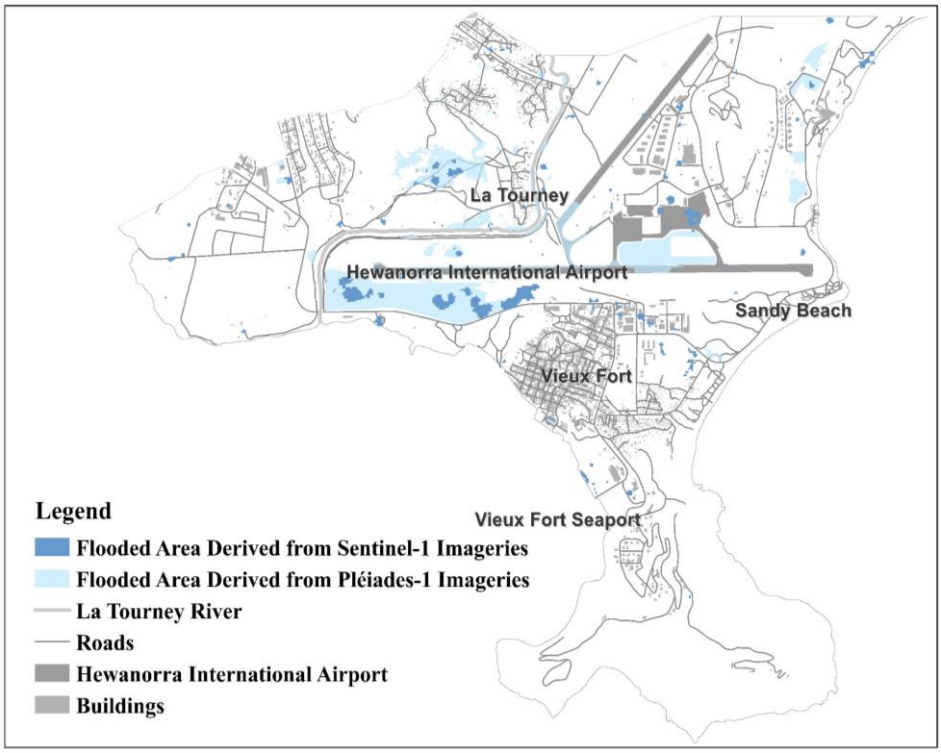

Figure 12. The flood map that is generated based on the combination of flood area derived from the Pléiades-1 and Sentinel-1 imagery.

As in Figure 12, the flood map used for model validation of LISFLOOD-FP is generated by combining flooded areas derived from Pléiades-1 and Sentinel-1 imagery. The resultant flood map provides valuable insights into flood conditions of the event; however, it is not expected to provide a comprehensive understanding of flood inundation area during the event for the following reasons: (i) available collections of Pléiades-1 and Sentinel-1 imagery were taken after the event, by which time the flood-induced water was largely receded; (ii) no flood-induced water was observed but only flood-related erosions, which are generally associated with severe flooding, were spotted in the Pléiades-1 imagery; (iii) unidentifiable areas exist in the Pléiades-1 imagery

due to the presence of clouds and high-density buildings in the communities; (iv) in order to minimize the impacts of speckle noise of Sentinel-1A imagery, pre-defined thresholds are set to have conservative estimations of flood areas.

3.3.4. Hydrodynamic Modelling

Flood extents and water depths are simulated using the latest version of the simplified two-dimensional raster-based hydrodynamic model LISFLOOD-FP (J. Neal et al. 2018). Studies have shown that the LISFLOOD-FP model has capabilities to simulate combined floods in coastal environments (Lewis et al. 2013; Skinner et al. 2015). The computational grid used within the model is of Cartesian coordinates (WGS 1984 UTM Zone 20N) with a horizontal resolution of 5m. Two subroutines are included to route river flows in sub-grid channels (J. Neal, Schumann, and Bates 2012) as well as rainfall-induced flows over elevated structures (Sampson et al. 2013). The model is forced with estimated coastal water levels, estimated river discharges, and rainfall inputs to simulate the combined effects of multiple flood factors in the event of Tropical Storm Matthew. Model validation is based on the derived flood map (Figure 12), and the resultant validated model is used to conduct sensitivity analysis, scenario analysis, and the probabilistic flood hazard analysis.

Model Setup

The model is set up to explore flood conditions caused by the Tropical Storm Matthew from 00:00 am AST on September 28, 2016 to 00:00 am AST on September 30, 2016. The application of the sub-grid LISFLOOD-FP model requires the specification of floodplain topography, bank-full river widths, river bank elevations, river bed elevations, river channel shapes, Manning's roughness coefficients for the channel and the floodplain, parameters required for the rainfall routing scheme, as well as boundary conditions (i.e. coastal sea levels, inflow hydrographs, and hyetographs).

As discussed in Section 3.3.1.1, a DSM is produced from the correlated point clouds obtained from a high-resolution orthoimagery taken in April 2018. The DSM was levelled to the local mean sea level and is used to present the floodplain topography, while the orthoimagery is used to identify

the bank-full river widths of La Tourney River, which increases from 5m at the upstream to approximately 15m at the river mouth. Spatially-varied Manning's roughness coefficients assigned different land cover types are presentedin Table1, and the Manning's n for the channel is set as 0.035 (Jetten 2016). No resources are available to calibrate the Manning's n for the channel or for floodplains.

No surveyed cross sections are available for the La Tourney River, but there are several images taken in non-flood conditions providing information about the characteristics of the river channel such as the channel shape and elevation difference between the water surface and the banks. J.C. Neal et al. (2015) have introduced a shape parameter to simulate river channels of different shapes (Eq. (3-18) and Eq. (3-19)).

$$w_{flow} = w_{full} \times \left(\frac{h_{flow}}{h_{full}}\right)^{1/s} \tag{3-18}$$

$$A_{flow} = w_{flow} h_{flow} \left(1 - \frac{1}{s+1}\right) \tag{3-19}$$

where w_{flow} is the flow width for a given water depth of h_{flow}, w_{full} is the bank-full width corresponding to the bank-full depth of the channel h_{full}, s is the shape parameter, and A_{flow} is the flow area. The parameter s can take any value above 0 and produce various channel geometry; for example, a value of one will lead to a triangular channel, a value of two represents a parabolic channel, while the channel will change towards trapezoidal then rectangular as the value of s increases (J.C. Neal et al. 2015). Figure 13 shows some example channel shapes as in J.C. Neal et al. (2015). Preliminary results indicate that the optimal value of s is 20 in this study. This value represents a similar cross-sectional shape as the river channel and leads to realistic flow patterns in preliminary simulations.

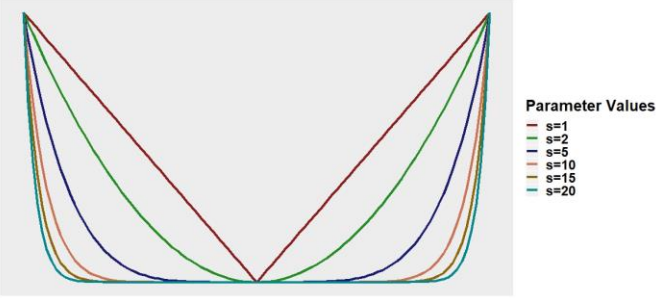

Figure 13. Example channel shapes.

Since abundant trees are grown at the river bank, the DSM did not capture the elevations of river banks but instead capture the elevations of trees, which are several meters higher than the banks. To obtain the river bank elevations, water surface elevations along the river are derived from the DSM, and the river banks are assumed to be 0.5m higher than the river surface under non-flood conditions. Bank-full river depths are calculated using the Equation (3-20) introduced in Jetten (2016). The river bed elevations are determined by subtracting bank-full river depth from the river bank elevations in surrounding pixels.

$$RiverDepth = a\left((1 - S) + c \times {D_{sea}}^{d}\right)^{e} \quad (3\text{-}20)$$

where S is the terrain slope (bounded 0-1), D_{sea} is the relative distance to the sea (bounded 0-1), and the scaling parameters are: a = 1.5, b = 0.5, c = 0.5, d = 0.1, e = 1.5. This equation shows that steeper slopes and/or closer to the sea will lead to the shallower river. Estimated river depths vary from 0.35m to 2.56m with an average value of 1.80m.

Instabilities arise when many two-dimensional hydrodynamic models attempting to model flow off elevated features such as buildings; introduction of the rainfall routing scheme enables LISFLOOD-FP to directly and stably simulate pluvial events by applying a relatively simple flood spreading algorithm than hydraulic equations (i.e. Eq. (2-1) and Eq. (2-2)) to shallow rainfall-induced flows (Sampson et al. 2013). Parameters required for the routing scheme are the specification of a depth threshold, a routing speed, and the Courant-Friedrichs-Lewy (CFL) coefficient. For cells where the water depth is below the user-defined threshold, the routing scheme will route water to the lowest neighbouring cell with a constant routing velocity (Sampson et al. 2013). As is in Sampson et al. (2013), the depth threshold is set as 5mm and the routing speed is 0.1m/s. A CFL coefficient of 0.4 is used to ensure model stability.

The soil map, which originates from 1966 soil map made by UWI Imperial College of Tropical Agriculture and is accessible in the Caribbean Handbook on Risk Information Management (CHARIM) website (http://charim-geonode.net/layers/geonode:soils_1), is utilized to estimate infiltration rate of the study area. Based on Hillel (1998), typical steady infiltration rates are assigned to each soil type and the spatially-uniform infiltration rate is calculated as 2.9×10^{-6} m/s. Evaporation and drainage capacity are not considered due to the lack of relevant data resources.

Minimum Flood Depth Threshold for Flooded Areas

A threshold of minimum depth should be defined to categorize the study area into flooded regions and non-flooded regions, which can help transfer the flood depth map to a binary map showing the locations of dry cells and wet cells. The choice of depth threshold is essential not only for the delineation of flood areas but also for decision-making during the development of the floodplain (Bharath and Elshorbagy 2018). Criteria for defining flood inundation areas used in the study are:

1) The runway, taxiway, and apron of the Hewanorra International Airport are considered to be flooded when the flood depth is greater than 0.001m since the movement of aircrafts would be affected whenever substances, such as standing water and snow, are present in these areas (Federal Aviation Administration 2019; Transport Canada 2019).

2) Other regions in the study area are considered as flooded when the depth of inundation is greater than 0.1m, which is the minimum depth threshold applied in many studies (Candela and Aronica 2017; Savage, Bates, et al. 2016; Savage, Pianosi, et al. 2016).

Model Validation and Verification Method

Model validation of the hydrodynamic model is based on the event of Tropical Storm Matthew. Combined effects of multiple flood factors during the event is simulated by using the combination of estimated coastal water levels, estimated river discharges, and observed precipitation as boundary conditions. As discussed in Section 3.3.1.4, the derived *mean* time series in Figure 7 represents the patterns of coastal water levels during the event and is used to force coastal boundaries. As discussed in Section 3.3.2.2.4, Table 8 presents the estimated daily runoff discharges when the rainfall inputs to the hydrologic model are provided by WRMA in Saint Lucia. Those daily runoff estimates are assumed to remain constant throughout the day and are utilized as the upstream inflow boundary conditions. As to the rainfall inputs to the hydrodynamic model, as discussed in Section 3.3.1.3, the 6-hour accumulated rainfall records provided by WRMA in Saint Lucia are utilized, and the derived time series of rainfall intensities are indicated in Figure 5.

The ability of the hydrodynamic model to simulate the spatial extents of flooding is evaluated by conducting a visual comparison between simulated flood extents and flood extents derived from

available satellite imagery. Comparison results are categorized into three types, namely, overestimation, underestimation, and correct simulation as flooding.

Sensitivity Analysis

There are many sources of uncertainties in the hydrodynamic modelling, and they can be categorized into three major types: model structures (e.g. different types of numerical equations and assumptions of the model), model parameters (e.g. roughness values for the channel and floodplain), and model inputs (e.g. channel and floodplain geometry, boundary conditions such as hyetographs, inflow hydrographs, and coastal water levels) (Liu and Merwade 2018; Teng et al. 2017). In this study, due to the lack of reliable hourly observations during the event, estimated boundary conditions are expected to be the major source of model uncertainties. As a result, the sensitivity analysis was conducted in this study not only to explore the individual effects of each flood factor as well as the combined effects of two flood factors, but also to identify and rank the influences of the three uncertain boundary conditions (i.e. rainfall input, upstream inflows, and coastal water levels) by perturbing one of them at a time. The configuration used in the model validation is considered as the reference model, and its simulation results are used as the base case for comparison with that of other configurations. Configurations of simulations conducted in sensitivity analysis are shown in Table 12. Simulation results from different model configurations are evaluated based on both the horizontal (flood extent) and vertical (water depth) flood estimates.

Scenario Analysis

Potential effects of wave run-up are investigated by considering the worst scenarios where the wave run-up is assumed to continuously affect the island along the coastline on top of storm tides with the heights of 0.5m, 1.5m, 2.5m, 3.5m, 4.5m, 5.5m, and 6m from 11:00 am AST on September 28, 2016 to 8:00 am AST on September 29, 2016. Simulations conducted in the scenario analysis and the corresponding boundary conditions are listed in Table 13. Evaluations are based on the comparison of simulation results obtained in scenarios of including wave run-up and excluding

wave run-up in regards to the differences in horizontal (flood extent) and vertical (water depth) flood estimates.

Probabilistic Flood Hazard Analysis

The combination of the uncertain coastal boundary conditions (estimated water levels and the uncertainty bounds; wave run-up is not included; Figure 7), rainfall inputs (time series of rainfall intensities derived from different sources; Figure 5), and upstream inflow conditions (estimated streamflow values and the uncertainty bounds associated with the selection of parameters as well as rainfall data sources; Table 8 and Table 9) leads to a total of 300 simulations (Table 14). Results of each simulation are evaluated by analyzing the maximum flood extent and maximum flood depths over the course of simulation for each pixel. The probability of inundation for each pixel is defined as Equation (3-21), and a probabilistic flood hazard map is accordingly derived in order to minimize the impacts of uncertain boundary conditions, identify the high-risk regions, and provide insights into local flood management.

$$P_i = \frac{N_i}{N_T} \tag{3-21}$$

where P_i is the probability of inundation calculated for the *i*-th pixel, N_i is the number of times when the *i*-th pixel is inundated (maximum flood depth $\geq$ 0.001m in the areas of runway, taxiway, and aprons, and maximum flood depth $\geq$ 0.1m in other areas), and N_T is the total number of simulations (i.e. 300).

Table 12. Characteristics of input data for the LISFLOOD-FP model in model validation and sensitivity analysis.

Simulation Number	Purpose	Coastal Boundary Conditions	Rainfall Input Data	Upstream Inflow Condition
R0 (Reference Model)	Model Validation	Mean	Rainfall Gauge (WRMA)	Mean (Rainfall input of HYMOD: data from WRMA)
R1	$SA_{Individual}$[1]	Mean	/	/
R2	$SA_{Individual}$[1]	/	/	Mean (Rainfall input of HYMOD: data from WRMA)
R3	$SA_{Individual}$[1]	Mean	/	Mean (Rainfall input of HYMOD: data from WRMA)
R4	$SA_{Individual}$[1]	/	Rainfall Gauge (WRMA)	/
R5	$SA_{Individual}$[1]	Mean	Rainfall Gauge (WRMA)	/

R6	$SA_{Coastal}^2$	Mean + σ	Rainfall Gauge (WRMA)	Mean (Rainfall input of HYMOD: data from WRMA)
R7	$SA_{Coastal}^2$	Mean + 2σ	Rainfall Gauge (WRMA)	Mean (Rainfall input of HYMOD: data from WRMA)
R8	$SA_{Coastal}^2$	Mean - σ	Rainfall Gauge (WRMA)	Mean (Rainfall input of HYMOD: data from WRMA)
R9	$SA_{Coastal}^2$	Mean - 2σ	Rainfall Gauge (WRMA)	Mean (Rainfall input of HYMOD: data from WRMA)
R10	$SA_{Rainfall}^3$	Mean	Rainfall Gauge (DS3505)	Mean (Rainfall input of HYMOD: data from WRMA)
R11	$SA_{Rainfall}^3$	Mean	ERA5	Mean (Rainfall input of HYMOD: data from WRMA)
R12	$SA_{Rainfall}^3$	Mean	MERRA-2	Mean (Rainfall input of HYMOD: data from WRMA)
R13	$SA_{Rainfall}^3$	Mean	TMPA-3B42 V7	Mean (Rainfall input of HYMOD: data from WRMA)
R14	$SA_{Rainfall}^3$	Mean	IMERGHH V05	Mean (Rainfall input of HYMOD: data from WRMA)

R15	$SA_{Inflow\text{-}Model}$[4]	Mean	Rainfall Gauge (WRMA)	Mean + σ (Rainfall input of HYMOD: data from WRMA)
R16	$SA_{Inflow\text{-}Model}$[4]	Mean	Rainfall Gauge (WRMA)	Mean + 2σ (Rainfall input of HYMOD: data from WRMA)
R17	$SA_{Inflow\text{-}Model}$[4]	Mean	Rainfall Gauge (WRMA)	Mean – σ (Rainfall input of HYMOD: data from WRMA)
R18	$SA_{Inflow\text{-}Model}$[4]	Mean	Rainfall Gauge (WRMA)	Mean - 2σ (Rainfall input of HYMOD: data from WRMA)
R19	$SA_{Inflow\text{-}Rainfall}$[5]	Mean	Rainfall Gauge (WRMA)	Mean (Rainfall input of HYMOD: data from DS3505 dataset)
R20	$SA_{Inflow\text{-}Rainfall}$[5]	Mean	Rainfall Gauge (WRMA)	Mean (Rainfall input of HYMOD: data from ERA5 dataset)

R21	$SA_{Inflow\text{-}Rainfall}$[5]	Mean	Rainfall Gauge (WRMA)	Mean (Rainfall input of HYMOD: data from MERRA-2)
R22	$SA_{Inflow\text{-}Rainfall}$[5]	Mean	Rainfall Gauge (WRMA)	Mean (Rainfall input of HYMOD: data from TMPA-3B42 V7)
R23	$SA_{Inflow\text{-}Rainfall}$[5]	Mean	Rainfall Gauge (WRMA)	Mean (Rainfall input of HYMOD: data from IMERGHH V05)

Note: The purposes of sensitivity analysis are to explore the individual effects of each flood factor[1] as well as to investigate the model's sensitivity to coastal water levels[2], rainfall input data[3], and upstream inflow with its uncertainty associated with the selection of HYMOD's parameters[4] and rainfall input data[5].

Table 13. Characteristics of input data for the LISFLOOD-FP model in the scenario analysis of including wave run-up.

Simulation Number	Reference Model	Coastal Boundary Conditions	Rainfall Input Data	Upstream Inflow Condition
W1	R1	Mean + Wave run-up: 0.5m	/	/
W2	R1	Mean + Wave run-up: 1.5m	/	/
W3	R1	Mean + Wave run-up: 2.5m	/	/
W4	R1	Mean + Wave run-up: 3.5m	/	/
W5	R1	Mean + Wave run-up: 4.5m	/	/

W6	R1	Mean + Wave run-up: 5.5m	/	/
W7	R1	Mean + Wave run-up: 6m	/	/
W8	R5	Mean + Wave run-up: 0.5m	/	Mean (Rainfall input of HYMOD: data from WRMA)
W9	R5	Mean + Wave run-up: 1.5m	/	Mean (Rainfall input of HYMOD: data from WRMA)
W10	R5	Mean + Wave run-up: 2.5m	/	Mean (Rainfall input of HYMOD: data from WRMA)
W11	R5	Mean + Wave run-up: 3.5m	/	Mean (Rainfall input of HYMOD: data from WRMA)

W12	R5	Mean + Wave run-up: 4.5m	/	Mean (Rainfall input of HYMOD: data from WRMA)
W13	R5	Mean + Wave run-up: 5.5m	/	Mean (Rainfall input of HYMOD: data from WRMA)
W14	R5	Mean + Wave run-up: 6m	/	Mean (Rainfall input of HYMOD: data from WRMA)
W15	R0	Mean + Wave run-up: 0.5m	Rainfall Gauge (WRMA)	Mean (Rainfall input of HYMOD: data from WRMA)
W16	R0	Mean + Wave run-up: 1.5m	Rainfall Gauge (WRMA)	Mean (Rainfall input of HYMOD: data from WRMA)
W17	R0	Mean + Wave run-up: 2.5m	Rainfall Gauge (WRMA)	Mean (Rainfall input of HYMOD: data from WRMA)

W18	R0	Mean + Wave run-up: 3.5m	Rainfall Gauge (WRMA)	Mean (Rainfall input of HYMOD: data from WRMA)
W19	R0	Mean + Wave run-up: 4.5m	Rainfall Gauge (WRMA)	Mean (Rainfall input of HYMOD: data from WRMA)
W20	R0	Mean + Wave run-up: 5.5m	Rainfall Gauge (WRMA)	Mean (Rainfall input of HYMOD: data from WRMA)
W21	R0	Mean + Wave run-up: 6m	Rainfall Gauge (WRMA)	Mean (Rainfall input of HYMOD: data from WRMA)

Table 14. Descriptions of boundary conditions used for the LISFLOOD-FP model in the probabilistic flood hazard analysis.

Boundary Condition Type	Characteristics	Number of Boundary Conditions
Coastal Water Levels	Five composite two-day time series of water levels (i.e. *mean, mean+σ, mean+2σ, mean-σ,* and *mean-2σ* values calculated for each hour)	5
Rainfall Inputs	Time series of rainfall intensities derived from six different sources: WRMA in Saint Lucia, DS3505 dataset, ERA5, MERRA-2, TMPA-3B42 V7, and IMERGHH V05 product	6
Upstream Inflows	Estimated runoff from the calibrated HYMOD model and uncertainty bounds associated with the selection of parameters and rainfall input data	10
		Total Number of Simulations = 5 × 6 × 10 = 300

3.4. Results and Discussions

3.4.1. Model Performance and Validation

Simulation R0, the reference model, is utilized for model validation as well as the analysis of model performance. In this study, the runway, taxiway, and apron of the Hewanorra International Airport are considered to be flooded when the flood depth is greater than 0.001m, while other regions are considered as flooded when the flood depth is greater than 0.1m. During the event of Tropical Storm Matthew (from 00:00 am AST on September 28, 2016 to 00:00 am AST on September 30, 2016), the maximum flood extent is 2.6018 km^2, which accounts for 27.244% of the total area, and the maximum flood depth for each pixel ranges from 0.01m to 10.202m (Figure

14). Maximum flood depths in the river channel vary from 0.3m to 3m, while for the floodplain is mostly less than 2m. Since topographic data used in this study also captures the elevations of trees and there are huge elevation differences between the trees and the ground, there are some pixels with low elevations surrounded by pixels with much higher elevations, resulting in significant accumulation of water and unrealistic extreme values of flood depths (i.e. flood depth greater than 2m). Those pixels are mostly located in the communities in the north and west of the study area, which are not the major areas of interest in this study.

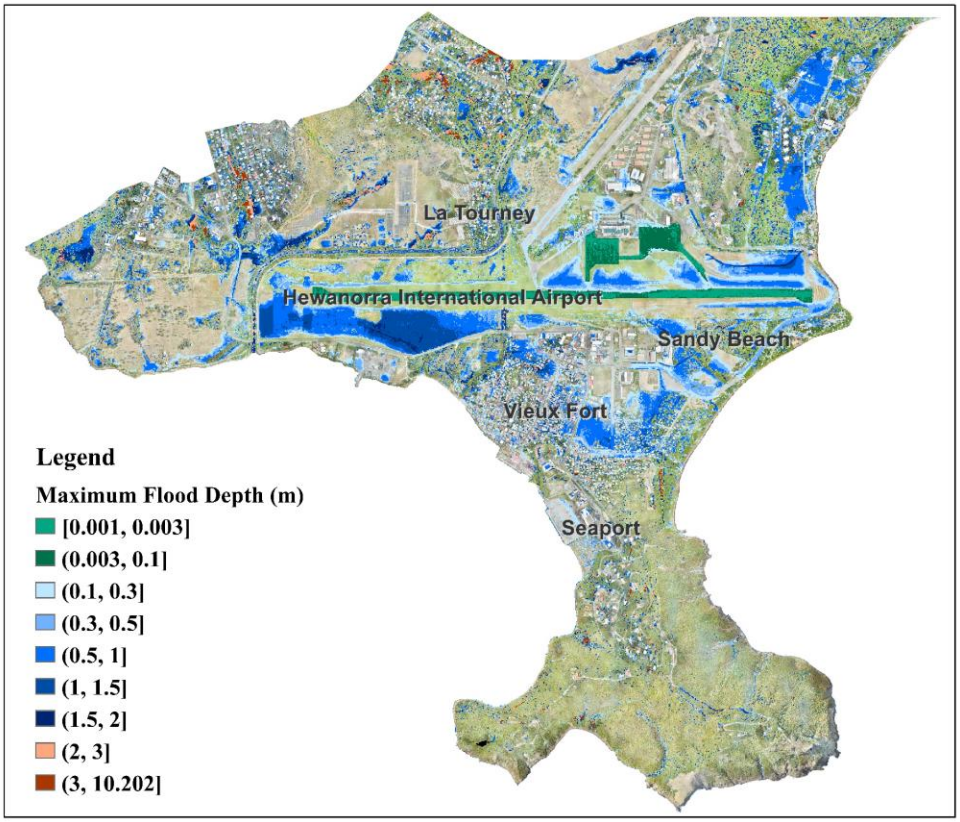

Figure 14. Map showing the maximum flood depth for each pixel over the course of the simulation R0 in the event of Tropical Storm Matthew.

Despite the significant role of Hewanorra International Airport in the tourism and local economy, it is located in the low-lying area and is at high risk of flooding. Figure 15 presents the maximum flood depth for each pixel within the airport boundary over the course of simulation R0. Most of the airport facilities such as the terminal building, cargo shed, fire station, and the control tower is not likely to be impacted by flood water. Parking areas are expected to be partially flooded with maximum flood depth ranging from 0.3m to 0.5m, and therefore, cars in the parking lot may be

swamped by the flood water. Maximum flood depths for the runway, taxiway, and apron vary from 0.001m to 0.3m, indicating the need for timely clearing of flood water during the event. Otherwise, operations of airplanes would be interrupted, leading to disruptions of regional and international transportation. Flood conditions are the most severe in the grassland (i.e. flood depth ranging from 0.3m to 3m) near the western end of runway due to the low elevations; however, such severe flood can lead to enormous erosion but limited impacts to the operations of the airport.

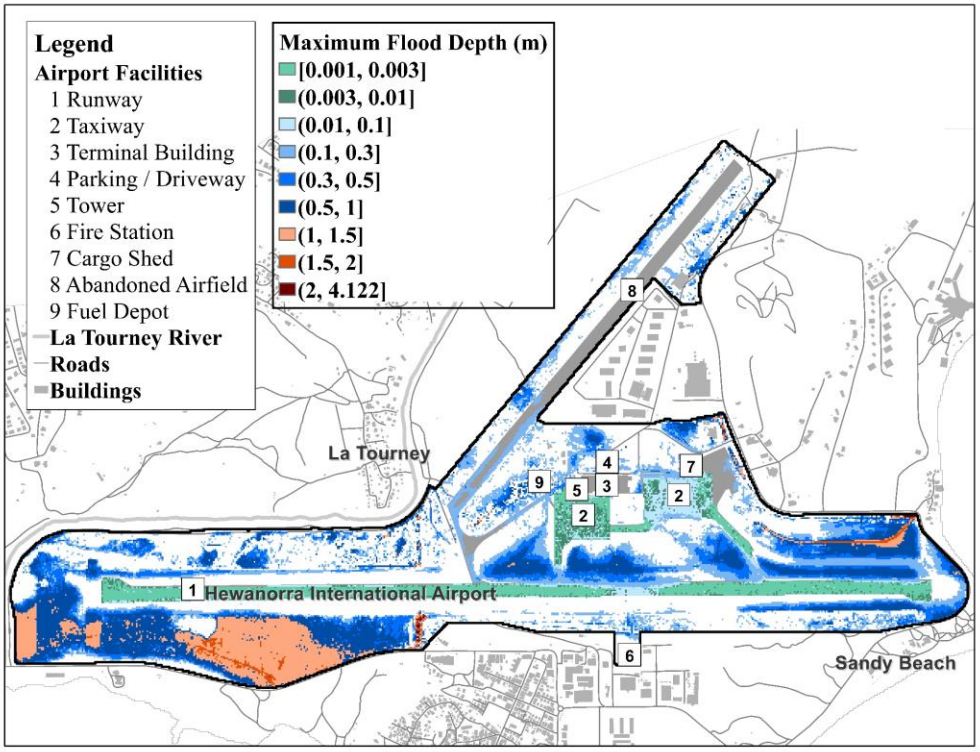

Figure 15. Map showing the maximum flood depth for each pixel over the course of the simulation R0 in the event of Tropical Storm Matthew within boundaries of Hewanorra International Airport.

Apart from the Hewanorra International Airport, areas affected by the flooding include the two human settlements (the town of La Tourney and Vieux Fort), the Vieux Fort Seaport, and coastal agricultural lands. Within the seaport boundary, estimated flood depths for flooded areas are mostly less than 0.2m, which is not likely to interrupt seaport operations. Agricultural areas are expected to be flooded with maximum flood depths ranging from 0.5m to 1m, which is consistent with the statement that at least 80% of the farms incurred losses during the event (Stewart 2017). Although sections of the major highway are estimated to be flooded with maximum flood depths less than 0.5m and the settlements are expected to experience flooding with maximum flood depths

varying from 0.1m to 2m, there may be significant overestimations in these regions since the hydrodynamic model does not consider the drainage systems, which are essential for flood water removal in these areas during the event. Inclusion of drainage systems, higher resolution of the model, and topographic data that excludes elevations of trees are needed to obtain more realistic and reliable simulation results in the environments with a high intensity of buildings and trees.

In the model validation, pixels with the maximum flood depth that is higher than the pre-defined threshold are all considered as flooded and will be compared with the flood map derived from the available satellite imageries. Comparison results are grouped into three types and are presented in Figure 16. Discussions on the three categories are as follows.

1) Overestimation: Overestimation indicates the pixels that are simulated as flooded but not shown as flooded in the derived flood map. A major reason for the overestimation is that the derived flood map cannot provide comprehensive information on the flood extents during the event but only indicates the areas that have potentially been severely flooded.

2) Underestimation: Underestimation indicates the pixels that are not simulated as flooded but are shown as flooded in the derived flood map. The topographic data was generated from the orthoimagery taken in 2018, while the Tropical Storm Matthew occurred in 2016. The land use change, such as the newly-developed structures near the town of La Tourney, is the major reason for the underestimation. Besides, to derive the flood map, eroded areas observed in Pléiades-1 imagery are considered to were severely flooded, but those erosions are not necessarily caused by flooding.

3) Correct simulation as flooding: Correct simulation as flooding indicates the pixels that are simulated as flooded and are also shown as flooded in the derived flood map. The results of simulation R0 indicate that the hydrodynamic model can accurately capture the severe flooding in the grasslands near the runway and in agricultural areas.

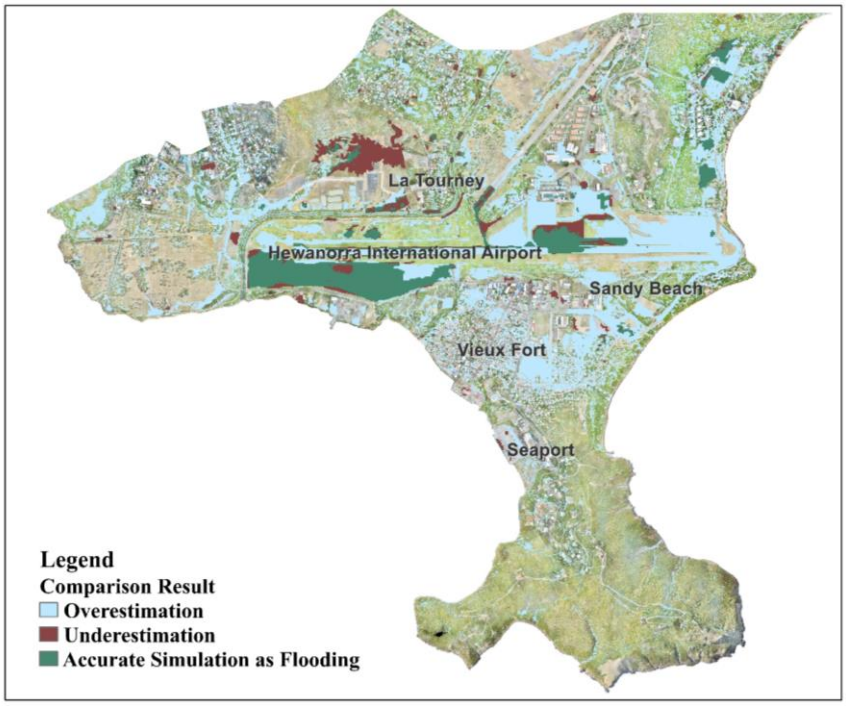

Figure 16. Comparison of the maximum flood extent from the model and flood extents derived from the satellite imageries.

3.4.2. Sensitivity Analysis

Due to the lack of reliable hourly observational data, major assumptions were made when generating boundary conditions for the hydrodynamic model. Influences of uncertain boundary conditions (i.e. coastal water levels, river discharges, and hyetographs) are explored in the sensitivity analysis by considering the uncertainty bounds of the three types of input data. Simulation results are analyzed in detail in this section.

Individual Effects of Flood Factors

Simulations R1~ R5 are conducted to investigate the individual effects of each flood factor and the combined effects of two flood factors, aiming to understand flood mechanisms in the event of Tropical Storm Matthew. Corresponding boundary conditions are presented in Table 12.

- **Effects of Coastal Water Levels**

Individual effects of coastal water levels in the event of Tropical Storm Matthew are explored in simulation R1. Wave run-up is not considered. The maximum flood depth for each pixel over the course of the simulation is presented in Figure 17. Backwater effects from the ocean are expected in La Tourney river channel, indicating the potential interactions between high river flows and high sea levels in extreme events. No coastal flooding is caused along the coastline, showing that the estimated sea levels during the event are not significantly high to induce flood at the coast.

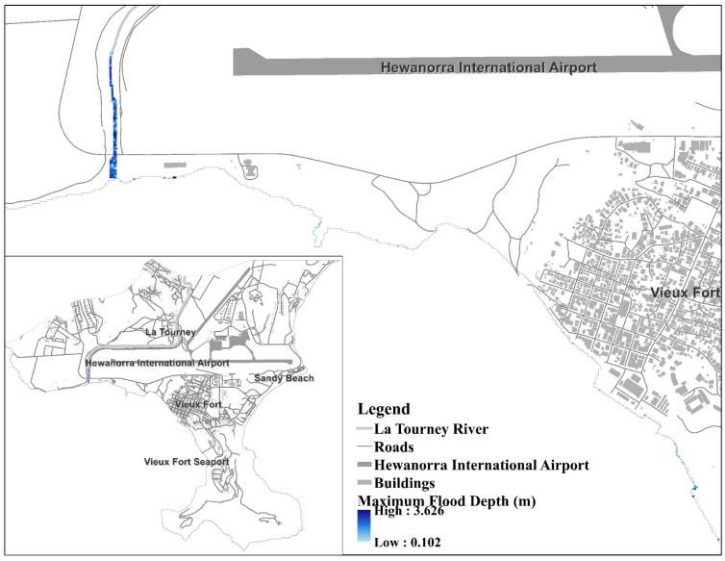

Figure 17. Map showing the maximum flood depth for each pixel over the course of the simulation R1 in the event of Tropical Storm Matthew.

- **Effects of River Discharges and Coastal Water Levels**

Based on the maximum flood depth conditions of simulations R2 and R3 (Figure 18), major conclusions are as follows: 1) closed coastal boundaries in simulation R2 cause significant water accumulations at the river mouth and at the river floodplain, thus leading to unrealistic flood estimations; 2) river discharges during the events are not expected to cause overbank flows along the channel; 3) there are no estimated floods in simulation R3, indicating that the inclusion of coastal water levels majorly enables river flows discharging into the sea while the interactions between river flows and coastal water levels are not likely to induce floods in the floodplain.

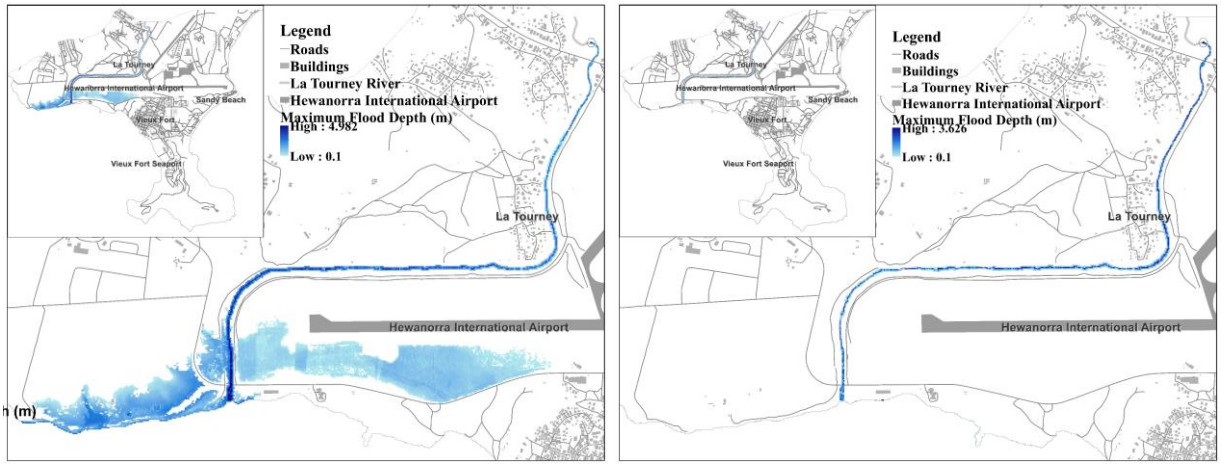

Figure 18. Map showing the maximum flood depth for each pixel over the course of the simulation R2 (left) and simulation R3 (right) in the event of Tropical Storm Matthew.

However, the assumption of constant river discharge throughout the day can lead to significant underestimation of flood estimates. The catchment has a quick response to rainfall, and considering the rainfall patterns, hourly river discharges have the potential to dramatically increase when the rainfall volume dramatically increases. Moreover, if peak river discharges occur simultaneously with the peak sea levels, resultant flooding conditions can be much more severe.

- **Effects of Rainfall and Coastal Water Levels**

Comparing the maximum flood depth conditions obtained from simulation R1 (Figure 17), simulations R2 and R3 (Figure 18) as well as R4 and R5 (Figure 19) with that of the reference model R0 (Figure 14), major conclusions are as follows: 1) closed coastal boundaries in simulation R4 cause significant water accumulations along the coastline, thus resulting in unreasonable flood estimations; 2) including coastal water levels as in simulations R5 leads to more reliable flood estimates since it enables the rainfall-induced water draining into the sea; 3) it is determined that rainfall is the major contributor of flooding in the event of Tropical Storm Matthew because simulations R0 and R5 yield similar simulated flood patterns, the results of simulation R3 indicate that river discharges do not lead to overbank floods, and the results of simulation R1 show that coastal water levels during the event are not likely to incur flood along the coastline or the river.

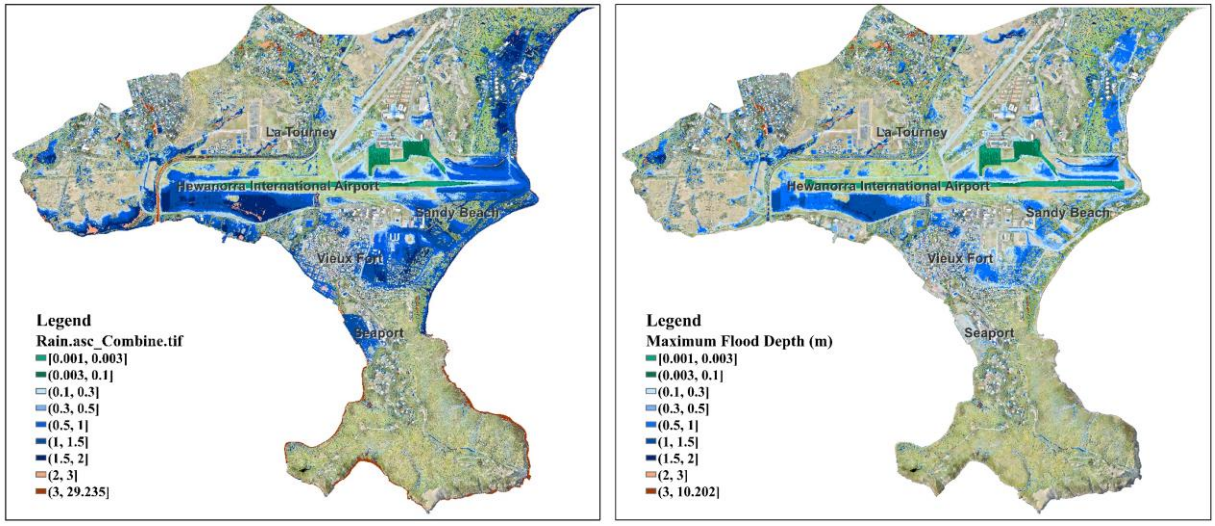

Figure 19. Map showing the maximum flood depth for each pixel over the course of the simulation R4 (left) and simulation R5 (right) in the event of Tropical Storm Matthew.

Effects of Uncertain Rainfall Patterns

Due to the lack of knowledge in hourly rainfall patterns as well as the inconsistency of rainfall data from different sources, time series of rainfall intensities derived from different datasets and products are utilized as rainfall inputs to the LISFLOOD-FP model in the sensitivity analysis to investigate model uncertainties associated with rainfall volume and temporal distributions of rainfall. For this purpose, simulation R10~R14 are conducted. As in Table 12, coastal and riverine boundary conditions for R10~R14 are the same as that of the reference model R0. Selected sources of rainfall data for simulations R0, R10, R11, R12, R13, and R14 are 6-hourly accumulated rainfall gauge data provided by WRMA, 6-hourly accumulated rainfall gauge data from the DS3505 dataset, hourly rainfall data from ERA5, hourly rainfall data from MERRA-2, three-hourly rainfall data from the TMPA-3B42 V7 product, and half-hourly rainfall data from the IMERGHH V05 product, respectively. 6-hourly data and 3-hourly data are transformed to hourly data by assuming that the rainfall intensities are constant within every 6 hours and 3 hours, respectively. The resultant hyetographs are presented in Figure 5.

Figure 20 shows the spatial patterns of maximum flood depth for each pixel over the course of simulation when using rainfall inputs derived from different sources, and Figure 21 presents the

temporal patterns of flood inundation area throughout the event. Characteristics of different rainfall inputs and corresponding flood estimations are summarized in Table 15. Since rainfall is the major contributor to flooding in the event of Tropical Storm Matthew, spatial patterns of floods are strongly dependent on the characteristics of rainfall volume and temporal distributions of rainfall intensities. Using rainfall data with higher total rainfall volume leads to larger flood-impacted areas, higher flood depths for inundated pixels, and higher values of maximum flood inundation area. However, the runway, taxiway, and apron of the Hewanorra International Airport as well as coastal lowland agriculture areas are at risk of flooding in all simulations, indicating the need for further study in regards to the flood risk of the airport in extreme events. In addition, temporal patterns of flood inundation area are related to the temporal distributions of rainfall intensities. The increase of rainfall intensities causes the increase of flood inundation area, the time for the peak rainfall intensity affects the time reaching the maximum flooded area, and the flood would start receding when the rainfall intensity drops. Also, considering that the flood inundation estimations are sensitive to the dramatic increases in rainfall intensities, the assumption that the rainfall intensities are constant within every 6 hours and 3 hours when utilizing the 6-hourly and 3-hourly rainfall data could lead to underestimations in the flooded area since there may be significant variations in rainfall intensities within each time interval. Therefore, reliable hourly or sub-hourly rainfall patterns would be needed to obtain more accurate flood estimations for the event of Tropical Storm Matthew.

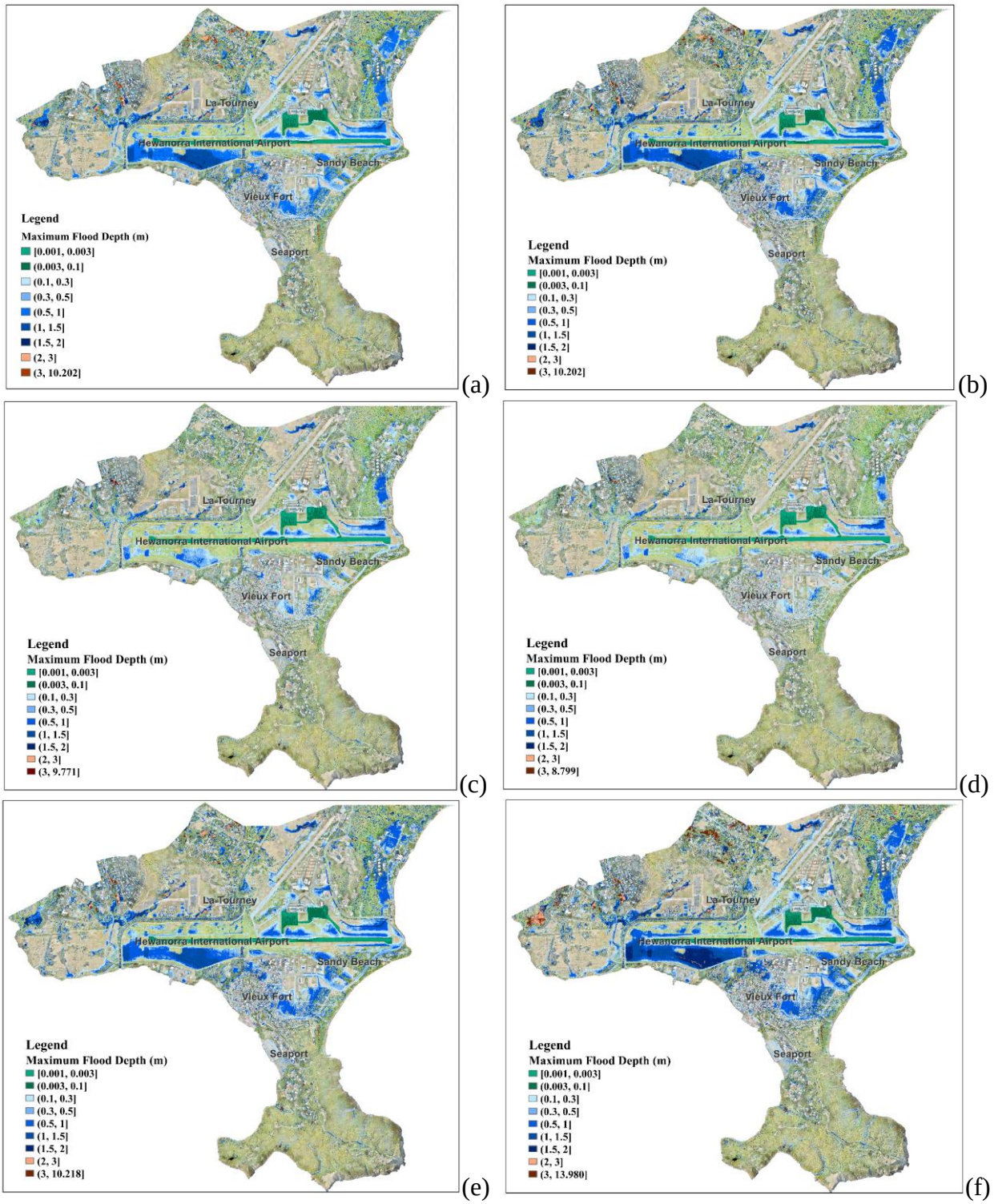

Figure 20. Maps showing the maximum flood depth for each pixel over the course of simulations when the rainfall input is derived from (a) rainfall gauge (WRMA), (b) rainfall gauge (DS3505), (c) ERA5, (d) MERRA-2, (e) TMPA-3B42 V7, and (f) IMERGHH V05.

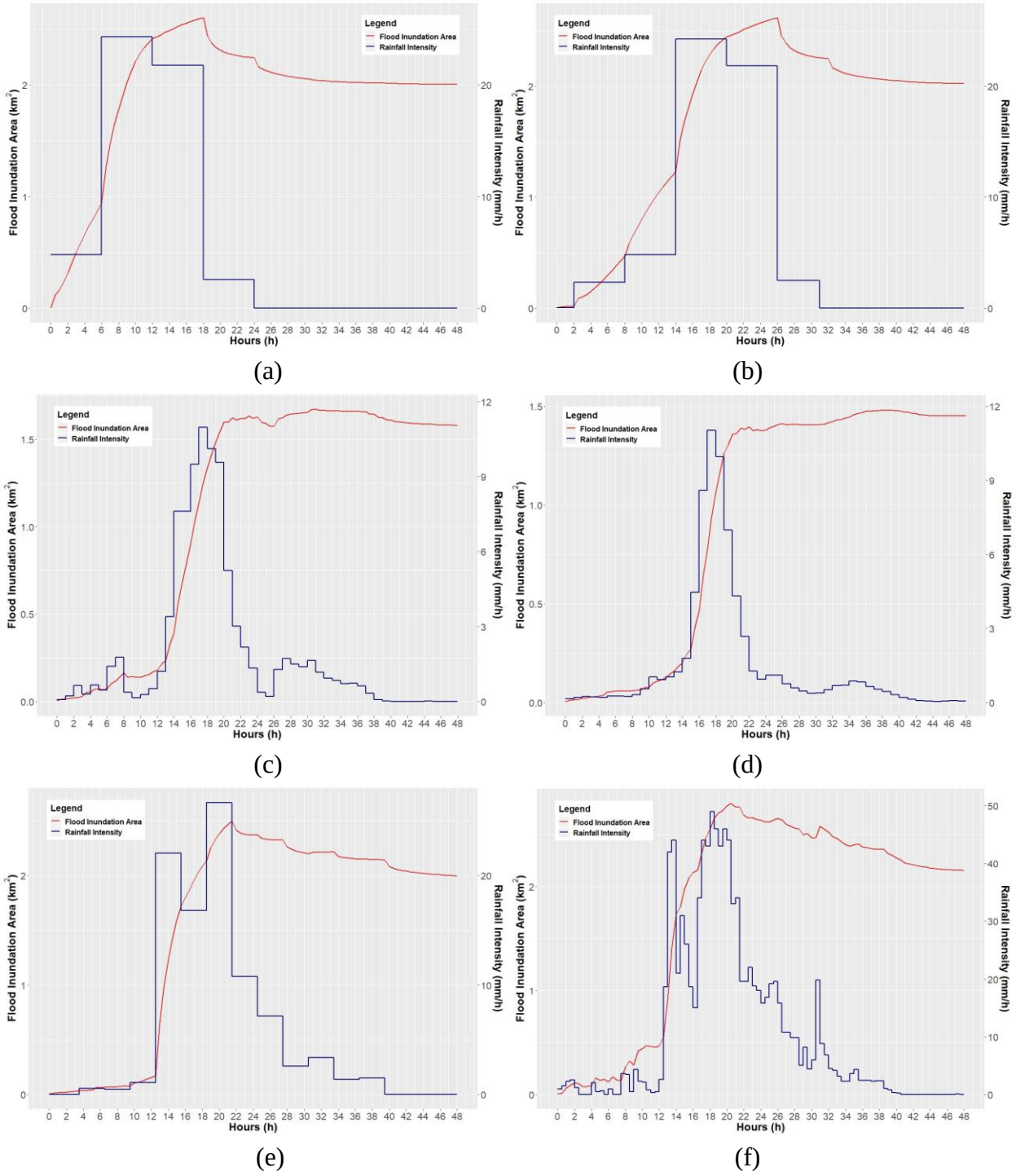

Figure 21. Graphs showing the flood inundation area over the course of simulations when the rainfall input is from (a) rainfall gauge (WRMA), (b) rainfall gauge (DS3505), (c) ERA5, (d) MERRA-2, (e) TMPA-3B42 V7, and (f) IMERGHH V05.

Table 15. Characteristics of rainfall derived from different sources and corresponding flood inundation estimations.

Source of Rainfall Data	Rainfall Characteristics			Flood Inundation	
	Total Rainfall Volume (mm)	Differences in Total Rainfall Volume (%)	Peak Rainfall Intensity (mm/h)	Maximum Flooded Area over the Course of Simulation (km^2)	Differences in the Maximum Flooded Area (%)
Rainfall Gauge (WRMA)	320.7	/	24.317	2.6018	/
Rainfall Gauge (DS3505)	332.11	3.56	24.257	2.6179	0.617
ERA5	92.08	-71.29	10.983	1.6724	-35.721
MERRA-2	70.06	-78.15	11.010	1.4812	-43.072
TMPA-3B42 V7	283.05	-11.74	26.680	2.4994	-3.938
IMERGHH V05	495.66	54.56	49.000	2.7999	7.612

Note: The formula for calculating the differences in total rainfall is (total rainfall from other sources – total rainfall from the WRMA rainfall gauge)/total rainfall from the WRMA rainfall gauge), and the formula for calculating the differences in the maximum flooded area is (maximum flooded area when using rainfall inputs from other sources – maximum flooded area when using rainfall inputs from the WRMA rainfall gauge)/maximum flooded area when using rainfall inputs from the WRMA rainfall gauge.

Effects of Uncertain Coastal Boundary Conditions

Since there is no tide gauge in the study area, time series of coastal water levels of tide gauges in surrounding islands are utilized. Extreme sea levels for Saint Lucia proposed in the study of Monioudi et al. (2018) are used to rescale the observed time series in order to generate possible patterns of sea levels during the event. In total, there are 3 time series of observed sea levels and 21 time series of rescaled sea levels, representing the potential effects of astronomical tides, the episodic water level rise due to storm surges, as well as wave setup. Based on these 24 time series,

values of *mean* and *standard deviation (σ)* can be calculated for each hour during the simulated period. The *mean* time series is assumed as the *true* time series of sea levels, and to investigate the effects of uncertainties in the estimations of coastal water levels, *mean+σ*, *mean+2σ*, *mean-σ*, and *mean-2σ* time series are regarded as the uncertainty bounds in sea levels and utilized as the coastal boundary conditions for the LISFLOOD-FP model (Figure 7). Accordingly, simulation R6~R9 were conducted. As in Table 12, pluvial and riverine boundary conditions for R6~R9 are the same as that of the reference model R0, but the coastal boundary conditions are different to explore the effects of uncertainties in sea levels.

As in Table 16, uncertainties in the estimations of coastal water levels have limited impacts on the maximum flooded area. The major reason is that, when considering uncertainty bounds, the individual contribution of coastal water levels to flooding remain insignificant, indicating unlikely occurrences of overbank or coastal floods as discussed in Section 3.4.2.1.1.

Table 16. Flood area estimations when considering the uncertainties in coastal water levels.

Time Series of Coastal Water Levels	Flood Inundation Condition	
	Maximum Flooded Area over the Course of Simulation (km^2)	Differences in Maximum Flooded Area (%)
Mean	2.6018	/
Mean + σ	2.6023	0.019
Mean + 2σ	2.6032	0.055
Mean - σ	2.6013	-0.019
Mean - 2σ	2.5998	-0.079

Note: The formula for calculating the differences in the maximum flooded area is (maximum flooded area when using *mean+σ/mean+2σ/mean-σ/mean-2σ* time series – maximum flooded area when using *mean* time series)/maximum flooded area when using *mean* time series.

Effects of Uncertain River Discharges

A hydrological model HYMOD was set up and calibrated to simulate daily river discharges of La Tourney River. Uncertainties in the runoff estimations majorly come from the selection of model parameters and the sources of rainfall inputs.

- **Uncertainties associated with the Selection of Model Parameters**

As discussed in Section 3.3.2.2.3, 1000 optimal parameter sets were derived by using the leave-three-out cross-validation method, thus leading to 1000 simulation results. From these results, values of *mean* and *standard deviation (σ)* can be calculated for each day. Time series of *mean* is assumed to be the *true* time series of river flows, while *mean+2σ*, *mean+σ*, *mean-σ*, and *mean-2σ* time series were regarded as the uncertainty bounds of runoff estimations. These uncertainty bounds (Table 8) are utilized as upstream inflow boundary conditions for the hydrodynamic model in order to investigate the effects of uncertainties associated with the selection of model parameters. Simulation R15~R18 were accordingly conducted. As in Table 12, pluvial and coastal boundary conditions for R15~R18 are the same as that of the reference model R0, but the upstream inflow boundary conditions are different.

As in Table 17, uncertainties in river flow estimations associated with the selection of model parameters have limited impacts on the maximum flooded area. The major reason is that, when considering uncertainties, the individual contribution of river discharges to flooding remain insignificant due to the unlikely occurrence of overbank floods as discussed in Section 3.4.2.1.2.

Table 17. Flood area estimations when considering the uncertainties in river flow estimations associated with the selection of model parameters.

Time Series of Simulated River Inflows	Flood Inundation Condition	
	Maximum Flooded Area (km^2)	Differences in Maximum Flooded Area (%)
Mean	2.6018	/
Mean + σ	2.6028	0.038

Mean + 2σ	2.6039	0.079
Mean - σ	2.6004	-0.056
Mean - 2σ	2.5990	-0.109

Note: The formula for calculating the differences in the maximum flooded area is (maximum flooded area when using *mean+σ/mean+2σ/mean-σ/mean-2σ* time series – maximum flooded area when using *mean* time series)/maximum flooded area when using *mean* time series.

- **Uncertainties associated with the Source of Rainfall Data**

The HYMOD model was set up and calibrated based on the rainfall inputs derived from the gauge data provided by WRMA. Considering that different sources of rainfall data lead to different daily rainfall volume (Table 2), the effects of uncertainties associated with the selection of rainfall data sources should be considered. For this purpose, simulations R19~R23 were conducted. As in Table 12, pluvial and coastal boundary conditions for R19~R23 are the same as that of the reference model R0, but the upstream inflow boundary conditions are the simulated river flows using rainfall data derived from the DS3505 dataset, ERA5, MERRA-2, TMPA-3B42 V7, and IMERGHH V05, respectively (Table 9).

As in Table 18, the effects of uncertainties in river flows associated with the selection of rainfall data have insignificant impacts on the flood area estimations. The major reason is that, regardless of the rainfall input sources to the HYMOD model, resultant river discharges are not likely to cause overbank floods and accordingly have limited contributions to the flooding in the event of Tropical Storm Matthew as discussed in Section 3.4.2.1.2.

Table 18. Flood area estimations when considering the uncertainties in upstream river inflows associated with the sources of rainfall data used in the HYMOD model.

Source of Rainfall Data	Flood Inundation Condition	
	Maximum Flooded Area (km^2)	Differences in Maximum Flooded Area (%)
Rainfall Gauge (WRMA)	2.6018	/
Rainfall Gauge (DS3505)	2.6006	-0.045

ERA5	2.5976	-0.163
MERRA-2	2.5975	-0.164
TMPA-3B42 V7	2.5998	-0.076
IMERGHH V05	2.6028	0.038

Note: The formula for calculating the differences in the maximum flooded area is (maximum flooded area when using rainfall inputs from other sources – maximum flooded area when using rainfall inputs from the WRMA rainfall gauge)/maximum flooded area when using rainfall inputs from the WRMA rainfall gauge.

3.4.3. Scenario Analysis

As discussed in Section 3.3.1.4, coastal boundary conditions used for model validation (simulation R0) and sensitivity analysis (simulation R1~R23) do not consider the effects of wave run-up, and the results indicate that the contribution of estimated sea levels to flooding is limited. However, as in Table 4, heights of wave run-up are significantly higher than storm surges in Saint Lucia, indicating that the effects of wave run-up can be dominant in extreme events and induce severe flooding in the study area. The scenario analysis, as a result, is conducted to explore the potential impacts of wave run-up in the event of Tropical Storm Matthew. Due to the lack of knowledge in temporal patterns of wave run-up, the worst scenarios are considered by adding 0.5m, 1.5m, 2.5m, 3.5m, 4.5m, 5.5m, and 6m to the *mean* time series of sea levels from 11:00 am AST on September 28, 2016 to 8:00 am AST on September 29, 2016. The resultant time series of coastal water levels, as in Figure 8, are used as the coastal boundary conditions to conduct simulations W1-W28. Results are analyzed based on the comparisons with their corresponding reference models that have the same pluvial and riverine boundary conditions but do not consider the effects of wave run-up (Table 13). Overestimations are expected since the worst scenarios are considered in the scenario analysis; however, the results provide insights on areas that are at high risk of temporary floods caused by high waves.

Individual Effects of Coastal Water Levels

Simulations W1~W7 are conducted to explore individual effects of coastal boundary conditions when considering the wave run-up. Table 19 presents the flood area estimations for simulation R0

and W1~W7, and Figure 22 shows the spatial patterns of maximum flood depth for each pixel over the course of simulations in scenarios of including wave run-up heights in the coastal boundary conditions. The results indicate the significant potential impacts of wave run-up. When the wave run-up height is 0.5m, greater backwater effects are observed in the La Tourney River. When the wave run-up height is 1.5m, there are not only overbank flooding caused by seawater draining into the river channel but also coastal flooding occurring along the coastline and in the town of Vieux Fort. Flood inundation area dramatically increases when the heights of wave run-up increase from 2.5m to 6m. The town of Vieux Fort, the runway of the airport, and the coastal agriculture area are at risk of flooding when the wave run-up heights are greater than 2.5m, the Hewanorra International Airport area are at significant risk when the wave run-up heights are larger than 3.5m, and the flood hazards are farther inland when the wave run-up heights are above 4.5m. Flood hazards in different scenarios within the Hewanorra International Airport boundary are presented in Figure 23. When the height of wave run-up reaches 3.5m, the runway, taxiway, and aprons of the airport are under the risk of flooding, leading to disruptions of the airport if there is no effective removal of flood water. As the heights of wave run-up increase from 3.5m to 6m, flood hazards go farther inland, severely impacting the airport facilities such as the control tower, the cargo shed, and the terminal building. Discontinued operations of the airport are expected with the failures of all these facilities, and therefore, further study on the effects of wave run-up and effective flood management in the airport is needed.

Table 19. Flood area estimations in scenarios of excluding wave run-up and including wave run-up in the coastal boundary conditions.

Simulation Number	Heights of Wave Run-up (m)	Flood Inundation Condition	
		Maximum Flooded Area over the Course of Simulations (km^2)	Differences in Maximum Flooded Area
R0	0	0.0099	/
W1	0.5	0.0294	1.985
W2	1.5	0.2030	19.612

W3	2.5	1.0725	107.878
W4	3.5	2.4481	247.563
W5	4.5	3.0076	304.343
W6	5.5	3.5002	354.348
W7	6.0	3.6929	373.916

Note: The formula for calculating the differences in the maximum flooded area is (maximum flooded area when considering wave run-up – maximum flooded area when excluding wave run-up)/maximum flooded area when excluding wave run-up.

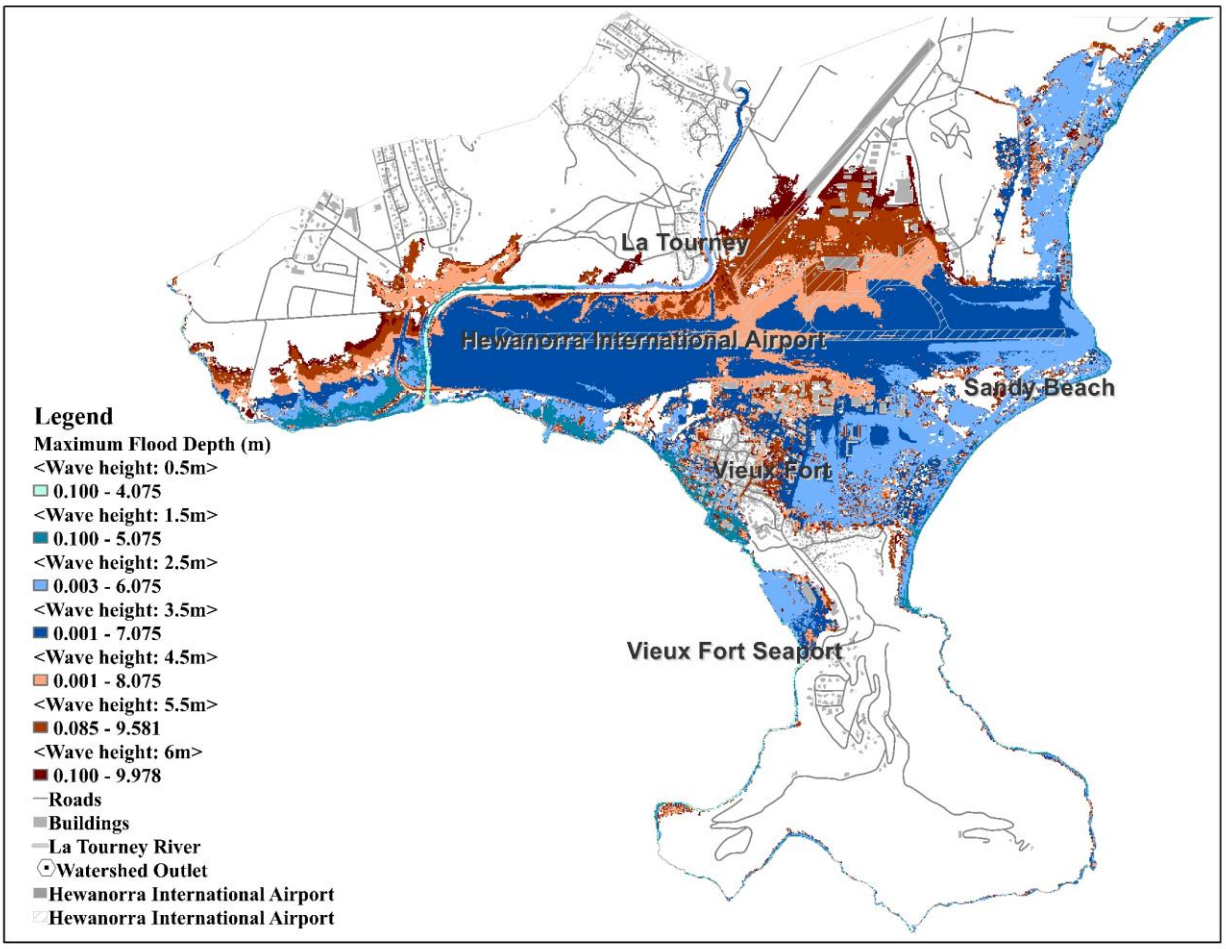

Figure 22. Map showing the maximum flood depth for each pixel over the course of simulations in scenarios of including wave run-up in the coastal boundary conditions.

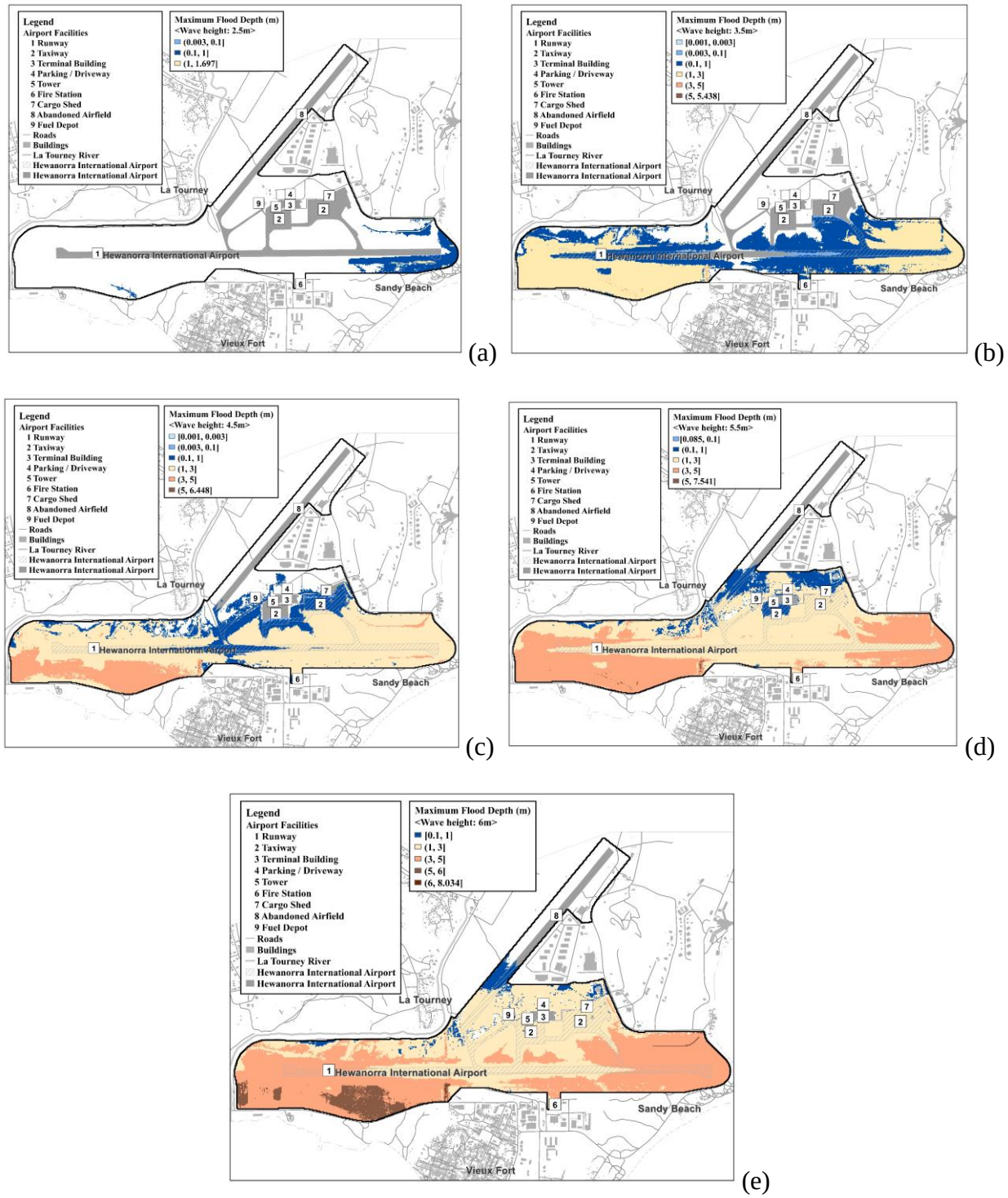

Figure 23. Maps showing the maximum flood depth for each pixel within the Hewanorra International Airport boundary over the course of simulations when the heights of wave run-up are (a) 2.5m, (b) 3.5m, (c) 4.5m, (d) 5.5m, and (e) 6m.

Combined Effects of River Discharges and Coastal Water Levels

As in Section 3.4.2.1.2, based on the results of the reference model R0, it is determined that river discharges do not lead to overbank floods, coastal water levels do not incur flood along the coastline, and the interactions between sea levels and river flows are insignificant. However, when including wave run-up in coastal boundary conditions, the flood mechanisms are expected to be different. Figure 24 presents spatial patterns of the maximum flood depth for each pixel over the course of simulations, and Table 20 summarizes the flood area estimations under different scenarios. As in Figure 24, when the height of wave run-up reaches 1.5m, overbank flooding is expected in the river floodplains due to the interactions of high sea levels and river discharges. As the heights of wave run-up increase, compared to the interactions between seawater and river flows, the role of coastal water levels becomes dominant, leading to the significant increase in the flood inundation area, more intense backwater effects, more serious coastal flooding along the coastline, as well as farther-inland flood hazards.

Table 20. Flood area estimations in scenarios of excluding wave run-up and including wave run-up in the coastal boundary conditions.

Simulation Number	Heights of Wave Run-up (m)	Flood Inundation Condition	
		Maximum Flooded Area over the Course of Simulations (km^2)	Differences in Maximum Flooded Area
R5	0	0.0409	/
W8	0.5	0.0597	0.459
W9	1.5	0.2245	4.484
W10	2.5	1.0754	25.278
W11	3.5	2.4481	58.820
W12	4.5	3.0076	72.491

W13	5.5	3.5001	84.524
W14	6.0	3.6929	89.236

Note: The formula for calculating the differences in the maximum flooded area is (maximum flooded area when considering wave run-up – maximum flooded area when excluding wave run-up)/maximum flooded area when excluding wave run-up.

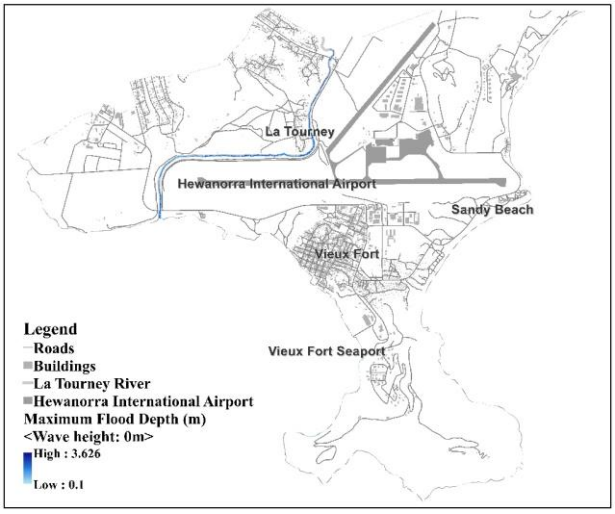

(a)

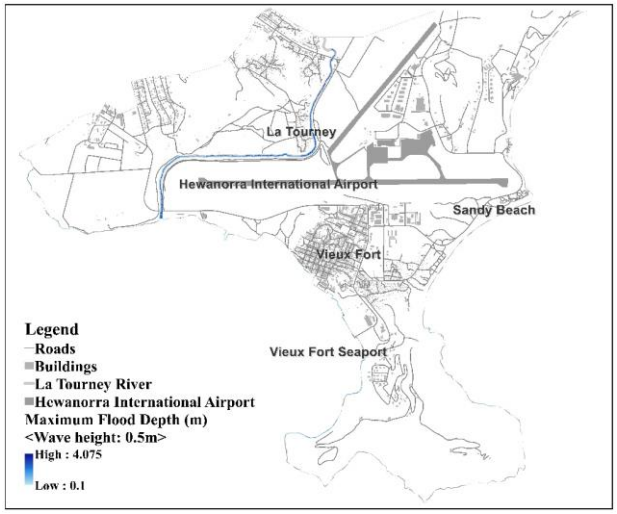

(b)

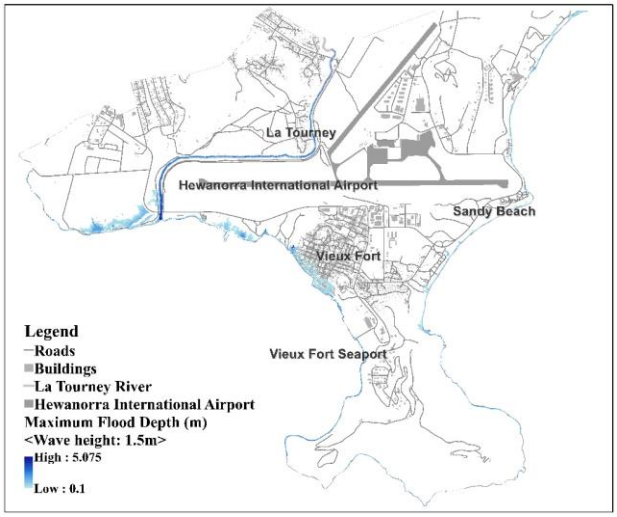

(c)

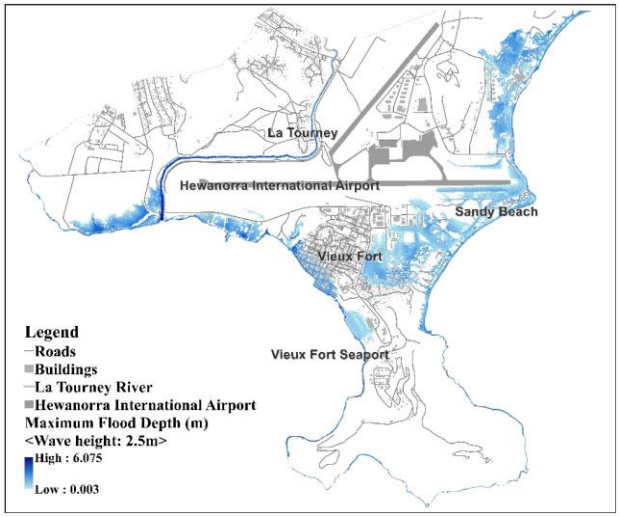

(d)

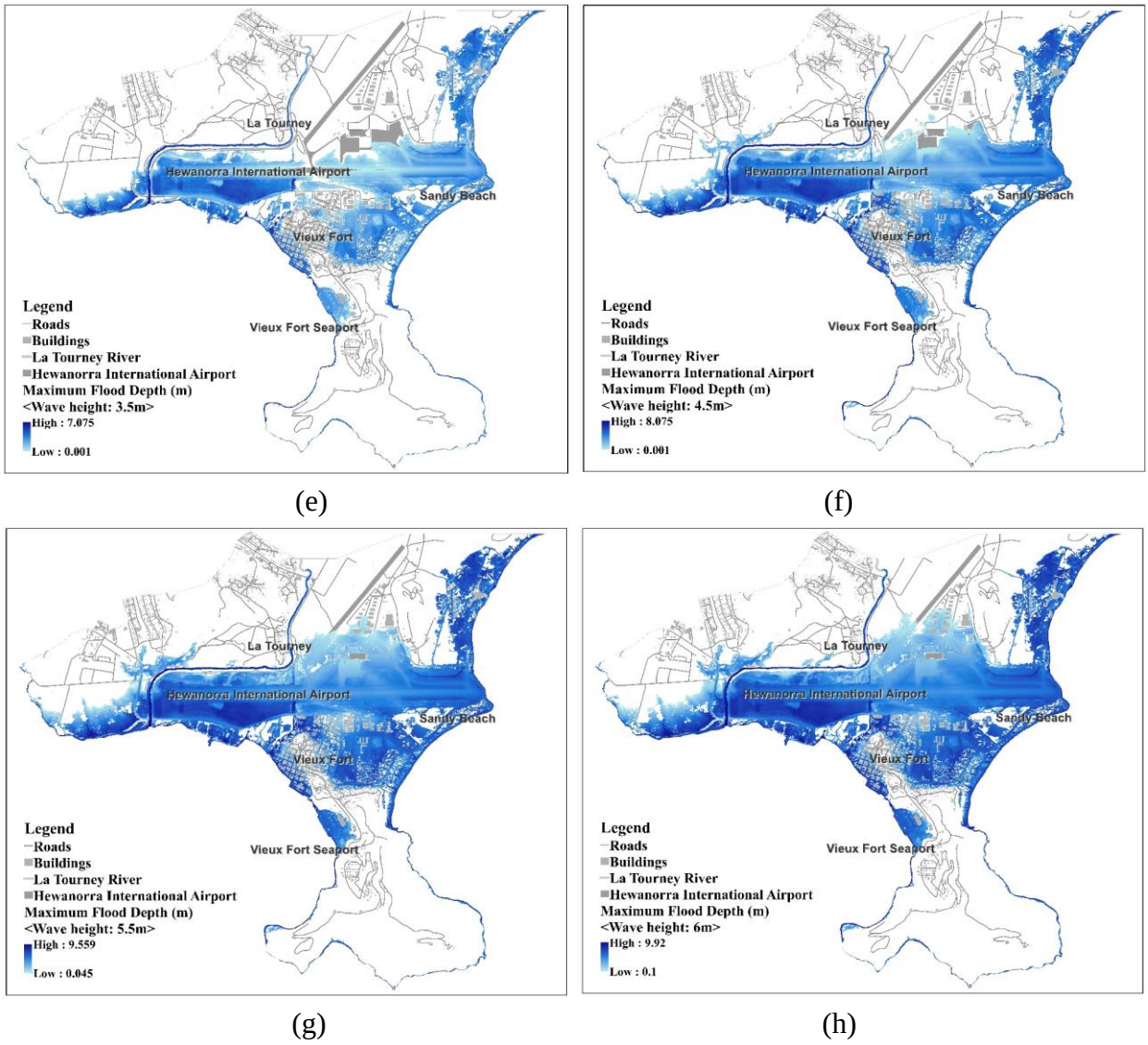

Figure 24. Maps showing the maximum flood depth for each pixel within the Hewanorra International Airport boundary over the course of simulations when the heights of wave run-up are (a) 0m, (b) 0.5m, (c) 1.5m, (d) 2.5m, (e) 3.5m, (f) 4.5m, (g) 5.5m, and (h) 6m.

Combined Effects of River Discharges, Rainfall Inputs, and Coastal Water Levels

Simulations W15~W21 were conducted to investigate the combined effects of rainfall, river discharges, and coastal water levels when considering the effects of wave run-up. Figure 25 presents the spatial patterns of the maximum flood depth for each pixel over the course of simulations, and Table 21 summarizes the flood area estimations under different scenarios. As the

heights of wave run-up increase, high sea levels begin to interact with river flows in the river channel causing overbank floods in the river floodplains, coastal floods are expected along the coastline affecting the town of Vieux Fort and lowland agriculture areas, and more severe flooding are estimated within the Hewanorra International Airport boundary impacting the operations of airport facilities. Comparing Figure 22, 24, and 25, it can be concluded that effects of wave run-up are significant and would cause extensive impacts to compound flood patterns in extreme events, especially in the Hewanorra International Airport and the town of Vieux Fort.

Table 21. Flood area estimations in scenarios of excluding wave run-up and including wave run-up in the coastal boundary conditions

Simulation Number	Heights of Wave Run-up (m)	Flood Inundation Condition	
		Maximum Flooded Area over the Course of Simulations (km^2)	Differences in Maximum Flooded Area (%)
R0	0	2.6018	/
W15	0.5	2.6121	0.626
W16	1.5	2.6812	3.289
W17	2.5	2.9845	14.970
W18	3.5	3.6251	39.649
W19	4.5	3.9793	53.296
W20	5.5	4.3310	66.843
W21	6.0	4.4812	72.629

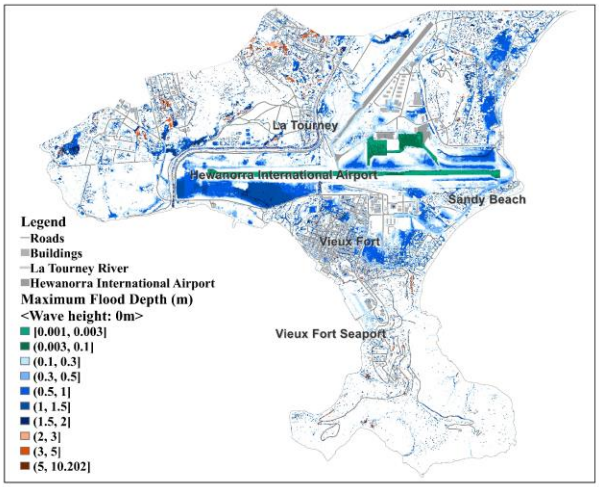
La Tourney
Hewanorra International Airport
Sandy Beach
Vieux Fort
Vieux Fort Seaport
Legend
Roads
Buildings
La Tourney River
Hewanorra International Airport
Maximum Flood Depth (m)
<Wave height: 0m>
[0.001, 0.003]
(0.003, 0.1]
(0.1, 0.3]
(0.3, 0.5]
(0.5, 1]
(1, 1.5]
(1.5, 2]
(2, 3]
(3, 5]
(5, 10.202]

(a)

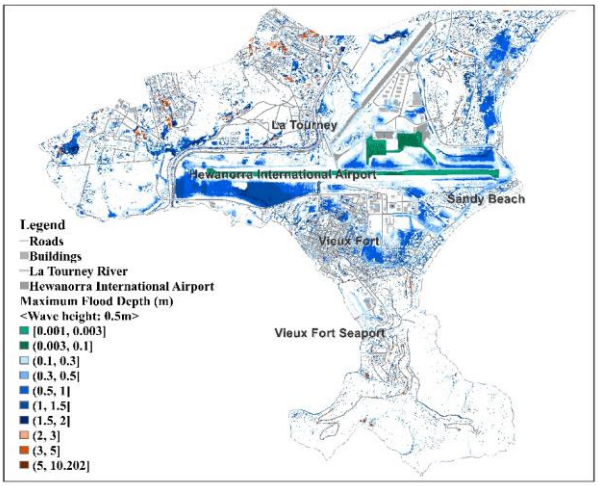
La Tourney
Hewanorra International Airport
Sandy Beach
Vieux Fort
Vieux Fort Seaport
Legend
Roads
Buildings
La Tourney River
Hewanorra International Airport
Maximum Flood Depth (m)
<Wave height: 0.5m>
[0.001, 0.003]
(0.003, 0.1]
(0.1, 0.3]
(0.3, 0.5]
(0.5, 1]
(1, 1.5]
(1.5, 2]
(2, 3]
(3, 5]
(5, 10.202]

(b)

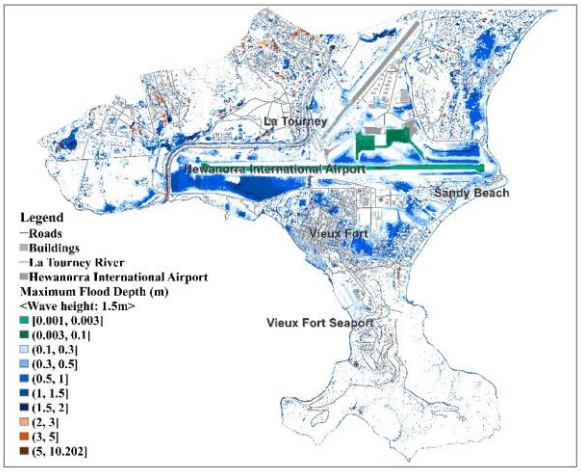
La Tourney
Hewanorra International Airport
Sandy Beach
Vieux Fort
Vieux Fort Seaport
Legend
Roads
Buildings
La Tourney River
Hewanorra International Airport
Maximum Flood Depth (m)
<Wave height: 1.5m>
[0.001, 0.003]
(0.003, 0.1]
(0.1, 0.3]
(0.3, 0.5]
(0.5, 1]
(1, 1.5]
(1.5, 2]
(2, 3]
(3, 5]
(5, 10.202]

(c)

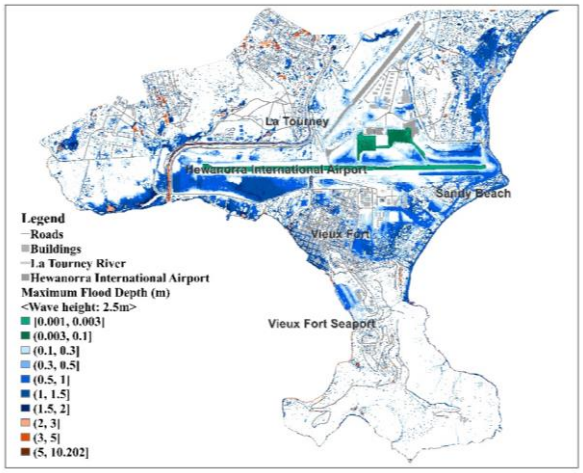
La Tourney
Hewanorra International Airport
Sandy Beach
Vieux Fort
Vieux Fort Seaport
Legend
Roads
Buildings
La Tourney River
Hewanorra International Airport
Maximum Flood Depth (m)
<Wave height: 2.5m>
[0.001, 0.003]
(0.003, 0.1]
(0.1, 0.3]
(0.3, 0.5]
(0.5, 1]
(1, 1.5]
(1.5, 2]
(2, 3]
(3, 5]
(5, 10.202]

(d)

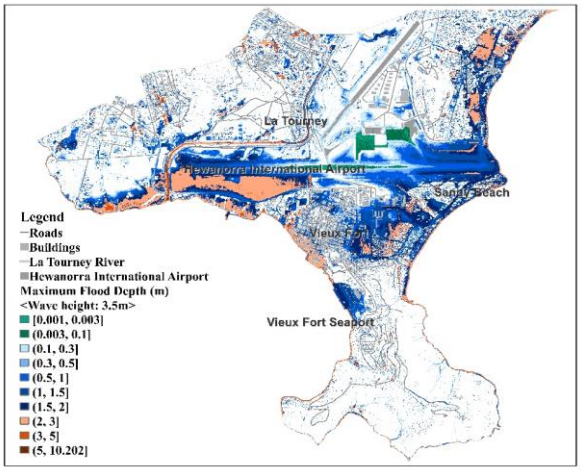
La Tourney
Hewanorra International Airport
Sandy Beach
Vieux Fort
Vieux Fort Seaport
Legend
Roads
Buildings
La Tourney River
Hewanorra International Airport
Maximum Flood Depth (m)
<Wave height: 3.5m>
[0.001, 0.003]
(0.003, 0.1]
(0.1, 0.3]
(0.3, 0.5]
(0.5, 1]
(1, 1.5]
(1.5, 2]
(2, 3]
(3, 5]
(5, 10.202]

(e)

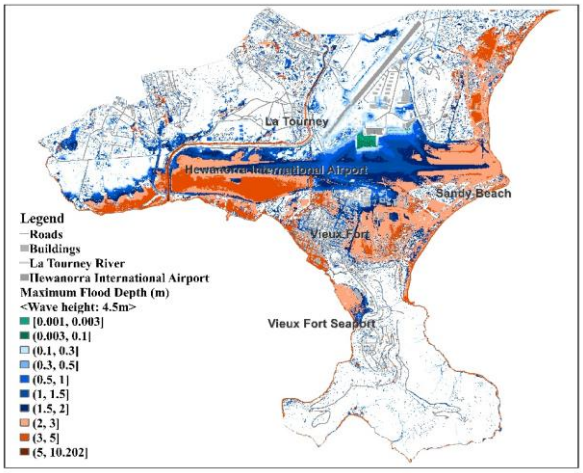
La Tourney
Hewanorra International Airport
Sandy Beach
Vieux Fort
Vieux Fort Seaport
Legend
Roads
Buildings
La Tourney River
Hewanorra International Airport
Maximum Flood Depth (m)
<Wave height: 4.5m>
[0.001, 0.003]
(0.003, 0.1]
(0.1, 0.3]
(0.3, 0.5]
(0.5, 1]
(1, 1.5]
(1.5, 2]
(2, 3]
(3, 5]
(5, 10.202]

(f)

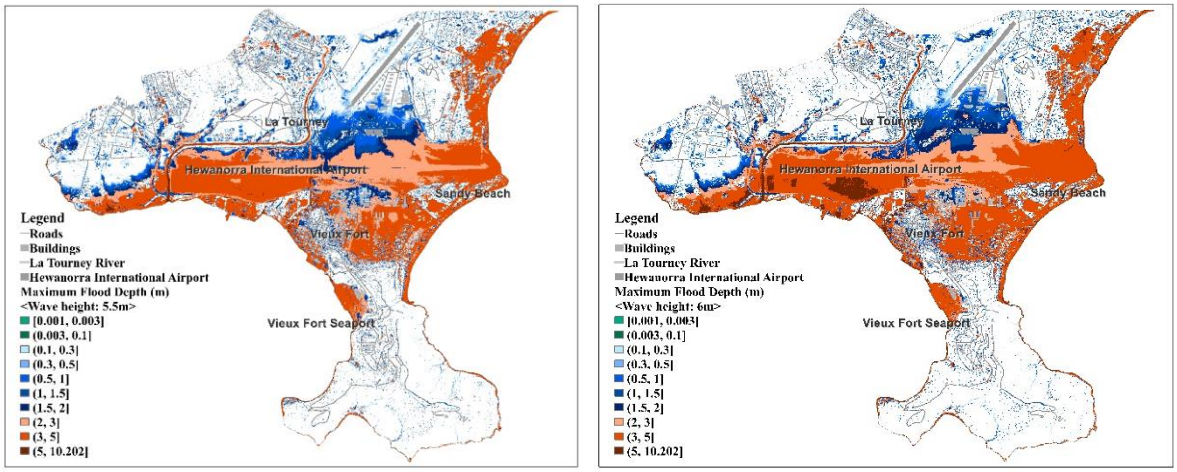

(g) (h)

Figure 25. Maps showing the maximum flood depth for each pixel over the course of simulations when the heights of wave run-up are (a) 0m, (b) 0.5m, (c) 1.5m, (d) 2.5m, (e) 3.5m, (f) 4.5m, (g) 5.5m, and (h) 6m.

3.4.4. Probabilistic Flood Hazard Analysis

As in Table 14, a total of 300 simulations were conducted to investigate the combined effects of the three uncertain boundary conditions by considering all possible coastal boundary conditions (estimated water levels and the uncertainty bounds; wave run-up effects are not included), all selected rainfall inputs (time series of rainfall intensities derived from different sources), and all potential river discharges (estimated streamflow values and the uncertainty bounds associated with the selection of parameters as well as sources of rainfall inputs). Simulation results are analyzed in three aspects, namely, the maximum flood inundation area, the maximum flood depth for each pixel, and the probability of flooding.

Maximum Flood Inundation Area

Figure 26 presents the maximum flood inundation area for each simulation, and it can be concluded that in terms of the estimations of flood inundation area, uncertainties in the rainfall inputs play an

important role in flooding in the event of Tropical Storm Matthew, while uncertainties in the coastal and riverine boundary conditions are relatively insignificant.

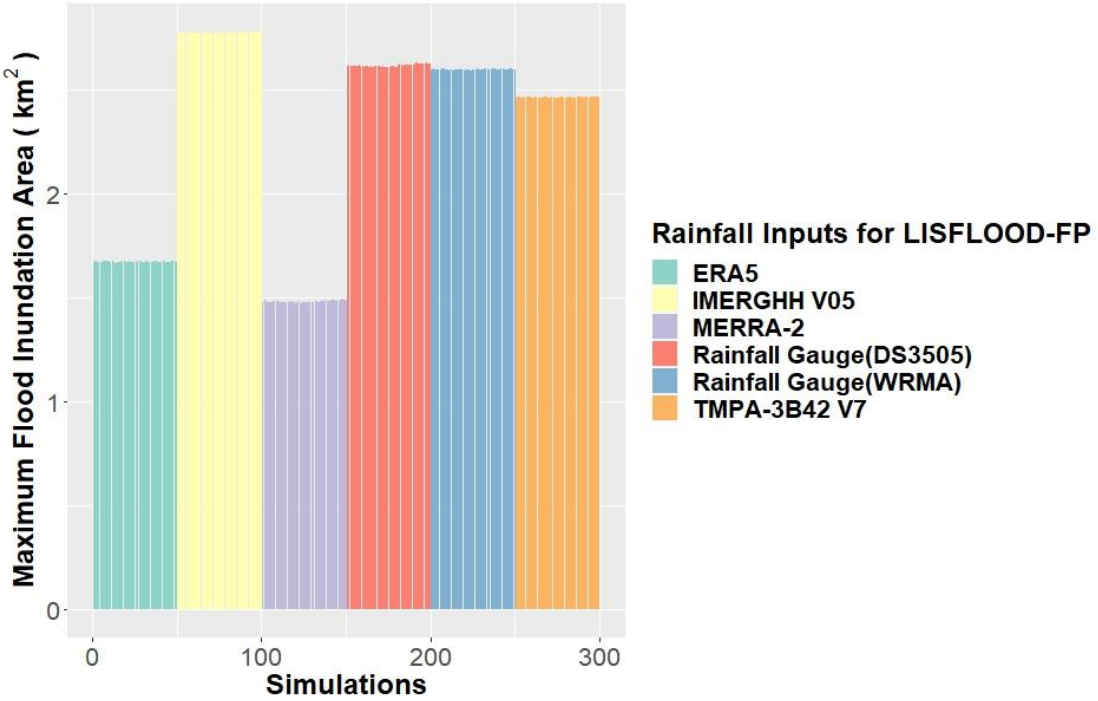

Figure 26. Maximum flood inundation area over the course of simulations in the probabilistic flood hazard analysis.

Maximum Flood Depth Estimations

A total of 300 estimations of maximum flood depth were generated for each pixel in the study area, and it is expected that the estimates for the same pixel do not necessarily have the same value because the boundary conditions are different in each simulation. The impacts of uncertain boundary conditions on flood depth estimations can be determined by calculating the ranges, which is defined as the differences between the maximum estimated values of maximum flood depth and the minimum estimated values maximum flood depth for each pixel.

Figure 27 shows spatial patterns of the ranges calculated for each pixel, and it is found that the ranges derived from the total of 300 simulations are less than 1m or equal to 0m in most inundated pixels. It can be concluded that in terms of maximum flood depth estimations, uncertainties in the boundary conditions have limited impacts.

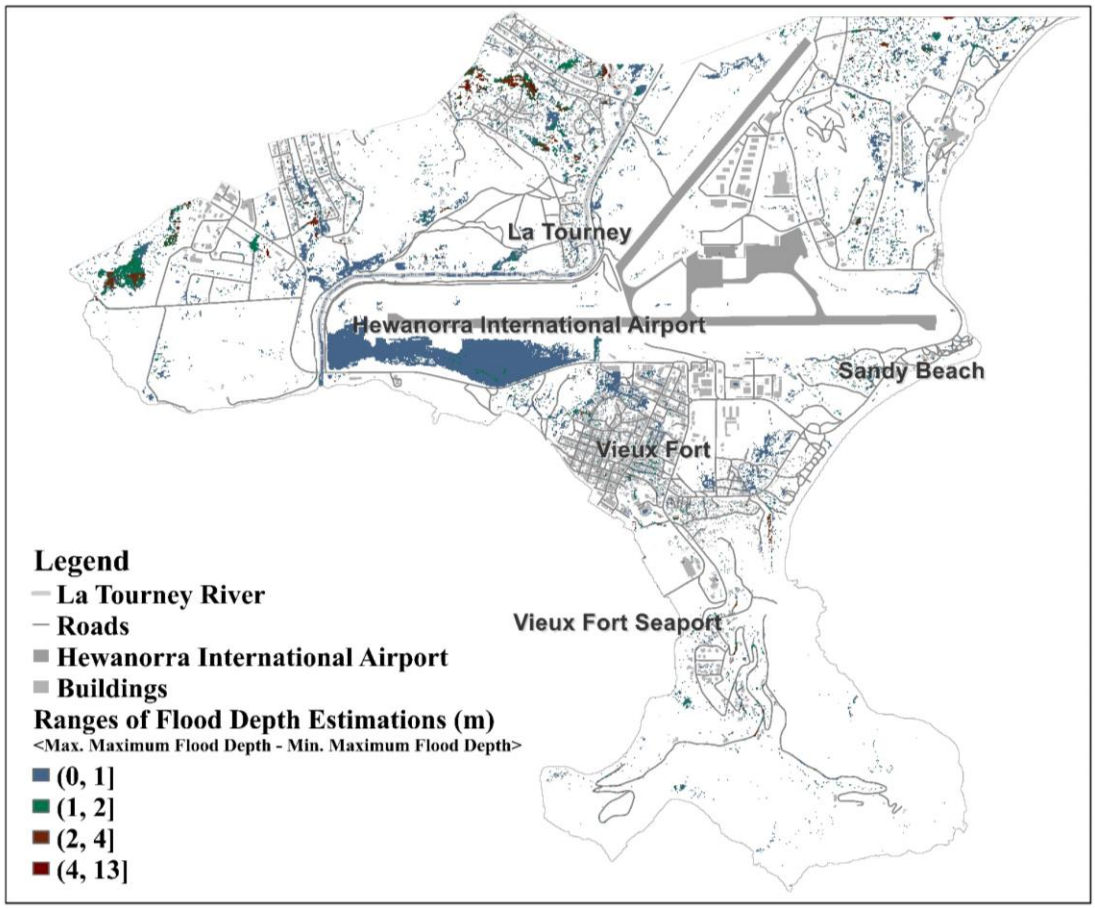

Figure 27. Map showing the ranges of maximum flood depth estimations for each pixel.

Probability of Flooding

In each simulation, each pixel can be classified into flooded or non-flooded areas based on the pre-defined criteria as in Section 3.3.4.2, and the probability of flooding can be calculated as in Section 3.3.4.6. Figure 28 and Figure 29 show the probability of flooding calculated from the total of 300 simulations for pixels in the study area and within the Hewanorra International Airport boundary. The figures indicate that areas at high risk of flooding are the lowland agriculture areas, the major highway, the town of Vieux Fort, the grassland around the runway, as well as the runway, taxiway, and apron of the airport.

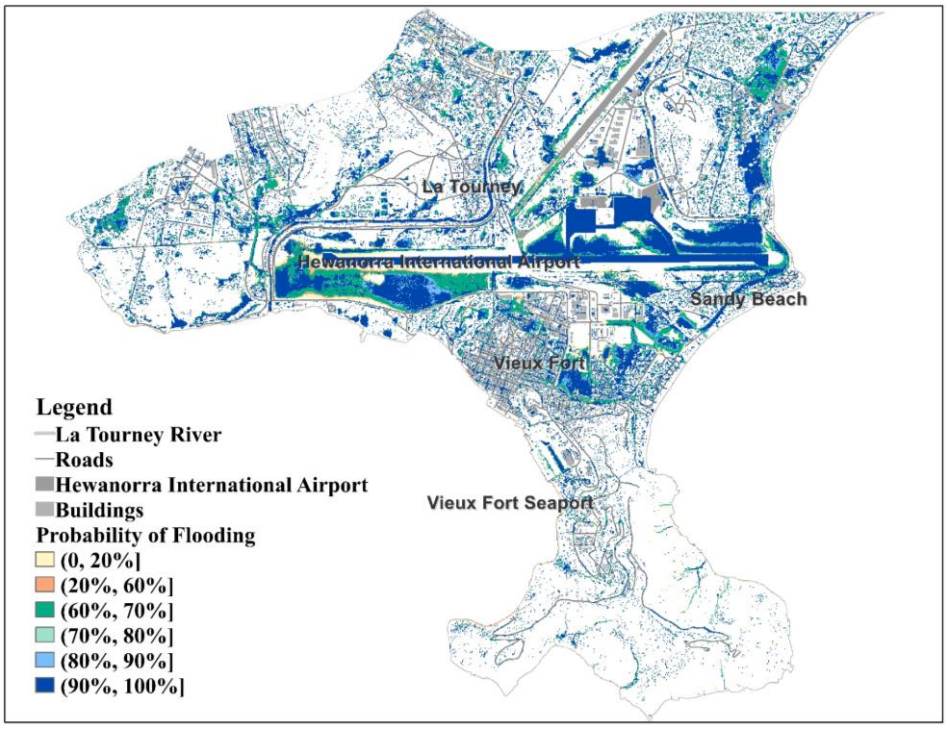

Figure 28. Map showing the probability of flooding calculated from all simulations for each pixel in the study area.

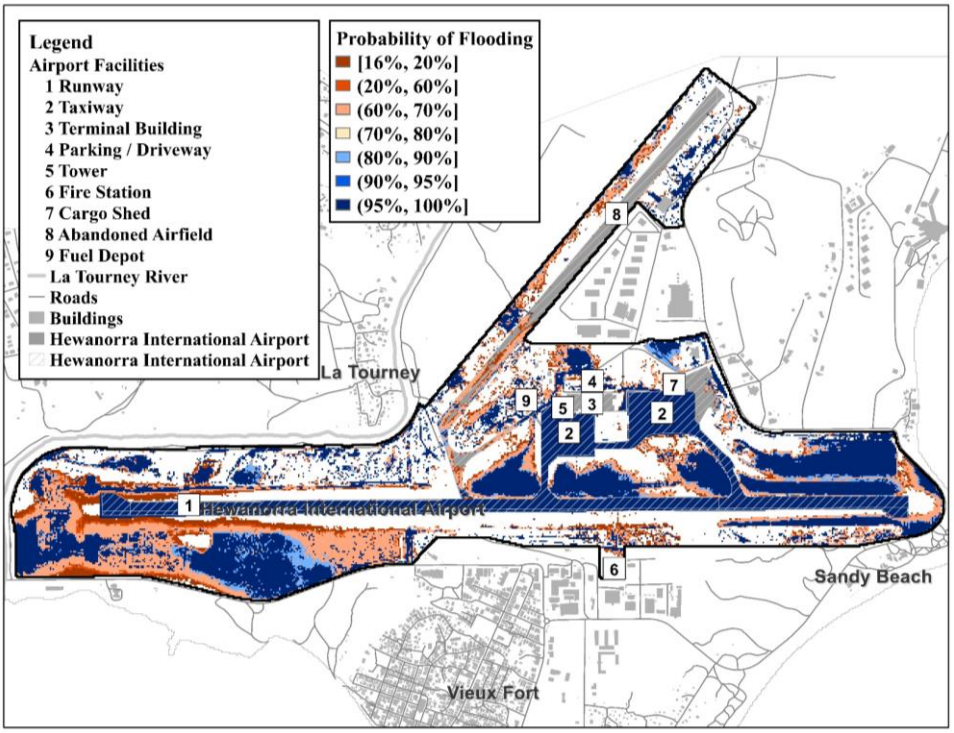

Figure 29. Map showing the probability of flooding calculated from all simulations for each pixel within the Hewanorra International Airport.

3.5.Conclusions

The study area, located at the southern coast of Saint Lucia, is highly vulnerable to weather-related extreme events and at risk of compound flooding, especially in the condition of climate change. There are high concentrations of infrastructures and human communities in the low-lying areas. Major assets include the Hewanorra International Airport, the Vieux Fort Seaport, the north-south major highway, and the towns of Vieux Fort and La Tourney.

A two-dimensional hydrodynamic model LISFLOOD-FP was set up to simulate the combined effects of coastal water levels, river discharges, and rainfall in the event of Tropical Storm Matthew. The model was validated using the flood map derived from available Pléiades-1 and Sentinel-1 imagery. However, due to the lack of imagery taken during the event, the derived flood map reveals areas that have potentially experienced severe flooding but could not provide a comprehensive understanding of the actual flood extents. In addition, not considering the drainage system can lead to overestimation of flood conditions because it plays an important role when floodwater is receding in urban areas and in the highway. As to the impacts of changing climate, although it is expected to be significant to the flooding, it is not included in this study.

Due to the lack of reliable hourly rainfall patterns, the lack of observational coastal water levels, and the uncertainties in river flow estimations from the hydrological model HYMOD, assumptions were made in the preparations of boundary conditions. Therefore, boundary conditions become the major source of model uncertainties in hydrodynamic modelling. Sensitivity analysis has according been conducted to explore the uncertainties associated with the uncertain input data as well as to investigate individual contributions of different flood factors. It is determined that rainfall is the major contributor to flooding in the event of Tropical Storm Matthew when not considering the effects of wave run-up. Uncertainties in the rainfall volume and in the hourly patterns of rainfall intensities have significant impacts on flood patterns such as maximum flood inundation area and water depths. Although rainfall plays a major role in flooding in the event of Tropical Storm Matthew, the inclusion of coastal and riverine boundary conditions is significant for more accurate and reliable flood estimations not only because the interactions between seawater and river flows are expected but also because the temporal patterns of coastal water levels determine how the river flows and rainfall-induced water drain into the sea. Nevertheless, the interaction mechanisms between river flows and sea levels are not well studied due to the lack of

reliable hourly patterns for these two factors. The assumption of constant river discharge throughout the day may result in significantly underestimated flood estimations. The drainage area of the river is characterized as steep and mountainous, indicating that the river discharges have a quick response to the rainfall, and therefore, in the event of Tropical Storm Matthew, hourly river discharges have the potential to dramatically increase when the rainfall intensity significantly increases. Moreover, if there are simultaneous occurrences of peak river discharges and peak sea levels, resultant floods can be much more severe.

The wave run-up has significantly higher values than the storm surges in Saint Lucia. The scenario analysis was conducted to analyze the potential impacts of wave run-up. It can be concluded that wave run-up can lead to severe coastal flooding along the coastline, the river overflows in the floodplains due to the interactions between river flows and high sea levels, as well as more severe compound floods caused by the rainfall, river discharges, and coastal water levels. The maximum flood area for compound floods increases from 2.6018km^2 to 4.4812 km^2 when the heights of wave run-up increases from 0m to 6m. Hewanorra International Airport and the town of Vieux Fort are at especially high risk of flooding when considering the effects of wave run-up.

Taking uncertainty bounds of the three types of boundary conditions into consideration, the probabilistic flood hazard analysis was conducted. In terms of maximum flood inundation area, the sources of rainfall inputs for the hydrodynamic model play the most significant role since rainfall is the major contributor to flooding in the event of Tropical Storm Matthew. In terms of maximum flood depths, uncertainties in boundary conditions have limited impacts on the estimations. Probabilistic flooding maps were derived to estimate the flood probabilities for each pixel in the total of 300 simulations. In the event of Tropical Storm Matthew, areas at high risk of flooding are the lowland agriculture areas, the major highway, the town of Vieux Fort, the grassland around the runway, as well as the runway, taxiway, and apron of the airport.

In summary, major conclusions from the analysis of compound flooding are as follows: (i) Rainfall is the major contributor of flooding in the event of Tropical Storm Matthew, but considering multiple flood factor leads to more accurate flood estimations; (ii) Uncertainties in the rainfall volume and temporal rainfall patterns have significant impacts on simulation results in terms of flood inundation area; (iii) It is expected that the potential impacts of wave run-up include stronger

interactions between sea levels and river flows, more severe coastal flooding at the coastline and even farther inland, as well as more severe pluvial flooding due to the reduced ability of rainfall-induced water draining into the sea, thus resulting in more intense compound flooding; (iv) High-risk flood areas in the study area are the Hewanorra International Airport, the town of Vieux Fort, the north-south major highway, and coastal agricultural lands.

Despite the limitations, this study evaluates the compound flooding caused by river flows, rainfall, and coastal water levels in the event of Tropical Storm Matthew. The results have provided insights into the areas that are at high risk of flooding. Hewanorra International Airport, as the assessed critical transportation asset in the study area, is at particularly high risk of disruptions because the runway, taxiway, and apron have high potential to be flooded especially when considering the impacts of wave run-up. As a result, further study on flood risk analysis is needed for the airport.

3.6. References

Ajami, Newsha K., Hoshin Gupta, Thorsten Wagener, and Soroosh Sorooshian. 2004. "Calibration of a semi-distributed hydrologic model for streamflow estimation along a river system." *Journal of Hydrology* 298 (1): 112-135. https://doi.org/https://doi.org/10.1016/j.jhydrol.2004.03.033.

Argenti, Fabrizio, Alessandro Lapini, Tiziano Bianchi, and Luciano Alparone. 2013. "A Tutorial on Speckle Reduction in Synthetic Aperture Radar Images." *IEEE Geoscience and Remote Sensing Magazine* 1 (3): 6-35. https://doi.org/10.1109/MGRS.2013.2277512.

Armaroli, C., P. Ciavola, M. Masina, and L. Perini. 2009. "Run-up computation behind emerged breakwaters for marine strom risk assessment." *Journal of Coastal Research*: 1612-1616.

Ban, Yifang, O. A. Yousif, miljö Samhällsplanering och, samhällsbyggnad Skolan för arkitektur och, geoinformatik Geodesi och, and Kth. 2012. "Multitemporal Spaceborne SAR Data for Urban Change Detection in China." *IEEE Journal of Selected Topics in Applied Earth Observations and Remote Sensing* 5 (4): 1087-1094. https://doi.org/10.1109/JSTARS.2012.2201135.

Bates, Paul D, Matthew S Horritt, and Timothy J Fewtrell. 2010. "A simple inertial formulation of the shallow water equations for efficient two-dimensional flood inundation modelling." *Journal of Hydrology* 387 (1-2): 33-45.

Bender, Morris A., Thomas R. Knutson, Robert E. Tuleya, Joseph J. Sirutis, Gabriel A. Vecchi, Stephen T. Garner, and Isaac M. Held. 2010. "Modeled Impact of Anthropogenic

Warming on the Frequency of Intense Atlantic Hurricanes." *Science* 327 (5964): 454-458. https://doi.org/10.1126/science.1180568.

Beven, John L. 2017. "National Hurricane Center Annual Summary: 2016 Atlantic Hurricane Season." National Hurricane Center. https://www.nhc.noaa.gov/data/tcr/summary_atlc_2016.pdf.

Bharath, R., and Amin Elshorbagy. 2018. "Flood mapping under uncertainty: a case study in the Canadian prairies." *Natural Hazards* 94 (2): 537-560. https://doi.org/10.1007/s11069-018-3401-1.

Biondi, Esteban L., and Greg Guannel. 2018. "Practical tools for quantitative analysis of coastal vulnerability and sea level rise impacts—application in a Caribbean island and assessment of the 1.5 °C threshold." *Regional Environmental Change* 18 (8): 2227-2236. https://doi.org/10.1007/s10113-018-1397-4.

Bioresita, Filsa, Anne Puissant, André Stumpf, and Jean-Philippe Malet. 2018. "A method for automatic and rapid mapping of water surfaces from Sentinel-1 imagery." *Remote Sensing* 10 (2): 217. https://doi.org/10.3390/rs10020217.

Boyle, Douglas Patrick. 2001. "Multicriteria Calibration of Hydrologic Models." Ph.D. Dissertation, Department of Hydrology and Water

Resources, University of Arizona.

Brunner, D., L. Bruzzone, A. Ferro, J. Fortuny, and G. Lemoine. 2008. *Analysis of the double bounce scattering mechanism of buildings in VHR SAR data*. Vol. 7109.*SPIE Remote Sensing*: SPIE.

Bueno, Ramon, Cornelia Herzfeld, Elizabeth A Stanton, and Frank Ackerman. 2008. "The Caribbean and climate change: the costs of inaction." *Stockholm Environment Institute, US Center and Global Development and Environment Institute, Tufts University*.

Caldwell, PC, MA Merrifield, and PR Thompson. 2015. "Sea level measured by tide gauges from global oceans–the Joint Archive for Sea Level holdings (NCEI Accession 0019568), Version 5.5, NOAA National Centers for Environmental Information, Dataset." *Centers Environ. Information, Dataset* 10: V5V40S7W.

Candela, Angela, and Giuseppe T. Aronica. 2017. "Probabilistic Flood Hazard Mapping Using Bivariate Analysis Based on Copulas." *ASCE-ASME Journal of Risk and Uncertainty in Engineering Systems, Part A: Civil Engineering* 3 (1): A4016002. https://doi.org/10.1061/AJRUA6.0000883.

Central Intelligence Agency. 2019. "The World Factbook." Accessed September 6, 2019.

Cian, Fabio, Mattia Marconcini, and Pietro Ceccato. 2018. "Normalized Difference Flood Index for rapid flood mapping: Taking advantage of EO big data." *Remote Sensing of Environment* 209: 712-730. https://doi.org/10.1016/j.rse.2018.03.006.

Clement, M. A., C. G. Kilsby, and P. Moore. 2018. "Multi-temporal synthetic aperture radar flood mapping using change detection: Multi-temporal SAR flood mapping using change detection." *Journal of Flood Risk Management* 11 (2): 152-168. https://doi.org/10.1111/jfr3.12303.

Copernicus Climate Change Service. 2017. ERA5: Fifth generation of ECMWF atmospheric reanalyses of the global climate.

de Almeida, Gustavo AM, Paul Bates, Jim E Freer, and Maxime Souvignet. 2012. "Improving the stability of a simple formulation of the shallow water equations for 2-D flood modeling." *Water Resources Research* 48 (5).

Dechant, Caleb M., and Hamid Moradkhani. 2012. "Examining the effectiveness and robustness of sequential data assimilation methods for quantification of uncertainty in hydrologic forecasting." *Water Resources Research* 48 (4). https://doi.org/10.1029/2011WR011011.

Duan, Q. Y., V. K. Gupta, and S. Sorooshian. 1993. "Shuffled complex evolution approach for effective and efficient global minimization." *Journal of Optimization Theory and Applications* 76 (3): 501-521. https://doi.org/10.1007/BF00939380.

Duan, Qingyun, Soroosh Sorooshian, and Vijai Gupta. 1992. "Effective and efficient global optimization for conceptual rainfall- runoff models." *Water Resources Research* 28 (4): 1015-1031. https://doi.org/10.1029/91WR02985.

Duan, Qingyun, Soroosh Sorooshian, and Vijai K. Gupta. 1994. "Optimal use of the SCE-UA global optimization method for calibrating watershed models." *Journal of Hydrology* 158 (3): 265-284. https://doi.org/10.1016/0022-1694(94)90057-4.

Farr, Tom G., Paul A. Rosen, Edward Caro, Robert Crippen, Riley Duren, Scott Hensley, Michael Kobrick, Mimi Paller, Ernesto Rodriguez, Ladislav Roth, David Seal, Scott Shaffer, Joanne Shimada, Jeffrey Umland, Marian Werner, Michael Oskin, Douglas Burbank, and Douglas Alsdorf. 2007. "The Shuttle Radar Topography Mission." *Reviews of Geophysics* 45 (2): RG2004. https://doi.org/10.1029/2005RG000183.

Fay, Marianne, Luis Alberto Andres, Charles Fox, Ulf Narloch, Stephane Straub, and Michael Slawson. 2017. *Rethinking infrastructure in Latin America and the Caribbean: Spending better to achieve more*. The World Bank.

Federal Aviation Administration. 2019. Aeronautical Information Manual: Official Guide to Basic Flight Information and ATC Procedures. edited by United States Department of Transportation. United States Department of Transportation.

Federal Emergency Management Agency. 2016. Guidance for Flood Risk Analysis and Mapping: Coastal Water Levels.

Fewtrell, T. J., P. D. Bates, M. Horritt, and N. M. Hunter. 2008. "Evaluating the effect of scale in flood inundation modelling in urban environments." *Hydrological Processes* 22 (26): 5107-5118. https://doi.org/10.1002/hyp.7148.

Fewtrell, TJ, A Duncan, CC Sampson, JC Neal, and PD Bates. 2011. "Benchmarking urban flood models of varying complexity and scale using high resolution terrestrial LiDAR data." *Physics and Chemistry of the Earth* 36 (7-8): 281-291. https://doi.org/10.1016/j.pce.2010.12.011.

Global Facility for Disaster Reduction and Recovery. 2014. Saint Lucia Flood Event of December 24-25, 2013: A Report by the Government of Saint Lucia and the World Bank.

Global Modeling and Assimilation Office. 2015. MERRA-2 tavg1_2d_flx_Nx: 2d,1-Hourly,Time-Averaged,Single-Level,Assimilation,Surface Flux Diagnostics V5.12.4. Greenbelt, MD, USA, Goddard Earth Sciences Data and Information Services Center (GES DISC),.

Google Earth Engine. 2015. Sentinel-1: C-band Synthetic Aperture Radar (SAR) Ground Range Data.

Gorelick, Noel, Matt Hancher, Mike Dixon, Simon Ilyushchenko, David Thau, and Rebecca Moore. 2017. "Google Earth Engine: Planetary-scale geospatial analysis for everyone." *Remote Sensing of Environment* 202: 18-27. https://doi.org/10.1016/j.rse.2017.06.031.

Government of Saint Lucia. 2018a. Economic and Social Review 2017. Ministry of Finance, Economic Growth, Job Creation, External Affairs and the Public Service.

---. 2018b. Saint Lucia's National Adaptation Plan (NAP): 2018–2028. Department of Sustainable Development, Ministry of Education, Innovation, Gender Relations and Sustainable Development.

Gupta, Hoshin V., Harald Kling, Koray K. Yilmaz, and Guillermo F. Martinez. 2009. "Decomposition of the mean squared error and NSE performance criteria: Implications for improving hydrological modelling." *Journal of Hydrology* 377 (1): 80-91. https://doi.org/10.1016/j.jhydrol.2009.08.003.

Hillel, Daniel. 1998. *Environmental soil physics: Fundamentals, applications, and environmental considerations*. Elsevier.

Hostache, R., P. Matgen, and W. Wagner. 2012. "Change detection approaches for flood extent mapping: How to select the most adequate reference image from online archives?" *International Journal of Applied Earth Observation and Geoinformation* 19 (1): 205-213. https://doi.org/10.1016/j.jag.2012.05.003.

Huffman, G. J. 2017. GPM IMERG Final Precipitation L3 Half Hourly 0.1 degree x 0.1 degree V05. Greenbelt, MD, Goddard Earth Sciences Data and Information Services Center (GES DISC),.

Hunter, NM, PD Bates, S Neelz, G Pender, I Villanueva, NG Wright, D Liang, Roger Alexander Falconer, B Lin, and S Waller. 2008. "Benchmarking 2D hydraulic models for urban flood simulations." Proceedings of the institution of civil engineers: water management.

International Federation of Red Cross and Red Crescent Societies. 2017. DREF Operations Final Report Saint Lucia: Hurricane Matthew.

Jetten, V. 2016. CHARIM Project Saint Lucia National Flood Hazard Map: Methodology and Validation Report. Caribbean Handbook on Risk Information Management.

Jiang, Yan, Changming Liu, Lifang Liu, Xuyong Li, and Hongrui Wang. 2015. "Rainfall-runoff modeling, parameter estimation and sensitivity analysis in a semiarid catchment." *Environmental Modelling and Software* 67: 72-88. https://doi.org/10.1016/j.envsoft.2015.01.008.

Kumbier, Kristian, Rafael C. Carvalho, Athanasios T. Vafeidis, and Colin D. Woodroffe. 2018. "Investigating compound flooding in an estuary using hydrodynamic modelling: A case study from the Shoalhaven River, Australia." *Natural Hazards and Earth System Sciences* 18 (2): 463-477. https://doi.org/10.5194/nhess-18-463-2018.

Lee, J. H., A. W. Jayawardena, and N. Muttil. 2006. "Comparative Analysis of Data-Driven and GIS-Based Conceptual Rainfall-Runoff Model." *Journal of Hydrologic Engineering* 11 (1): 1-11. https://doi.org/10.1061/(ASCE)1084-0699(2006)11:1(1).

Lenderink, Geert, Adri Buishand, and Willem Van Deursen. 2007. "Estimates of future discharges of the river Rhine using two scenario methodologies: Direct versus delta approach." *Hydrology and Earth System Sciences* 11 (3): 1145-1159. https://doi.org/10.5194/hess-11-1145-2007.

Lewis, Matt, Paul Bates, Kevin Horsburgh, Jeff Neal, and Guy Schumann. 2013. "A storm surge inundation model of the northern Bay of Bengal using publicly available data." *Quarterly Journal of the Royal Meteorological Society* 139 (671): 358-369. https://doi.org/10.1002/qj.2040.

Li, Yu, Sandro Martinis, Simon Plank, and Ralf Ludwig. 2018. "An automatic change detection approach for rapid flood mapping in Sentinel-1 SAR data." *International journal of applied earth observation and geoinformation* 73: 123-135.

Lin, Ning, Kerry Emanuel, Michael Oppenheimer, and Erik Vanmarcke. 2012. "Physically based assessment of hurricane surge threat under climate change." *Nature Climate Change* 2 (6): 462-467. https://doi.org/10.1038/nclimate1389.

Liu, Zhu, and Venkatesh Merwade. 2018. "Accounting for model structure, parameter and input forcing uncertainty in flood inundation modeling using Bayesian model averaging." *Journal of Hydrology* 565: 138-149. https://doi.org/10.1016/j.jhydrol.2018.08.009.

Long, Stephanie, Temilola E. Fatoyinbo, and Frederick Policelli. 2014. "Flood extent mapping for Namibia using change detection and thresholding with SAR." *Environmental Research Letters* 9 (3): 35002. https://doi.org/10.1088/1748-9326/9/3/035002.

Madsen, H. 2000. "Automatic calibration of a conceptual rainfall–runoff model using multiple objectives." *Journal of Hydrology* 235 (3): 276-288. https://doi.org/10.1016/S0022-1694(00)00279-1.

Marcos, Marta, Jérémy Rohmer, Michalis Ioannis Vousdoukas, Lorenzo Mentaschi, Gonéri Le Cozannet, and Angel Amores. 2019. "Increased Extreme Coastal Water Levels Due to the Combined Action of Storm Surges and Wind Waves." *Geophysical Research Letters* 46 (8): 4356-4364. https://doi.org/10.1029/2019GL082599.

Martinis, Sandro, and Christoph Rieke. 2015. "Backscatter analysis using multi-temporal and multi-frequency SAR data in the context of flood mapping at River Saale, Germany." *Remote Sensing* 7 (6): 7732-7752. https://doi.org/10.3390/rs70607732.

Monioudi, Isavela N, Regina Asariotis, Austin Becker, Cassandra Bhat, Danielle Dowding-Gooden, Miguel Esteban, Luc Feyen, Lorenzo Mentaschi, Antigoni Nikolaou, Leonard Nurse, Willard Phillips, David A Y Smith, Mizushi Satoh, Ulric O'Donnell Trotz, Adonis F. Velegrakis, Evangelos Voukouvalas, Michalis I. Vousdoukas, and Robert Witkop. 2018. "Climate change impacts on critical international transportation assets of Caribbean Small Island Developing States (SIDS): the case of Jamaica and Saint Lucia." *Regional Environmental Change* 18 (8): 2211-2225. https://doi.org/10.1007/s10113-018-1360-4.

Moore, RJ. 1985. "The probability-distributed principle and runoff production at point and basin scales." *Hydrological Sciences Journal* 30 (2): 273-297.

Moradkhani, Hamid, Kuo-Lin Hsu, Hoshin Gupta, and Soroosh Sorooshian. 2005. "Uncertainty assessment of hydrologic model states and parameters: Sequential data assimilation using the particle filter." *Water Resources Research* 41 (5): W05012-n/a. https://doi.org/10.1029/2004WR003604.

Mycoo, Michelle. 2011. "Natural Hazard Risk Reduction: Making St. Lucia Safe in an Era of Increased Hurricanes and Associated Events." *Natural Hazards Review* 12 (1): 37-45. https://doi.org/10.1061/(ASCE)NH.1527-6996.0000023.

Mycoo, Michelle A. 2018. "Beyond 1.5 °C: vulnerabilities and adaptation strategies for Caribbean Small Island Developing States." *Regional Environmental Change* 18 (8): 2341-2353. https://doi.org/10.1007/s10113-017-1248-8.

Najafi, MR, H Moradkhani, and IW Jung. 2011. "Assessing the uncertainties of hydrologic model selection in climate change impact studies." *Hydrological processes* 25 (18): 2814-2826.

Neal, Jeffrey C., Nicholas A. Odoni, Mark A. Trigg, Jim E. Freer, Javier Garcia-Pintado, David C. Mason, Melissa Wood, and Paul D. Bates. 2015. "Efficient incorporation of channel cross-section geometry uncertainty into regional and global scale flood inundation models." *Journal of Hydrology* 529 (1): 169-183. https://doi.org/10.1016/j.jhydrol.2015.07.026.

Neal, Jeffrey, Toby Dunne, Chris Sampson, Andrew Smith, and Paul Bates. 2018. "Optimisation of the two-dimensional hydraulic model LISFOOD-FP for CPU architecture." *Environmental Modelling and Software* 107: 148-157. https://doi.org/10.1016/j.envsoft.2018.05.011.

Neal, Jeffrey, Guy Schumann, and Paul Bates. 2012. "A subgrid channel model for simulating river hydraulics and floodplain inundation over large and data sparse areas." *Water Resources Research* 48 (11). https://doi.org/10.1029/2012WR012514.

Neal, Jeffrey, Ignacio Villanueva, Nigel Wright, Thomas Willis, Timothy Fewtrell, and Paul Bates. 2012. "How much physical complexity is needed to model flood inundation?" *Hydrological Processes* 26 (15): 2264-2282. https://doi.org/10.1002/hyp.8339.

Nurse, L.A., R.F. McLean, J. Agard, L.P. Briguglio, V. Duvat-Magnan, N. Pelesikoti, E. Tompkins, and A. Webb. 2014. "Small Islands." In *ClimateChange 2014: Impacts, Adaptation, and Vulnerability. Part B: Regional Aspects.Contribution of Working Group II to the Fifth Assessment Report of the Intergovernmental Panel on Climate Change*, edited by Barros, C.B. Field V.R., D.J. Dokken, M.D. Mastrandrea, K.J. Mach, T.E. Bilir, M., K.L. Ebi Chatterjee, Y.O. Estrada, R.C. Genova, B. Girma, E.S. Kissel, A.N. and S. MacCracken Levy, P.R. Mastrandrea, & L.L. White, 1613-1654. Cambridge University Press, Cambridge, United Kingdom and New York, NY, USA.

Pasch, R. J., and T. B Kimberlain. 2011. *National Hurricane Center Tropical Cyclone Report: Hurricane Tomas.* https://www.nhc.noaa.gov/data/tcr/AL212010_Tomas.pdf.

Perini, L., L. Calabrese, G. Salerno, P. Ciavola, and C. Armaroli. 2016. "Evaluation of coastal vulnerability to flooding: Comparison of two different methodologies adopted by the Emilia-Romagna region (Italy)." *Natural Hazards and Earth System Sciences* 16 (1): 181-194. https://doi.org/10.5194/nhess-16-181-2016.

Pulwarty, Roger S., Leonard A. Nurse, and Ulric O. Trotz. 2010. Caribbean Islands in a Changing Climate. 52 (6): 16-27. https://doi.org/10.1080/00139157.2010.522460.

Rhiney, Kevon. 2015. "Geographies of Caribbean Vulnerability in a Changing Climate: Issues and Trends." *Geography Compass* 9 (3): 97-114. https://doi.org/10.1111/gec3.12199.

Saleh, F., V. Ramaswamy, Y. Wang, N. Georgas, A. Blumberg, and J. Pullen. 2017. "A multi-scale ensemble-based framework for forecasting compound coastal-riverine flooding: The Hackensack-Passaic watershed and Newark Bay." *Advances in Water Resources* 110: 371-386. https://doi.org/10.1016/j.advwatres.2017.10.026.

Sampson, Christopher C., Paul D. Bates, Jeffrey C. Neal, and Matthew S. Horritt. 2013. "An automated routing methodology to enable direct rainfall in high resolution shallow water models." *Hydrological Processes* 27 (3): 467-476. https://doi.org/10.1002/hyp.9515.

Savage, James Thomas Steven, Paul Bates, Jim Freer, Jeffrey Neal, and Giuseppe Aronica. 2016. "When does spatial resolution become spurious in probabilistic flood inundation

predictions?" *Hydrological Processes* 30 (13): 2014-2032. https://doi.org/10.1002/hyp.10749.

Savage, James Thomas Steven, Francesca Pianosi, Paul Bates, Jim Freer, and Thorsten Wagener. 2016. "Quantifying the importance of spatial resolution and other factors through global sensitivity analysis of a flood inundation model." *Water Resources Research* 52 (11): 9146-9163. https://doi.org/10.1002/2015WR018198.

Schaefli, Bettina, and Hoshin V. Gupta. 2007. "Do Nash values have value?" *Hydrological Processes* 21 (15): 2075-2080. https://doi.org/10.1002/hyp.6825.

Schumann, Guy, Paul D. Bates, Matthew S. Horritt, Patrick Matgen, and Florian Pappenberger. 2009. "Progress in integration of remote sensing-derived flood extent and stage data and hydraulic models." *Reviews of Geophysics* 47 (3). https://doi.org/10.1029/2008RG000274.

Schumann, Guy J. P., and Delwyn K. Moller. 2015. "Microwave remote sensing of flood inundation." *Physics and Chemistry of the Earth* 83-84: 84-95. https://doi.org/10.1016/j.pce.2015.05.002.

Shultz, James M., James P. Kossin, J. Marshall Shepherd, Justine M. Ransdell, Rory Walshe, Ilan Kelman, and Sandro Galea. 2019. "Risks, Health Consequences, and Response Challenges for Small-Island-Based Populations: Observations from the 2017 Atlantic Hurricane Season." *Disaster Medicine and Public Health Preparedness* 13 (1): 5-17. https://doi.org/10.1017/dmp.2018.28.

Singh, Prabhishek, and Raj Shree. 2016. "Analysis and effects of speckle noise in SAR images." 2016 2nd International Conference on Advances in Computing, Communication, & Automation (ICACCA) (Fall), 30 Sept.-1 Oct. 2016.

Skinner, Christopher J., Thomas J. Coulthard, Daniel R. Parsons, Jorge A. Ramirez, Liam Mullen, and Susan Manson. 2015. "Simulating tidal and storm surge hydraulics with a simple 2D inertia based model, in the Humber Estuary, U.K." *Estuarine, Coastal and Shelf Science* 155: 126-136. https://doi.org/10.1016/j.ecss.2015.01.019.

Sentinel Application Platform.

Stewart, S.R. 2017. *National Hurricane Center Tropical Cyclone Report: Hurricane Matthew*. https://www.nhc.noaa.gov/data/tcr/AL142016_Matthew.pdf.

Stockdon, Hilary F., Rob A. Holman, Peter A. Howd, and Asbury H. Sallenger. 2006. "Empirical parameterization of setup, swash, and runup." *Coastal Engineering* 53 (7): 573-588. https://doi.org/10.1016/j.coastaleng.2005.12.005.

Tavus, B., S. Kocaman, C. Gokceoglu, and H. A. Nefeslioglu. 2018. "CONSIDERATIONS ON THE USE OF SENTINEL-1 DATA IN FLOOD MAPPING IN URBAN AREAS: ANKARA (TURKEY) 2018 FLOODS." *The International Archives of the*

Photogrammetry, Remote Sensing and Spatial Information Sciences XLII-5: 575-581. https://doi.org/10.5194/isprs-archives-XLII-5-575-2018.

Teng, J., A. J. Jakeman, J. Vaze, B. F. W. Croke, D. Dutta, and S. Kim. 2017. "Flood inundation modelling: A review of methods, recent advances and uncertainty analysis." *Environmental Modelling and Software* 90: 201-216. https://doi.org/10.1016/j.envsoft.2017.01.006.

The Caribbean Catastrophe Risk Insurance Facility. 2016. *Tropical Cyclone Matthew (AL142016) Wind and Storm Surge: Preliminary Event Briefing.* https://www.ccrif.org/sites/default/files/publications/20160928-1001_CCRIF_PreliminaryEventBriefing_TCMatthew_WindwardIslands%26Barbados_20161004_Final.pdf.

Thornthwaite, C. W. 1948. "An Approach toward a Rational Classification of Climate." *Geographical Review* 38 (1): 55-94. https://doi.org/10.2307/210739.

Tian, Haifeng, Wang Li, Mingquan Wu, Ni Huang, Guodong Li, Xiang Li, and Zheng Niu. 2017. "Dynamic monitoring of the largest freshwater lake in China using a new water index derived from high spatiotemporal resolution sentinel-1A data." *Remote Sensing* 9 (6): 521. https://doi.org/10.3390/rs9060521.

Torres, Ramon, Paul Snoeij, Dirk Geudtner, David Bibby, Malcolm Davidson, Evert Attema, Pierre Potin, BjÖrn Rommen, Nicolas Floury, Mike Brown, Ignacio Navas Traver, Patrick Deghaye, Berthyl Duesmann, Betlem Rosich, Nuno Miranda, Claudio Bruno, Michelangelo L'Abbate, Renato Croci, Andrea Pietropaolo, Markus Huchler, and Friedhelm Rostan. 2012. "GMES Sentinel-1 mission." *Remote Sensing of Environment* 120: 9-24. https://doi.org/10.1016/j.rse.2011.05.028.

Transport Canada. 2019. Aeronautical Information Manual (TC AIM).

Tropical Rainfall Measuring Mission. 2011. TRMM (TMPA) Rainfall Estimate L3 3 hour 0.25 degree x 0.25 degree V7. Greenbelt, MD, Goddard Earth Sciences Data and Information Services Center (GES DISC),.

Twele, André, Wenxi Cao, Simon Plank, and Sandro Martinis. 2016. "Sentinel-1-based flood mapping: a fully automated processing chain." *International Journal of Remote Sensing* 37 (13): 2990-3004. https://doi.org/10.1080/01431161.2016.1192304.

U.S. Army Corps of Engineers. 2002. *Coastal engineering manual*. 6 vols. Vol. Report. U.S. Army Corps of Engineers. Washington, DC.

United Nations Conference on Trade and Development. 2017. Climate change impacts on coastal transportation infrastructure in the Caribbean: enhancing the adaptive capacity of Small Island Developing States (SIDS), SAINT LUCIA: a case study UNDA Project 1415O.

Vrugt, Jasper A., Hoshin V. Gupta, Willem Bouten, and Soroosh Sorooshian. 2003. "A Shuffled Complex Evolution Metropolis algorithm for optimization and uncertainty assessment of

hydrologic model parameters." *Water Resources Research* 39 (8): 1201-SWC116. https://doi.org/10.1029/2002WR001642.

Wagener, Thorsten, Douglas P. Boyle, Matthew J. Lees, Howard S. Wheater, Hoshin V. Gupta, and Soroosh Sorooshian. 2001. "A framework for development and application of hydrological models." *Hydrology and Earth System Sciences* 5 (1): 13-26. https://doi.org/10.5194/hess-5-13-2001.

Wang, Jingzhe, Jianli Ding, Guannan Li, Jing Liang, Danlin Yu, Tayierjiang Aishan, Fang Zhang, Jinming Yang, Aerzuna Abulimiti, and Jie Liu. 2019. "Dynamic detection of water surface area of Ebinur Lake using multi-source satellite data (Landsat and Sentinel-1A) and its responses to changing environment." *Catena* 177: 189-201. https://doi.org/10.1016/j.catena.2019.02.020.

Woodhouse, Iain H., and C. R. C. Press. 2017. *Introduction to microwave remote sensing*. First ed. Vol. Book, Whole. Boca Raton, FL: CRC Press.

World Travel and Tourism Council. 2019. St Lucia 2019 Annual Research: Key Highlights. World Travel and Tourism Council, London.

Yan, Kun, Giuliano Di Baldassarre, Dimitri P. Solomatine, Guy J. -P Schumann, vetenskapsområdet Teknisk-naturvetenskapliga, universitet Uppsala, sektionen Geovetenskapliga, geovetenskaper Institutionen för, and vatten och landskapslära Luft. 2015. "A review of low-cost space-borne data for flood modelling: topography, flood extent and water level." *Hydrological Processes* 29 (15): 3368-3387. https://doi.org/10.1002/hyp.10449.

Chapter 4

4 Flood Risk Analysis in Saint Lucia

Significant infrastructures in the study area include Hewanorra International Airport, Vieux Fort Seaport, the town of Vieux Fort and La Tourney, as well as the north-south highway. Those assets, along with other entities, ensure services and activities of key economic sectors in Saint Lucia such as tourism, agriculture, manufacturing, housing and human settlements, information and communications technology, health, food, energy, water, electricity, transportation, physical planning and infrastructure, watershed management, and disaster risk management. Interdependence is expected among infrastructures from different sectors, and therefore, failures of entities could propagate through the network and cause cascading effects. In this study, RiskLogik software was used to set up a network analysis model in order to investigate the impacts of indirect connections among entities, to explore the relative importance of entities in the system, as well as to prioritize risk for more efficient allocation of resources. Aside from normal conditions, flood scenarios were also introduced in the risk assessment. Flood conditions in the event of Tropical Storm Matthew, simulated by the hydrodynamic model LISFLOOD-FP in Chapter 3, were utilized to explore how flooding within the airport boundary affect the risk of entities. Results indicate that normal operation of Hewanorra International Airport is of fundamental significance in the system. To reduce risks of the airport especially in scenarios of flooding, prioritization should be given to those airport facilities whose risk indices are expected to dramatically increase due to floods. Moreover, essential services, such as transport, electricity services, as well as information and communication services, are at high risk in all scenarios, indicating the need to ensure those services all times regardless of in normal conditions or in floods.

4.1 Introduction

Saint Lucia, a tropical island in the Caribbean Sea, is located in the tropical cyclone belts and is highly exposed to multiple natural hazards such as storm surges, tide waves, landslides, tropical

storms, and hurricanes (ICF GHK 2012). Flood risks generated from these climate-related extreme events are exacerbated due to the mountainous topography in Saint Lucia, increasing impermeable surfaces associated with the coastal urbanization, inadequate and poorly maintained drainage systems in the city area, as well as the high concentration of infrastructures and settlements at coastal lowlands (ICF GHK 2012; Global Facility for Disaster Reduction and Recovery 2019). Historical events have revealed that critical infrastructures in the island, such as airports, seaports, roads, electricity networks, water systems as well as health facilities, are highly susceptible to flooding and landslides. Their potential failures in extreme events can lead to interruptions of essential services, tourism, agriculture, and other key economic sectors in Saint Lucia, thus leading to considerable economic losses (Global Facility for Disaster Reduction and Recovery 2019). For example, in August 2007, the storm surge associated with the Hurricane Dean occurred simultaneously with the normal high tide and the recorded maximum sea level was 10.2m (Augustine 2007). The northwest coast of the island was majorly impacted, leading to significant coastline erosion, damages to the marine equipment and infrastructure particularly in the Castries harbor and resort areas, as well as rock and sand washing back to the end of the runway of the George Charles Airport (Economic Commission for Latin America and the Caribbean 2007; Augustine 2007). According to Economic Commission for Latin American and the Caribbean (2011), in October 2010, Hurricane Tomas attacked Saint Lucia and the associated waves were equivalent to a 1:15 year event while the associated rainfall was classified as a 1:180 year event, triggering severe flooding across the island and leading to the total impact that is equivalent to 43.4% of GDP. Critical infrastructures, including the water supply and distribution utilities, roads and bridges, airports and seaports, electricity networks, as well as telecommunications, were heavily damaged and accounts for 43% of the total impact. Tourism was also greatly impacted mainly due to the flooding in the main tourist hub, damages to the hotels, disruptions of water supply, and the closure of the two airports during the event. Increased costs for the facilities include the fees for the cleanup of mud at the runway, dramatic loss of passengers immediately following the event, and the shuttle fees utilized to transfer passengers due to the loss of road connections. In December 2013, as reported in Global Facility for Disaster Reduction and Recovery (2014), a tropical trough system passed over Saint Lucia and generated extraordinarily heavy rainfall. The rainfall incurred intense and rapid flash floods, whose effects were enhanced due to the mountainous topography and the already saturated soil, leading to the total damages and losses

equivalent to 8.3% of the GDP. As is in the event of Hurricane Tomas, the major impact was sustained in the infrastructure sector, primarily related to transportation (72.31%) and water systems (6.44%). The impacts on the transportation largely refer to the damaged roads, bridges, the highway, and the closure of Hewanorra International Airport due to the temporal flooding in the runway and terminal building. Agriculture (12.99%) and tourism (2.12%) were also severely affected. In 2016, the passage of Hurricane Matthew produced heavy rainfall, strong winds, and rough seas, severely damaging the infrastructures and human settlements (Global Facility for Disaster Reduction and Recovery 2019). Major impacts include power outages observed in several communities, flooding in Vieux Fort and other cities, impassable roads, as well as the interruptions of water supply (International Federation of Red Cross and Red Crescent Societies 2017).

Current weather-related threats are expected to intensify under the changing climate. Sea level rise, increasing sea surface temperature and wind speed, as well as more intense tropical storms and hurricanes are projected in Saint Lucia, indicating the possibility of increased coastal erosion and loss of natural defences, higher storm tides and breaking of waves further inshore, higher possibility of severe inundation in low-lying coastal areas, as well as more frequent landslides and flooding from the intense seasonal rainfall and hurricanes (Government of Saint Lucia 2018). Key economic assets in Saint Lucia are mainly located at coastal lowlands and therefore at particularly high risk (United Nations Conference on Trade and Development 2017). Potential impacts of climate change on the infrastructure sector majorly relate to the loss of coastal properties and tourism utilities, reduced effectiveness of drainage systems, as well as destructions of critical infrastructures, thus resulting in increased risks of injuries, significant economic loss due to the interruptions of essential services provided by the commercial properties and critical infrastructures, as well as increased costs for relocating, replacing, and/or repairing the damaged infrastructures (Government of Saint Lucia 2018, 2017). Risk assessment, as a result, is necessary to protect significant assets from current and future extreme events.

Networks of critical infrastructures, which provide a broad range of fundamental services that are critical to social security and economic development, are highly interdependent and vulnerable to both internal and external threats (Eleutério, Hattemer, and Rozan 2013). According to Rinaldi, Peerenboom, and Kelly (2001), there are four principal types of interdependencies between two infrastructures: (i) physical interdependency means that there are material linkages between two

infrastructures; (ii) cyber interdependency represents information links that connect information infrastructures to others; (iii) geographic interdependency occurs when two infrastructures are spatially close to each other, and therefore, although there is no material or information linages, failures of one infrastructure can affect the other infrastructure; (iv) logical interdependency refers to the connections that are not physical, cyber, or geographic. Disruptions or failures of infrastructures can propagate to other infrastructures through the feedback loops, leading to much more severe consequences (Rinaldi, Peerenboom, and Kelly 2001). To prevent catastrophic infrastructure failures and mitigate damage, it is critical to identify the interdependence relationships among infrastructures as well as the pathways of possible failures.

O'Neill (2014) has proposed the Strongest Path Method (SPM) for performing risk analysis on interdependent infrastructures, which can not only identify the potential impact of one entity to another but also the compound effects of all possible pathways of failures. In SPM, risk is defined as the possibility of loss and is assessed through two dimensions: (i) the degree of impact, referring to the measures of the positive or negative consequences of an event; and (ii) the likelihood of occurrence, indicating the measures of the possibility or the relative level of belief in the possibility that an event would occur. Potential risks arising from the direct and indirect dependencies are considered in the modelling through directed graphs, where entities are represented as nodes and the direct connections are presented as directional edges. Modelling results can be used to evaluate the risk and relative importance of entities, which helps decision-makers prioritize risks and determine effective mitigation strategies. The RiskLogik software, developed by RiskLogik Inc. on the basis of SPM theory, was used in this study to identify connections among major assets, to analyze the pathways for potential failures, as well as to prioritize risks for preventing cascading consequences caused by interdependencies between infrastructures.

4.2 Methodology

4.2.1 Terminology

As discussed in O'Neill (2014), Strongest Path Method (SPM) can be used to understand indirect relationships and to conduct risk analysis for interdependent assets. Well defined terminology is the foundation of SPM and therefore is introduced in Table 22.

Table 22. Defined terminology in Strongest Path Method.

Terms	Definition
Entity	A distinct and individual existence in each sector. Entities can be physical or non-physical. They can be inputs and outputs, enablers and activities that require inputs and produce outputs, controls and regulations that govern the enablers and activities, or monitoring and verification agents that oversee the activities and processes.
Degree of Impact	A weight assigned to each entity reflecting its importance relative to the other entities in the networks.
Likelihood of Failure	A weight assigned to each entity indicating the relative likelihood that a node will fail in the condition of random internal causes or non-random external threats such as natural hazards.
System	A collection of entities that collaborate together to produce outputs.
Input	An entity or a system requires or receives inputs.
Output	An entity or a system produces outputs.
Direct Dependency Relationship	A direct relationship refers to the directional connections between two entities. The number of connections can be 0, 1, or 2. If there is zero connection, the two entities have no interaction. If there is 1 connection, one entity is dependent on the other entity. If there are 2 connections, the two entities are interdependent. The dependency or interdependency can be physical, cyber, geographic, or logical.
Degree of Dependence	A weight assigned to each relationship to reflect the strength of a relationship between two entities.
Directed Graph	SPM is developed based on the directed graphs, in which entities are represented as nodes and each pair of them may have directional connections represented as directed edges. In this modelling diagram, each entity has two weight indices, which are the degree of impact

	and the likelihood of failure, while the degree of dependence would be assigned to each directional relationship.
Global Impact	The global impact can be calculated for each entity. It means the impact of any node *x* on the entire model. The higher the global impact, the more important the entity is to the system, and accordingly, the more severe the consequences are if the entity fails.
Global Vulnerability	The global vulnerability can be calculated for each entity. It considers two factors, which are the likelihood of failure of any node *x*, and the cumulative vulnerability of node *x* from all nodes in the model. The higher the global vulnerability, the more vulnerable the entity is to the internal and external threats.
Risk Index	Risk index, defined as the product of global impact and global vulnerability, can be calculated for each entity and is used in SPM to compare risk among all entities. Prioritization should be given to entities that have a high risk index in the system.

4.2.2 Scoring Systems

The modeling diagram used in the RiskLogik software is called the directed graph, which consists of a set of nodes and a set of directional edges. Each node has two weight indices, namely, the degree of impact and the likelihood of failure, whose definitions are presented in Table 22. These two indices are assigned to nodes without regard for any of their explicit relationships in the networks. In the context of RiskLogik modelling, failure of an entity is defined as falling below the Minimum Acceptable Level of Service (MASL), which refers to the lowest level of functionality of an entity that allows its dependents to normally operate. Aside from MASL, other operational statuses of an entity are clarified in Table 23. If necessary, the likelihood of failure can be estimated in terms of “degree of belief” or “expert judgement”. Whether the analysis is quantitative or qualitative depends upon the data availability. Each edge should be assigned a weight called the degree of dependence to reflect the strength of direct connections between two entities. The degree of impact, the likelihood of failure, and the degree of dependence are pre-

defined parameters and are assigned as integers ranging from 0 to 10. The scoring criteria of those parameters, as indicated in Table 24, 25, and 26, are provided by the RiskLogik Inc. and applied consistently to every node and edge in this study.

Table 23. Operational status of an entity.

Operational Status	Definition
Minimum Operational Capability (MOC) Levels	MOC encompasses the required resource demands and the critical functions that enable an entity to survive. The MOC level is the lowest level of functionality of an entity. In this level, the operation of the entity is not sustainable since revenues do not cover costs. An entity is deemed to be "failed" when its functionality falls below MOC levels.
Minimum Sustainable Capability (MSC) Levels	MSC encompasses the operations to achieve a balance so that costs can be covered by revenues in the short term, enabling the entity to continue operating under adverse conditions. However, sustainability is not in the long term because the revenues do not allow for growth or capital investment.
Routine Operating Levels	Routine operations encompass the operations that allow the entities to operate under normal conditions. Under internal or external threats, routine operating levels indicate that entities could recover quickly or continue to operate at routine.

Table 24. Criteria used for assigning the Likelihood of Failure of an entity.

Likelihood of Failure	Value	Descriptions
Very Low	1	Unlikely to happen (once/10 years)
Low	3	May or may not happen (2 or 3 times/10 years)
Medium	5	Happens occasionally (2 or 3 times/5 years)
High	7	Happens frequently (once every 1-2 years)
Very High	9	Happens regularly (>once every year)

Table 25. Criteria used for assigning the Degree of Impact of an entity.

Degree of Impact	Value	Descriptions
Very Low	1	Little or no disruption to operations, or max $1 per capita loss expected
Low	3	Minor impact on operations (short term, <6 hours loss of operations expected), or max $10 per capita loss expected
Medium	5	Moderate impact on operations (between 6 and 24 hours loss of operations expected), or max $100 per capita loss expected
High	7	Major impact on operations (between 24 hours and 7 days loss of operations expected), or max $500 per capita loss expected
Very High	9	Disastrous impact (>7 days loss of operations expected), or >$500 per capita loss expected

Table 26. Criteria used for assigning the Degree of Dependence to a direct connection between two entities.

Degree of Dependence	Value	Descriptions
Low	2	Without invoking a contingency plan, the dependent entity will remain at Routine Operating levels if the reference entity fails.
Medium-Low	4	By invoking a contingency plan, the dependent entity will remain at MSC levels if the reference entity fails.
Medium-High	6	By invoking a contingency plan, the dependent entity will remain MOC levels if the reference entity fails.
High	8	The dependent entity will unavoidably fall below MOC levels if the reference entity fails.

4.2.3 Analytical Tools

In SPM, the risk is considered in two dimensions, namely the impact and the vulnerability. The modelling would start from the standalone risk assessment for each entity, which means assigning the degree of impact and the likelihood of failure to individual entities. Ordered pairs of entities are then connected by directional edges and the degree of dependence is assigned to each edge to represent the strength of the connections. Multiple directed paths can accordingly be generated. In each path, a node can be directly connected to its respective successor by an edge or indirectly connected to other nodes through one or more intervening nodes and edges. The length between the two entities is the number of intervening edges between them. The global impact and global vulnerability can subsequently be calculated for each entity in the system based on all its pathways of impacts on other entities and all its pathways of vulnerability from other entities.

To calculate the global impact of each entity in the networks, rules for propagating impact along the directed paths should be first defined. In SPM, the propagated impact can be no higher than the lesser of the degree of impact and the degree of dependence because it is expected that the failure of an entity with high degree of impact can have little impact on its dependent entities if their connections are weak, and if their connections are strong, the propagated impact depends on the degree of impact of the failed entity. Equation (4-1) can be used to illustrate the ***propagation of impact*** along each edge in the selected path.

$$I(z) = \min\{I(x), D(x,z)\} \tag{4-1}$$

where *x* and *z* are the entities, (*x*, *z*) indicates the edge directed from *x* to *z*, $I(z)$ is the degree of impact at *z* propagated from *x*, $I(x)$ is the degree of impact of *x*, $D(x,z)$ is the degree of direct dependence of *z* on *x*.

The propagation rule indicates that the greatest impact from entity *x* to *z* is propagated by the path or paths whose lowest degree edge has the highest degree of dependence among all pathways connecting the two entities. The ***strongest path*** is accordingly defined to indicate the path or paths carrying the largest impact with the shortest length. As indicated in Equation (4-2), when the strongest path between two entities do exist, the ***strongest path impact*** of *x* on *z* is the degree of dependence of the strongest path multiplied by the degree of impact of *x* raised to the power of the length of the strongest path. In other words, the more intervening edges between two indirectly connected entities, the less impact would propagate from the entity to its dependent entities.

$$I(\llbracket x,z \rrbracket) = D(\llbracket x,z \rrbracket) \times I(x)^{L(\llbracket x,z \rrbracket)} \tag{4-2}$$

where *x* and *z* are individual nodes, $\llbracket x,z \rrbracket$ is the strongest path from *x* to *z*, $I(\llbracket x,z \rrbracket)$ is the strongest path impact of *x* on *z*, $D(\llbracket x,z \rrbracket)$ is the degree of dependence of the strongest path, that is the degree of dependence of the lowest degree edge, and $L(\llbracket x,z \rrbracket)$ is the length of the strongest path.

Equation (4-3) can be used to estimate the ***cumulative impact*** of each entity to the other entity by considering all pathways that exist between them.

$$If\ [x,z] = \emptyset, then\ I([x,z]) = 0; otherwise,$$

$$I([x,z]) = 1 - \prod_{y \in E}(1 - min\{D(\llbracket x,y \rrbracket), D(y,z)\}) \times I(x)^{L(\llbracket x,y \rrbracket)+1} \tag{4-3}$$

where $[x, z]$ indicates all paths from x to z, $y \in E$ is the set of nodes on which z is directly dependent, $[\![x, y]\!]$ is the strongest path from x to y, (y, z) indicates the edge directed from y to z, $L([\![x, y]\!])$ is the length of the strongest path from x to y. This formula calculates the strongest path impact from x to z through y, and similar to the binomial probability function, it compounds the effects of all pathways from x to z. Based on the calculation of the cumulative impact, Equation (4-4) can be used to estimate the ***global impact*** of each entity.

$$I([x, G]) = \sum_{z \in N}\big(I[x, z] \times I(z)\big) / \sum_{z \in N} I(z) \tag{4-4}$$

where G denotes the directed graph with a set of nodes N, $z \in N$ means that z represents any node in the graph, $[x, G]$ indicates all paths from x to all nodes in G (including x itself), $[x, z]$ indicates all paths from x to z (including x itself), $I[x, z]$ is the cumulative impact of x on z, $I(z)$ is the degree of impact of the entity z showing the relative importance of z. The term $I[x, z] \times I(z)$ gives the global importance of the impact of x on z, and the sum of these products for all nodes z in the graph can be regarded as a sum of cumulative impact values weighted by the direct impact, giving the impact of x on the entire model. $\sum_{z \in N} I(z)$, the sum of the direct impact of all nodes, is used for normalization so that the global impact factor can be utilized to evaluate the relative impact of each entity to the model.

To calculate the global vulnerability of each entity, the source of vulnerability should be defined. In SPM, the possible failure of any entity z could be influenced by its likelihood of failure as well as the cumulative impact of other entities on it. The ***cumulative vulnerability*** of each entity from other entities could be calculated as Equation (4-5), and the ***global vulnerability*** of each entity could be represented as Equation (4-6).

$$\mathrm{F}([x, z]) = I([x, z]) \times F(x) \tag{4-5}$$

where x and z are entities, $\mathrm{F}([x, z])$ is the cumulative vulnerability of z from x, $I([x, z])$ is the cumulative impact of x on z, and $F(x)$ is the likelihood of failure of x.

$$\mathrm{F}([G, z]) = 1 - \prod_{x \in N}\big(1 - F([x, z])\big) \tag{4-6}$$

where G denotes the directed graph with a set of nodes N, $x \in N$ means that x represents any node in the graph, $\mathrm{F}([G, z])$ is the global vulnerability of z from the model, and $\mathrm{F}([x, z])$ is the

cumulative vulnerability of *z* from *x*. The binomial probability function is used to compound the effects of cumulative vulnerability from all nodes in the model.

Risk is in two dimensions in SPM, namely, the impact and the vulnerability. The ***risk index*** of each entity is defined as the product of its global impact and global vulnerability. Equation (4-7) is used to calculate the risk index and the results can be used to prioritize risks of entities.

$$\mathrm{R}(x) = I([x, G]) \times \mathrm{F}([G, x]) \tag{4-7}$$

where *x* denotes any entity in the model, $\mathrm{R}(x)$ is the risk index of *x*, $I([x, G])$ is the global impact of *x* on the model, and $\mathrm{F}([G, x])$ is the global vulnerability of *x* from the model.

In our study, the global impact, the global vulnerability, and the risk index would be calculated for each entity with the help of RiskLogik software. Those risk indices, as the evaluation criteria, would be utilized to explore the risk of different entities in the system.

4.3 Model Setup

According to Government of Saint Lucia (2017), key economic sectors in Saint Lucia include Tourism, Agriculture, Manufacturing, Housing and Human Settlements, Information and Communications Technology, Physical Planning and Infrastructure, Health, Energy, Water, Electricity, Transportation, Watershed Management, and Disaster Risk Management. Major assets pertaining to these sectors in the study area are Hewanorra International Airport, Vieux Fort Seaport, the town of Vieux Fort and La Tourney, and the north-south highway. To explore the role of those assets and how the failure of them propagate through the infrastructure network, the RiskLogik software was used to develop a network analysis model. The initial model was set up by RiskLogik Inc., and has subsequently been refined in our study for conducting the flood risk analysis. Considered entities, as is presented in Table 27, consist of inputs and outputs, enablers and activities, controls and regulations, as well as monitoring and verification agents, all of which support major services and assets in the study area, and by extension, the economy of the island. Entities in the network analysis framework could be categorized into the following classes: agriculture, assets and operations of Hewanorra International Airport, Eastern Caribbean Civil

Aviation Authority, electricity generation, electric power transmission, electricity distribution, energy, food, goods, government services, health, housing and human settlements, information and communication technology, manufacturing, physical planning and infrastructure, safety, tourism, transportation, flood control, floodplain development, water, and watershed management. Each entity is assigned two weights, namely, the degree of impact and the likelihood of failure, to illustrate its relative importance in the networks and the relative degree of belief that it would fail under internal and external threats. Due to the limited resources, weight indices are assessed in a qualitative manner. Major references are official reports from the Government of Saint Lucia and professional experience from RiskLogik Inc.

Adapted from Rinaldi, Peerenboom, and Kelly (2001), the direct connections between two entities in this study can be physical, cyber, and logical. Physical connections mean that the state of one entity is dependent on the material output(s) of the other entity. For example, freshwater resources, including the rivers, springs, streams, and wetlands, are water supplies to drinking water treatment plants. Operations of airports, housing and human settlements, manufacturing, as well as hotels and restaurants are also highly dependent on the electricity brought by the distribution systems. Cyber connections indicate that the state of one entity depends on the information that is transmitted and delivered by the other entity. Flood control systems, especially the emergency measures such as sandbags, are dependent on the monitoring of water levels and rainfall intensities at gauges, as well as the outcomes of flood risk analysis. Logical connections denote connections that are not physical, cyber, or geographic, majorly referring to human decisions and regulations that link an agent in one entity to an agent in the other entity. For example, departments that propose stormwater management plans would have significant impacts on departments that are responsible for the design of the local sewer system. Geographic connections, indicating that the state of one entity would be affected by the other entity if they are geographically close to each other, are not considered in this study due to the lack of data resources. The strength of the direct connections is assigned based on Table 26. The directed graph set up for the study area in the RiskLogik software and the model setup (i.e. the degree of impact of each entity, the likelihood of failure of each entity, and the degree of dependence between two entities) are presented in Figure 30 and Table 28, respectively.

Table 27. The hierarchical system of considered entities.

Level 1	Level 2	Level 3	Level 4	Level 5
Agriculture	Banana			
	Fisheries			
	Livestock			
	Non-banana Crops			
Airport Processes	Air Traffic Control			
	Air Traffic Management			
	Aircraft Fueling			
	Airplane Landing and Taking Off			
	Baggage and Disembarkation of Passengers			
	Cargo Loading and Unloading			
	Crash, Fire, and Rescue Services			
	Lighting of Runway and Taxiway			
	Meteorological Services			
	Parking			
	Security and Screening Services	Baggage		
		Cargo		
		People		

Airport Resources	Hewanorra International Airport	Air Terminal	Baggage Handling Equipment	
			Gate Counters	
			Purchase and Check-in Counters	
			Security Screening	
		Aircraft and Cargo Capacity	Aircrews	
			Ground Support Crews	
			Ground Support Equipment	Aircraft Fueling and Refueling
				Cargo Loading and Unloading
				Cargo Shed for Storage
				Engine and Fuselage Examination
				Food and Beverage Catering
				Lavatory Waste Tank Drainage
				Maintenance
				Passenger Loading and Unloading
				Portable Water Storage

		Backup Electricity Generators	For the Control Tower and Air Traffic Systems	
			For the Crash, Fire and Rescue Services	
			For the Terminal Building	
		Control Tower		
		Drainage System	Drainage System in the Parking Lots	
			Drainage System in the Runway	
			Drainage System in the Taxiway/Apron	
		Fire and Rescue Building		
		Fuel Depot		
		Fuel Supplies to the Airport	Aviation Fuel	
			Diesel	
			Vehicle Gasoline	
		Runway Conditions	Clearing of the Runway	Clearing Crews
				Clearing Efficiency
				Clearing Equipment
			Runway Status	Contamination Conditions
				Runway Length

		Taxiway/Apron Conditions	Clearing of the Taxiway/Apron	Clearing Crews
				Clearing Efficiency
				Clearing Equipment
			Taxiway/Apron Status	Contamination Conditions
		Meteorological Office		
		Parking Lot Status	Flood/Rain Water Depth	
			Flood/Rain Water Extent	
		Runway and Taxiway Lighting Systems		
Airport's Normal Operations				
Eastern Caribbean Civil Aviation Authority	Air Traffic Control System	Communication System		
		Radar		
		Visual		
	Terminal Control System	Communication System		
		Radar		
		Visual		
Electric Power Transmission	Castries Substation			
	Cul-De-Sac Substation			
	Praslin Substation			
	Reduit Substation			
	Soufriere Substation			

	Union Substation			
	Vieux Fort Substation			
Electricity Generation	Saint Lucia Electricity Services Limited	Cul-de-Sac Power Station		
		Solar Farms		
Energy	Distribution Systems	Fuel Lines		
		Gas Pipelines		
		Petrol Stations		
		Road Transportation		
	Imported Petroleum Products			
	Storage Facilities	Liquefied Petroleum Gas Storage Facility in the South		
		Oil Storage Facility in the North		
Food	Processing			
	Retailing	Convenience Stores		
		Grocery Stores		
		Public Markets		
	Wholesale and Food Distribution			
Goods	Exports			
	Imports			
Government Services	Ministry of External Affairs, International Trade and Civil Aviation	Regulations on External Affairs and International Trade		
		St Lucia Air and Sea Ports Authority		

	Ministry of Finance and Economic Affairs	Customs and Excise Services		
Health	Health Facilities			
Housing and Human Settlements	Other Human Settlements			
	The Town of La Tourney			
	The Town of Vieux Fort			
Information and Communication Technology	Cell Towers			
	Data Communications			
	Internet Access			
	Voice Communications			
Manufacturing	Heavy Industry	Chemical Industry		
		Petroleum and Coal Industry		
		Primary Metals Industry		
		Pulp and Paper Industry		
	Light Industry	Food Industry		
		Paper Making		
Physical Planning and Infrastructure	Energy and Utilities	Electricity Distribution		
		Heating Oil Distribution		
		Natural Gas Distribution		
		Vehicle Fuel Distribution	Diesel	
			Gasoline	
	Transportation Assets	Bridges		
		Major North-South Highway		

		Roads		
		Vieux Fort Seaport		
Safety	Emergency Services	EMS		
		Fire		
		Police		
	Emergency Shelters			
Tourism	Hotels and Restaurants Performance			
	Near-shore Tourist Attractions	Beaches		
		Reef-based Activities		
	Soft Adventure Activities	Biking		
		Eco-tours to waterfalls and rainforests		
		Hiking		
		Mountain Climbing		
	Tourist Arrivals	Cruise Ship and Yacht Arrivals		
		Flight Arrivals	International Flights	
			Regional Flights	
Transportation	Goods and Freight	Road Transportation		
		Water Transportation		
	People	Inter-city Road Transportation		
		Intra-city Road Transportation		
		Water Transportation		

Watershed Sub-sectors	Flood Control	Coastal Defenses	Hard Engineering Options	Groynes
				Sea Wall
			Natural Coastal Protection	Reef
			Soft Engineering Options	Beach Nourishment
				Managed Retreat
		Rainwater Control	Dams	
			Dykes	
			Low-impact Development	
			Municipal Drains	
			Open Channels	
		River Defences	Floodplain and Groundwater Replenishment	
			Levees	
			Weirs	
		Temporary Perimeter Barriers		
	Floodplain Development Controls	Flood Risk Analysis		
		Floodplain Development Standards		
		Floodplain Mapping		
	Freshwater Resources	Rivers		
		Springs		

		Streams		
		Wetlands		
	Wastewater Treatment and Discharge			
	Water Consumption	Drinking Water	Drinking Water Distribution	
			Drinking Water Treatment	
		Water for Agricultural Uses	Animal Production	
			Crop Production	
		Water for Firefighting		
		Water for Industrial Uses		
	Water Monitoring	Land Use Practices		
		Marine Ecosystem	Coral Reefs	
			Mangroves	
			Sea Grass Beds	
		Rainwater		
		Sea Level		
		Streamflow		
		Urban Flood Conditions		
		Water Quality		
	Watershed Management Plans	Allocation and Use of Water Resources		
		Protection and Control of Water Resources		
		Stormwater Management		

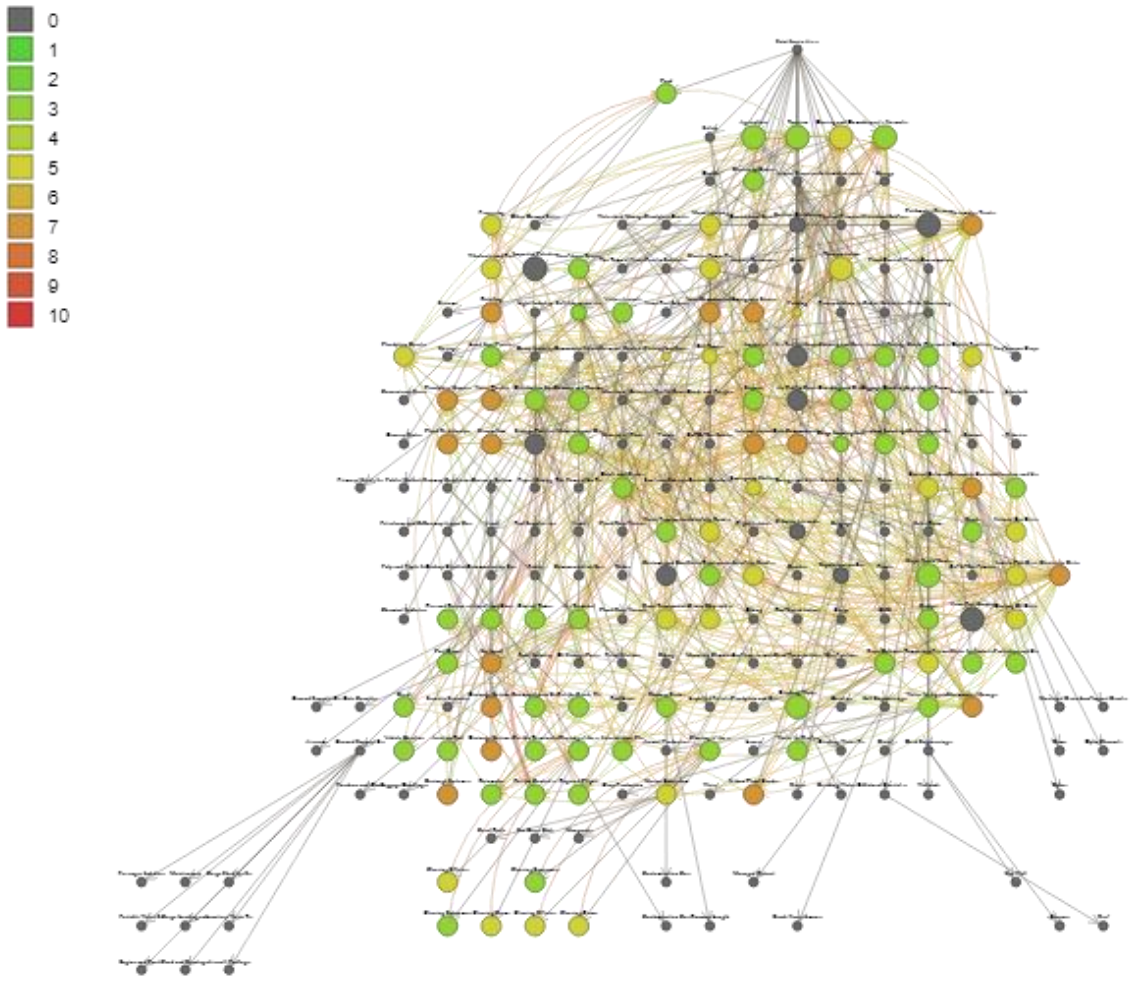

Figure 30. The directed graph set up in the RiskLogik software.

Table 28. Pre-defined parameters values in the model setup.

Entity	Degree of Impact	Likelihood of Failure	Downstream Direct Connections		Upstream Direct Connections	
			Entity Name	Degree of Dependence	Entity Name	Degree of Dependence
Agriculture	7	3	Processing	6	Electricity Distribution	6
			Exports	6	Water for Agricultural Uses	6
			Wastewater Treatment and Discharge	6	Manufacturing	4
			Tourism	4	Distribution Systems	6
					Floodplain Development Standards	4
					Coastal Defences	7
					Rainwater Control	6
Air Traffic Control	5	1	Air Traffic Management	4	Control Tower	9
			Airplane Landing and Taking Off	9	Meteorological Services	6
			Airport's Normal Operations	9	Air Traffic Management	4
					Eastern Caribbean Civil Aviation Authority	4
Air Traffic Management	5	1	Airport's Normal Operations	8	Meteorological Services	6
			Airplane Landing and Taking Off	8	Air Traffic Control	4

			Air Traffic Control	4	Eastern Caribbean Civil Aviation Authority	4
					St Lucia Air and Sea Ports Authority	4
Aircraft Fueling	5	3	Airplane Landing and Taking Off	8	Aircraft and Cargo Capacity	8
					Taxiway/Apron Status	8
					Aviation Fuel	6
					Fuel Depot	6
Airplane Landing and Taking Off	5	3	Airport's Normal Operations	9	Aircraft and Cargo Capacity	8
					Lighting of Runway and Taxiway	6
					Aircraft Fueling	8
					Runway Status	9
					Air Traffic Management	8
					Air Traffic Control	9
Baggage Handling Services	5	3	Airport's Normal Operations	8	Air Terminal	8
					Aircraft and Cargo Capacity	8
					Taxiway/Apron Status	8
Boarding and Disembarkation of Passenger	5	3	Airport's Normal Operations	8	Air Terminal	8
					Aircraft and Cargo Capacity	8
					Taxiway/Apron Status	8

Cargo Loading/Unloading	3	3	Airport's Normal Operations	6	Aircraft and Cargo Capacity	8
					Taxiway/Apron Status	8
Crash, Fire and Rescue Services	5	3	Airport's Normal Operations	8	Fire and Rescue Building	8
					Aircraft and Cargo Capacity	6
Lighting of Runway and Taxiway	5	3	Airplane Landing and Taking Off	6	Runway and Taxiway Lighting Systems	8
Meteorological Services	5	3	Air Traffic Management	6	Meteorological Office	8
			Air Traffic Control	6		
Parking	1	5	Airport's Normal Operations	2	Parking Lot Status	6
Security and Screening Services	5	3	Airport's Normal Operations	8	Air Terminal	8
Air Terminal	5	3	Baggage Handling Services	8	Electricity Distribution	6
			Boarding and Disembarkation of Passenger	8	For the Terminal Building	9
			Security and Screening Services	8	Drinking Water	6
			Wastewater Treatment and Discharge	6	Wholesale and Food Distribution	4
					Rainwater Control	6
					River Defences	8
Aircraft and Cargo Capacity	5	3	Airplane Landing and Taking Off	8	Diesel	6
			Aircraft Fueling	8	Vehicle Gasoline	6

			Boarding and Disembarkation of Passenger	8	Electricity Distribution	6
			Cargo Loading/Unloading	8	For the Control Tower and Air Traffic Systems	9
			Baggage Handling Services	8		
			Crash, Fire and Rescue Services	6		
For the Control Tower and Air Traffic Systems	5	3	Control Tower	9	Diesel	6
			Runway and Taxiway Lighting Systems	9	Rainwater Control	6
			Meteorological Office	9		
			Aircraft and Cargo Capacity	9		
For the Crash, Fire and Rescue Services	5	3	Fire and Rescue Building	9	Diesel	6
					Rainwater Control	6
For the Terminal Building	5	3	Air Terminal	9	Diesel	6
					Rainwater Control	6
Control Tower	5	3	Air Traffic Control	9	Electricity Distribution	6
			Wastewater Treatment and Discharge	6	For the Control Tower and Air Traffic Systems	9
					Drinking Water	6
					Rainwater Control	4
Drainage System in the Parking Lots	5	7	Parking Lot Status	6		
			Wastewater Treatment and Discharge	4		

Drainage System in the Runway	5	7	Runway Status	6		
			Wastewater Treatment and Discharge	4		
Drainage System in the Taxiway/Apron	5	7	Taxiway/Apron Status	6		
			Wastewater Treatment and Discharge	4		
Fire and Rescue Building	5	3	Crash, Fire and Rescue Services	8	Electricity Distribution	6
					For the Crash, Fire and Rescue Services	9
					Water for Firefighting	6
					Rainwater Control	4
Fuel Depot	5	3	Aircraft Fueling	6	Aviation Fuel	6
					Rainwater Control	4
Fuel Supplies of Aviation Fuel to the Airport	5	3	Fuel Depot	6	Distribution Systems	8
			Aircraft Fueling	6		
Fuel Supplies of Diesel to the Airport	5	3	Aircraft and Cargo Capacity	6	Distribution Systems	8
			For the Control Tower and Air Traffic Systems	6		
			For the Crash, Fire and Rescue Services	6		
			For the Terminal Building	6		
Fuel Supplies of Vehicle Gasoline to the Airport	5	3	Aircraft and Cargo Capacity	6	Distribution Systems	8

Clearing of the Runway	5	3	Runway Status	9	Clearing Crews	8
					Clearing Efficiency	8
					Clearing Equipment	8
Clearing Crews	5	5	Clearing of the Runway	8		
Clearing Efficiency	5	5	Clearing of the Runway	8		
Clearing Equipment	5	3	Clearing of the Runway	8		
Runway Status	5	3	Airplane Landing and Taking Off	9	Clearing of the Runway	9
					Drainage System in the Runway	6
					Coastal Defences	6
					Rainwater Control	6
					River Defences	6
Clearing of the Taxiway/Apron	5	3	Taxiway/Apron Status	9	Clearing Crews	8
					Clearing Efficiency	8
					Clearing Equipment	8
Clearing Crews	5	5	Clearing of the Taxiway/Apron	8		
Clearing Efficiency	5	5	Clearing of the Taxiway/Apron	8		
Clearing Equipment	5	3	Clearing of the Taxiway/Apron	8		
Taxiway/Apron Status	5	3	Aircraft Fueling	8	Clearing of the Taxiway/Apron	9
			Baggage Handling Services	8	Drainage System in the Taxiway/Apron	6

			Boarding and Disembarkation of Passenger	8	Coastal Defences	6
			Cargo Loading/Unloading	8	Rainwater Control	6
					River Defences	6
Meteorological Office	5	3	Meteorological Services	8	Electricity Distribution	6
			Rainwater	6	Internet Access	6
			Wastewater Treatment and Discharge	6	For the Control Tower and Air Traffic Systems	9
					Data Communications	6
					Drinking Water	6
					Rainwater Control	4
Parking Lot Status	1	5	Parking	6	Drainage System in the Parking Lots	6
					Rainwater Control	4
Runway and Taxiway Lighting Systems	5	3	Lighting of Runway and Taxiway	8	Electricity Distribution	6
					For the Control Tower and Air Traffic Systems	9
					Rainwater Control	4
Airport's Normal Operations	7	3	Imports	4	Airplane Landing and Taking Off	9
			Exports	4	Baggage Handling Services	8
			International Flights	9	Boarding and Disembarkation of Passenger	8
			Regional Flights	6	Cargo Loading/Unloading	6

			Transportation	8	Crash, Fire and Rescue Services	8
					Parking	2
					Security and Screening Services	8
					Internet Access	8
					Voice Communications	8
					Air Traffic Management	8
					Eastern Caribbean Civil Aviation Authority	4
					Air Traffic Control	9
					Data Communications	8
					St Lucia Air and Sea Ports Authority	4
Eastern Caribbean Civil Aviation Authority	3	1	Airport's Normal Operations	4		
			Air Traffic Management	4		
			Air Traffic Control	4		
Electric Power Transmission	5	5	Electricity Distribution	9	Electricity Generation	9
					Rainwater Control	6
Electricity Generation	5	3	Electric Power Transmission	9	Distribution Systems	6
					Rainwater Control	6
Distribution Systems	5	3	Heating Oil Distribution	8	Storage Facilities	8
			Natural Gas Distribution	8	Bridges	4
			Vehicle Fuel Distribution	8	Major North-South Highway	4
			Electricity Generation	6	Roads	4

			Agriculture	6	Electricity Distribution	6
			Aviation Fuel	8	Rainwater Control	6
			Diesel	8		
			Vehicle Gasoline	8		
Imported Petroleum Products	7	1	Storage Facilities	6	Customs and Excise Services	6
					Vieux Fort Seaport	6
Storage Facilities	5	1	Distribution Systems	8	Imported Petroleum Products	6
Food	5	3	Tourism	6	Processing	6
					Retailing	6
					Wholesale and Food Distribution	6
Processing	5	5	Wholesale and Food Distribution	8	Agriculture	6
			Wastewater Treatment and Discharge	6	Manufacturing	4
			Food	6	Drinking Water	8
					Imports	6
					Electricity Distribution	6
					Water for Industrial Uses	8
Retailing	5	7	Housing and Human Settlements	6	Wholesale and Food Distribution	8
			Near-shore Tourist Attractions	4	Electricity Distribution	8
			Food	6	Drinking Water	6
Wholesale and Food Distribution	5	5	Retailing	8	Road Transportation	6
			Air Terminal	4	Electricity Distribution	6

			Hotels and Restaurants Performance	6	Processing	8
			Housing and Human Settlements	6		
			Food	6		
Exports	5	3			Water Transportation	6
					Airport's Normal Operations	4
					Manufacturing	6
					Regulations on External Affairs and International Trade	4
					Agriculture	6
					Customs and Excise Services	6
Imports	5	3	Processing	6	Customs and Excise Services	6
			Manufacturing	6	Water Transportation	6
					Airport's Normal Operations	4
					Regulations on External Affairs and International Trade	4
Regulations on External Affairs and International Trade	3	1	Imports	4		
			Exports	4		

St Lucia Air and Sea Ports Authority	3	1	Vieux Fort Seaport	4		
			Airport's Normal Operations	4		
			Air Traffic Management	4		
Customs and Excise Services	5	1	Imports	6		
			Imported Petroleum Products	6		
			Exports	6		
			Cruise Ship and Yacht Arrivals	6		
			International Flights	6		
			Regional Flights	6		
Health Facilities	5	5	Wastewater Treatment and Discharge	6	Electricity Distribution	6
					Natural Gas Distribution	6
					Drinking Water	6
					Heating Oil Distribution	6
					Rainwater Control	6
					Temporary Perimeter Barriers	8
Housing and Human Settlements	7	5	Wastewater Treatment and Discharge	7	Electricity Distribution	6
					Heating Oil Distribution	6
					Natural Gas Distribution	6
					Drinking Water	8
					Retailing	6
					Wholesale and Food Distribution	6

					Data Communications	6
					Internet Access	6
					Voice Communications	6
					Floodplain Development Standards	6
					Coastal Defences	6
					Rainwater Control	8
					River Defences	6
					Temporary Perimeter Barriers	8
					Wastewater Treatment and Discharge	6
					Transportation	6
Cell Towers	3	5	Voice Communications	6	Electricity Distribution	6
			Data Communications	6	Rainwater Control	6
			Internet Access	6		
Data Communications	5	7	Meteorological Office	6	Cell Towers	6
			Manufacturing	6	Electricity Distribution	6
			Airport's Normal Operations	8		
			Housing and Human Settlements	6		
			Emergency Services	6		
			Urban Flood Conditions	6		
			Water Quality	6		
			Streamflow	6		
			Sea Level	6		
			Rainwater	6		
			Marine Ecosystem	6		

			Land Uses Practices	6		
			Tourism	6		
Internet Access	5	7	Meteorological Office	6	Electricity Distribution	6
			Airport's Normal Operations	8	Cell Towers	6
			Manufacturing	6		
			Housing and Human Settlements	6		
			Emergency Services	6		
			Urban Flood Conditions	6		
			Water Quality	6		
			Streamflow	6		
			Sea Level	6		
			Rainwater	6		
			Marine Ecosystem	6		
			Land Uses Practices	6		
			Tourism	6		
Voice Communications	5	7	Airport's Normal Operations	8	Cell Towers	6
			Emergency Services	6	Electricity Distribution	6
			Housing and Human Settlements	6		
			Urban Flood Conditions	6		
			Streamflow	6		
			Water Quality	6		
			Sea Level	6		
			Rainwater	6		
			Marine Ecosystem	6		

			Land Uses Practices	6		
			Tourism	6		
Manufacturing	5	5	Exports	6	Electricity Distribution	6
			Agriculture	4	Natural Gas Distribution	6
			Processing	4	Data Communications	6
			Wastewater Treatment and Discharge	7	Internet Access	6
			Tourism	6	Water for Industrial Uses	8
					Drinking Water	6
					Imports	6
					Heating Oil Distribution	6
Electricity Distribution	5	7	Emergency Services	6	Electric Power Transmission	9
			Cell Towers	6	Rainwater Control	6
			Internet Access	6		
			Emergency Shelters	8		
			Health Facilities	6		
			Data Communications	6		
			Voice Communications	6		
			Agriculture	6		
			Air Terminal	6		
			Control Tower	6		
			Fire and Rescue Building	6		
			Meteorological Office	6		
			Runway and Taxiway Lighting Systems	6		
			Housing and Human Settlements	6		

			Aircraft and Cargo Capacity	6		
			Manufacturing	6		
			Hotels and Restaurants Performance	6		
			Distribution Systems	6		
			Processing	6		
			Retailing	8		
			Drinking Water	6		
			Wholesale and Food Distribution	6		
			Wastewater Treatment and Discharge	6		
			Land Uses Practices	6		
			Rainwater	6		
			Sea Level	6		
			Streamflow	6		
			Water Quality	6		
			Urban Flood Conditions	6		
			Marine Ecosystem	6		
			Water for Agricultural Uses	4		
			Water for Firefighting	4		
			Water for Industrial Uses	4		
			Tourism	6		
Heating Oil Distribution	5	5	Emergency Shelters	8	Distribution Systems	8
			Housing and Human Settlements	6		

			Hotels and Restaurants Performance	6		
			Health Facilities	6		
			Manufacturing	6		
Natural Gas Distribution	5	5	Health Facilities	6	Distribution Systems	8
			Emergency Shelters	8	Rainwater Control	6
			Housing and Human Settlements	6		
			Manufacturing	6		
			Hotels and Restaurants Performance	6		
Vehicle Fuel Distribution	5	5	Emergency Services	6	Distribution Systems	8
			Road Transportation	8	Rainwater Control	6
			Water Transportation	8		
			Inter-city Road Transportation	8		
			Intra-city Road Transportation	8		
			Water Transportation	8		
Bridges	5	3	Road Transportation	6	Rainwater Control	6
			Inter-city Road Transportation	6		
			Intra-city Road Transportation	6		
			Distribution Systems	4		
			Wastewater Treatment and Discharge	4		

Major North-South Highway	7	3	Road Transportation	6	Rainwater Control	6
			Inter-city Road Transportation	8		
			Distribution Systems	4		
			Intra-city Road Transportation	6		
			Wastewater Treatment and Discharge	4		
Roads	5	3	Road Transportation	6	Rainwater Control	6
			Inter-city Road Transportation	6		
			Intra-city Road Transportation	6		
			Distribution Systems	4		
			Wastewater Treatment and Discharge	4		
Vieux Fort Seaport	7	1	Water Transportation	6	St Lucia Air and Sea Ports Authority	4
			Water Transportation	6	Rainwater Control	6
			Imported Petroleum Products	6		
			Wastewater Treatment and Discharge	4		
Emergency Services	5	7			Electricity Distribution	6
					Vehicle Fuel Distribution	6
					Voice Communications	6
					Inter-city Road Transportation	6

					Intra-city Road Transportation	6
					Water for Firefighting	6
					Data Communications	6
					Internet Access	6
Emergency Shelters	3	5	Wastewater Treatment and Discharge	6	Electricity Distribution	8
					Heating Oil Distribution	8
					Natural Gas Distribution	8
					Drinking Water	6
Tourism	7	3			Transportation	8
					Hotels and Restaurants Performance	8
					Near-shore Tourist Attractions	8
					Soft Adventure Activities	6
					Visitor Arrivals	8
					Manufacturing	6
					Agriculture	4
					Data Communications	6
					Internet Access	6
					Voice Communications	6
					Electricity Distribution	6
					Food	6
Hotels and Restaurants Performance	5	3	Wastewater Treatment and Discharge	7	Inter-city Road Transportation	6
			Tourism	8	Intra-city Road Transportation	6
					Heating Oil Distribution	6

					Natural Gas Distribution	6
					Electricity Distribution	6
					International Flights	7
					Regional Flights	7
					Cruise Ship and Yacht Arrivals	7
					Drinking Water	6
					Wholesale and Food Distribution	6
					Floodplain Development Standards	6
					Coastal Defences	7
					Rainwater Control	6
					Wastewater Treatment and Discharge	6
					Temporary Perimeter Barriers	8
Near-shore Tourist Attractions	5	3	Cruise Ship and Yacht Arrivals	6	Inter-city Road Transportation	6
			International Flights	7	Intra-city Road Transportation	6
			Regional Flights	6	Retailing	4
			Wastewater Treatment and Discharge	4	Floodplain Development Standards	6
			Tourism	8	Coastal Defences	7
					Wastewater Treatment and Discharge	6
					Rainwater Control	4
					Marine Ecosystem	6

Soft Adventure Activities	3	3	Cruise Ship and Yacht Arrivals	6	Inter-city Road Transportation	6
			International Flights	6	Intra-city Road Transportation	6
			Regional Flights	6	Rainwater Control	6
			Tourism	6		
Visitor Arrivals	5	3	Tourism	8	Cruise Ship and Yacht Arrivals	6
					International Flights	6
					Regional Flights	6
Cruise Ship and Yacht Arrivals	5	5	Hotels and Restaurants Performance	7	Water Transportation	8
			Visitor Arrivals	6	Near-shore Tourist Attractions	6
					Soft Adventure Activities	6
					Customs and Excise Services	6
International Flights	5	3	Hotels and Restaurants Performance	7	Airport's Normal Operations	9
			Visitor Arrivals	6	Near-shore Tourist Attractions	7
					Soft Adventure Activities	6
					Customs and Excise Services	6
Regional Flights	5	3	Hotels and Restaurants Performance	7	Airport's Normal Operations	6
			Visitor Arrivals	6	Near-shore Tourist Attractions	6

Transportation	7	5	Tourism	8	Soft Adventure Activities	6
					Customs and Excise Services	6
					Airport's Normal Operations	8
			Housing and Human Settlements	6	Road Transportation	8
					Water Transportation	8
					Inter-city Road Transportation	8
					Intra-city Transportation	8
					Water Transportation	8
					Water Transportation	8
Road Transportation	5	5	Wholesale and Food Distribution	6	Vehicle Fuel Distribution	8
			Transportation	8	Bridges	6
					Major North-South Highway	6
					Roads	6
Water Transportation	5	3	Imports	6	Vehicle Fuel Distribution	8
			Exports	6	Vieux Fort Seaport	6
			Transportation	8		
Inter-city Road Transportation	5	5	Hotels and Restaurants Performance	6	Vehicle Fuel Distribution	8
			Near-shore Tourist Attractions	6	Bridges	6
			Soft Adventure Activities	6	Major North-South Highway	8

			Emergency Services	6	Roads	6
			Transportation	8		
			Hotels and Restaurants Performance	6	Vehicle Fuel Distribution	8
Intra-city Road Transportation	5	5	Near-shore Tourist Attractions	6	Bridges	6
			Soft Adventure Activities	6	Roads	6
			Emergency Services	6	Major North-South Highway	6
			Transportation	8		
Water Transportation	5	3	Cruise Ship and Yacht Arrivals	8	Vehicle Fuel Distribution	8
			Transportation	8	Vieux Fort Seaport	6
Coastal Defences	5	5	Agriculture	7	Sea Level	6
			Runway Status	6	Land Uses Practices	6
			Taxiway/Apron Status	6	Floodplain Development Standards	6
			Housing and Human Settlements	6	Flood Risk Analysis	6
			Hotels and Restaurants Performance	7	Floodplain Mapping	6
			Near-shore Tourist Attractions	7	Marine Ecosystem	6
			Floodplain Development Standards	6	Stormwater Management	4
					Wastewater Treatment and Discharge	6
Rainwater Control	5	7	Agriculture	6	Rainwater	7
			Air Terminal	6	Land Uses Practices	6

Control Tower	4	Floodplain Development Standards	6
Fuel Depot	4	Flood Risk Analysis	6
Runway Status	6	Floodplain Mapping	6
Taxiway/Apron Status	6	Stormwater Management	8
Meteorological Office	4		
Parking Lot Status	4		
Electric Power Transmission	6		
Distribution Systems	6		
Electricity Generation	6		
Housing and Human Settlements	8		
Electricity Distribution	6		
Natural Gas Distribution	6		
Vehicle Fuel Distribution	6		
Bridges	6		
Major North-South Highway	6		
Roads	6		
Vieux Fort Seaport	6		
Fire and Rescue Building	4		
Health Facilities	6		
Cell Towers	6		
Hotels and Restaurants Performance	6		
For the Control Tower and Air Traffic Systems	6		

			For the Crash, Fire and Rescue Services	6		
			For the Terminal Building	6		
			Soft Adventure Activities	6		
			Near-shore Tourist Attractions	4		
			Floodplain Development Standards	6		
			Runway and Taxiway Lighting Systems	4		
River Defences	5	3	Air Terminal	8	Sea Level	6
			Runway Status	6	Rainwater	6
			Taxiway/Apron Status	6	Streamflow	7
			Housing and Human Settlements	6	Land Uses Practices	6
			Floodplain Development Standards	6	Floodplain Development Standards	6
					Flood Risk Analysis	6
					Floodplain Mapping	6
					Stormwater Management	4
Temporary Perimeter Barriers	5	5	Housing and Human Settlements	8	Sea Level	6
			Health Facilities	8	Streamflow	6
			Hotels and Restaurants Performance	8	Rainwater	6
					Land Uses Practices	4
					Urban Flood Conditions	7

Flood Risk Analysis	5	7	Floodplain Development Standards	6	Land Uses Practices	6
			Coastal Defences	6	Floodplain Mapping	8
			Rainwater Control	6	Stormwater Management	4
			River Defences	6		
			Stormwater Management	4		
Floodplain Development Standards	5	5	Housing and Human Settlements	6	Flood Risk Analysis	6
			Near-shore Tourist Attractions	6	Stormwater Management	4
			Hotels and Restaurants Performance	6	Land Uses Practices	6
			Agriculture	4	Coastal Defences	6
			River Defences	6	Rainwater Control	6
			Rainwater Control	6	River Defences	6
			Coastal Defences	6	Floodplain Mapping	6
			Stormwater Management	4		
Floodplain Mapping	5	7	Coastal Defences	6	Land Uses Practices	6
			Rainwater Control	6	Rainwater	6
			River Defences	6	Sea Level	6
			Stormwater Management	4	Streamflow	6
			Floodplain Development Standards	6	Marine Ecosystem	4
			Flood Risk Analysis	8	Urban Flood Conditions	4
					Stormwater Management	4
Freshwater Resources	7	1	Drinking Water	8	Land Uses Practices	6

			Water for Agricultural Uses	8	Water Quality	6
			Water for Firefighting	8	Protection and Control of Water Resources	6
			Water for Industrial Uses	8	Stormwater Management	6
			Stormwater Management	6	Allocation and Use of Water Resources	6
					Wastewater Treatment and Discharge	7
			Freshwater Resources	7	Agriculture	6
			Near-shore Tourist Attractions	6	Air Terminal	6
			Hotels and Restaurants Performance	6	Control Tower	6
			Housing and Human Settlements	6	Drainage System in the Parking Lots	4
			Coastal Defences	6	Drainage System in the Runway	4
Wastewater Treatment and Discharge	5	7			Drainage System in the Taxiway/Apron	4
					Meteorological Office	6
					Processing	6
					Health Facilities	6
					Housing and Human Settlements	7
					Manufacturing	7
					Bridges	4

					Major North-South Highway	4
					Roads	4
					Vieux Fort Seaport	4
					Emergency Shelters	6
					Hotels and Restaurants Performance	7
					Near-shore Tourist Attractions	4
					Electricity Distribution	6
					Water Quality	6
					Marine Ecosystem	6
Drinking Water	7	3	Control Tower	6	Electricity Distribution	6
			Air Terminal	6	Freshwater Resources	8
			Meteorological Office	6	Allocation and Use of Water Resources	6
			Housing and Human Settlements	8		
			Hotels and Restaurants Performance	6		
			Health Facilities	6		
			Manufacturing	6		
			Emergency Shelters	6		
			Processing	8		
			Retailing	6		
Water for Agricultural Uses	5	3	Agriculture	6	Freshwater Resources	8
					Allocation and Use of Water Resources	6
					Electricity Distribution	4

Water for Firefighting	5	3	Emergency Services	6	Freshwater Resources	8
			Fire and Rescue Building	6	Allocation and Use of Water Resources	6
					Electricity Distribution	4
Water for Industrial Uses	5	3	Manufacturing	8	Freshwater Resources	8
			Processing	8	Allocation and Use of Water Resources	6
					Electricity Distribution	4
Land Uses Practices	5	3	Freshwater Resources	6	Electricity Distribution	6
			Floodplain Mapping	6	Data Communications	6
			Stormwater Management	6	Internet Access	6
			Allocation and Use of Water Resources	6	Voice Communications	6
			Floodplain Development Standards	6		
			Flood Risk Analysis	6		
			Rainwater Control	6		
			River Defences	6		
			Temporary Perimeter Barriers	4		
			Coastal Defences	6		
			Protection and Control of Water Resources	6		
Marine Ecosystem	5	5	Coastal Defences	6	Data Communications	6
			Near-shore Tourist Attractions	6	Internet Access	6
			Stormwater Management	6	Voice Communications	6

			Floodplain Mapping	4	Electricity Distribution	6
			Wastewater Treatment and Discharge	6		
Rainwater	5	3	Floodplain Mapping	6	Meteorological Office	6
			Rainwater Control	7	Electricity Distribution	6
			River Defences	6	Data Communications	6
			Temporary Perimeter Barriers	6	Internet Access	6
			Stormwater Management	6	Voice Communications	6
Sea Level	5	7	Floodplain Mapping	6	Electricity Distribution	6
			Coastal Defences	6	Data Communications	6
			River Defences	6	Internet Access	6
			Temporary Perimeter Barriers	6	Voice Communications	6
			Stormwater Management	6		
Streamflow	5	7	Floodplain Mapping	6	Electricity Distribution	6
			Allocation and Use of Water Resources	6	Data Communications	6
			River Defences	7	Internet Access	6
			Temporary Perimeter Barriers	6	Voice Communications	6
			Stormwater Management	6		
Urban Flood Conditions	5	7	Temporary Perimeter Barriers	7	Data Communications	6
			Floodplain Mapping	4	Internet Access	6
			Stormwater Management	6	Voice Communications	6
					Electricity Distribution	6

Water Quality	5	7	Freshwater Resources	6	Electricity Distribution	6
			Protection and Control of Water Resources	6	Data Communications	6
			Allocation and Use of Water Resources	6	Internet Access	6
			Stormwater Management	6	Voice Communications	6
			Wastewater Treatment and Discharge	6		
Allocation and Use of Water Resources	5	3	Drinking Water	6	Water Quality	6
			Water for Agricultural Uses	6	Land Uses Practices	6
			Water for Firefighting	6	Streamflow	6
			Water for Industrial Uses	6	Protection and Control of Water Resources	4
			Freshwater Resources	6		
			Protection and Control of Water Resources	4		
Protection and Control of Water Resources	5	3	Freshwater Resources	6	Water Quality	6
			Allocation and Use of Water Resources	4	Land Uses Practices	6
					Allocation and Use of Water Resources	4
Stormwater Management	5	7	Floodplain Development Standards	4	Water Quality	6
			Freshwater Resources	6	Land Uses Practices	6
			Rainwater Control	8	Rainwater	6
			Floodplain Mapping	4	Marine Ecosystem	6
			Flood Risk Analysis	4	Streamflow	6

Coastal Defences	4	Flood Risk Analysis	4
River Defences	4	Floodplain Mapping	4
		Floodplain Development Standards	4
		Urban Flood Conditions	6
		Sea Level	6
		Freshwater Resources	6

4.4 Results and Discussions

Based on the hierarchical system of considered entities (Table 27) and the direct connections identified between each pair of entities (Table 28), a directed graph (Figure 30) was set up in the RiskLogik software. The model has subsequently been used to conduct risk assessment under three different scenarios: (i) no existing external threats; (ii) compound flooding in the event of Tropical Storm Matthew without considering the effects of wave run-up; (iii) compound flooding in the event of Tropical Storm Matthew when considering the effects of wave run-up. Evaluated indices include the global impact of each entity, the global vulnerability of each entity, as well as the risk index of each entity. By comparing the indices calculated for different entities, the relative importance of entities in the system is explored, which can help identify and prioritize risk.

With the help of RiskLogik software, the risk of entities can be categorized into five classes, which are extreme, very high, high, moderate, and low. The category of risk is a measure used to indicate the relative importance of entities, and therefore, it is not based on a set of constant threshold values. Discussions in this study majorly focus on the entities that are at extreme/very high/high risk in order to provide insights for the prioritization of risk.

4.4.1 Risk Assessment under Normal Condition

In the first scenario, there are no external threats to the system in order to investigate the risk of different entities under normal conditions. Risk indices, including the global impact, the global vulnerability, and the risk index, were calculated for each entity and are presented in Figure 31. Figure 32 presents entities that are at extreme/very high/high risk and their corresponding risk indices. According to the simulation results, 3 entities (i.e. airport's normal operations, rainwater control, and electricity distribution) are at extreme risk, 2 entities (i.e. transportation as well as housing and human settlements) are at very high risk, 4 entities (i.e. internet access, data communications, voice communications, and tourism) are at high risk, 33 entities are moderate risk, and the remaining 201 entities are at low risk.

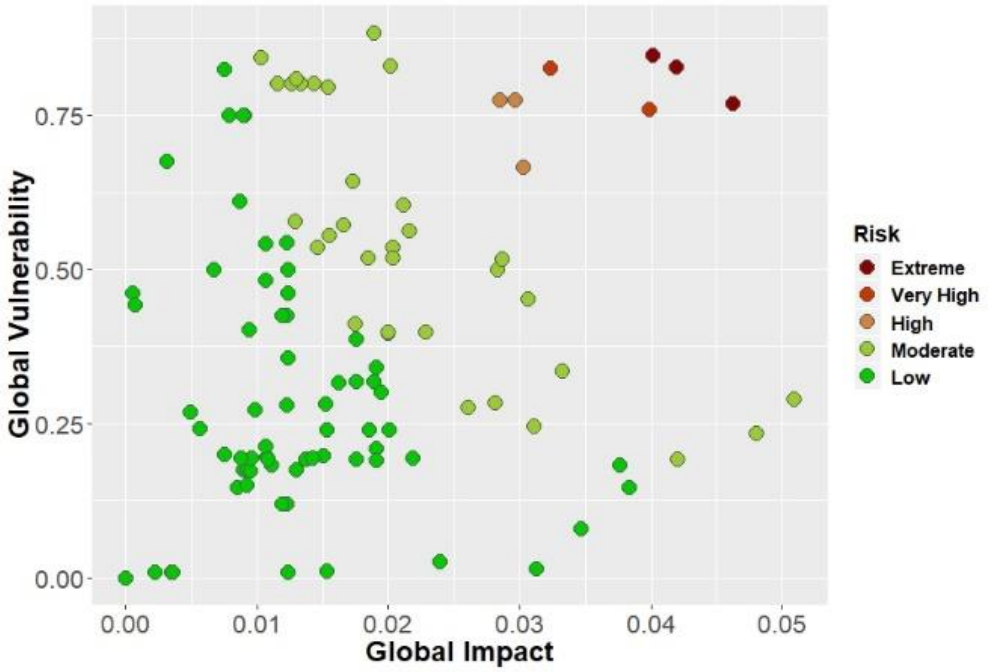

(a)

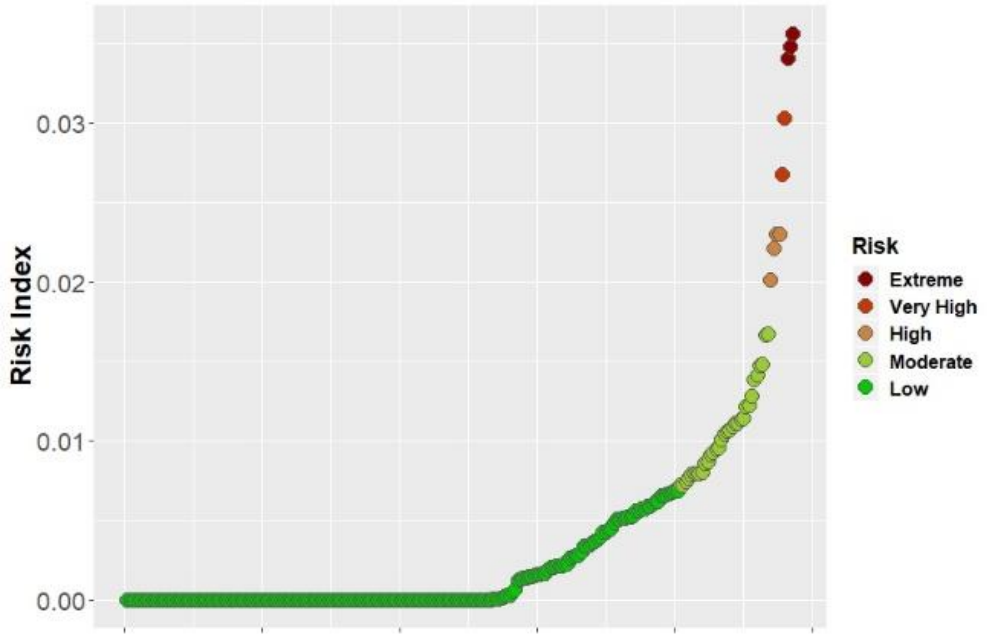

(b)

Figure 31. Risk indices of each entity in the non-flood condition: (a) global vulnerability and global impact; (b) risk index.

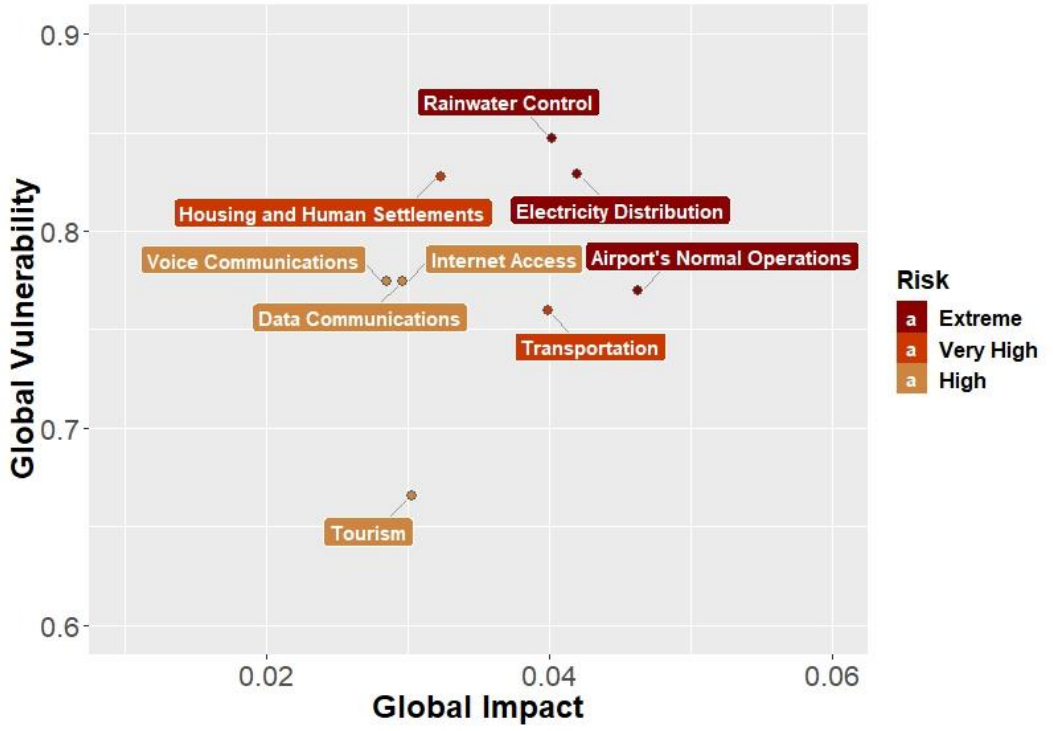

(a)

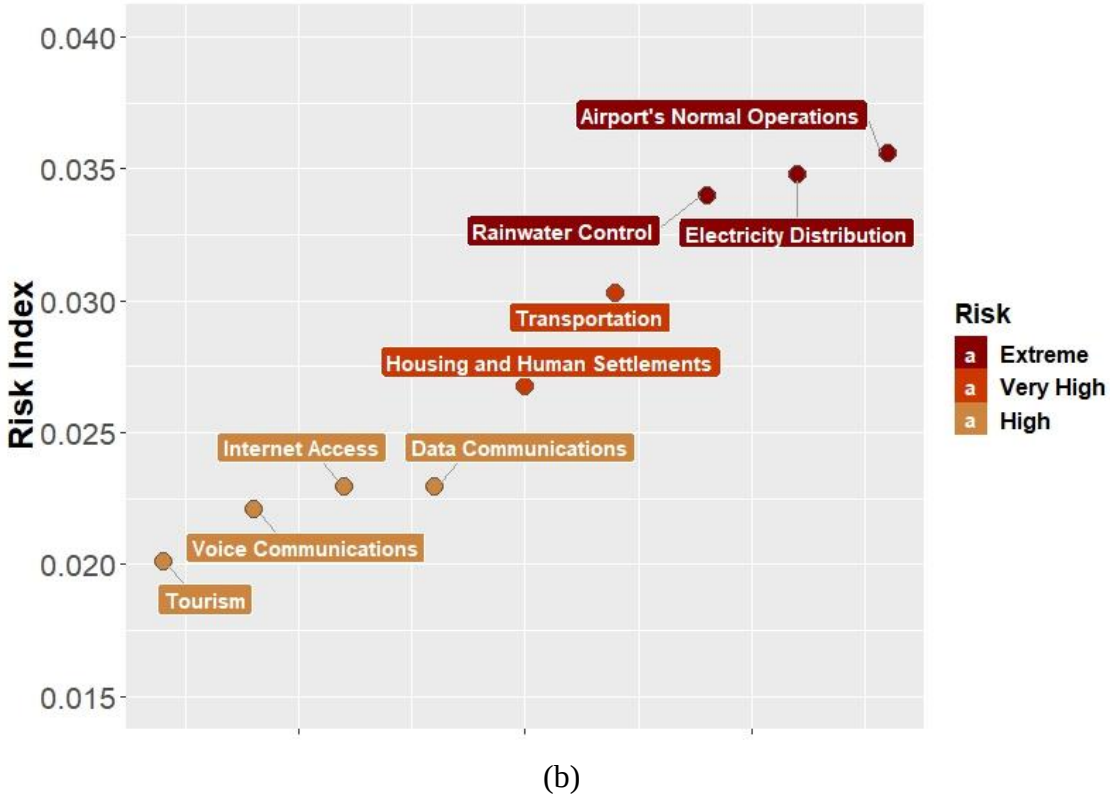

(b)

Figure 32. Risk indices of entities that are at high/very high/extreme risk in the non-flood condition: (a) global vulnerability and global impact; (b) risk index.

Under normal conditions, it is extremely significant to maintain normal operations of Hewanorra International Airport because it has the highest risk index and the highest global impact. Electricity distribution, as the entity that has the second-highest risk index, has high values of global vulnerability but is indispensable to numerous entities in the system, especially to those that do not have backup electricity generators. Rainwater control, including dams, dykes, municipal drains, open channels, and low-impact development, have the highest value of global vulnerability. The failure of rainwater control can lead to significant flooding, hugely affecting the normal operations of entities, such as cell towers providing communication services, bridges and highway connecting cities across the island, and the houses in human communities.

Transportation, as well as housing and human settlements, are both at very high risk. Major transportation in Saint Lucia includes inter-city road transportation, intra-city road transportation, water transportation such as cruise ships and yachts, and air transportation, providing services for citizens, visitors, as well as carrying goods. Major human communities within the study area are the town of La Tourney and the town of Vieux Fort, which are vulnerable to the disruptions of essential services such as electricity and water supplies. Tourism, as well as information and communication technology (i.e. data communications, internet access, and voice communications), are at high risk. All these four entities are key economic sectors in Saint Lucia, indicating the need to conduct further risk analysis and develop efficient risk mitigation strategies.

The optimized Monte Carlo analysis provided by the RiskLogik software was used to investigate the model uncertainty that comes from the pre-defined parameters. The values bounds are ± 1 for all pre-defined weighting indices, which are the degree of impact, the likelihood of failure, and the degree of dependence. Monte Carlo analysis results are presented in Figure 33. Based on the mean and median values, it is believed that the model uncertainty regarding pre-defined parameters has little impact when identifying the relative importance of entities. However, entities that have relatively high values of risk index also have larger ranges between the maximum and minimum values, indicating their relatively high sensitivity to pre-defined parameters.

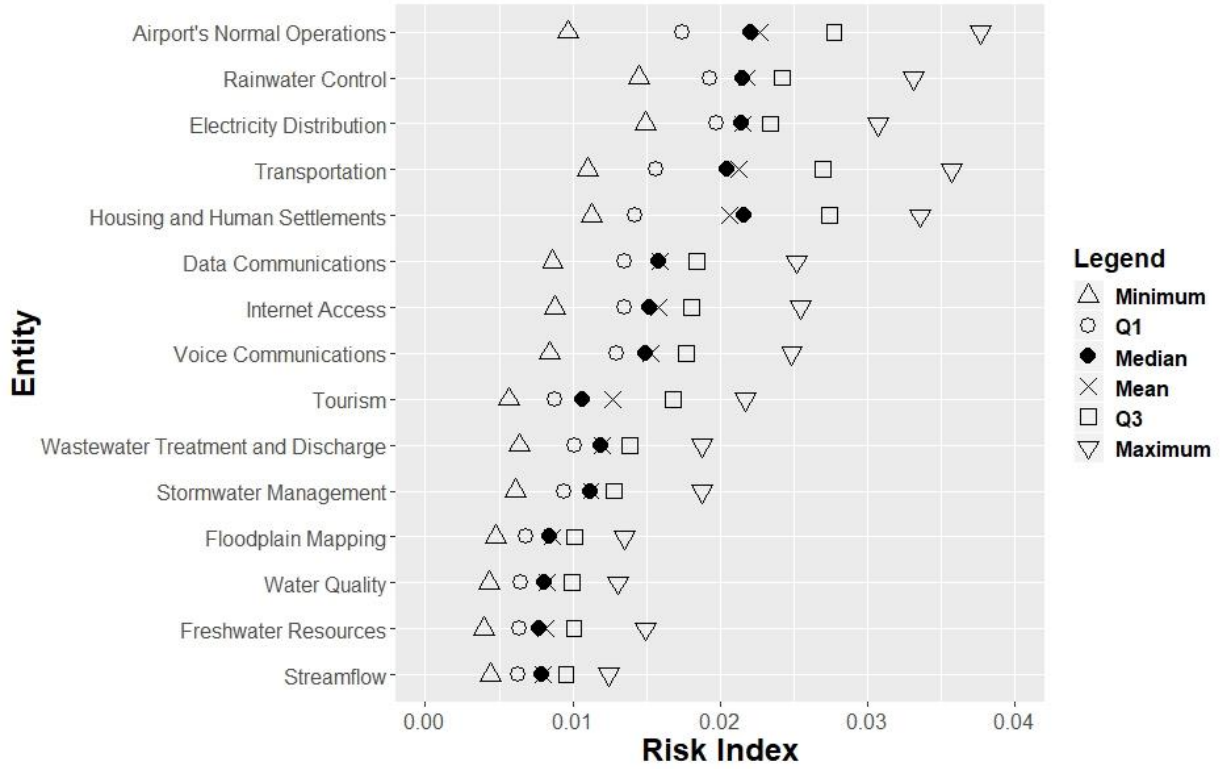

Figure 33. Results of the Monte Carlo analysis in the non-flood condition.

In conclusion, under normal conditions, following entities are at relatively high risk: Hewanorra International Airport, rainwater control, electricity distribution, transportation, housing and human settlements, data communications, Internet access, voice communications, and tourism.

4.4.2 Risk Assessment under Flood Scenarios

As in Chapter 3, a two-dimensional hydrodynamic model LISFLOOD-FP was set up to simulate compound flooding in the event of Tropical Storm Matthew. Simulated flood extents can be utilized in flood risk assessment. Since Hewanorra International Airport is at high risk of flooding while its normal operations is at extreme risk under normal conditions as illustrated in Section 4.1.1, the major focus of this section is to explore how floods occurring within the airport boundary affect airport facilities, and if they fail in the flooding, to understand how the failures propagate through the network and cause cascading effects.

Flood Conditions when not considering Wave Run-up

Flood factors for this scenario are river flows, rainfall, as well as coastal water levels but not considering the effects of wave run-up. According to the simulation results, flood extents reach the maximum value at 18h, and the simulated flood depth for each pixel within the airport boundary is presented in Figure 34.

The RiskLogik model that was set up in Section 4.4.1 is utilized as the base model. Since standing water is expected in the runway and taxiway/apron, the likelihood of failure of these two entities are set to 10, indicating their failures in flooding.

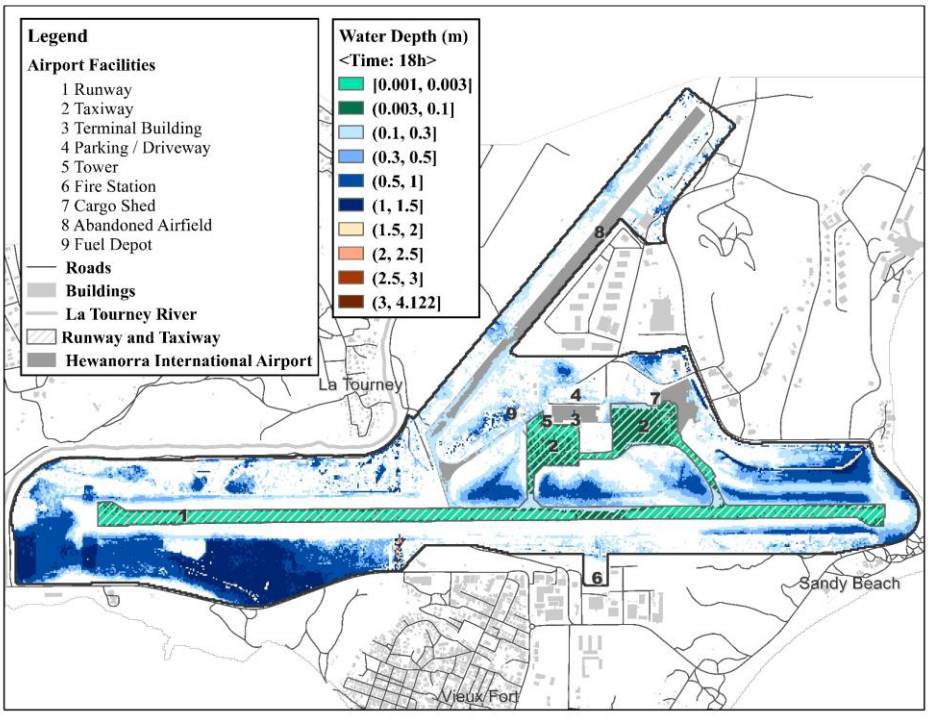

Figure 34. Map showing the flood conditions when flood extents reach the maximum value over the course of the simulation R0 in the event of Tropical Storm Matthew within the boundary of Hewanorra International Airport.

Risk indices, including global impact, global vulnerability, and risk index, were calculated for each entity and are presented in Figure 35. Figure 36 presents entities that are at extreme/very high/high risk and their corresponding risk indices. According to the simulation results, 1 entity (i.e. airport's normal operations) is at extreme risk, 3 entities (i.e. electricity distribution, rainwater control, and transportation) are at very high risk, 8 entities (i.e. housing and human settlements, internet access,

data communications, runway status, voice communications, airplane landing and taking off, tourism, and taxiway/apron status) are at high risk, 25 entities are moderate risk, and the remaining 204 entities are at low risk.

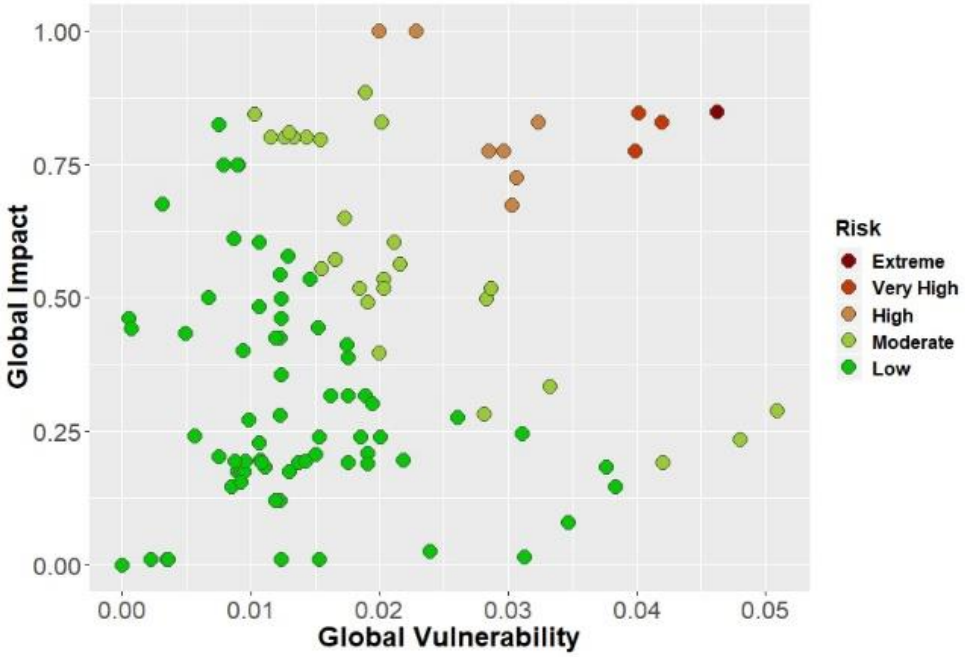

(a)

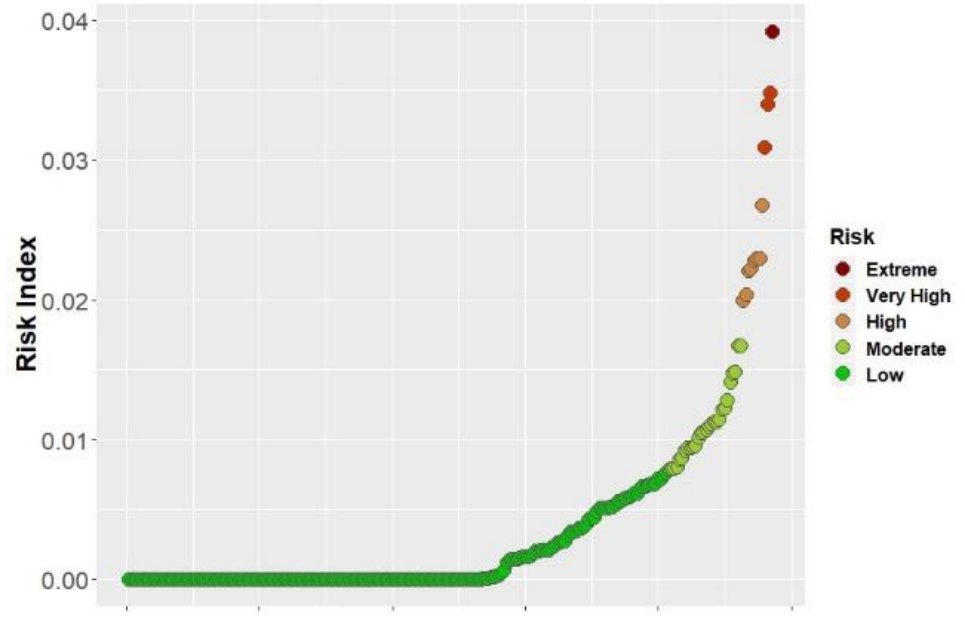

(b)

Figure 35. Risk indices of each entity in flood conditions when not considering the effects of wave run-up: (a) global vulnerability and global impact; (b) risk index.

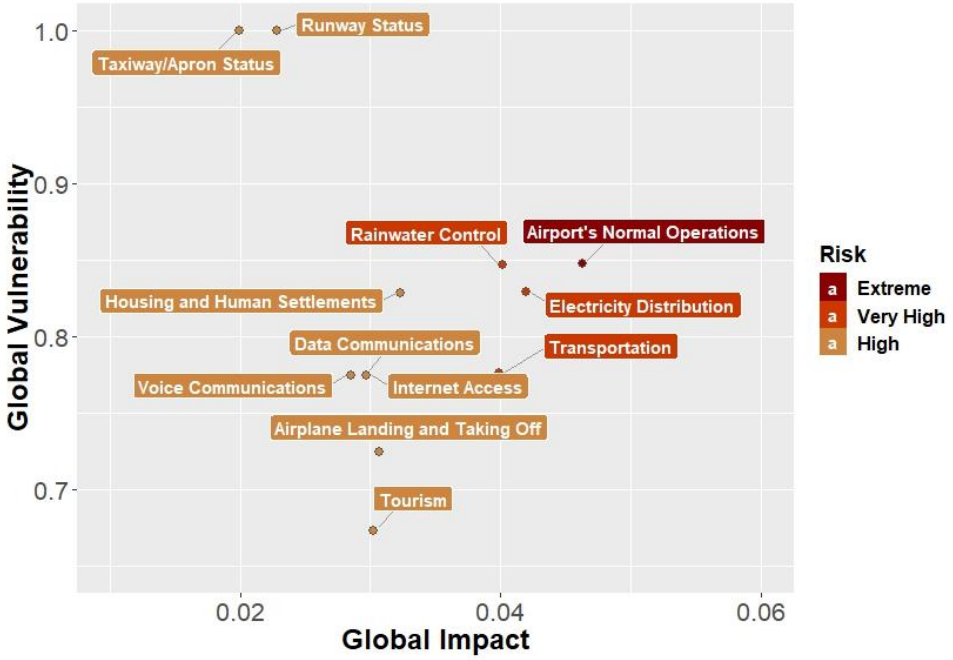

(a)

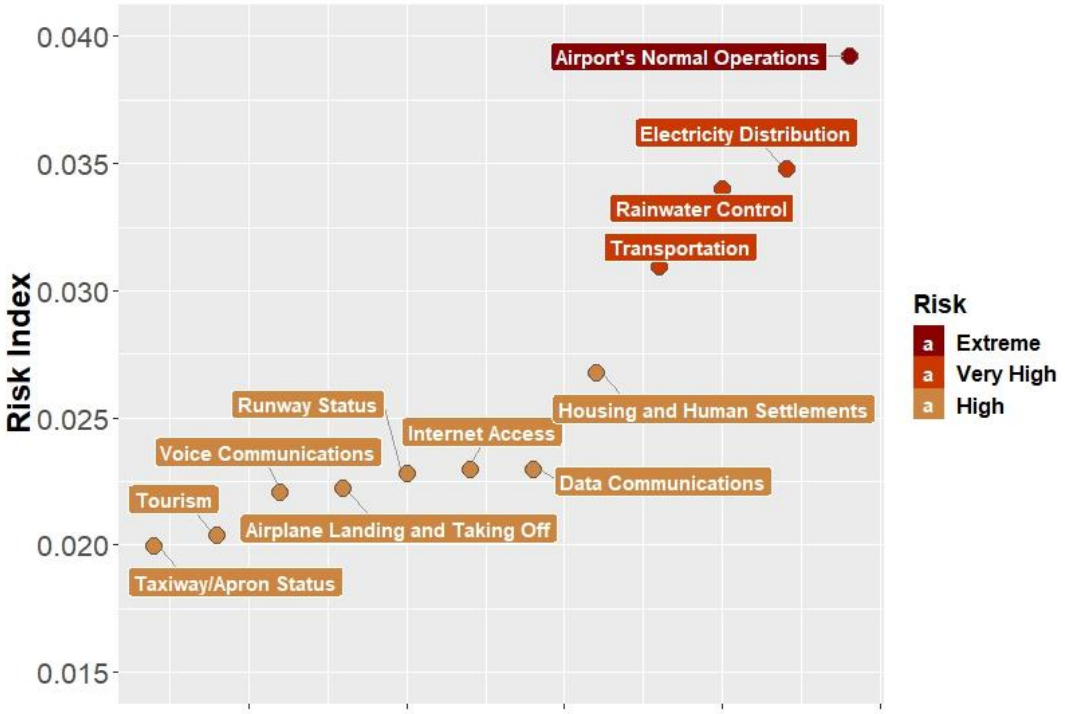

(b)

Figure 36. Risk indices of entities that are at high/very high/extreme risk in flood conditions when not considering effects of wave run-up: (a) global vulnerability and global impact; (b) risk index.

The normal operation of Hewanorra International Airports has the highest values of both global impact and risk index. Compared to Figure 32, it can be concluded that external threats in this flooding scenario not only increase the risk index of the airport's normal operations but also significantly increase the risk of runway status, taxiway/apron status, as well as airplane landing and taking off. As a result, it is important to timely clear the standing water in the runway and taxiway/apron; otherwise, airplanes cannot land or take off normally greatly affecting the normal operations of the airport. Similar conclusions can be drawn from the results of the Monte Carlo analysis (Figure 37). In addition, as discussed in Section 4.1.1, entities that have higher risk index have a higher sensitivity to the pre-defined parameters, such as the normal operations of the airport, transportation, rainwater control, and electricity distribution.

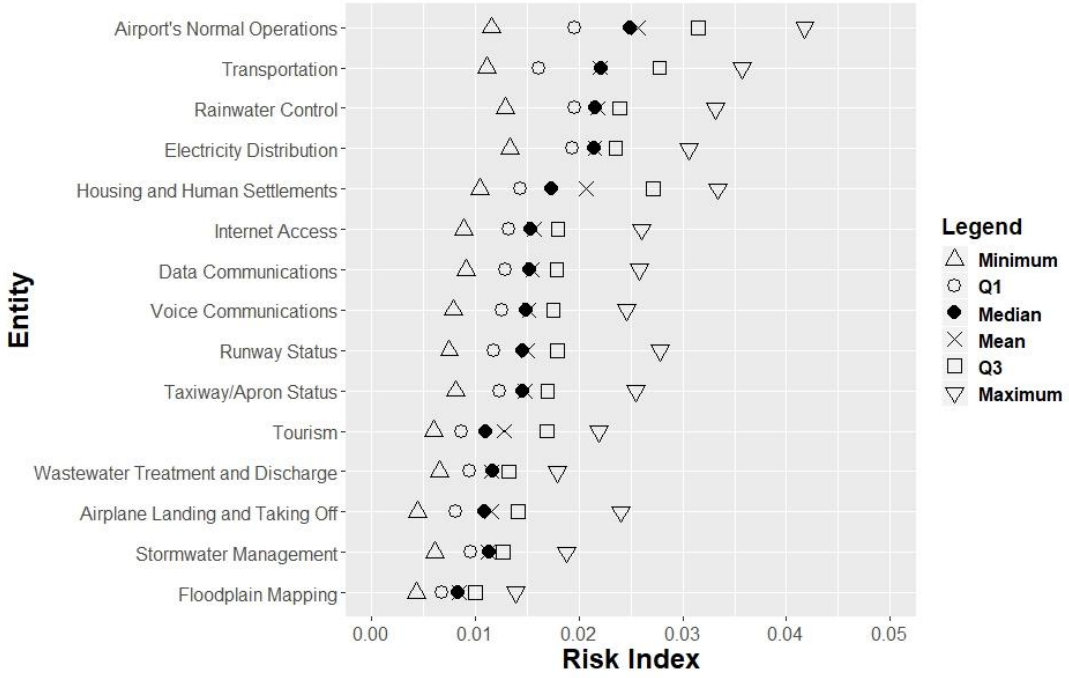

Figure 37. Results of the Monte Carlo analysis in flood conditions when not considering the effects of wave run-up.

In conclusion, under the scenario of flooding in the event of Tropical Storm Matthew without considering the effects of wave run-up, it is of fundamental importance to maintain normal operations of Hewanorra International Airport. In addition, significant attention should be paid to following entities with high values of risk index: transportation, rainwater control, electricity distribution, housing and human settlements, data communications, Internet access, runway status, airplane landing and taking off, voice communications, tourism, as well as taxiway/apron status.

Flood Conditions when considering Wave Run-up

Flood factors for this scenario are river flows, rainfall, as well as coastal water levels which include the effects of wave run-up. As in Chapter 3, due to the lack of knowledge in temporal patterns, the worst scenarios are considered by adding 0.5m, 1.5m, 2.5m, 3.5m, 4.5m, 5.5m, and 6m to the *mean* time series of sea levels from 11:00 am AST on September 28, 2016 to 8:00 am AST on September 29, 2016. Much more severe flood conditions are expected when considering the effects of wave run-up, indicating the urgent need to conduct the risk assessment in these scenarios.

Figure 38 shows the maximum flood depth for each pixel within the airport boundary under different conditions. When the heights of wave run-up are less than or equal to 2.5m, majorly affected entities are the runway and taxiway/apron. When the heights increase from 3.5m to 4.5m, besides runway and taxiway/apron, the fire and rescue building also has the risk of being inundated. When the heights are equal to or larger than 4.5m, most of the airport facilities are expected to be flooded, including the air terminal, fuel depot, ground support equipment, backup electricity generators, meteorological office, parking lots, the fire and rescue building, the runway, as well as the taxiway/apron. As a result, two scenarios are considered in this section: (i) failed airport entities include the runway, taxiway/apron, as well as fire and rescue building; (ii) failed airport entities include the air terminal, aircraft and cargo capacity, backup electricity generators, fuel depot, meteorological office, parking lots, the fire and rescue building, the runway, as well as the taxiway/apron. The RiskLogik model set up in Section 4.4.1 is utilized as the base model, and the likelihood of failure of failed entities is subsequently set to be 10, indicating their failures in flooding. Modelling results would be used to investigate the impacts of failed entities.

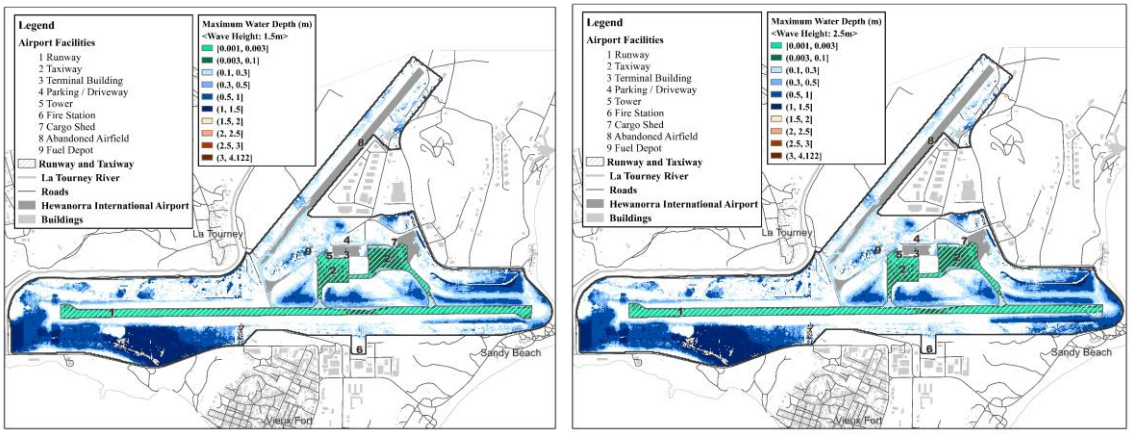

(a) (b)

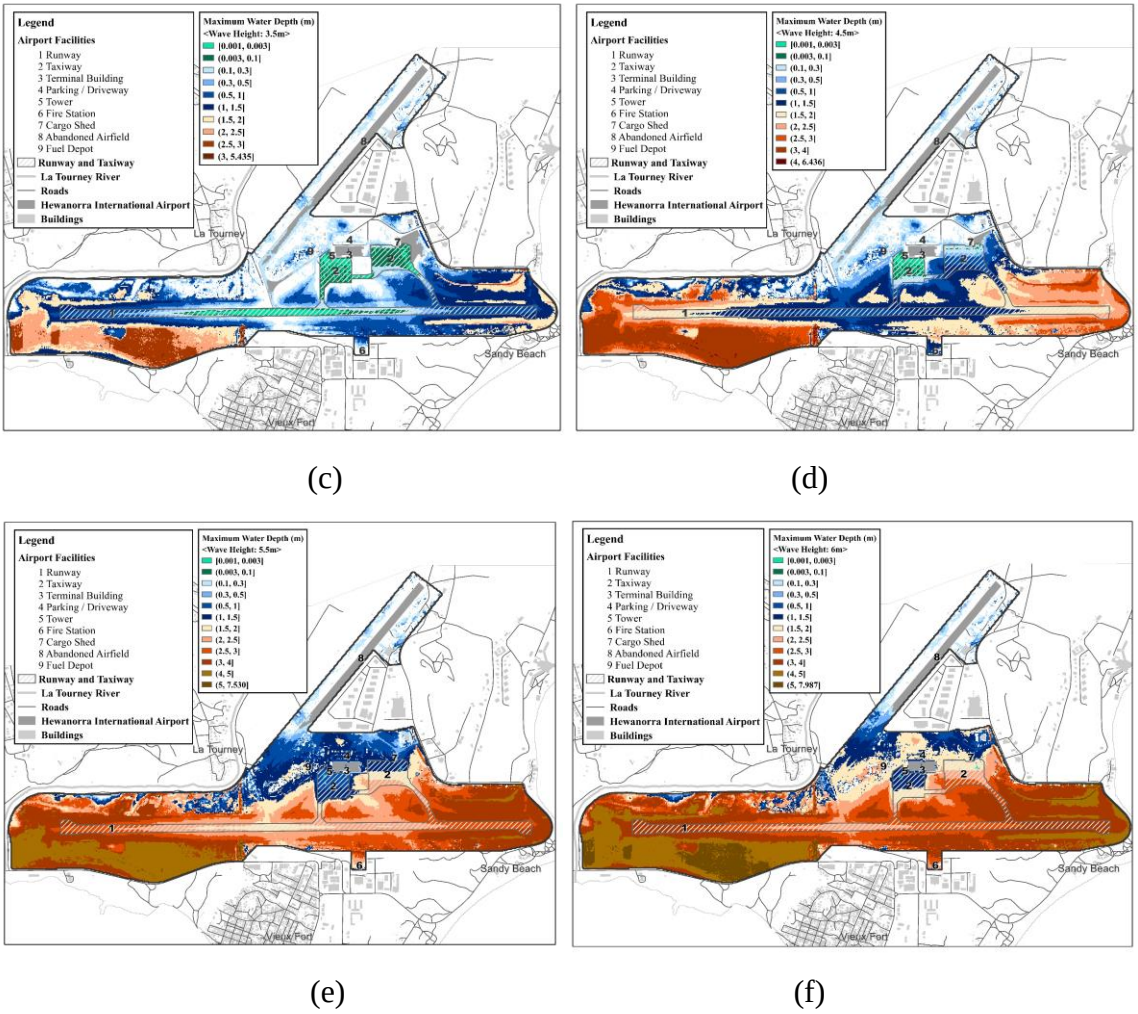

Figure 38. Maps showing the maximum flood depth of each pixel within the airport boundary when wave run-up heights are: (a) 1.5m, (b) 2.5m, (c) 3.5m, (d) 4.5m, (e) 5.5m, and (f) 6m.

Results of the first scenario are presented in Figure 39, 40, and 41. The failure of the fire and rescue building does increase the risk of normal operations of Hewanorra International Airport, but it has negligible impacts on other entities that also have high values of risk index.

Results of the second scenario are presented in Figure 42, 43, and 44. Since most of the airport facilities are expected to fail, Hewanorra International Airport is at extreme risk of failure. Among all failed airport facilities, the backup electricity generator for the control tower and air traffic system has the highest global impact. Electricity distribution, rainwater control, and transportation are at very high risk, while entities at high risk include housing and human settlements, airplane landing and taking off, aircraft and cargo capacity, data communications, internet access, runway

status, as well as voice communications. According to the results of Monte Carlo analysis, other entities such as the air terminal, taxiway/apron, as well as tourism are also at relatively high risk.

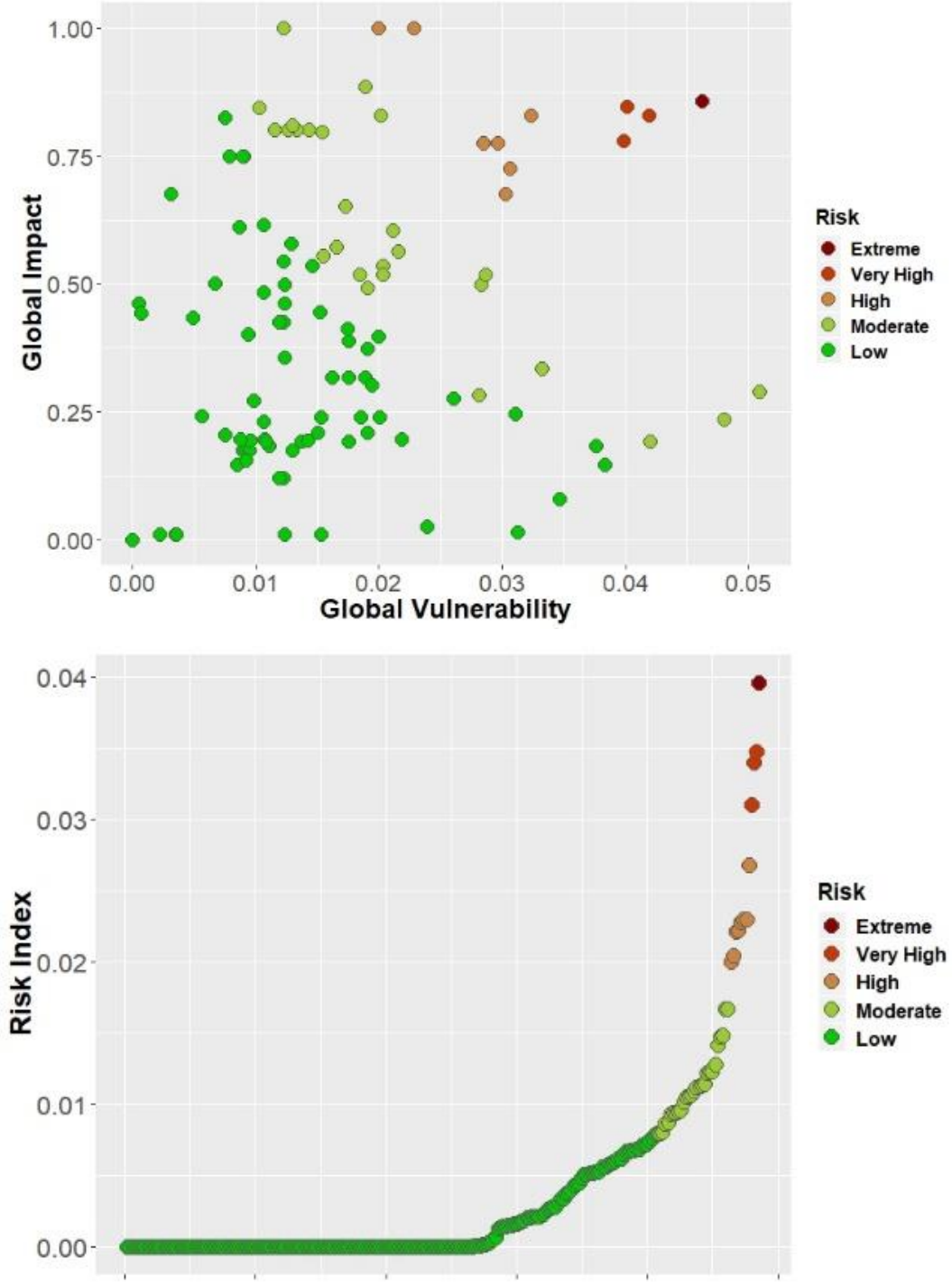

Figure 39. Risk indices of each entity in the first scenario of flooding when considering the effects of wave run-up: (a) global vulnerability and global impact; (b) risk index.

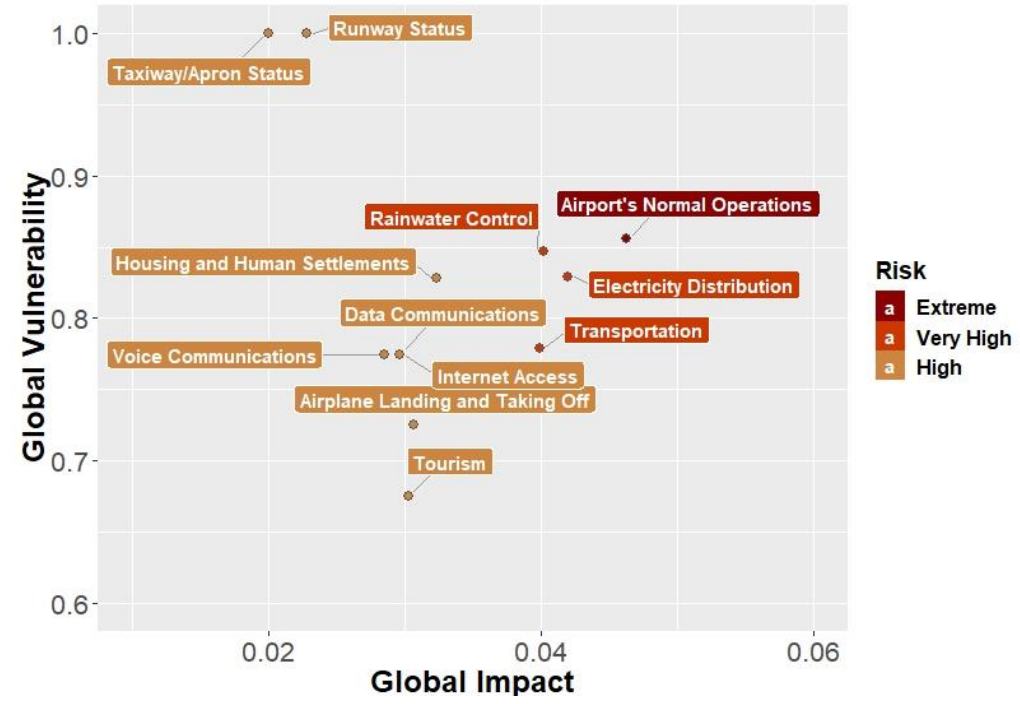

(a)

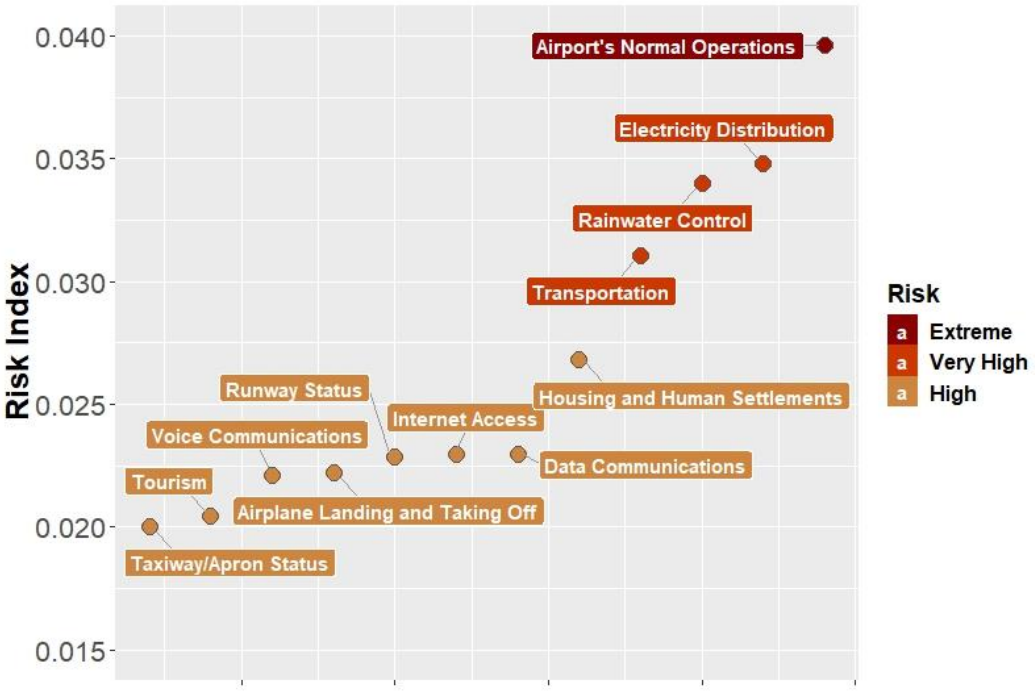

(b)

Figure 40. Risk indices of entities that are at high/very high/extreme risk in the first scenario of flooding when considering the effects of wave run-up: (a) global vulnerability and global impact; (b) risk index.

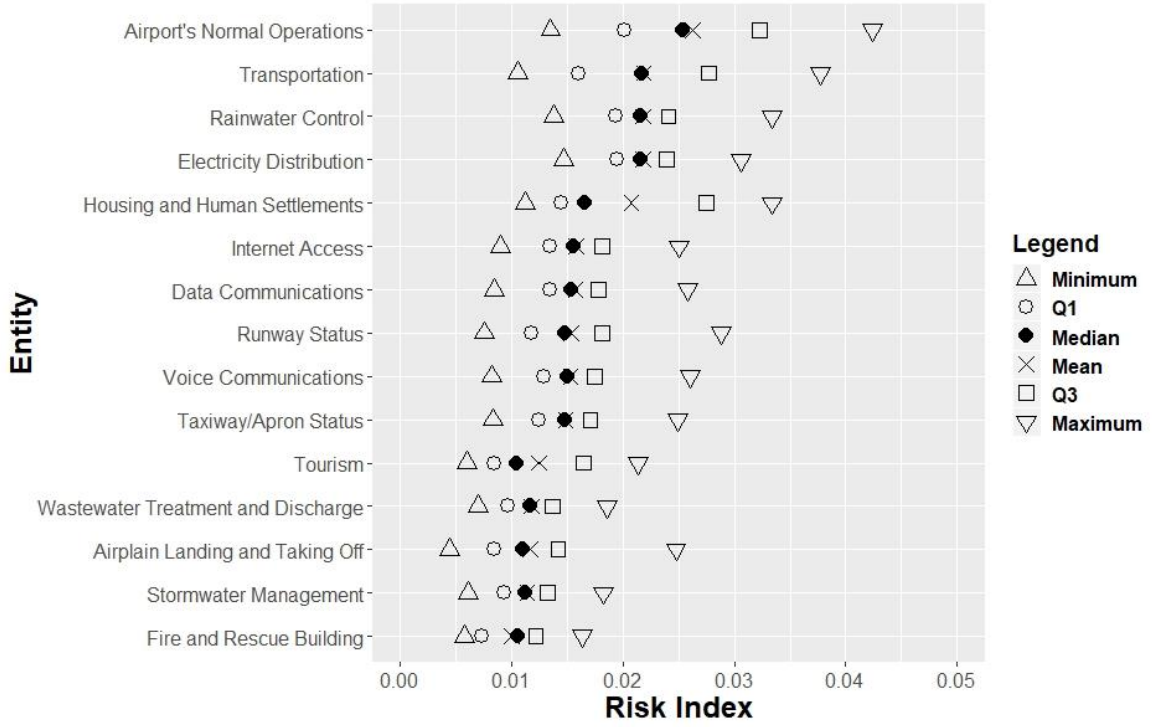

Figure 41. Results of the Monte Carlo analysis in the first scenario of flooding when considering the effects of wave run-up.

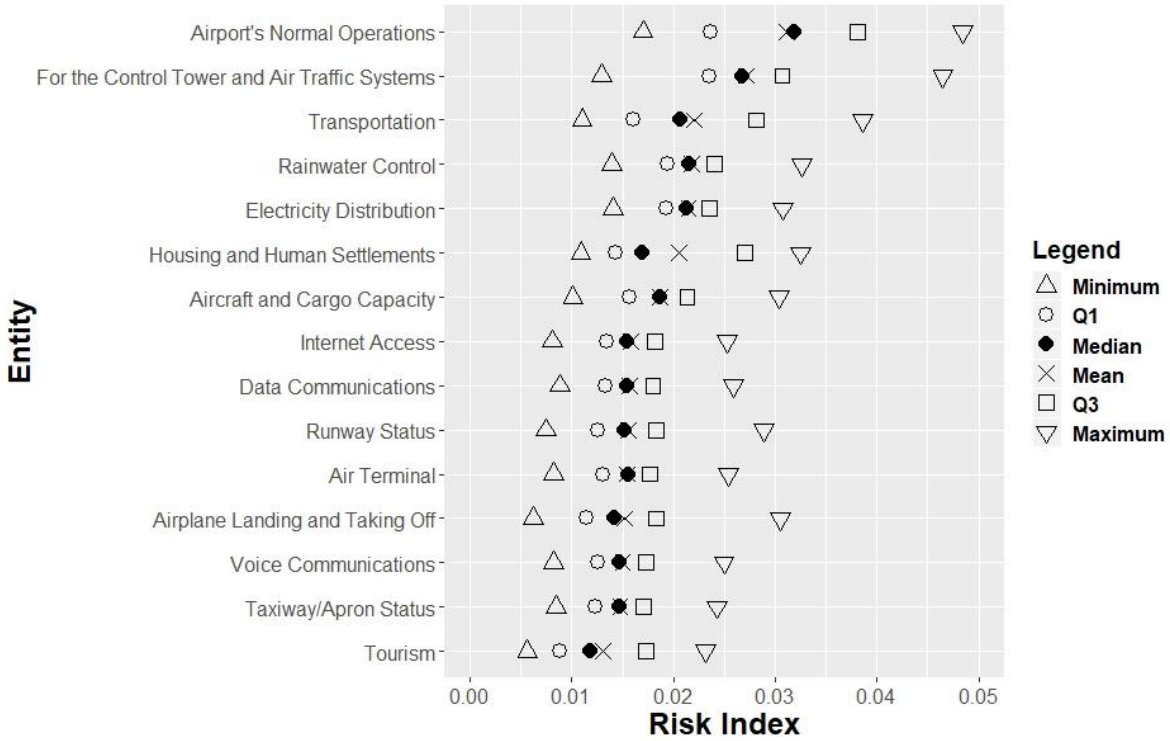

Figure 42. Results of the Monte Carlo analysis in the second scenario of flooding when considering the effects of wave run-up.

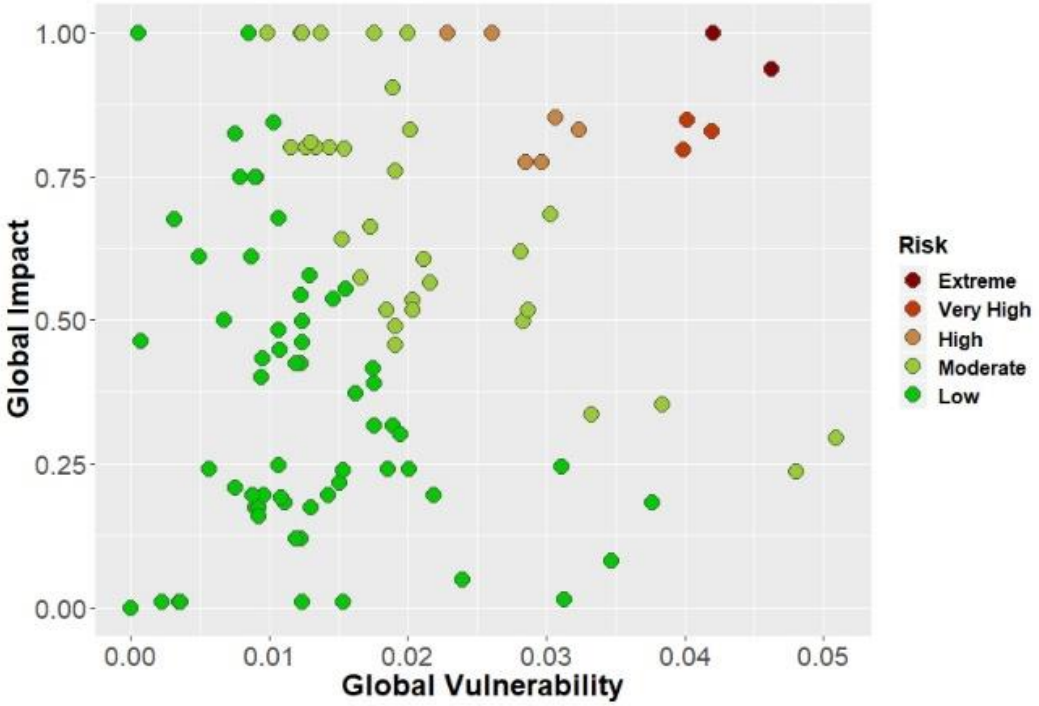

(a)

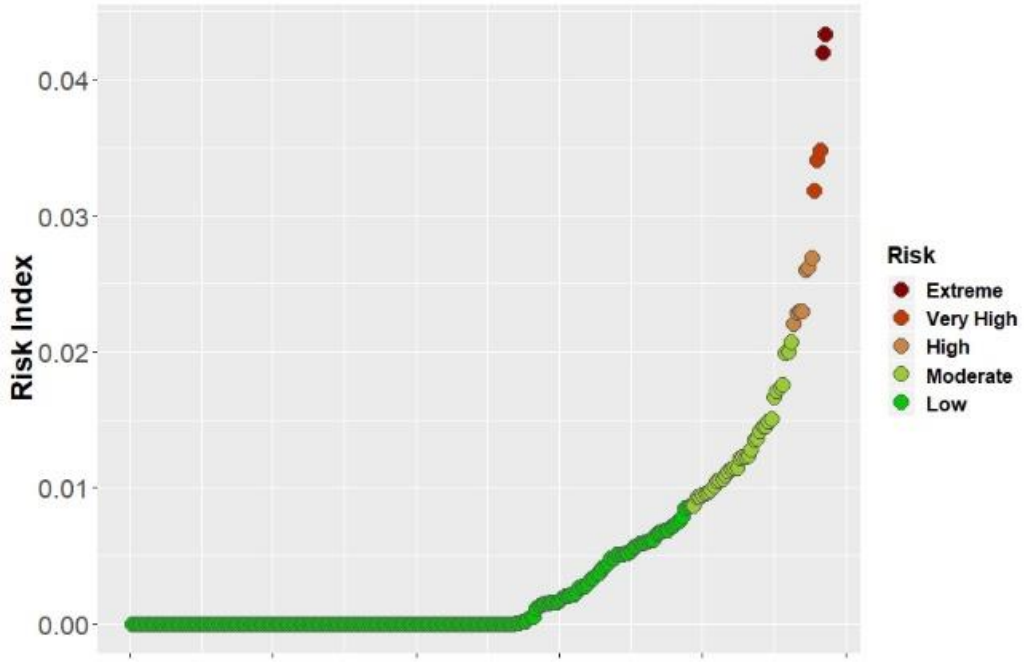

(b)

Figure 43. Risk indices of each entity in the second scenario of flooding when considering the effects of wave run-up: (a) global vulnerability and global impact; (b) risk index.

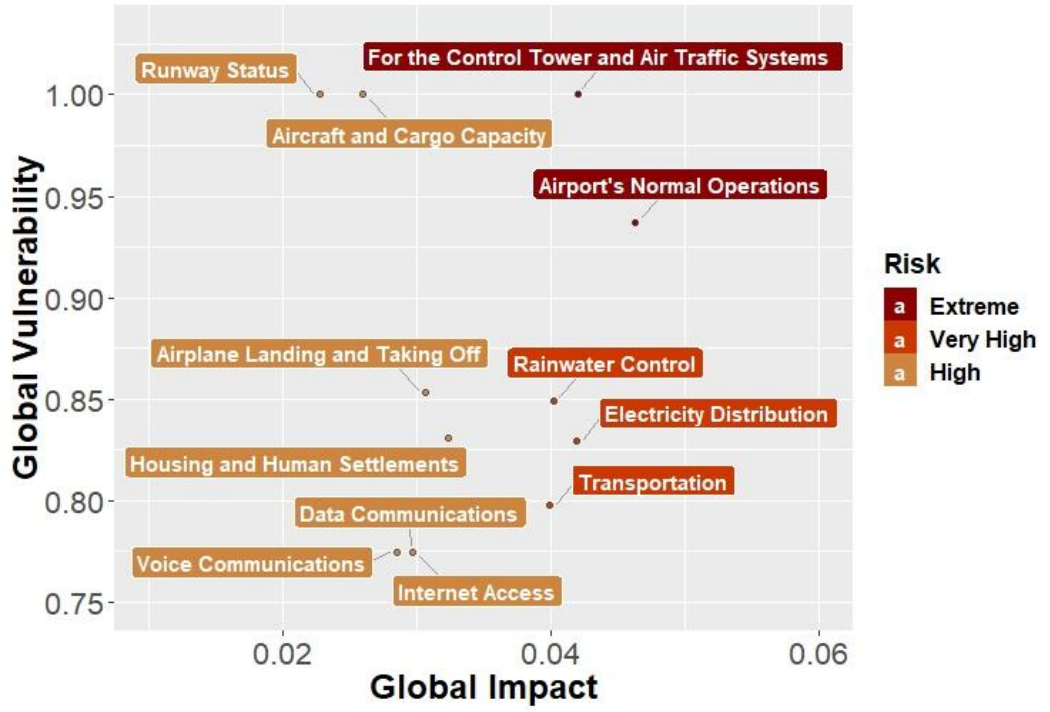

(a)

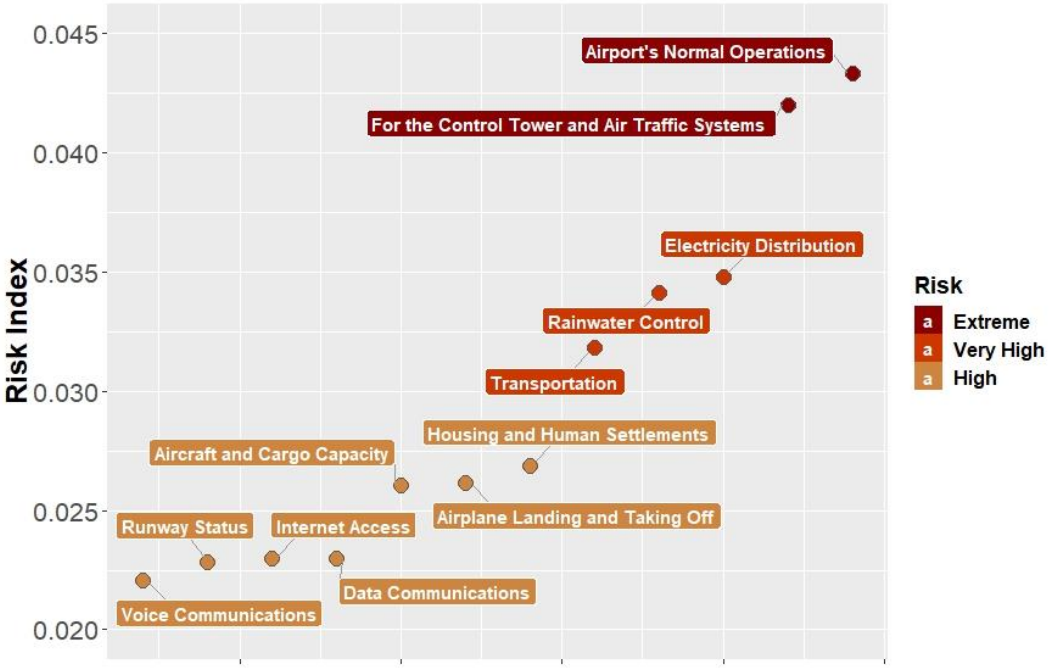

(b)

Figure 44. Risk indices of entities that are at high/very high/extreme risk in the second scenario of flooding when considering the effects of wave run-up: (a) global vulnerability and global impact; (b) risk index.

4.5 Conclusions

Major assets in the study area include Hewanorra International Airport, Vieux Fort Seaport, coastal agricultural land, the town of Vieux Fort and La Tourney, as well as the north-south highway, whose normal operations along with other entities pertain to key economic sectors in Saint Lucia, such as Tourism, Agriculture, Manufacturing, Housing and Human Settlements, Information and Communications Technology, Physical Planning and Infrastructure, Health, Food, Energy, Water, Electricity, Transportation, Watershed Management, and Disaster Risk Management. Dependence relationships are expected among all involved entities. With the help of RiskLogik software, a network analysis model was set up to investigate the relative importance of those interdependent entities in the system as well as to understand how the failures of airport facilities propagate through the network in the scenarios of flooding. Considered entities are presented in Table 27, and the direct connections between each pair of entities are presented in Table 28.

In the perspective of failed entities, four scenarios are considered in the risk assessment: (1) no existing external threats; (2) flooding conditions in the event of Tropical Storm Matthew when the heights of wave run-up is 0m, 0.5m, 1.5m, or 2.5m ; (3) flooding conditions in the event of Tropical Storm Matthew when the heights of wave run-up is 3.5m or 4.5m; (4) flooding conditions in the event of Tropical Storm Matthew when the heights of wave run-up is equal to or larger than 5.5m. Failed entities in each scenario are presented in Table 29. Entities that are at extreme/very high/high risk in each scenario are summarized in Figure 45.

Table 29. Scenario number and failed entities in each scenario.

Scenario Number	Failed Entities[1]
1	None
2	Runway, Taxiway/Apron
3	Runway, Taxiway/Apron, Fire and Rescue Building
4	Air Terminal, Aircraft and Cargo Capacity, Backup Electricity Generators, Fuel Depot, Meteorological Office, Parking Lots, Fire and Rescue Building, Runway, as well as the Taxiway/apron

Note: The likelihood of failure of failed entities is set to 10^{1}.

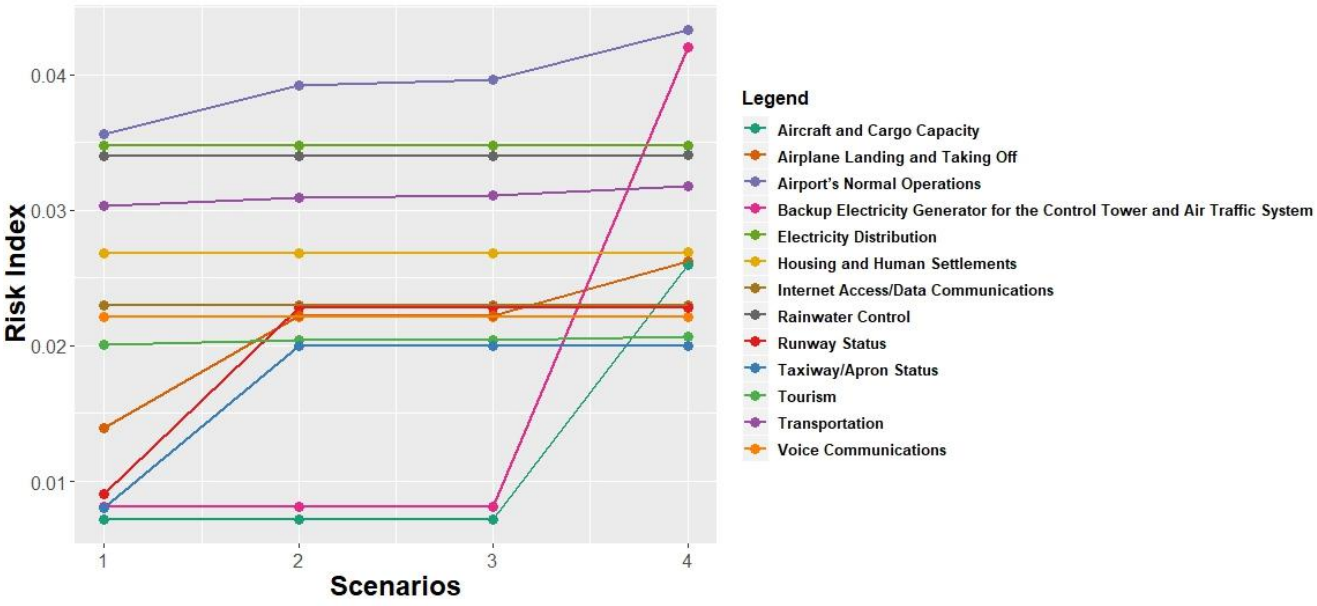

Figure 45. Risk index of entities that are at extreme/very high/high risk in each scenario.

In all scenarios, the normal operation of Hewanorra International Airport has the highest value of risk index, indicating its fundamental significance in the system. Moreover, when the flooding becomes more severe, the global vulnerability of the airport increases, and accordingly, the value of risk index increases. Effective flood control is indispensable since services of the airport are majorly provided by airport facilities such as the air terminal, ground support crews and equipment, backup electricity generators, the control tower, drainage systems, the fire and rescue building, fuel depot, the runway, the taxiway/apron, meteorological office, parking lots, and the lighting system of runway and taxiway/apron.

The presence of flooding within the airport boundary dramatically increases the risk index of airplane landing and taking off, runway status, taxiway/apron status, aircraft and cargo capacity, and particularly the backup electricity generator for the control tower and air traffic system. Those entities are at moderate risk when there are no external threats. To effectively maintain the normal operations of Hewanorra International Airport, further risk analysis should be conducted and prioritization should be given to those airport facilities. Among them, the backup generator has the highest risk index in Scenario 4, indicating its significance in the system. Deep Logic Solutions Inc. conducted field surveys in the airport, and according to the reports documented for this field

trip, the backup generator building is highly vulnerable to flooding. Therefore, mitigation measures should be developed particularly for protecting the backup generators from the flooding.

Both transportation and tourism have high values of risk index in all scenarios, and slightly higher values of risk index in the scenarios of flooding, which indicates that flooding in the airport has impacts on the sectors of transportation and tourism. This is reasonable since the disruption of Hewanorra International Airport would affect air transportation and lead to disruptions of visitor arrivals and departures by international flights and regional flights.

Entities that are at high risk but not sensitive to the flooding within the airport boundary include electricity distribution, rainwater control, housing and human settlements, internet access, data communications, as well as voice communications. It can be concluded that essential services, which includes electricity services, flood control, as well as information and communication services, should be maintained no matter in normal conditions or in flooding scenarios.

Due to the limited data resources, not all major entities are taken into consideration in each sector. Pre-defined parameters, including the degree of impact, the likelihood of failure, and the degree of dependence, are assigned majorly in a qualitative manner. Moreover, floods outside the airport boundary, such as flooding in human communities and agricultural lands, and their possible outcomes, such as power outages and disruptions of water supplies, are not considered, which could lead to significant underestimation of flood risk in the system. However, further risk analysis could be conducted when more detailed information is available. The RiskLogik model that was set up in this study, as well as the findings derived from the modelling results, could provide valuable insights for future risk assessment in Saint Lucia.

4.6 References

Augustine, Thomas. 2007. *Report on The Passage of Hurricane Dean: St. Lucia.* (Saint Lucia Meteorological Services). http://www.cmo.org.tt/docs/cmc47/PDFs/St._Lucia_Hurricane_Dean.pdf.

Economic Commission for Latin American and the Caribbean. 2011. *Saint Lucia: Macro Socio-economic and Environmental Assessment of the Damage and Losses caused by*

Hurricane Tomas: A Geo-environmental Disaster. https://www.finance.gov.lc/resources/download/290.

Economic Commission for Latin America and the Caribbean. 2007. *Saint Lucia: Macro Socio-economic Assessment of the Damage and Losses caused by Hurricane Dean.*

Eleutério, J., C. Hattemer, and A. Rozan. 2013. "A systemic method for evaluating the potential impacts of floods on network infrastructures." *Natural Hazards and Earth System Science* 13 (4): 983-998. https://doi.org/10.5194/nhess-13-983-2013.

Global Facility for Disaster Reduction and Recovery. 2014. Saint Lucia Flood Event of December 24-25, 2013: A Report by the Government of Saint Lucia and the World Bank.

---. 2019. "Saint Lucia." https://www.gfdrr.org/en/saint-lucia.

Government of Saint Lucia. 2017. *Third National Communication on Climate Change for Saint Lucia.* https://www.climatechange.govt.lc/wp-content/uploads/2017/10/THIRD-NATIONAL-COMMUNICATION-_-SAINT-LUCIA-2017.pdf.

---. 2018. Saint Lucia's National Adaptation Plan (NAP): 2018–2028. Department of Sustainable Development, Ministry of Education, Innovation, Gender Relations and Sustainable Development.

ICF GHK. 2012. *Climate Change Adaptation Planning in Latin American and Caribbean Cities Complete Report: Castries, Saint Lucia* http://www.worldbank.org/content/dam/Worldbank/document/LAC/Climate%20Change%20Adaptation%20Planning%20for%20Castries_FINAL.pdf.

International Federation of Red Cross and Red Crescent Societies. 2017. DREF Operations Final Report Saint Lucia: Hurricane Matthew.

O'Neill, Philip. 2014. "Decision Support Through Strongest Path Method Risk Analysis." In *Networks and Network Analysis for Defence and Security*, 247-263. Springer.

Rinaldi, S. M., J. P. Peerenboom, and T. K. Kelly. 2001. Identifying, understanding, and analyzing critical infrastructure interdependencies. 21 (6): 11-25. https://doi.org/10.1109/37.969131.

United Nations Conference on Trade and Development. 2017. Climate change impacts on coastal transportation infrastructure in the Caribbean: enhancing the adaptive capacity of Small Island Developing States (SIDS), SAINT LUCIA: a case study UNDA Project 1415O.

Chapter 5

5 Concluding Remarks and Future Work

The study area, located at the southern coast of Saint Lucia, is highly exposed to weather-related extreme events and at risk of compound flooding that is caused by the multiple contributing factors such as river flows, heavy rainfall, and coastal water levels. The associated risk is exacerbated due to the high concentrations of infrastructure and human communities at coastal lowlands. Major assets in the study area include Hewanorra International Airport, the towns of Vieux Fort and La Tourney, Vieux Fort Seaport, coastal agricultural lands, as well as the north-south highway.

A hydrologic model (i.e. HYdrological MODel) and a two-dimensional hydrodynamic model (i.e. LISFLOOD-FP) was set up and calibrated to investigate the combined effects of storm tides, wave run-up, rainfall, and river flow in the event of Tropical Storm Matthew. Simulated flood extents are validated based on the flood inundation map derived from available satellite imagery. Due to the limited data resources, boundary conditions are expected to be the major source of model uncertainties in hydrodynamic modelling. Sensitivity analysis was accordingly used to investigate impacts of uncertain boundary conditions, as well as to determine individual contributions of different contributing factors. Probabilistic flood hazard analysis was utilized to derive conditional probabilistic flood hazard map and to gain understanding of high-risk regions. In addition, scenario analysis was conducted to evaluate the potential impacts of wave run-up. Results indicate that although heavy rainfall is the major contributing factor in the flooding in the event of Tropical Storm Matthew, it is necessary to include sea levels and river discharges in modelling to obtain more reliable and accurate flood estimates. Uncertainties in the rainfall volume and in temporal patterns of rainfall intensities have significant impacts on the flood estimates, including water depths as well as the magnitude and peak time of flood inundation areas. The potential effects of wave run-up are severe, which can induce overbank flooding and flood water from the coast running much farther inland, affecting numerous assets.

The RiskLogik software, a network-based risk analysis platform, was used in this study to explore the relative importance of infrastructures and prioritize risks in conditions of non-flooding and flooding. The model setup was based on major assets that pertain to key economic sectors in Saint Lucia. Interdependencies are expected among those assets. Direct connections between entities were pre-identified while effects of indirect connections were simulated in the RiskLogik model. Modelling results revealed the fundamental importance of the normal operations of Hewanorra International Airport, which has the greatest impact on the system and has the highest risk index. In scenarios of flooding, to ensure the normal operations of the airport, it is critical to timely clear the standing water in the runway and taxiway. Uncertainty analysis indicates that the subjectivity in pre-defined parameters (i.e. the degree of impact, the likelihood of failure, and the degree of dependence) has limited impacts on the ranking of risk of entities. Prioritization should be given to following entities: airplane landing and taking off, runway status, taxiway/apron status, aircraft and cargo capacity, and particularly the backup electricity generator for the control tower and air traffic system. Other entities that are found at high risk include transportation, tourism, as well as essential services such as electricity distribution, rainwater control, and communication services.

This study considers inland flooding caused by rainfall as well as flooding caused by coastal water levels (i.e. storm tides and waves) along with the effects of interactions between river flows and sea levels, which can help complete current understanding of compound flooding in the research. This study also reveals the potential of using simplified two-dimensional hydrodynamic models in data-scarce regions with the appropriate preprocess of topographic and forcing data as well as the characterization of the effects of uncertain boundary conditions to simulation results. In addition, risk analysis is conducted for interdependent infrastructures that support major services in the study area and the economy of the island, which provides insights for local flood management.

Major limitations of this study are as follows. Firstly, due to the lack of data resources, uncertain boundary conditions can result in significant uncertainties in simulated results of LISFLOOD-FP, which are investigated but not comprehensively quantified in this study. Secondly, interaction mechanisms between different factors and their impacts to flooding patterns are not well studied. Hourly runoff is assumed to be constant during one day, but in reality, river discharge rates can dramatically increase and then decrease due to the quick response of the catchment to heavy

rainfall. Wave run-up is assumed to continuously affect the island for 21 hours along the coastline with different heights on top of storm tides, while in real events, extreme wave run-up heights may only last for seconds or minutes. The inability to reproduce hourly patterns of river flows and coastal water levels (including wave run-up) can lead to significant underestimation of flood risks because peak river discharges and peak sea levels can occur simultaneously and induce substantial overbank flooding or significant overestimation of flood risks due to the continuing high wave run-up heights for hours. Thirdly, consideration of drainage systems, higher resolutions of the hydrodynamic model, and topographic data that excludes elevations of trees are needed to obtain more realistic and reliable simulation results especially in the environments with high intensities of buildings and trees. Besides, surveyed cross sections are needed for more reliable simulations on overbank flooding. Fourthly, in model validation, since available satellite imagery are taken one day after the event and flood water has mostly receded, the derived flood inundation map cannot provide a comprehensive understanding of flood conditions during the event. Lastly, due to limited resources, risks of assets are assessed in a qualitative and relative manner, not all spatial relationships between assets are considered, and subjectivity is expected when assigning pre-defined parameters in the RiskLogik software.

To address the limitations of this study and obtain more reliable simulation results, the major task is to investigate and quantify the impacts of uncertain boundary conditions. It is critical to understand how the uncertainties propagate through the model and influence the simulation results including flood extents and water depths. Secondly, sensitivity analysis should be conducted to evaluate the effects of different temporal distributions of river flows, coastal water levels, and rainfall to flood patterns. To obtain higher-quality forcing data, hydrological models can be set up to simulate sub-daily runoff when there is available data, and hydrodynamic circulation models can be utilized to generate reliable time series of sea levels.

Analysis of this study is restricted to the event of Tropical Storm Matthew. To further extend the scope, effects of storms with different characteristics (e.g. different magnitudes and temporal patterns of rainfall, river flows, and coastal water levels) can be simulated using the validated hydrodynamic model. Analysis can also be conducted to evaluate the impacts of changing climate on compound flooding, which includes earlier snow melt (M.R. Najafi, Zwiers, and Gillett 2017a;

M.R. Najafi, Zwiers, and Gillett 2016), more intense precipitation events (M.R. Najafi and Moazami 2016; Halmstad, Najafi, and Moradkhani 2013), changes in the flow characteristics including its peaks (M. Najafi and Moradkhani 2014; Reza Najafi and Moradkhani 2013; M.R. Najafi, Zwiers, and Gillett 2017b), more intense storm surge events among others. In addition, copulas and Bayesian approaches can be used to evaluate the statistical dependencies between multiple contributing factors, characterize the uncertainties and develop more robust estimations based on multi-modelling (M.R. Najafi and Moradkhani 2015).

References

Halmstad, Andrew, Mohammad Reza Najafi, and Hamid Moradkhani. 2013. "Analysis of precipitation extremes with the assessment of regional climate models over the Willamette River Basin, USA." Hydrological Processes 27 (18): 2579-2590.

Najafi, Mohammad Reza, and Saber Moazami. 2016. "Trends in total precipitation and magnitude–frequency of extreme precipitation in Iran, 1969–2009." International Journal of Climatology 36 (4): 1863-1872.

Najafi, Mohammad Reza, and Hamid Moradkhani. 2015. "Multi-model ensemble analysis of runoff extremes for climate change impact assessments." Journal of Hydrology 525: 352-361.

Najafi, Mohammad Reza, Francis Zwiers, and Nathan Gillett. 2017a. "Attribution of the observed spring snowpack decline in British Columbia to anthropogenic climate change." Journal of Climate 30 (11): 4113-4130.

Najafi, Mohammad Reza, Francis W Zwiers, and Nathan P Gillett. 2016. "Attribution of the spring snow cover extent decline in the Northern Hemisphere, Eurasia and North America to anthropogenic influence." Climatic Change 136 (3-4): 571-586.

---. 2017b. "Attribution of observed streamflow changes in key British Columbia drainage basins." Geophysical Research Letters 44 (21): 11,012-11,020.

Najafi, MR, and H Moradkhani. 2014. "A hierarchical Bayesian approach for the analysis of climate change impact on runoff extremes." Hydrological processes 28 (26): 6292-6308.

Reza Najafi, Mohammad, and Hamid Moradkhani. 2013. "Analysis of runoff extremes using spatial hierarchical Bayesian modeling." Water Resources Research 49 (10): 6656-6670.

Curriculum Vitae

Name	Ying Zhang
Post-secondary Education and Degrees	Sun Yat-sen University Guangzhou, Guangdong, China 2013-2017 B.A. Western University London, Ontario, Canada 2017-2019 M.A.
Honours and Awards	2nd Scholarship for Excellent Student 2013-2015 3rd Scholarship for Excellent Student 2015-2016
Related Work Experience	Teaching Assistant (ES4498G, CEE4465a) Western University 2018-2019
Conference Poster Presentations	2018 Joint Meeting of CGU, CSSS, CIG, ES-SSA, and CSAFM Niagara Falls, Ontario, Canada, 2018 2018 AGU Fall Meeting Washington, D.C., America, 2018 Workshop on Correlated Extremes Manhattan, NYC, America, 2019 27th IUGG General Assembly Montreal, Quebec, Canada, 2019
Professional Skills	ArcGIS, R, HEC-RAS, HEC-GeoRAS, LISFLOOD-FP, Matlab, HEC-HMS, Google Earth Engine, AutoCAD, Python